# UNIVERSITÀ DEGLI STUDI DI FIRENZE

FACOLTÀ DI INGEGNERIA

Tesi di dottorato

*2009*

# Solutions for $CO_2$ capture from coal-fired power plants

## Influence on plant performance and environmental impact

**Relatore:** *Prof. Ing. G.MANFRIDA*

**Co-relatore:** *Ing. D.FIASCHI*

**Contro-relatore:** *Prof. Ing. P. CONSONNI*

**Candidato:**

Robert Strube

# Acknowledgments

# Introduction

Global warming caused by the emission of anthropogenic greenhouse gases, especially of $CO_2$, is nowadays one of the major environmental issues. However, there are a number of mitigation options that can help reduce the emission of greenhouse gases. These options comprise, for example, reforestation and a change in agriculture. For the energy sector, some of these options are energy savings, increased power plant efficiency, e.g. by using co-generation of heat and electricity, the use of renewables and switching to low-carbon fuels such as natural gas. It is clear that one of these choices alone is not capable of sufficiently reducing greenhouse gas emissions. All possibilities for the reduction of greenhouse gas emissions have to be employed in order to at least significantly slow down global warming.

In this thesis, the author concentrated on a relatively new mitigation option. Fossil fuels still are - and in the short to medium term will remain - the main resource for energy production. Especially coal is a fossil resource that is expected to be available for some hundred years or more. Therefore, greenhouse gas emissions due to its use have to be reduced by some sort of $CO_2$ elimination in the so-called carbon capture and storage process (CCS).

In order to reduce $CO_2$ emissions from a power plant, $CO_2$ can either be captured from the flue gases or from the syngas stream in a gasification plant. Although smaller pilot plants already exist to study their performance, CCS needs to be applied to larger power plants of about or more than 500 MW output such as the ones studied in this thesis in order for this mitigation to be effective on a global scale.

The author developed models with the flowsheet simulation program Aspen Plus to study the most common power plant processes and their performance with and without capture. All models were designed to achieve a nominal $CO_2$ capture efficiency of 90%. In a first step, models were developed that assume chemical and vapour-liquid equilibrium. In order for the models to be as realistic as possible, focus was then laid on rate-based models that take into account the kinetics of the occurring chemical reactions and of mass transfer.

The rate-based models studied in this thesis are for

i)      a 500 MW pulverized coal power plant using monoethanolamine (MEA) and ammonia as chemical solvents for post-combustion $CO_2$ capture,

ii)     a 500 MW Internal Gasification Combined Cycle (IGCC) with pre-combustion capture, using the physical solvent Selexol for either separate or co-capture of $CO_2$ and $H_2S$, and

iii)    a 500 MW oxy-fuel power plant with cryogenic $CO_2$ purification.

For all models, the author compares the effect of $CO_2$ capture on power plant performance. In accordance with literature, the largest energy penalty due to $CO_2$ capture was caused by the necessary thermal regeneration of chemical solvents used in post-combustion capture in this study.

In order to determine the environmental impact of the investigated power plants, a consecutive Life Cycle Assessment (LCA) was carried out with the commercial software SimaPro. The LCA confirmed the findings of the energy analysis.

The highest environmental impact per net energy output is observed for post-combustion capture. This impact was not only caused by the high energy penalty but also by the necessary solvent production to compensate for solvent losses to the atmosphere and solvent degradation. The environmental impact of the IGCC with pre-combustion capture was lower and of similar magnitude as for the oxy-fuel power plant.

Finally an Exergetic Life Cycle Assessment was carried out for all capture options. In this analysis, the impact of the power plants and of $CO_2$ capture is calculated in the form of irreversibility caused to the environment. The lowest process irreversibilities, i.e. exergy destruction, were observed for pre-combustion $CO_2$ capture, followed by oxy-fuel $CO_2$ purification. The exergy destruction in the latter power plant type would be significantly reduced, if the exergy content of the compressed nitrogen stream leaving the ASU could be integrated, e.g. by expansion in a gas turbine together with the inerts separated in the $CO_2$ purification section. Without $CO_2$ capture the irreversibilities in the pulverised coal power plant are similar to the IGCC plant.

For the respective capture method, i.e. pre-combustion, post-combustion, or oxy-fuel, the lowest calculated cumulative irreversibility or exergy destruction could be considered as synonymous to the result for a zero-emission process.

Despite the inferior performance of post-combustion capture in both energy and environmental impact analyses, this process is very important, because it can be applied (also as a retrofit option) to a wide range of processes such as cement or steel production, in which fuel is burned with air at atmospheric pressure. This fuel conversion process is also the most common technology for power plants today. In these cases, apart from using lower carbon fuels or biomass, post-combustion capture is the only feasible means to reduce greenhouse gas emissions.

# Contents

# List of Figures

# List of Tables

# Nomenclature

| | |
|---|---|
| a | Stoichiometric coefficient |
| AA | Aqueous ammonia |
| aMDEA | Activated MDEA process, licensed by BASF |
| ASC | Advanced supercritical |
| ASU | Air separation unit |
| CAP | Chilled ammonia process |
| CCS | Carbon capture and storage |
| CExC | Cumulative exergy consumption |
| d | Change (delta) |
| DALY | Disability adjusted life years |
| DGA | Diglycolamine |
| DEPG | mixture of dimethyl ethers of polyethylene glycols |
| e | Specific exergy |
| E | Exergy |
| $\dot{E}$ | Exergy stream |
| EAA | Aqueous ethanol-ammonia solvent |
| EC | European Community |
| EGR | Enhanced gas recovery |
| ELCA | Exergy life cycle assessment |
| EOR | Enhanced oil recovery |
| EOS | Equation of state |
| ESP | Electrostatic precipitator |
| FG | Flue gas |
| FGD | Flue gas desulphurisation |
| FSU | Former Soviet Union |
| G | Gibbs free energy |
| GE | General Electrics |
| GHG | Greenhouse gases |
| GT | Gas turbine |
| GWP | Global warming potential |
| h | Specific enthalpy |
| H | Enthalpy |
| H&MB | Heat and mass balances |
| HE | Heat exchanger |
| HHV | Higher heating value |
| HP | High pressure |

| | |
|---|---|
| HRSG | Heat recovery steam generator |
| İ | Irreversibility |
| IEA GHG | IEA Greenhouse Gas R&D programme |
| IGCC | Internal gasification combined cycle |
| IP | Intermediate pressure |
| IPCC | International Panel on Climate Change |
| ISO | International Standards Organization |
| K | Equilibrium constant |
| KEPCO | Kansai Electric Power Company |
| KS-1 | Proprietary hindered amine solvent from KEPCO/MHI |
| k | pre-exponential kinetic factor |
| LCA | Life-cycle assessment or life-cycle analysis |
| LCI | Life-cycle inventory |
| LCIA | Life-cycle impact assessment |
| LCM | Life-cycle management |
| LP | Low pressure |
| LULUFC | Land use, land-use change and forestry |
| LHV | Lower heating value |
| m | Mass flow |
| MDEA | Methyl-diethanolamine |
| MEA | Monoethanolamine |
| MHI | Mitsubishi Heavy Industries |
| n | Mole flow |
| NGCC | Natural gas combined cycle |
| NMR | Nuclear magnetic resonance spectroscopy |
| NRTL | Non-Random Two-Liquid activity coefficient model |
| OC | Other countries |
| OECD | Organisation for Economic Co-operation and Development |
| OME | Other major economies |
| p | Pressure |
| $p_i$ | Partial pressure |
| PAF | Potentially affected fraction |
| PC | Pulverised coal |
| PC-SAFT | Perturbed chain statistical associating fluid theory |
| PDF | Potentially disappeared fraction |
| ppb | Parts per billion |
| ppm | Parts per million |
| PR-BM | Peng-Robinson equation of state with Boston-Mathias correction |
| r | Reaction rate |

| | |
|---|---|
| Rectisol | Commercial name for physical solvent methanol |
| RK | Redlich-Kwong equation of state |
| s | Specific entropy |
| S | Entropy |
| SCR | Selective catalytic reduction |
| SD | Standard deviation |
| Selexol | Mixture of dimethyl ethers of polyethylene glycol |
| SETAC | Society of environmental toxicology |
| SOFC | Solid oxide fuel cell |
| ST | Steam turbine |
| UNEP | United Nations Environment Programme |
| UNFCCC | United Nations Framework Convention on Climate Change |
| VLE | Vapour-liquid equilibrium |
| $\dot{W}$ | Work stream |
| WEO | World Energy Outlook (Models and Scenarios by the IEA) |
| WGS | Water-gas-shift |
| x | mole fraction |

## Greek letters

| | |
|---|---|
| α | Activity coefficient |
| ε | Simple exergy efficiency |
| ψ | Rational exergy efficiency |

## Subscripts

| | |
|---|---|
| 0 | Standard or environmental state |
| ch | Chemical |
| D | Destruction |
| i | Component i |
| in | Incoming |
| mix | Mixing |
| out | Outgoing |
| ph | Physical |
| q | Heat |

# 1. Climate change

The effect of human action on the climate is now widely accepted. In this chapter the major causes of global warming by greenhouse gases such as $CO_2$ and its effect on the environment will be discussed, with the focus on its industrial origins. Here, power generation by fossil fuels is the prominent contribution [1]. For this sector then technical solutions for the mitigation of greenhouse gases will be presented.

## 1.1. Climate change by global warming

The IPCC defines climate change as the state of the climate that can be identified by changes in the mean value and/or the variability of its properties, and that persists for an extended period, typically decades or longer. It refers to any change in climate over time, whether due to natural variability or as a result of human activity [2]. In contrast, the UNFCCC uses a definition, which attributes climate change directly or indirectly to human activity that alters the composition of the global atmosphere in addition to natural climate variability observed over comparable time periods [3].

As presented in Figure 1, it can be observed that the linear warming trend for the 50 years between 1956 and 2005 is nearly twice as steep as that for the 100 years between 1906 and 2006. This trend is especially pronounced in the northern hemisphere. The average arctic temperatures have increased with almost twice the average global rate over the past 100 years. Sea levels have risen accordingly, a major contribution, 57% since 1993, being the thermal expansion of the oceans, while the melting of glaciers and ice caps contributed with 28% over the same period.

These stated changes have observable impacts on the environment. For natural systems related to snow, ice and frozen ground, it is observed that glacial lakes have increased in number and extension, permafrost regions show increasing ground instability, rock avalanches in mountain regions have increased in number. For terrestrial biological systems there is very high confidence that a wide range of species is affected by earlier spring events. Marine and freshwater biological systems are affected by rising water temperatures, changes in ice cover, salinity, oxygen levels and circulation [2].
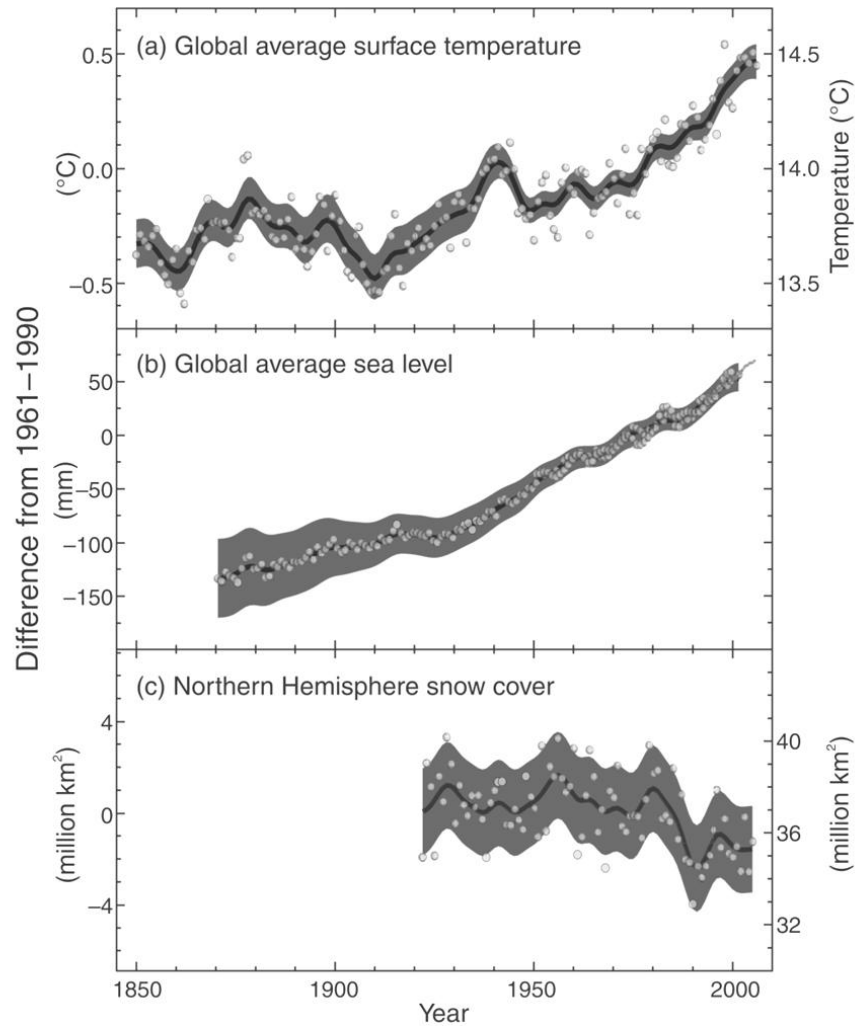
**Figure 1.** Observed changes in global average surface temperature, global average sea level, and Northern hemisphere snow cover for March-April with decadal averaged values (curves), yearly values (dots) and uncertainty intervals (shaded) [2].

Global warming is caused by natural and anthropogenic drivers, the emission of long-lived greenhouse gases (GHG) being the major contribution. GHGs contribute to global warming by changing the radiation balance of the earth. While the existence of greenhouse gases is important for the thermal balance of the earth by preventing the release of all reflected solar radiation from the earth's surface, the increased emission of these gases leads to a lower release of the infrared part of the spectrum and thus to an increase in the earth's temperature as shown in Figure 2. This effect of altering the balance of incoming and outgoing energy in the earth-atmosphere system is often measured with the radiative forcing value. This value in $W/m^2$ is an index standing for the importance of a potential climate change mechanism and is used in the IPCC reports for changes relative to pre-industrial conditions defined at 1750 [2].

Anthropogenic GHG emissions have increased globally by about 70% between 1970 and 2004. Due to their different radiative properties and lifetimes in the atmosphere the warming influence of

the greenhouse gases varies. However, these influences can be expressed and compared by a common metric, the so-called global warming potential (GWP).
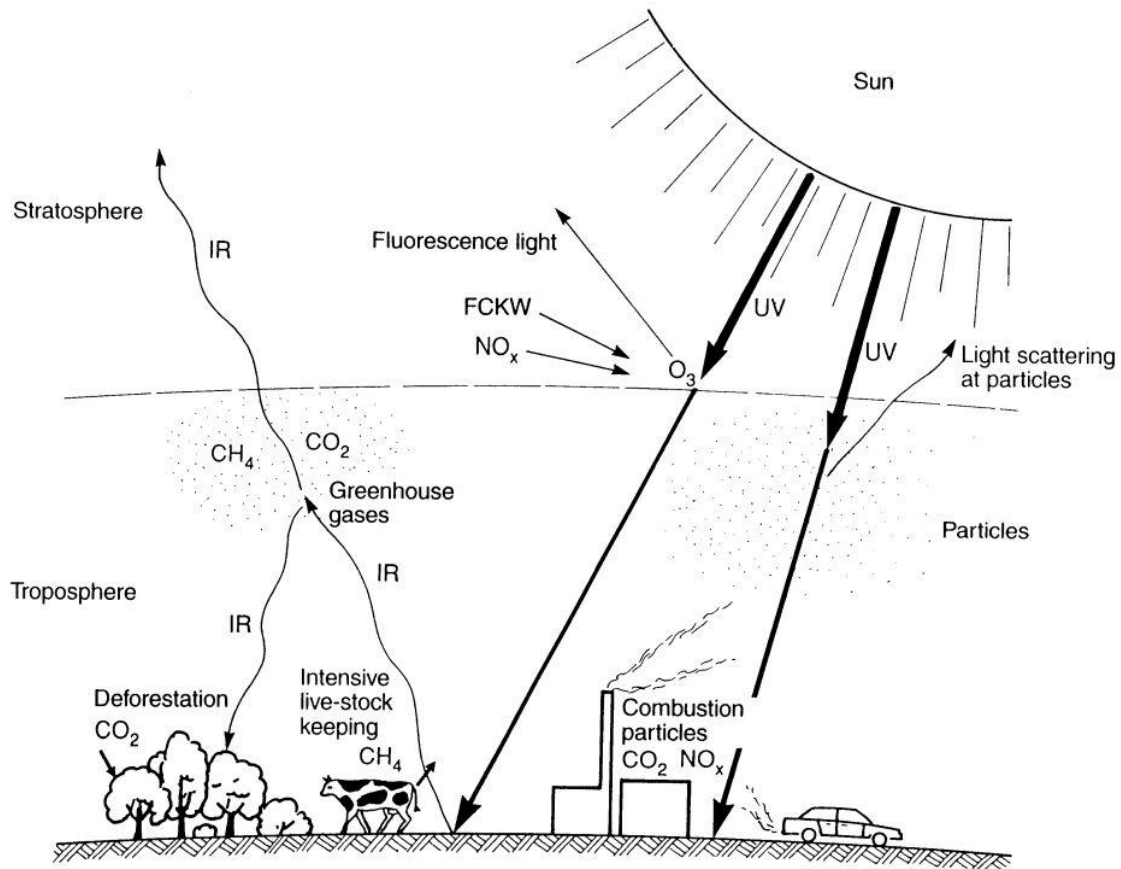


**Figure 2.** The greenhouse effect [4].

The characteristics of the most important greenhouse gases are presented in Table 1. The equivalent $CO_2$ emission of greenhouse gases other than $CO_2$ is obtained by multiplying its emission with its global warming potential. The equivalent $CO_2$ concentration is the concentration of $CO_2$ that would cause the same amount of radiative forcing.

**Table 1.** Characteristics of greenhouse gases [5].

| Gas | Residence time in atmosphere | GWP | | |
| --- | --- | --- | --- | --- |
| | | after 20 years | after 100 years | after 500 years |
| $CO_2$ | variable | 1 | 1 | 1 |
| $CH_4$ | 9 – 15 | 72 | 25 | 7.6 |
| $N_2O$ | 120 | 289 | 298 | 153 |
| HFC – 125 | 33 | 6,350 | 3,500 | 1,100 |
| $SF_6$ | 3200 | 16,300 | 22,800 | 32,600 |

The observed increase in global average temperatures over the last 100 years is very likely due to the increase in anthropogenic GHG emissions as shown in Figure 4.
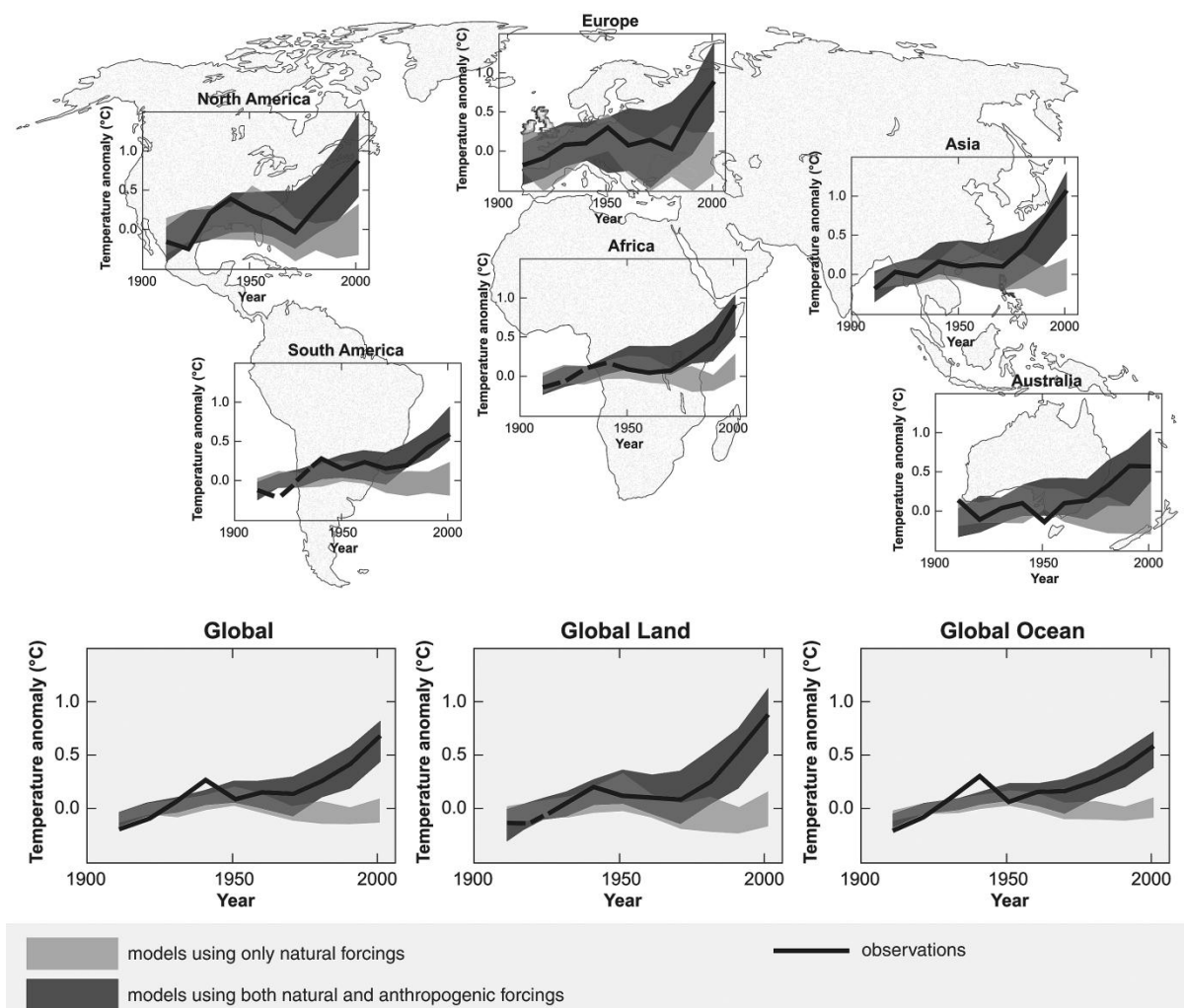


**Figure 3.** Observed decadal averages of surface temperature with overlay of uncertainty bands for climate models with and without anthropogenic GHG emissions [6].

In Figure 4, the emission of anthropogenic GHGs is shown in terms of $CO_2$ equivalents for the years 1974 to 2004. For 2004, the distribution of GHG emissions across the different sectors of anthropogenic activity is given. It is obvious that the most important greenhouse gas is $CO_2$, while the emissions are caused mainly by the industrial sector, in particular the energy supply. The still rising demand for energy and the increase in $CO_2$ emissions typically involved has become one of the most important environmental topics. Coal is a resource still readily available. Its use in power generation comes with a cost, however. The combustion or gasification of coal releases a high amount of $CO_2$.
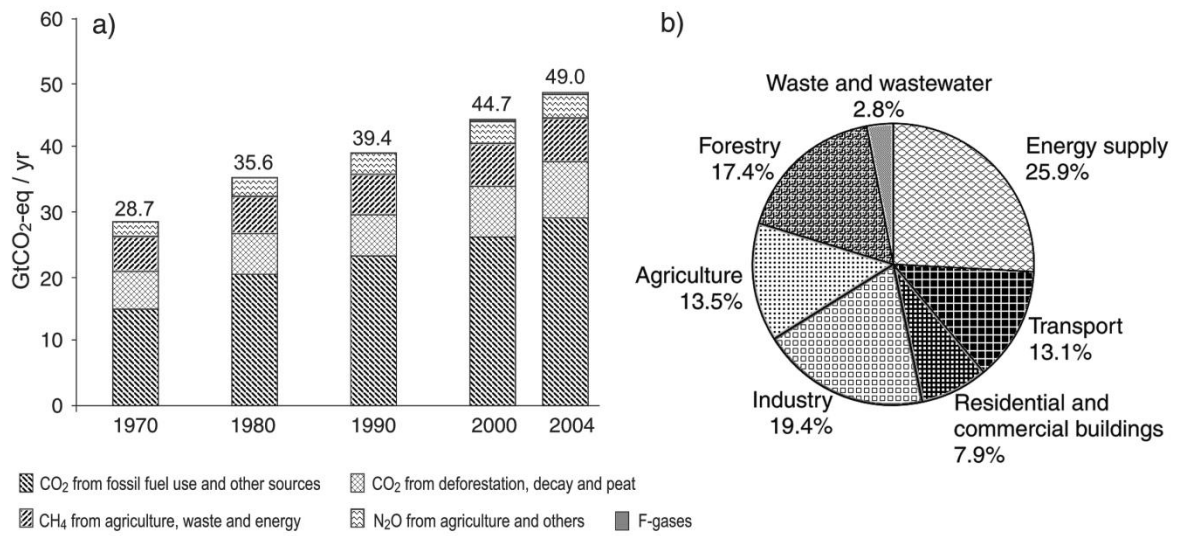
**Figure 4.** a) Global annual emissions of anthropogenic GHGs,
    b) share of different sectors in total anthropogenic GHG emissions in 2004 in $CO_2$-eq [2].

It is obvious that without a change in policy global warming will increase further and thus will have major environmental and social effects caused by extreme weather and climate events.

## 1.2. Responding to climate change

### 1.2.1. Alternative responses

There are two possible responses to climate change. One of them is the adaptation to its effects and the other, also called mitigation, is the reduction of GHG emissions in order to reduce the rate and magnitude of climate change. The possibility to adapt to climate change is limited and dependent on the society's financial, technological, political, and cultural resources. However, even highly adaptive societies are vulnerable to extremes such as the heat wave in Europe in 2003 and hurricane Katrina in the United States in 2005, both causing large human costs.

An important factor for the implementation of mitigation options is the regional environmental and socio-economic situation and the availability of information and technology. In order for this option to be effective, a concerted global approach needs to be taken.

### 1.2.2. Objectives of the Kyoto Protocol

For establishing a global response to climate change, the environmental treaty UNFCCC was produced at the United Nations Conference on Environment and Development (UNCED) in Rio de Janeiro in 1992 and entered into force in 1994, ratified by over 50 countries. The treaty, although considered legally non-binding, requires for updates called "protocols". Since 1995, the UNFCCC countries meet annually in Conferences of the Parties (COP). The principal update, the Kyoto Protocol, established national greenhouse gas inventories and created the 1990 benchmark of national greenhouse gas emissions. The Kyoto Protocol was concluded in 1997 and established legally binding obligations in the Annex I countries for a reduction of GHG emissions ($CO_2$, $CH_4$, $N_2O$, $SF_6$) as well as the emissions of hydrofluorcarbons and perfluorcarbons from 1990 levels by an average of 5% over the period 2008-2012. The states that signed the Kyoto Protocol can be divided in three groups. The industrialised countries committed to complying with the emission targets form the Annex I group. A subgroup of these countries that pays for costs arising in developing countries is formed by the Annex II states. These are OECD members except those countries that were economies in transition in 1992. The third group of countries, the developing countries, are not required to reduce GHG emissions to avoid restrictions to their development. They can sell emission credits to nations with difficulty of meeting the emission targets and receive financial and technological help for the implementation of

low-carbon technologies. Developing countries may volunteer to become Annex I countries when they are sufficiently developed [7].

Emission restrictions do not include international shipping and aviation. These limits are integrated in the 1987 Montreal Protocol on Substances that deplete the Ozone Layer with the industrial gases chlorofluorocarbons, or CFCs [7].

At the 2008 UNFCCC COP 14 in Poznan, Poland, the following objective was formulated [8]:

*"The ultimate objective of this Convention and any related legal instruments that the Conference of the Parties may adopt is to achieve, in accordance with the relevant provisions of the Convention, stabilization of greenhouse gas concentrations in the atmosphere at a level that would prevent dangerous anthropogenic interference with the climate system. Such a level should be achieved within a time frame sufficient to allow ecosystems to adapt naturally to climate change, to ensure that food production is not threatened and to enable economic development to proceed in a sustainable manner."*

In November 2009, 186 countries and one regional economic organisation, the EU, have signed and ratified the Kyoto protocol, representing over 63.9% of the 1990 emissions from Annex I countries. The United States, which are a signatory of UNFCCC and responsible for 36.1% of the 1990 emission levels, are still a non-member. India and China are excluded from complying with the emission limits, as they are considered developing countries despite a massive increase of their GHG emissions.

The so far 37 Annex I countries that agreed to binding emission targets may only exceed their allocations if they buy emission allowances or take other measures that all UNFCCC parties have to agree upon. The Kyoto Protocol allows for so-called flexible mechanisms that enable Annex I countries to acquire GHG emission credits either by financing emission reducing projects in other Annex I or non-Annex I countries or by purchasing credits from Annex I countries with excess credits [7]. These mechanisms are:

Emissions Trading (ET):
> Countries with permitted but "unused" emissions may sell this excess capacity to countries that are exceeding their emission targets. Carbon dioxide being the principal greenhouse gas, a so-called carbon market has been created, on which emission permits are now tracked and traded like any other commodity.

Clean Development Mechanism (CDM):

> A country with an emission limit commitment under the Kyoto Protocol may implement an emission-reduction project in developing countries. With such projects saleable certified emission reduction (CER) credits can be acquired. A CDM project activity can be, for example, a rural electrification project with solar panels or the installation of more energy-efficient boilers.

Joint Implementation (JI):

> Emission reduction units (ERUs) can be acquired from an emission-reduction or emission removal project in another Annex I country, from which the host country benefits by investment and technology transfer.

At the COP 15 United Nations climate Change Conference in Denmark a global climate agreement was to be established due to the near expiration of the first commitment period of the Kyoto Protocol in 2012. However, only a less specific politically binding agreement was reached, postponing a binding post-Kyoto agreement to a second summit meeting in Mexico City to be held in December 2010 [7].

For countries that ratified the Kyoto protocol, the development of GHG emissions from fuel combustion is shown in Table 2. On average, in 2007 the participating countries were below the specified emission limits of the Kyoto Protocol, but recent increases in emissions may threaten the compliance with the set targets. While the 36 Kyoto countries are on pace to meet the 5% reduction target by 2012, most of the emission reduction is due to the decline in the Eastern European countries' emissions after the collapse of communism in the 1990s.

The overall target of emission reduction in the EU under the Kyoto Protocol is 8% from 1990 levels by 2008-2012. However, the GHG reduction targets of the EU and member countries were agreed on in June 1998 under the so-called "Burden Sharing Agreement" specified in the EC ratification decision. The reduction targets specified under this agreement are generally stricter than the originally fixed targets under the Kyoto Protocol.

**Table 2.** GHG emissions from fuel combustion and reduction targets for Kyoto parties [9].

| Country | 1990 | 2007 | change 1990-2007 | Reduction target |
|---|---|---|---|---|
| KYOTO PARTIES | 8792.2 | 8162.1 | -7.2% | -4.7% |
| North America | 432.3 | 572.9 | 32.5% | -6% |
| Canada | 432.3 | 572.9 | 32.5% | -6% |
| Europe | 3158.7 | 3281.3 | 3.9% | (-8%) |
| Austria | 56.2 | 69.7 | 24.0% | -13.0% |
| Belgium | 107.9 | 106.0 | -1.8% | -7.5% |
| Denmark | 50.4 | 50.5 | 2.0% | -21.0% |
| Finland | 54.4 | 64.4 | 1.9% | 0.0% |
| France | 352.1 | 369.3 | 4.9% | 0.0% |
| Germany | 950.4 | 798.4 | -16.0% | -21.0% |
| Greece | 70.1 | 97.8 | 39.5% | 25.0% |
| Iceland | 1.9 | 2.3 | 24.6% | 10.0% |
| Ireland | 30.6 | 44.1 | 44.1% | 13.0% |
| Italy | 397.8 | 437.6 | 10.0% | -6.5% |
| Luxembourg | 10.5 | 10.7 | 2.5% | -28.0% |
| Netherlands | 156.6 | 182.2 | 16.4% | -6.0% |
| Norway | 28.3 | 36.9 | 30.6% | 1.0% |
| Portugal | 39.3 | 55.2 | 40.5% | 27.0% |
| Spain | 205.8 | 344.7 | 67.5% | 15.0% |
| Sweden | 52.8 | 46.2 | -12.4% | 4.0% |
| Switzerland | 40.7 | 42.2 | 3.6% | -8.0% |
| United Kingdom | 533.0 | 523.0 | -5.4% | -12.5% |
| Pacific | 1346.5 | 1668.1 | 23.9% | |
| Australia | 259.8 | 396.3 | 52.5% | 8.0% |
| Japan | 1065.3 | 1236.3 | 16.1% | -6.0% |
| New Zealand | 21.3 | 35.5 | 66.4% | 0.0% |
| Economies in transition | 3854.7 | 2639.8 | -31.5% | |
| Bulgaria | 74.9 | 50.2 | -33.0% | -8.0% |
| Croatia | 22.0 | 22.0 | 2.1% | -5.0% |
| Czech Republic | 155.4 | 122.1 | -21.4% | -8.0% |
| Estonia | 36.2 | 18.0 | -50.1% | -8.0% |
| Hungary | 66.7 | 53.9 | -19.1% | -6.0% |
| Latvia | 18.4 | 8.3 | -54.6% | -8.0% |
| Lithuania | 33.1 | 14.4 | -56.4% | -8.0% |
| Poland | 343.7 | 304.7 | -11.4% | -8.0% |
| Romania | 167.1 | 91.9 | -45.0% | -8.0% |
| Russian Federation | 2179.9 | 1587.4 | -27.2% | 0.0% |
| Slovak Republic | 56.7 | 36.8 | -35.1% | -8.0% |
| Slovenia | 13.1 | 15.9 | 21.2% | -8.0% |
| Ukraine | 687.9 | 314.0 | -54.4% | 0.0% |

When looking at the development of GHG emissions of the non-Kyoto parties and of world-wide emissions as shown in Table 3, it becomes obvious that efforts to reduce these emissions are crucial.

**Table 3.** GHG emissions from fuel combustion and for non-Kyoto parties and worldwide [9].

| Country | 1990 | 2007 | change 1990-2007 | Reduction target |
|---|---|---|---|---|
| NON-KYOTO PARTIES | 11577.8 | 19778.3 | 70.8% | |
| Non-participating Annex I Parties | 5106.3 | 6097.0 | 19.4% | |
| Belarus | 116.1 | 62.7 | -46.0% | |
| Turkey | 126.9 | 265.0 | 1.1% | |
| United States | 4863.3 | 5769.3 | 18.6% | -7.0% |
| Other regions | 6471.5 | 13681.3 | 111.4% | |
| Africa | 546.2 | 882.0 | 61.5% | |
| Middle East | 588.2 | 1389.0 | 136.1% | |
| Non-OECD Europe | 106.1 | 91.4 | -13.9% | |
| Other FSU | 581.6 | 406.7 | -30.1% | |
| Latin America | 897.0 | 1453.9 | 62.1% | |
| Asia (excl. China) | 1508.4 | 3387.1 | 124.6% | |
| China | 2224.0 | 6071.2 | 170.6% | |
| Int. Marine Bunkers | 356.9 | 610.4 | 71.1% | |
| Int. Aviation Bunkers | 253.6 | 411.6 | 62.3% | |
| World | 20980.5 | 28962.4 | 38.0% | |

In Figure 5 the development of international GHG emissions is presented graphically, high-lighting the importance of emissions by non-Annex I parties.
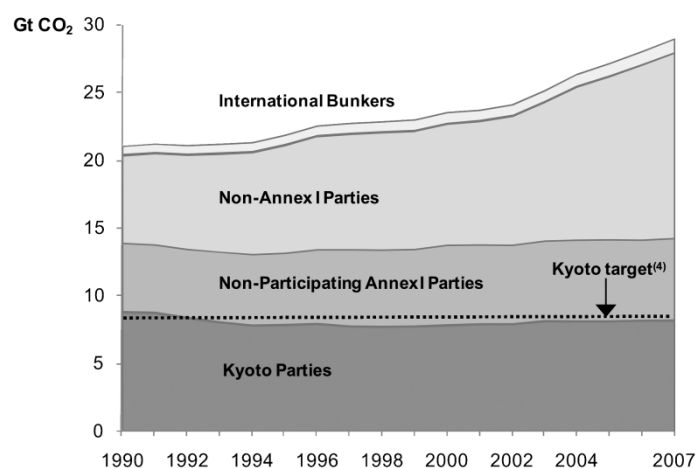


**Figure 5.** Development of GHG emissions worldwide [9].

In the context of this work, it is important to note that the energy sector is the major contributor to anthropogenic GHG emissions, especially in the Annex I countries. For the year 2006, the distribution of GHG emissions over the different sectors is shown in Figure 6, excluding land use, land-use change and forestry (LULUFC).
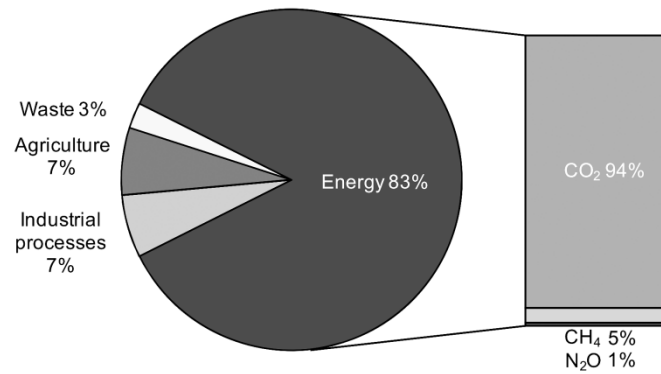


**Figure 6.** Anthropogenic GHG emissions without LULUFC in Annex I parties for 2006 [1].

The strong contribution of the energy sector to GHG emissions is caused by the extensive use of fossil fuels. In Figure 7 the projected development of worldwide primary energy consumption according to the reference scenario in the World Energy Outlook model (WEO) by the IEA is shown.
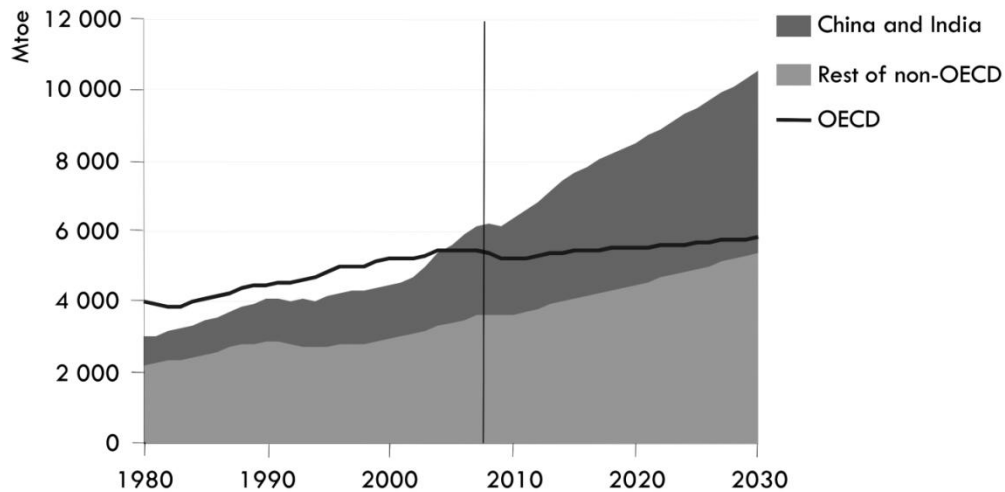


**Figure 7.** World primary energy demand in the Reference Scenario [10].

According to this model, non-OECD countries, here especially India and China, are responsible for 93% of the increase in global energy demand between 2007 and 2030. For this reference scenario, 77% of this increase is caused by fossil fuel consumption as presented in Figure 8.
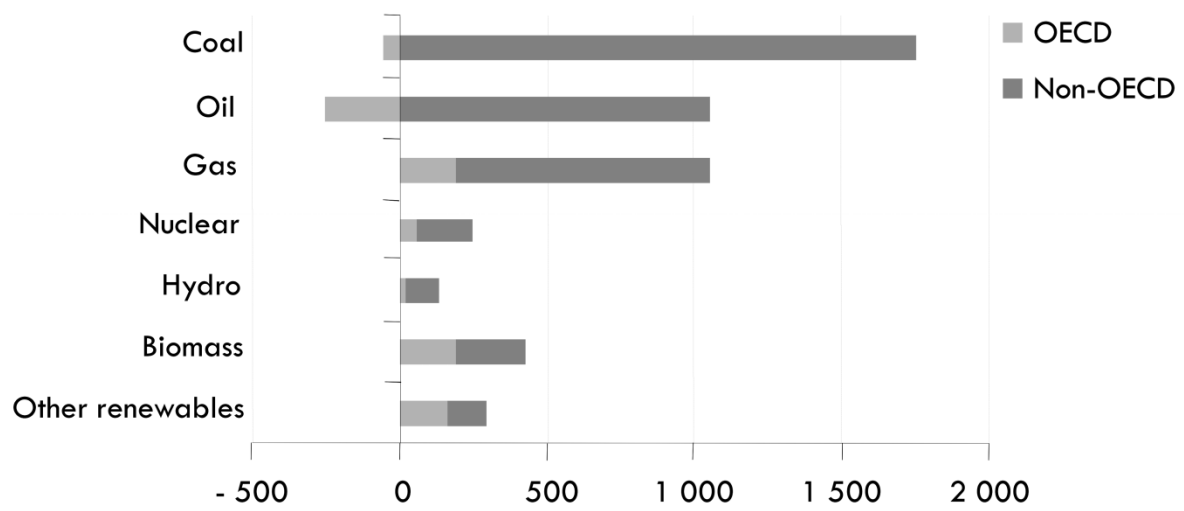
**Figure 8.** Change in global primary energy demand between 2007 and 2030 by fuel type [10].

## 1.3. Mitigation options

If the global temperature rise is to be limited, mitigation has to be applied with an ample portfolio of technologies. The reference scenario predicts a temperature rise of 6 °C. So limiting the temperature rise to 2°C requires big emission reductions in all regions and sectors. There is large uncertainty concerning the future contribution of the different mitigation technologies. The different stabilisation scenarios foresee that 60 to 80% of GHG emission reductions will be achieved in the sectors of energy supply and industrial processes. Emphasis is laid on higher efficiency and the use of low-carbon energy sources, which include the shift from coal to gas-fired power plants and the increased use of renewables. Including LULUFC mitigation options, such as reforestation, improved crop yields with reduced use of fertilizers, and manure management for decreased release of $CH_4$, allows for greater flexibility and cost-effectiveness [10].

In the WEO 450 Scenario, with a stabilisation of atmospheric $CO_2$ concentration to 450 ppm, demand for fossil fuels will peak by 2020, and by 2030 zero-carbon fuels will contribute to a third of the world's primary sources of energy demand. In this scenario, improved energy efficiency will account for most of the abatement as shown in Figure 9.
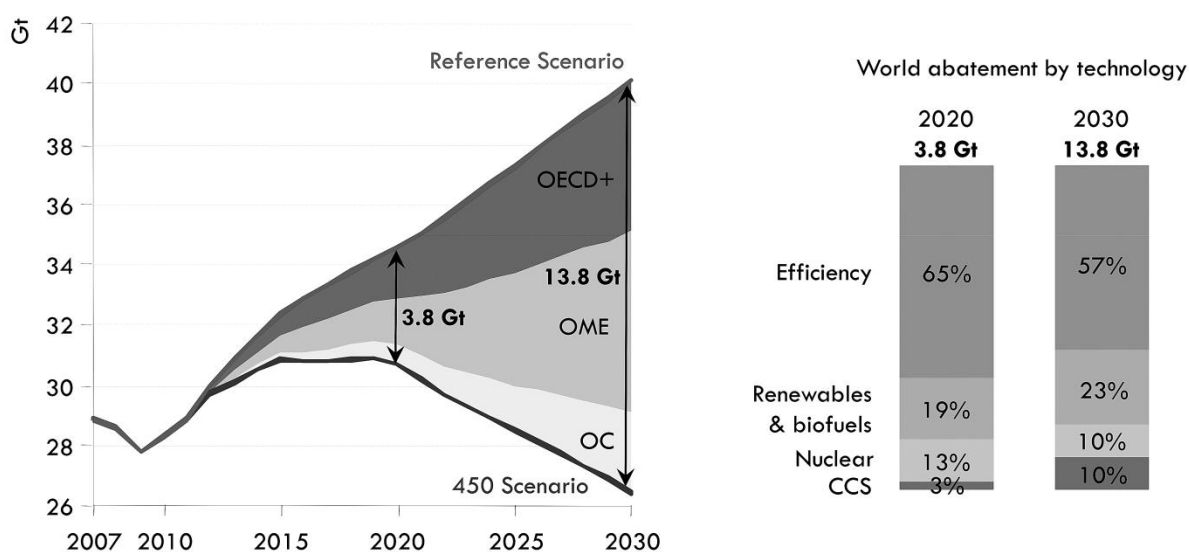


**Figure 9.** Role of abatement technologies in 450 scenario for OECD countries, other major economies (OME) and other countries (OC) compared to reference scenario [10].

In the context of this work, it should be stressed that renewables, nuclear power plants and plants fitted with carbon capture and sequestration account for around 60% of global electricity generation in 2030 in the 450 scenario, while today it is only one third. There would be additional benefits to energy security by reduced oil and gas imports, and less air pollution.

### 1.3.1. Importance of fossil fuels

Modern economies strive for securing energy supply by safe and stable power generation as well as independence from importing fossil fuels. More recently climate protection became an important factor in the planning of new power plants. Potential solutions such as renewable energies will not be able to secure our actual (and growing) need of power in the near future. Coal, however, will be available in Europe for about another 400 years. It is also an important fuel in fast-growing economies such as in China.

Large point sources such as power plants make up about 40% of all anthropogenic $CO_2$ emissions, especially in fast developing countries with large coal reserves. Other important point sources are sites of the cement and steel industry, fermentation processes for food and ammonia production.

One of the main problems with coal is the high $CO_2$ emission its use causes. In the next section, an option for reducing the environmental impact of fossil fuel burning is discussed.

### 1.3.2. Climate change mitigation by Carbon Capture and Storage

In Carbon Capture and Storage (CCS) as a major decarbonisation technology, a concentrated $CO_2$ stream is produced, which can be transported to an adequate storage site. CCS is an important mitigation option, since it allows for the continued use of fossil fuels even in scenarios with low GHG intensity. Large point sources such as power plants are ideal for the application of CCS. Combining CCS with the use of biomass, e.g. when co-fired in coal power plants, allows for effective net removal of $CO_2$ from the atmosphere.

The four basic systems for $CO_2$ capture in processes using fossil fuels and/or biomass are presented in Figure 10. Post-combustion $CO_2$ capture is the capture from flue gases produced by fuel combustion, while in pre-combustion capture $CO_2$ is removed from a syngas stream to be burned in a successive process step. The syngas stream is produced by reacting a fuel with air or oxygen. In oxy-fuel combustion, the fuel is burned with nearly pure oxygen, resulting in a very high concentration of $CO_2$ in the flue gas stream, which is then concentrated further to allow for storage. These processes are described in more detail in the corresponding chapters of this thesis. $CO_2$ separation has been applied for more than 80 years to large industrial plants for natural gas processing and in ammonia production [11] In these processes carbon capture is applied to meet process demands and not for storage due to lack of economical and policy incentives.
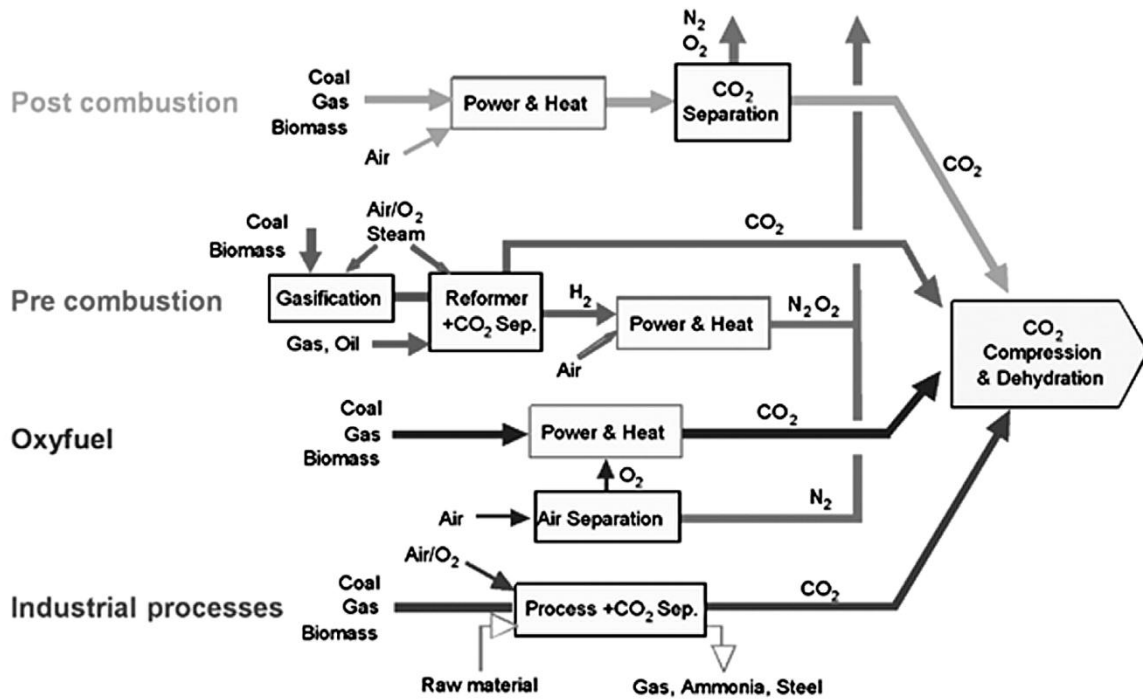
**Figure 10.** The four principal systems of $CO_2$ capture [12].

The main $CO_2$ capture technologies (absorption, membrane separation, distillation and cryogenic separation) are presented in Figure 11.



a) *Separation with sorbents/solvents*

b) *Separation with a membrane*

c) *Separation by cryogenic distillation*
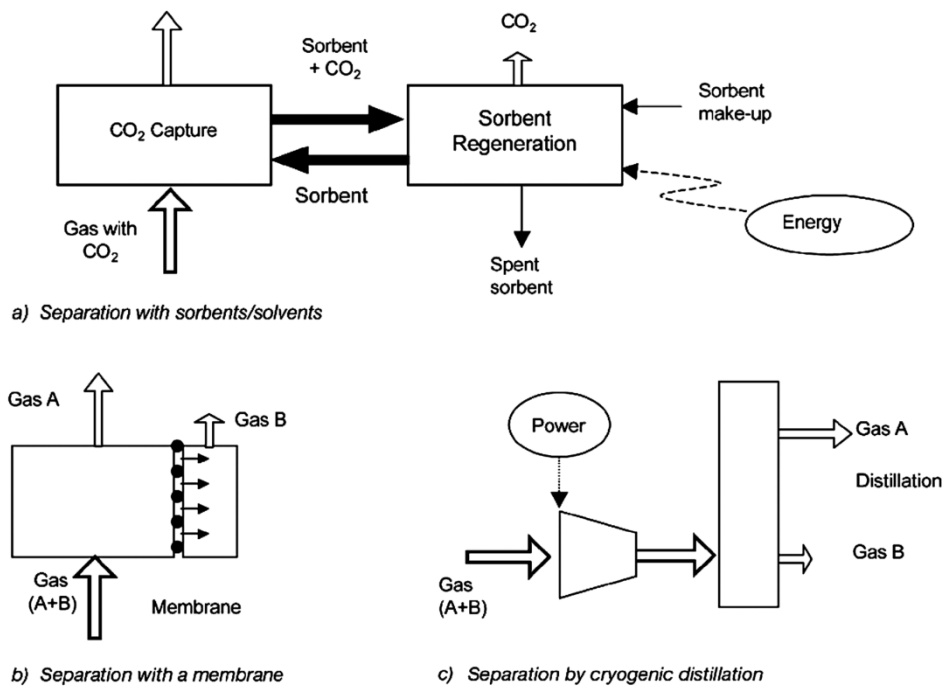
**Figure 11.** The main gas separation processes for $CO_2$ capture [12].

The principal disadvantage of CCS is that it energy is required, leading to a reduction in plant efficiency and increased fuel consumption. The influence of $CO_2$ capture on the latter is shown in Figure 12. Here, the power plants including $CO_2$ capture are compared to identical plants without capture
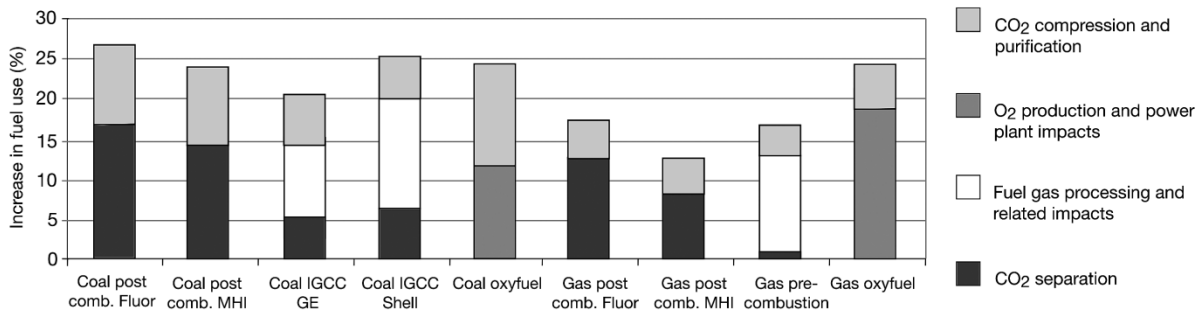


**Figure 12.** Increase in fuel consumption due to $CO_2$ capture [12].

After the $CO_2$ has been separated from the point source, the captured $CO_2$ may be stored underground, in the deep ocean or by industrial fixation as inorganic carbonates. Injection into geological storage sites is the most mature storage option. A number of commercial projects are already in operation. The other mentioned options show important disadvantages. Deep sea storage may not retain the $CO_2$ permanently and its ecological impacts are still unclear. Industrial fixation in mineral carbonates is very costly and requires a large amount of energy [13]. Total estimates for geological storage of $CO_2$ range from 1,000 to 10,000 Gt of $CO_2$, which represents more than 26 to 260 times the projected energy related emissions in 2030 [14, 9]. Storage may occur in depleted oil and gas reservoirs (920 Gt $CO_2$), saline aquifers (400 - 10,000 Gt $CO_2$) and unminable coal seams (40 Gt $CO_2$) [15]. The integrity of these storage sites needs to be ensured to prevent the possibly dangerous and at least counterproductive release of the stored gases. Most screening activities to explore adequate reservoirs are concentrated in North America, Europe, Japan and Australia due to political commitments there to reduce $CO_2$ emissions. Apart from storage, the $CO_2$ may also be used in industrial processes, e.g. for the production of methanol or fertilizers.

The drop in energy efficiency of the power plant due to $CO_2$ capture, the transport of the separated $CO_2$ stream and the storage of the captured gases lead to elevated costs. These costs per captured ton of $CO_2$ are listed in Table 4. However, as the large ranges show, such cost estimates are subject to assumptions and data inconsistencies. These estimates may also vary over time and depend on location and selected technology.

**Table 4.** Current cost ranges for CCS system components [12].

| CCS system components | Cost range in US$/t $CO_{2,net,captured}$ |
|---|:---:|
| Capture from coal- or gas-fired power plant | 15 - 75 |
| Capture from hydrogen and ammonia production or gas processing | 5 - 55 |
| Capture from other industrial sources | 25 - 115 |
| Transport | 1 - 8 |
| Geological storage (excl. possible additional long term costs for remediation and liabilities | 0.5 - 8 |
| Geological storage (monitoring and verification) | 0.1 - 0.3 |
| Ocean storage | 5 - 30 |
| Mineral carbonation | 50 - 100 |

As can be seen from this table, the most significant costs in CCS are caused by the capture process. Although this technology is promising, more research is necessary to reduce costs and to ensure the viability and safety of adequate storage sites to ensure a more widespread use of this technology. A cost reduction may be achieved with new or improved capture methods in combination with advanced design of power plants and industrial processes. At the moment, few commercial-scale demonstration projects for CCS are in operation as shown in Table 5. Larger power plants with CCS are planned to start operation in the near future. However, if CCS can be applied in large scale is also strongly dependent on public acceptance.

**Table 5.** Worldwide CCS Projects in operation [12, 15, 16, 17, 18, 19, 20, 21].

| CCS project | Operator | Description | Technology | Projected cost |
|---|---|---|---|---|
| Sleipner West (Norway) | Statoil and IEA | Injection of 1 Mt/yr of $CO_2$ from natural gas field into saline aquifers since 1996 | Physical absorption with Rectisol in gas cleanup train | € 350 M |
| Weyburn (Canada) | EnCana and IEA | Capture in the Great Plains synfuels plant in Beulah, ND, USA, transport by 325 km pipeline, injection of 7 Mt of $CO_2$ from 2000 to 2004, currently investigation of long-term sequestration suitability | Physical absorption with Rectisol, use of $CO_2$ for EOR | pipeline cost: US$ 100 M |
| In Salah (Algeria) | Sonatrach, BP, Statoil | Injection of 1 Mt/yr of $CO_2$ from natural gas production to a total 17 Mt into depleted gas reservoirs since 2004 | Chemical absorption with aMDEA | US$ 1700 M |
| K12B (Netherlands) | Gaz de France | Injection of $CO_2$ from natural gas production into the original gas reservoir (1 - 1.5 Billion $m^3$) since 2004 | Chemical absorption with aMDEA, use of $CO_2$ for EGR | n/a |
| Snøhvit (Norway) | Statoil | Injection of $CO_2$ from natural gas production beneath seabed since 2008, planned: 0.7 Mt/yr | n/a | total: $US 5200 M, injection: US$ 110 M |
| La Barge (Wyoming) | ExxonMobil | Injection of 4 Mt/yr of $CO_2$ from natural gas production into depleted gas reservoirs | Two-train physical acid gas removal with Selexol | n/a |
| Ketzin ($CO_2$SINK) (Germany) | GFZ Potsdam | Storage of $CO_2$ in saline aquifers since 2008, planned: 60 kt over 2 years | $CO_2$ from industrial gas supplier | € 15 M |
| Schwarze Pumpe (Germany) | Vattenfall | Capture of up to 100 kt $CO_2$ from 30 MW coal-fired power plant since 2008, storage in depleted gas field planned | Oxyfuel, 98% $CO_2$ purity | € 70 M |

# 2. Pre-combustion capture

Pre-combustion $CO_2$ capture is the separation of $CO_2$ from the fossil fuel before combustion. For an efficient capture, the fossil fuel is first converted into $CO_2$ and hydrogen gas. For natural gas, the conversion of the fuel into synthesis gas is achieved in a traditional steam reformer. Then, the carbon monoxide in the syngas reacts with steam and forms $CO_2$, as all remaining carbon monoxide is later burned to $CO_2$. As for coal used in an Internal Gasification Combined Cycle (IGCC), after gasification it is converted into $CO_2$ and $H_2$ in a water-gas-shift reaction.

## 2.1. Comparison of pre-combustion capture techniques

Either by membrane processes or in an absorption section, the $CO_2$ is separated from the converted hydrogen rich syngas stream, which is then mixed with air and burned in the combustion chamber of a gas turbine. The captured carbon dioxide is compressed and liquefied for transport and storage.

Pre-combustion capture allows for the removal of about 90% of the $CO_2$ from a power plant. However, this technology requires significant modifications of the power plant and is thus only viable for new plants. The investment costs for an IGCC with $CO_2$ capture is about twice as high as for a similar plant using post-combustion capture [22] as discussed in the next chapter.

Capture costs may be reduced in the future through improved gasification technology and through improved performance of the capture process. Highly selective membranes and ionic liquid membranes for this purpose are at the laboratory stage of development [23, 24, 25]. Furthermore, power plant efficiency may be improved by the integration of power fuel cells (SOFC) that use the $H_2$-rich syngas [26]. If economically feasible, part of the produced hydrogen can also be stored and sold as fuel.

Even though large-scale demonstration plants exist, highly efficient hydrogen turbines, which are optimised for CCS, are still under development [27, 28].

In case of IGCC, apart from $CO_2$, the acid gas component $H_2S$ also has to be removed to prevent formation of $SO_2$ in the combustion process, which would then be released with the flue gas stream. For acid gas removal by absorption, the available solvents can be divided in three groups. In physical solvents such as Selexol or methanol, absorption occurs according to Henry's law, so that the solubility of an acid gas in physical solvents increases linearly with its partial pressure [29]. In chemical solvents, such as monoethanolamine, the acid gas reacts chemically with the solvent. More infor-

mation can be found in the chapter on post-combustion capture. The third group, the mixed solvents, such as sterically hindered amine (MDEA) shows both types of capture, physical and chemical [30].

Physical solvents, such as Rectisol or Selexol, are favoured by a high partial pressure of the acid gas in the syngas and can be regenerated with lower energy consumption. This is due to the fact that usually the bulk of the regeneration duty is done by a simple flashing (pressure reduction). Chemical solvents have higher absorption capacity at relatively low acid gas partial pressures. However, their absorption capacities plateau at higher partial pressures as shown in Figure 13. Chemical solvents also require a significant amount of energy, usually in the form of LP steam for regeneration, because the chemical link between the acid gases and the solvent must be broken. The mixed solvents display a performance that is a compromise between the first two categories.
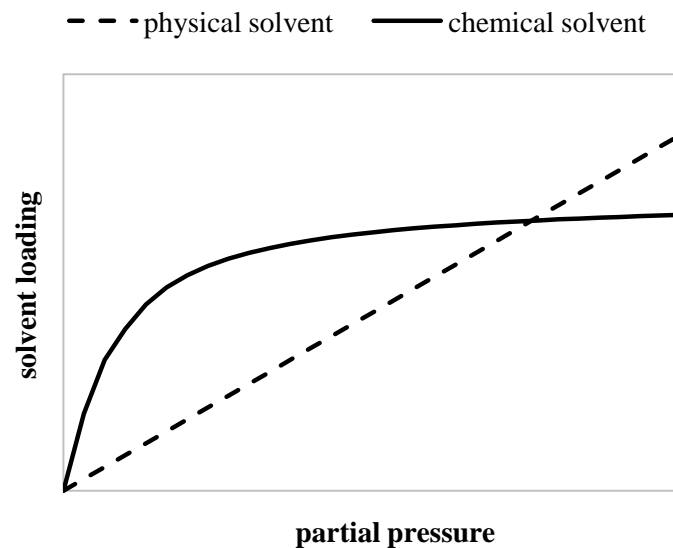


**Figure 13.** Characteristics for physical and chemical solvents [31].

Since the syngas from a gasification process usually is under pressure, physical solvents are attractive. Physical solvents also generally display a better selectivity than chemical solvents, which would permit to separately capture $H_2S$. This separation permits to convert $H_2S$ to sulphur (Claus process) and to obtain a pure $CO_2$ by-product. The same applies also for mixed solvents and hindered amines such as MDEA. However, a separate acid gas removal of $H_2S$ and $CO_2$ requires higher capital and operating costs than their combined removal [32] due to the sulphur recovery in a Claus process and tail gas treatment.

On the other hand, the combined removal produces a $CO_2$ by-product, which is contaminated with $H_2S$. Therefore, it has to be decided whether or not it would be acceptable and advantageous to transport and store the combined acid gas stream. Transporting and storing $CO_2$ containing significant concentrations of $H_2S$ and $CO_2$ may be expensive, and these extra costs may be greater than the reductions in capture costs. Other hurdles may be posed by regulations and permits for the combined stor-

age. However, $H_2S$ can be advantageous for $CO_2$ enhanced oil recovery, since it improves the misci-bility of $CO_2$. This would also depend on the nature of the oilfield. At the Weyburn field in Canada, $CO_2$ with about 2% $H_2S$ and other sulphur compounds is used for EOR [30].

Other than solely for power production, the hydrogen-rich syngas, from which the $CO_2$ has been removed, can be used partially or entirely for the production of fuel hydrogen, ammonia, and for Fischer-Tropsch liquids with a high H:C ratio, where the excess carbon is then made available for storage [33]. However, this technology will not be discussed in this work.
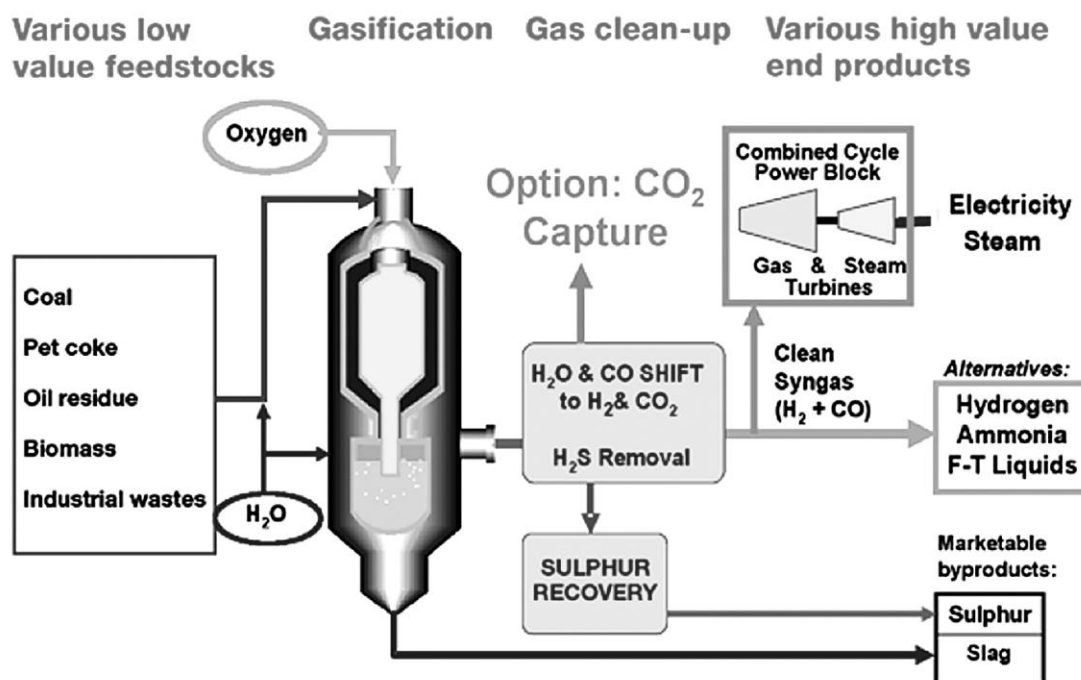


**Figure 14.** Schematics of IGCC with $CO_2$ capture, electricity generation, and by-products [12].

IGCC plants, as shown in Figure 14, are generally considered more costly than comparable pulverised coal (PC) power plants, if no $CO_2$ capture is applied. However, due to the reduced energy penalty they are considered less costly, if $CO_2$ capture is applied [12].

In this chapter, the performance of a chemical solvent, the tertiary amine MDEA, and the per-formance of a physical solvent Selexol is investigated and their influence on power plant performance compared. For a detailed analysis, the IGCC and the capture processes were modelled in Aspen Plus with and without consideration of the kinetics of chemical bonding and of mass transfer.

## 2.2. Equilibrium pre-combustion capture models

In this section, the performance of acid gas removal with a sterically hindered amine, MDEA, is compared to syngas sweetening with a physical solvent (Selexol). MDEA requires a lower solvent circulation rate than physical solvents and the steam consumption for regeneration is lower than for a true chemical solvent such as MEA. In order to investigate the influence of pre-combustion capture on power plant performance and to obtain the compositions of the relevant gas streams, models for the IGCC have been developed as well.

### 2.2.1. IGCC model for equilibrium pre-combustion capture models

Most commercial IGCC are based on entrained-flow gasifiers. This type of gasifier is able to gasify all types of coal. Due to the very short residence time in the gasifier, the coal has to be mechanically pre-treated to a very finely divided and homogenous state. It can be fed either dry or in a coal slurry. Oxidant requirements are high, but temperature inside the gasifier is uniform and very high, leading to a large amount of sensible heat in the raw gas and a lower cold gas efficiency than in other types of gasifiers (moving-bed and fluidised bed) [29].

The modelled gasifier shown in Figure 15 is of the dry fed entrained type and gasifies a coal stream of 10 kg/s at 19.3 bar. The gasification section was modelled using the VLE model PR-BM, which is recommended for the simulation of coal gasification, liquefaction and combustion.
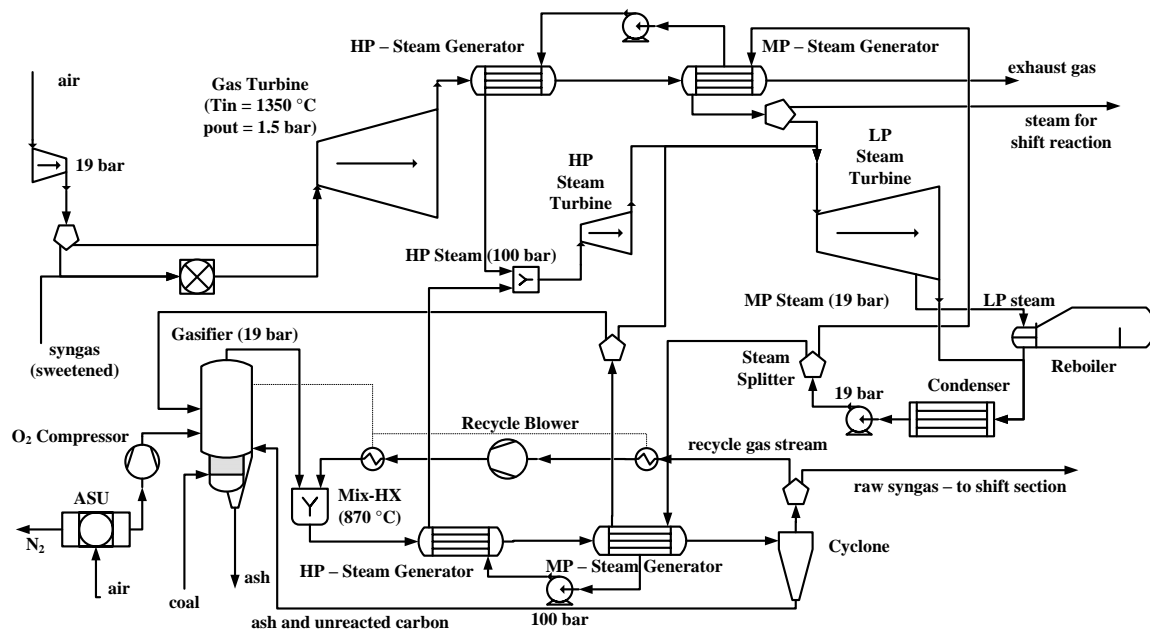


**Figure 15.** IGCC model for equilibrium pre-combustion capture simulations (after [34]).

The amount of oxygen inside the gasification reactor is limited so that only enough of the fuel is burned to provide the necessary heat for the chemical decomposition of the coal and to produce the syngas composed mainly of carbon monoxide and hydrogen. The LHV of the reference coal is 23.93 MJ/kg and its composition is presented in Table 6.

**Table 6.** Properties of coal used in IGCC for equilibrium pre-combustion capture models [34].

| Ultimate analysis | Dry basis %wt. | Proximate analysis | Dry basis %wt. | Sulfur analysis | Dry basis %wt. |
|---|---|---|---|---|---|
| Carbon | 69.5 | Moisture | 10 | Pyritic | 45.7 |
| Oxygen | 10 | Fixed Carbon (FC) | 60 | Sulfate | 8.86 |
| Nitrogen | 1.25 | Volatile Matter (VM) | 30 | Organic | 45.7 |
| Hydrogen | 5.3 | Ash | 10 | | |
| Sulphur | 3.95 | | | | |
| Chlorine | 0 | | | | |
| Ash | 10 | | | | |

The ash content and the moisture content were both set realistically to 10%. Based on the ultimate analysis, decomposition of the coal was modelled with an RYIELD reactor with the yields shown in Table 7.

**Table 7.** Component yields for pyrolysis in IGCC model for equilibrium pre-combustion capture.

| $H_2O$ | C | $H_2$ | $N_2$ | $Cl_2$ | S | $O_2$ | Ash |
|---|---|---|---|---|---|---|---|
| 0.1 | 0.6255 | 0.0477 | 0.01125 | 0 | 0.03555 | 0.09 | 0.09 |

The gasifier used 95 %mol pure oxygen (9.2 kg/s, i.e. equivalence ratio of 0.32) at ambient temperature and steam (0.75 kg/s) at 235 °C. For ash separation, the syngas is cooled down to 870 °C (below ash melting temperature) by recirculation. After a steam generation section, a cyclone removes all remaining ash as well as 95% of the unreacted carbon, which are both redirected to the gasifier.

Several chemical reactions occur in a gasifier, the two main series being pyrolysis and gasification. For the presented model, the main reactions are:

$$C \quad + 0.5\,O_2 \quad \leftrightarrow \quad CO \qquad\qquad \text{(Partial combustion)} \qquad\qquad (1)$$

$$C \quad + CO_2 \quad \leftrightarrow \quad 2\,CO \qquad\qquad \text{(Boudouard reaction)} \qquad\qquad (2)$$

$$C \quad + 2\,H_2 \quad \leftrightarrow \quad CH_4 \qquad\qquad \text{(Hydrogasification)} \qquad\qquad (3)$$

$$C \quad + H_2O \quad \leftrightarrow \quad CO \quad + H_2 \qquad \text{(Water gas reaction)} \qquad\qquad (4)$$

$$CO \quad + H_2O \quad \leftrightarrow \quad CO_2 \quad + H_2 \qquad \text{(Shift reaction)} \qquad\qquad (5)$$

$$CO \quad + 3\,H_2 \quad \leftrightarrow \quad CH_4 \quad + H_2O \quad \text{(Methanation)} \qquad\qquad (6)$$
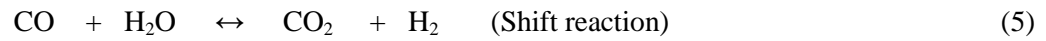
In some regions of the gasifier with excess oxygen, combustion may also take place:

$$C \quad + O_2 \quad \leftrightarrow \quad CO_2 \qquad\qquad \text{(Combustion)} \qquad\qquad (7)$$
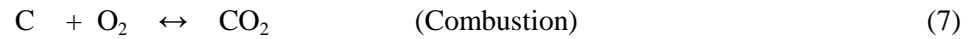
The sulphur and nitrogen contents of the coal are mainly released as hydrogen sulphide ($H_2S$), elemental nitrogen and ammonia ($NH_3$).

An RGIBBS reactor block with a restricted equilibrium approach was chosen, so chemical equilibrium was achieved by minimising Gibbs free energy for the above reactions. Of the coal, 5 % were realistically assumed to remain unreacted. Heat from this reactor as well as from the recycled gas stream in the HRSG section is used to provide the necessary energy for coal pyrolysis. The key input parameters for modelling the gasification section are shown in Table 8.

**Table 8.** IGCC operation parameters [34].

| | |
|---|---|
| Gasification temperature in °C | 1400 |
| Gasification pressure in bar | 19.3 |
| Combustion temperature in °C | 1350 |
| Coal flow rate in kg/s | 10 |
| Oxygen/Coal mass ratio | 0.9 |
| Steam/Coal mass ratio | 0.075 |
| Steam pressure levels in bar | 100, 19 |
| HP steam turbine inlet temperature in °C | 675 |

A very important part for $CO_2$ capture in an IGCC plant is the water-gas shift (WGS) section. Here, according to Reaction (5) almost the entire CO content of the raw gas is converted with steam to $CO_2$, which would otherwise be produced in the combustion turbine and leave the power plant without treatment. Equilibrium is favoured by high steam-to-CO ratios and low reaction temperatures due to the exothermic nature of the reaction. The shift reaction occurs in the presence of a catalyst and

reaction kinetics is favoured by a higher reaction temperature. Therefore, CO conversion in the shift reactors is determined by the exit temperature of the shift reactors as shown in Figure 16. A higher steam-to-CO ratio as a means to improve CO conversion leads to higher capital and operational costs, since the steam has to be supplied by water addition or by upstream steam extraction. The temperature rise in one shift reactor is limiting the conversion percentage. This limitation can be overcome by a two stage water-gas-shift reactor. After a first high-temperature shift reaction the gas stream is cooled down and further conversion is achieved in a low-temperature shift reactor.

There are two groups of catalysts used for the water-gas-shift reaction. For the so-called clean shift catalysts, which are mainly Cu or Fe-based, all sulphur compounds such as $H_2S$ and COS have to be removed from the gas stream prior to entering the shift reactors. These catalysts are poisoned and hence deactivated by the sulphur components. Although equilibrium is favoured by low temperatures, condensation of gas components would weaken the clean catalysts and has to be prevented. Sulphur tolerant so-called sour shift catalysts are generally cobalt-based and need sulphur in the gas stream to remain in activated state.

In the IGCC model used here, sour shift catalysts were applied, making expensive sulphur removal unnecessary. In this case, the sulphur components are then removed in the capture section after the WGS reactors.
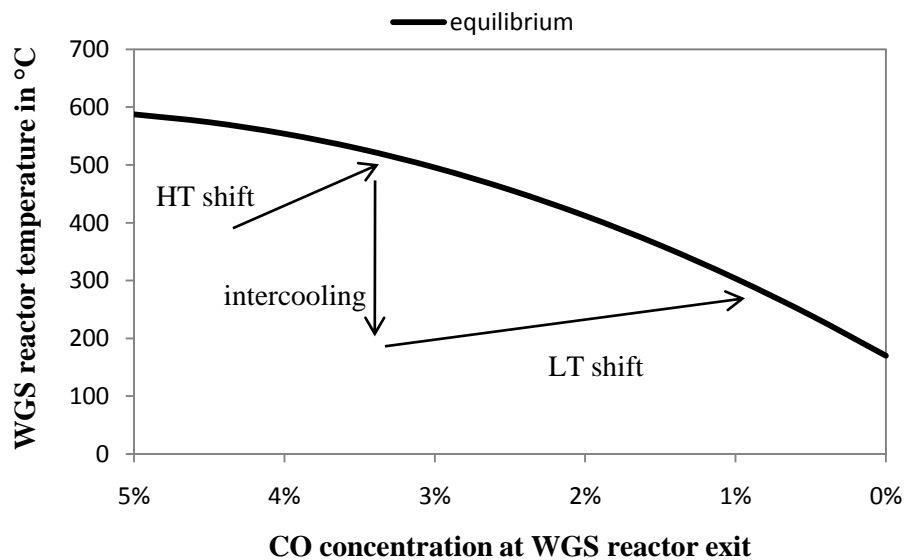


**Figure 16.** Influence of WGS reactor temperature on CO concentration in shifted syngas [31].

Before entering the first reactor, the syngas is heated up to 230 °C in a regenerative heat exchanger by the syngas leaving the second shift reactor. In the model, the first shift reactor, where most of the CO is converted, is held at 450 °C and the second reactor at 250 °C. In total, 94% of the CO is converted here. Of course, the better syngas quality - $H_2$ will be burnt to $H_2O$ without emission of greenhouse gas - is paid in terms of heating value (from 8860 kJ/kg to 6673 kJ/kg). The heat lost in

the exothermic shift reaction (-41097.871 kJ/kmol) has to be recovered in the form of steam generation in order to minimise its overall impact on the performance of the power plant. This steam (235 °C, 19.3 bar) is introduced into the shift reactor, leading to savings of 6 kg/s of extracted steam from the low pressure steam turbine. Simulations for this section were carried out with the VLE Model NRTL-RK (Non-Random Two Liquid model for the activity coefficient and Redlich-Kwong equation of state for the vapour fugacity coefficient).

In the combined cycle, the gaseous stream leaving the $CO_2$ absorption column is fed to the combustion chamber of a gas turbine. In this case, the maximum inlet temperature of the gas turbine was 1350 °C. The inlet conditions (amount of air, total gas flow) remained basically the same for all configurations of $CO_2$ removal, as almost exclusively $CO_2$ was removed, which has no effect on the product of syngas flow and heating value.

The combustion gas expands through the gas turbine from 19 bar down to 1.5 bar due to the expected pressure drop in the heat recovery steam generator, where around 56% of the total steam production (50 kg/s) takes place. The prerequisite condition is that the gas stream at the outlet still has higher than atmospheric pressure and possesses a higher temperature than 102 °C in order to prevent condensation.

The steam generated in the gasifier and in the heat recovery steam generator consists to 60% of high pressure steam, which expands through the high pressure steam turbine from 100 bar to 19 bar. After this steam turbine around 6 kg/s of steam are sent to the shift reactors and 0.75 kg/s to the gasifier. The rest is mixed with the medium pressure steam and expanded through the low pressure steam turbine with optional steam extraction for thermal solvent regeneration.

### 2.2.2.  Pre-combustion capture model with Selexol

The solvent Selexol is a mixture of dimethyl ethers of polyethylene glycol with the formula $CH_3(CH_2CH_2O)_nCH_3$, where n is in the range between 3 and 9 [35]. In this model, n = 5.3, leading to a molecular mass of 280 kg/kmol. The general properties of this solvent are given in Table 9.

**Table 9.** Properties of Selexol at T = 25 °C [29].

| | |
|---|---:|
| Molecular weight in kg/kmol | 280 |
| Density in kg/m$^3$ | 1030 |
| Vapour pressure in mmHg | 0.00073 |
| Viscosity in cp | 5.8 |
| Freezing point in °C | -28 °C |
| Maximum operating temperature in °C | 175 |

Higher partial pressure leads to a higher solubility in physical solvents of all components of the syngas stream, but Selexol shows a favourable solubility for the acid gases versus other light gases. For instance, $CO_2$ is 75 times more soluble than $H_2$ and 35 times more soluble than CO, and $H_2S$ is 670 times more soluble than $H_2$ in Selexol. These solubilities were incorporated in the capture simulation [36].

The Selexol solvent can either be regenerated thermally or by flashing the solvent stream. Due to lower energy requirements, depressurisation was chosen here despite the necessary recompression of the released acid gas stream. Beyond showing a high solubility for acid gases and the possibility for regeneration by simple depressurisation, Selexol shows other important advantages [37]. The extremely low vapour pressure of Selexol leads to negligible losses with the treated gas stream, and its low viscosity leads to very low pressure losses in the system. Selexol is thermally and chemically very stable. As a true physical solvent, it does not react with the absorbed gases, which could lead to the accumulation of reaction products in the solvent stream. It is non-toxic and non-corrosive, allowing for the use of carbon steel for the capture equipment. Operational stability is guaranteed, since the solvent does not show foaming. Additional advantages are the high solubility for HCN and $NH_3$, which can thus be removed without solvent degradation, and for nickel and iron carbyls, which could damage the blades of downstream steam turbines [29].
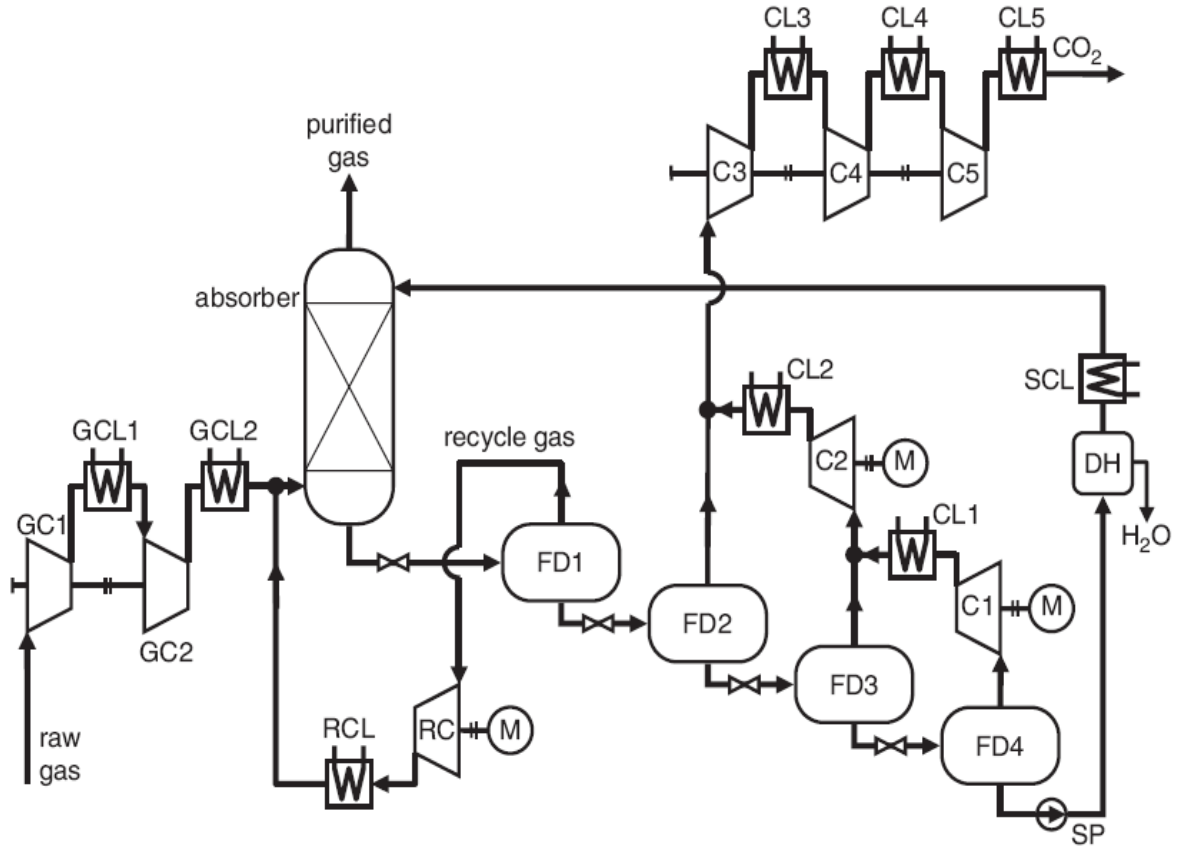
**Figure 17.** Schematics of physical absorption process with Selexol [38].

In the modelling of this physical absorption process the necessary solvent flow rate $m_{solv}$ was calculated using the temperature-dependent absorption factor AF [39]. This coefficient relates the Selexol solvent flow rate, the $CO_2$ partial pressure in the syngas stream, and the amount of $CO_2$ to be removed (which results from the assumed $CO_2$ removal efficiency).

At 25 °C, the solvent equilibrium coefficient is

$$AF(T = 25 \text{ °C}) = \frac{p_{CO_2}}{\left(\dfrac{n_{CO_2}}{m_{solvent}}\right)} = 6447.5 \frac{\text{bar}}{\left(\dfrac{\text{kmol}_{CO_2}}{\text{kg}_{solvent}}\right)} \tag{8}$$

For temperatures different from 25 °C, the equilibrium coefficient has to be corrected according to the following expression:

$$AF(T) = \frac{AF(T = 25 \text{ °C})}{9.433 \cdot T^{-0.6972}} \tag{9}$$

The $CO_2$-rich solvent is depressurised after the absorber to a pressure slightly lower than the solvent equilibrium pressure in order to release the absorbed CO and $H_2$ in a flash drum. Since also part of the captured $CO_2$ gets released, the gas leaving the flash drum gets repressurised and cooled, after which it enters the absorber again together with the syngas from the shift section. Recycle gas flow rate and composition strongly depend on the pressure in the first drum. The solvent gets nearly completely stripped of the absorbed $CO_2$ by further depressurisation in additional flash drums (at 4 bar, 2 bar and 1 bar). From there the released $CO_2$ is sent to an intercooled compressor for liquefaction and transport. The lean solvent is then recycled and cooled down to the desired absorber temperature again. At T = 30 °C and an absorber pressure of 18 bar the following linear relationship between solvent mass flow and removed $CO_2$ was found to be valid for solvent flows of 500 kg/s to 700 kg/s:
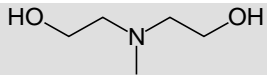
$$m_{CO2,rem} = 0.029 \cdot m_{solv} - 0.159 \tag{10}$$

This means that the necessary solvent flow for 90% $CO_2$ capture was 660 kg/s. For $H_2S$, a capture rate of 99.9% resulted. The solubilities and the necessary solvent mass flow were calculated in FORTRAN calculator blocks, which determined the component flows leaving the top and the bottom of the absorber and the flash drums. In order to be able to control these flows with the calculator blocks, the above mentioned system components were modelled with SEP2 columns.

### 2.2.3. Simulations of pre-combustion co-capture with MDEA

MDEA is a so called hindered tertiary amine. This means that $CO_2$ first has to dissolve into the solvent before it reacts with it [40]. The high syngas pressure facilitates this dissolution, however, so that in the case of pre-combustion capture, MDEA is a feasible option [41]. Being a chemical solvent, MDEA requires a significant amount of energy in the form of heat for its regeneration in order to break the chemical bonds with the captured $CO_2$. Usually steam is extracted from the steam turbine system to supply this heat. Due to their weaker chemical links, however, the energy requirements for tertiary amines are lower than for the regeneration of primary amines such as MEA. Generally, chemical solvents require less solvent circulation and thus less plant investment costs than physical solvents. As a compromise between necessary investment costs and high energy penalty, MDEA is also often applied in a mixed solvent processes, such as the Sulfinol process by Shell [42]. The molecular structure and other parameters of MDEA are shown in Table 10.

**Table 10.** Properties of MDEA at T = 20 °C [29, 43].

| | |
|---|---|
| Molecular structure | HO—N—OH |
| Molecular formula | $CH_3N(C_2H_4OH)_2$ |
| Molecular weight in kg/kmol | 119.163 |
| Density in kg/m$^3$ | 1043 |
| Vapour pressure in mmHg | < 0.01 |
| Viscosity in cp | 101 |
| Freezing point in °C | -21 °C |
| Boiling point in °C | 247 |

Due to the presence of ionic species, the electrolyte NRTL activity coefficient model is used for the liquid phase and the Redlich-Kwong equation of state for the vapour phase. The phase equilibrium model was regressed to VLE data from Jou *et al.* [44, 45, 46].

$H_2S$ and $CO_2$ in aqueous solutions react in an acid-base buffer mechanism with alkanolamines. These equilibrium reactions can be written as chemical dissociation:

$$2\,H_2O \quad\quad\quad\quad \leftrightarrow\; H_3O^+ \;+ OH^- \quad \text{(ionisation of water)} \quad\quad\quad\quad (11)$$

$$H_2O \;+ H_2S \quad \leftrightarrow\; HS^- \quad + H_3O^+ \;\; \text{(dissociation of hydrogen sulfide)} \quad (12)$$

$$H_2O \;+ HS^- \quad \leftrightarrow\; S^{-2} \quad + H_3O^+ \;\; \text{(dissociation of bisulfide)} \quad\quad\quad (13)$$

$$2\,H_2O \;+ CO_2 \quad \leftrightarrow\; HCO_3^- \;+ H_3O^+ \;\; \text{(dissociation of carbon dioxide)} \quad (14)$$

$$H_2O \;+ HCO_3^- \leftrightarrow\; CO_3^{-2} \;+ H_3O^+ \;\; \text{(dissociation of carbon dioxide)} \quad (15)$$
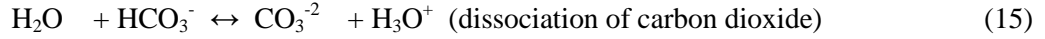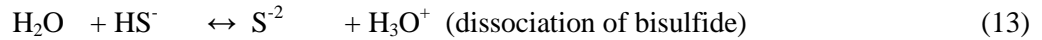
Maximum loading (moles of $CO_2$ per mole of amine in solution) achieved with MDEA in commercial absorbers is always less than 1 to avoid corrosion [47]. The recommended maximum loading in carbon steel equipment is 0.7 to 0.8 [48]. Table 11 and Table 12 show the reactions included in the KEMDEA data package [43] for the simulation of acid gas removal with MDEA.

**Table 11.** Equilibrium constants for absorption reactions with MDEA [43].

| Reaction | | A | B | C | D | |
|---|---|---|---|---|---|---|
| $2\,H_2O \;\leftrightarrow\; H_3O^+ + OH^-$ | | 132.899 | -1345.9 | -22.4773 | | (11) |
| $H_2O + H_2S \;\leftrightarrow\; HS^- + H_3O^+$ | | 214.582 | -12995.4 | -33.5471 | | (12) |
| $H_2O + HS^- \;\leftrightarrow\; S^{-2} + H_3O^+$ | | -9.742 | -8585.47 | | | (13) |
| $CO_2 + 2\,H_2O \;\leftrightarrow\; H_3O^+ + HCO_3^-$ | | 231.465 | -12092.1 | -36.7816 | | (14) |
| $HCO_3^- + H_2O \;\leftrightarrow\; H_3O^+ + CO_3^{-2}$ | | 216.049 | -12431.7 | -35.4819 | | (15) |
| $MDEAH^+ + H_2O \;\leftrightarrow\; MDEA + H_3O^+$ | | -9.4165 | -4234.98 | | | (16) |

$$\ln K(T) = A + B/T + C\cdot\ln(T) + D\cdot T, \quad T \text{ in Kelvin}$$

Tertiary amines such as MDEA and hindered amines can associate with $H^+$ to form $MDEAH^+$ as shown in Reaction (16), but they cannot react with $CO_2$ to form stable carbamates. Thus, the following rate-based reactions are included in this equilibrium type absorber model using a holdup correlation.

**Table 12.** Rate constants for kinetic reactions [43].

| Reaction | k | E | |
|---|---|---|---|
| $CO_2 + OH^- \rightarrow HCO_3^-$ | $4.3152\cdot10^{13}$ | 13249.00 cal/mol | (17a) |
| $HCO_3^- \rightarrow CO_2 + OH^-$ | $3.7486\cdot10^{14}$ | 25271.56 cal/mol | (17b) |

$$r = k\cdot T^n \cdot \exp\left(-\frac{E}{RT}\right)\cdot\prod_{i=1}^{N}\text{molarity}_i^{a_i}, \quad T \text{ in Kelvin}$$

For the uptake of the acid gas components in water the data for the Henry constants, which are regressed against solubility data from Jou *et al.*, are given in Table 13.

**Table 13.** Henry constants of acid gas components in water [43].

| i | j | $a_{ij}$ | $b_{ij}$ | $c_{ij}$ | $d_{ij}$ | $T_{lower}$ in K | $T_{upper}$ in K | |
|---|---|---------|---------|---------|---------|----------------|----------------|---|
| $CO_2$ | $H_2O$ | 170.7126 | -8477.711 | -21.9574 | 0.005781 | 273 | 500 | (18) |
| $H_2S$ | $H_2O$ | 358.138 | -13236.8 | -55.0551 | 0.059565 | 273 | 423 | (19) |

$$\ln H_{ij} = A + B/T + C \cdot \ln(T) + D \cdot T, \text{ T in Kelvin, } H_{ij} \text{ in N/m}^2$$

The basic configuration used for the simulations consists of a 6 stage absorber column (height 8 m, diameter 3.75 m) and a two-stage desorber column (height 4 m, diameter 4.95 m), both equipped with sieve trays.

In the simulations solutions of 50 %wt. MDEA were used. At atmospheric pressure, MDEA is easily regenerated to a near 100% at a temperature of around 103 °C, so that further heating has no effect on $CO_2$ capture performance. Keeping the reboiler temperature at 102 °C and elevating the solvent flow from 100 kg/s to 170 kg/s, reaching 97.8% removal efficiency, the amount of captured $CO_2$ increased with 0.109 kg per kg of solvent. Maintaining the stripper temperature requires 300 kW for every kg of solvent added. Since a higher solvent flow has a strong effect on equipment size and cost and also requires more heating to reach a given reboiler temperature, a balance between solvent flow and reboiler duty has to be found in order to achieve the desired capture efficiency.

The concentrations of absorbed carbon dioxide and hydrogen sulfide in the liquid phase along the absorber are shown in Figure 18 for the rich solvent loading of 0.8.
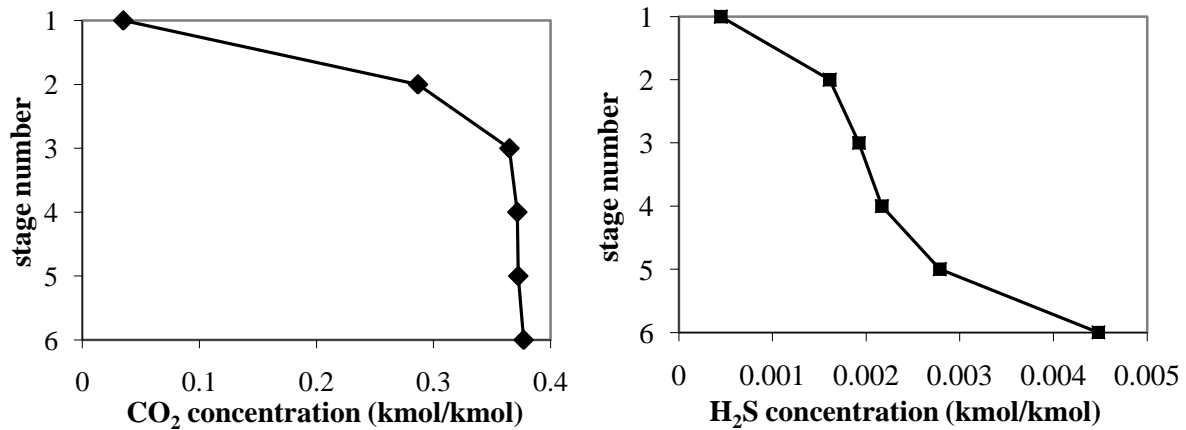


**Figure 18.** Acid gas concentrations in absorber with MDEA at a rich loading of 0.8.

As can be seen, in the equilibrium model $CO_2$ was absorbed almost up to maximum loading in the first two stages of the absorber. Thereafter, almost no change was observed. $H_2S$ got continuously absorbed along the absorber.

The desorber, or stripper, is equipped with a heat exchanger in the kettle reboiler, which is provided with energy by steam extraction from the low pressure steam turbine. A combination of de-pressurisation and thermal solvent regeneration was used for the release of the captured $CO_2$ from the solvent. Figure 19 shows the dependence of removal efficiency on reboiler duty. With a solvent flow of 153.6 kg/s and a reboiler duty of 51 MW, a $CO_2$ capture efficiency of 90% was achieved.
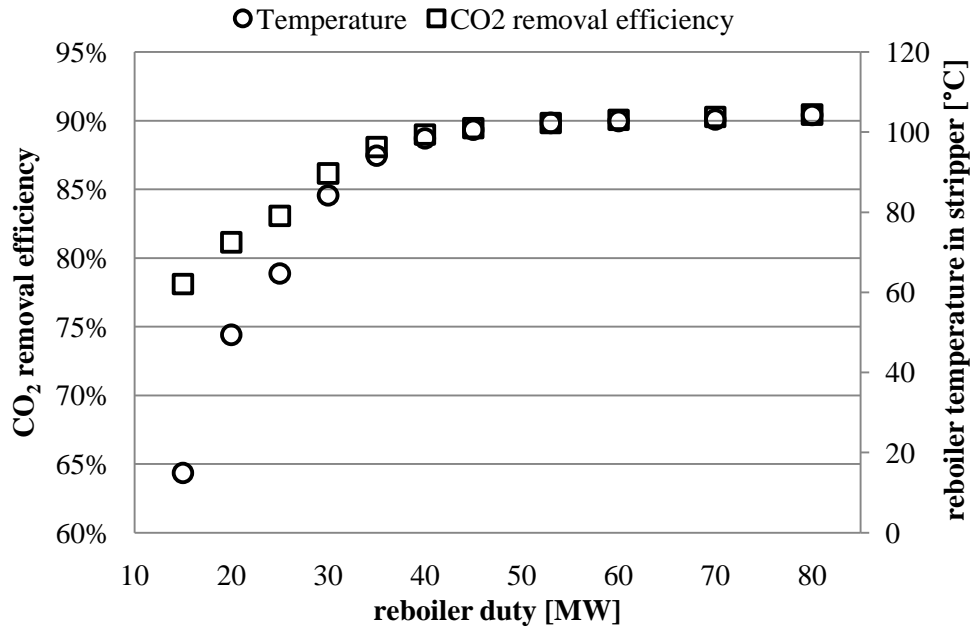


**Figure 19.** Desorption behaviour of MDEA.

The separated gases leaving the stripper are sent to a condenser, from where water and traces of amines are recirculated. The $CO_2$ is then liquified in a multistage compression unit with intercooling and condensation.

Whereas the reaction rates with $CO_2$ are slow with respect to mass transfer, the reaction with $H_2S$ is almost instantaneous. Therefore a kinetic selectivity for $H_2S$ exists. Both this effect as well as the influence of kinetics of the absorption of $CO_2$ have to be studied with a rate based absorber model. MDEA can also be used in combination with activating substances such as Piperazine or in a mixture with a primary amine to overcome the disadvantage of its very slow kinetics for $CO_2$ absorption [49].

### 2.2.4. Influence of pre-combustion capture on IGCC performance

For the calculation of the overall process efficiency, the influence of water-gas-shift reaction and acid gas capture on the heating value of the fuel gas streams for the combustion turbine are of great importance. The compositions and heating values of the key streams as obtained from the IGCC model are listed in Table 14.

**Table 14.** Compositions and heating values of gas streams in IGCC with acid gas capture.

| | Raw syngas | Shifted syngas | MDEA | | Selexol | |
|---|---|---|---|---|---|---|
| | | | Sweet gas | $CO_2$ stream | Sweet gas | $CO_2$ stream |
| Temperature in °C | 141 | 30 | 78.4 | 25 | 29.6 | 25 |
| Pressure in bar | 19 | 19 | 19 | 110 | 18 | 110 |
| Mass Flow in kg/s | 18.65 | 24.234 | 4.673 | 19.398 | 3.961 | 20.209 |
| LHV in MJ/kg | 9.8 | 6.8 | 35.2 | -- | 39.4 | -- |
| Enthalpy flow in MW | 182.1 | 164.8 | 164.6 | -- | 156.0 | -- |
| Mole fractions | | | | | | |
| $H_2O$ | 0.111 | 0.003 | 0.020 | -- | 10 ppm | -- |
| $CO_2$ | 0.072 | 0.420 | 0.067 | 0.976 | 0.071 | 0.938 |
| $N_2$ | 0.004 | 0.003 | 0.005 | -- | 0.005 | 37 ppm |
| CO | 0.449 | 0.024 | 0.038 | -- | 0.022 | 0.027 |
| $H_2S$ | 0.011 | 0.009 | 0.001 | 0.024 | 1 ppm | 0.022 |
| $H_2$ | 0.213 | 0.541 | 0.868 | -- | 0.902 | 0.013 |

The outlet stream from the low pressure steam turbine is directed through the kettle reboiler of the stripper, where it condenses and heats the solvent. The outlet pressure of the steam turbine depends on the heat duty requirement of the reboiler and the allowed minimum temperature difference there. At an assumed minimum temperature difference of 13 °C, the outlet pressure was 1.8 bar for the stripping of 153.6 kg/s loaded MDEA solution.

In Table 15, the cycle and the removal efficiencies of the different removal options are compared to direct firing of the gasified coal stream without capture. Here, steam extractions for shift section, reboiler duty, and power consumption for $CO_2$ compression and for driving the gas and solvent streams inside the absorption units are included. All compressors have an isentropic efficiency of 86%, while turbines have an isentropic efficiency of 90%.

**Table 15.** Parameters for IGCC with capture of $CO_2$ and $H_2S$.

|  | No capture | MDEA | Selexol |
|---|---|---|---|
| GT cycle net power output in $MW_{el}$ | 53.9 | 50.0 | 48.1 |
| Reboiler duty in $MW_{th}$ | -- | 51 | -- |
| ST cycle net power output in $MW_{el}$ | 64.7 | 47.0 | 56.4 |
| ASU in $MW_{el}$ | 28.7 | 28.7 | 28.7 |
| Capture efficiency for $CO_2$ and $H_2S$ | -- | 89.8%, 95.9% | 90.0%, 99.9% |
| $CO_2$ compression in $MW_{el}$ | -- | 6.6 | 5.1 |
| Work in capture section in $MW_{el}$ | -- | 1.0 | 3.8 |
| Power plant net output in $MW_{el}$ | 89.9 | 60.7 | 66.9 |
| Power plant efficiency (LHV-based) | 37.6% | 25.3% | 28.0% |
| Energy penalty for $CO_2$ capture in $MW_{el}$ | -- | 29.2 | 23 |
| Specific energy penalty in $GJ_{el}/t$ | -- | 1.51 | 1.18 |
| Specific $CO_2$ production in kg/MWh | 880.78 | 203.96 | 153.09 |
| Effective $CO_2$ removal | - | 76.8% | 82.6% |

The shift conversion leads to a decrease in available heating value of the syngas, which is burned in the gas turbine for all cases with $CO_2$ removal. Physical absorption in the case of pre-combustion capture yields a lower capture penalty. The IGCC with $CO_2$ removal shows a significant drop in power plant efficiency by about 25.6% in the case of physical absorption and by 32.5% when chemical absorption is used. The final calculated $CO_2$ removal efficiency on the basis of an equal power output, in the case with $CO_2$ removal as compared to the case without removal, is about 83% for physical absorption and 77% for chemical absorption.

It should be mentioned that the assumption of equilibrium for the absorption processes is not fully justified because the absorption process is kinetically controlled. Therefore, rate-based models for this process have been developed for acid gas removal from the IGCC. Increasing the gasification pressure was expected to favour physical absorption. Thus, chemical absorption for pre-combustion capture was not investigated further.

## 2.3. Rate-based pre-combustion capture models

In order to achieve more realistic results for capture performance and equipment size, the kinetics of absorption has to be taken into account. This is done in the following. The acid gas components are removed from the shifted syngas by physical absorption with Selexol. One configuration captures $H_2S$ and $CO_2$ separately, while the other one is used for co-capture of these gases.

### 2.3.1. IGCC for rate-based pre-combustion capture models

A 500 MW Internal Gasification Combined Cycle power plant with four pressure levels in the steam cycle was the basis for this study on pre-combustion $CO_2$ capture [50]. The plant uses an air separation unit to provide oxygen for the slurry-fed Texaco gasifier. As recommended for combustion processes, all blocks in this section were modelled using the Peng-Robinson equation of state.
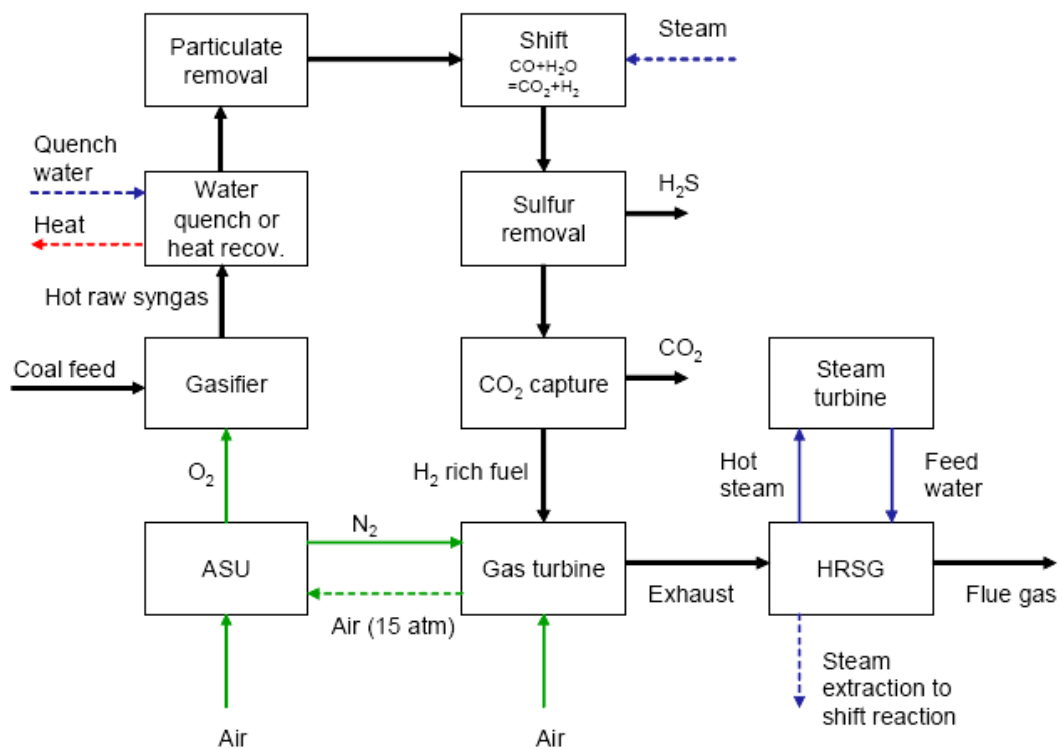


**Figure 20.** Process flowsheet of IGCC with acid gas removal [50].

The cryogenic air separation unit is modelled with RADFRAC column blocks, which are used in Aspen Plus for the calculation of chemical equilibrium processes. 165.9 kg/s air are separated into a nitrogen stream with a purity of 99.83 %mol and an oxygen stream of 38.4 kg/s with a purity of 95 %mol.

After mixing the coal feed (43.7 kg/s) with water (23.5 kg/s), the coal is crushed and screened, resulting in the coal slurry with 80% of the coal particles being smaller than 120 mu. This slurry with a total moisture content of 44.8% is then led to the gasifier together with the oxygen stream. The coal parameters are shown in Table 16.

**Table 16.** Properties of coal used in IGCC for rate-based pre-combustion capture models [50].

| Ultimate analysis | Dry basis %wt. | Proximate analysis | Dry basis %wt. | Sulfur analysis | Dry basis %wt. |
|---|---|---|---|---|---|
| Carbon | 74.455 | Moisture | 9.535 | Pyritic | 100 |
| Oxygen | 6.84 | Fixed Carbon (FC) | 50.909 | Sulfate | 0 |
| Nitrogen | 1.585 | Volatile Matter (VM) | 39.452 | Organic | 0 |
| Hydrogen | 4.955 | Ash | 9.639 | | |
| Sulphur | 2.44 | | | | |
| Chlorine | 0.065 | | | | |
| Ash | 9.66 | | | | |

Although gasification is a complicated chemical process, a simplified approach was chosen here. A fractional conversion approach inside an RSTOIC reactor block according to Reaction (20) was chosen for pyrolysis. This type of reactor model allows for the specification of the occurring reactions and of the conversion rate.

$$\text{Coal} \rightarrow C + O_2 + N_2 + H_2 + S + Cl_2 + Ash + H_2O \tag{20}$$

The stoichiometric coefficients for the conversion products are calculated in a FORTRAN calculator block based on the ultimate analysis. A conversion rate of 95% was assumed here. The decomposition results are shown in Table 17.

**Table 17.** Component yields for pyrolysis in IGCC model for rate-based pre-combustion capture.

| $H_2O$ | C | $H_2$ | $N_2$ | $Cl_2$ | S | $O_2$ | Ash |
|---|---|---|---|---|---|---|---|
| 0.00529 | 0.05608 | 0.02224 | 0.00051 | 8.29 ppm | 0.00069 | 0.00193 | 0.08739 |

The gasification reactions are not specified further. An equilibrium approach in an RGIBBS reactor block was chosen for this process. This approach considers all specified components as possible products and calculates equilibrium by minimisation of Gibbs free energy. The main parameters chosen for the IGCC are shown in Table 18. They agree well with realistic values.

**Table 18.** IGCC operation parameters.

| | |
|---|---|
| Gasification temperature in °C | 1455 |
| Gasification pressure in bar | 44 |
| Combustion temperature in °C | 1350 |
| Coal flow rate in kg/s | 34.7 |
| Oxygen/Coal mass ratio | 0.88 |
| Steam pressure levels in bar | 161.9, 40.6, 7.3, 3.1, 0.068 |
| HP steam turbine inlet temperature in °C | 563 |

After the gasification, impurities such as ash, unreacted coal, and nitrides are removed from the gas streams by a filter or cyclone, here modelled with a SEP block. This block allows for the specification of the solid components that leave the process. Denitrification was achieved by grey water wash (water and $NH_3$) in a FLASH2 block according to the following reactions:

**Table 19.** Equilibrium constants for grey water wash [50].

| Reaction | | | A | B | C | D | |
|---|---|---|---|---|---|---|---|
| $2\,H_2O$ | $\leftrightarrow$ | $H_3O^+ + OH^-$ | 132.899 | -1345.9 | -22.4773 | | (11) |
| $H_2O + H_2S$ | $\leftrightarrow$ | $HS^- + H_3O^+$ | 214.582 | -12995.4 | -33.5471 | | (12) |
| $H_2O + HS^-$ | $\leftrightarrow$ | $S^{-2} + H_3O^+$ | -9.742 | -8585.47 | | | (13) |
| $H_2O + NH_3$ | $\leftrightarrow$ | $NH_4^+ + OH^-$ | -1.257 | -3335.7 | 1.4971 | -0.0371 | (21) |
| $2\,H_2O + SO_2$ | $\leftrightarrow$ | $H_3O^+ + Cl^-$ | -5.979 | 637.396 | | -0.0151 | (22) |
| $H_2O + HSO_3^-$ | $\leftrightarrow$ | $H_3O^+ + SO_3^{-2}$ | -25.291 | 1333.4 | | | (23) |
| $2\,H_2O + CL_2$ | $\leftrightarrow$ | $H_3O^+ + Cl^- + HClO$ | -11.375 | -1286.972 | | | (24) |
| $H_2O + HClO$ | $\leftrightarrow$ | $H_3O^+ + ClO^-$ | -16.152 | -1602.87 | | | (25) |
| $NH_4Cl$ | $\xleftrightarrow{SALT}$ | $NH_4^+ + Cl^-$ | -141.676 | -880.103 | 27.7806 | -0.0632 | (26) |
| $(NH_4)_2SO_3$ | $\xleftrightarrow{SALT}$ | $2\,NH_4^+ + SO_3^{-2}$ | 920.378 | -44503.83 | -139.3449 | 0.0362 | (27) |
| $((NH_4)_2SO_3)_{aq}$ | $\xleftrightarrow{SALT}$ | $2\,NH_4^+ + SO_3^{-2} + H_2O$ | -1297.041 | 33465.89 | 224.2223 | -0.3516 | (28) |
| $NH_4HS$ | $\xleftrightarrow{SALT}$ | $NH_4^+ + HS^-$ | minimisation of Gibbs free energy | | | | (29) |
| $NH_4HSO_3$ | $\xleftrightarrow{SALT}$ | $NH_4^+ + HSO_3^-$ | minimisation of Gibbs free energy | | | | (30) |

$$\ln K(T) = A + B/T + C \cdot \ln(T) + D \cdot T, \quad T \text{ in Kelvin}$$

The pre-treated gas stream is then sent to COS hydrolysis, which is modelled with another RSTOIC reactor, showing a fractional conversion of 90% of the COS in the gas stream according to Reaction (31).

$$COS + H_2O \rightarrow CO_2 + H_2S \tag{31}$$
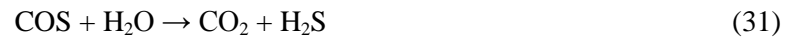
After passing the COS hydrolysis reactor, the gas stream enters the intercooled two-stage sour water-gas-shift section with reactor temperatures of 700 °C and 400 °C. With a necessary steam flow of 32.5 kg/s 98% of the CO content is converted.

Afterwards, $H_2S$ and $CO_2$ are removed in the capture section, while the remaining $H_2$-rich gas stream is burned in a gas turbine. The gas turbine exhaust gases are used to produce steam for electricity generation in steam turbines.

**2.3.2. Rate-based separate pre-combustion capture of $CO_2$ and $H_2S$ with Selexol**

In this study the author investigated two capture configurations with Selexol, either for simultaneous or for separate capture of $H_2S$ and $CO_2$. The first configuration captures $H_2S$ and $CO_2$ separately. For this purpose, the $H_2S$ absorber as presented in Figure 21 uses Selexol preloaded with $CO_2$ coming from the $CO_2$ absorber. In order to improve the selectivity of the $H_2S$ absorber, gas from the solvent regeneration of the $CO_2$ section is mixed to the cooled syngas stream coming from the water-gas-shift reactors. $H_2S$ is separated from the solvent stream in a stripper column. The energy for the solvent regeneration is provided by steam extraction from the combined cycle, reducing power plant efficiency [51].
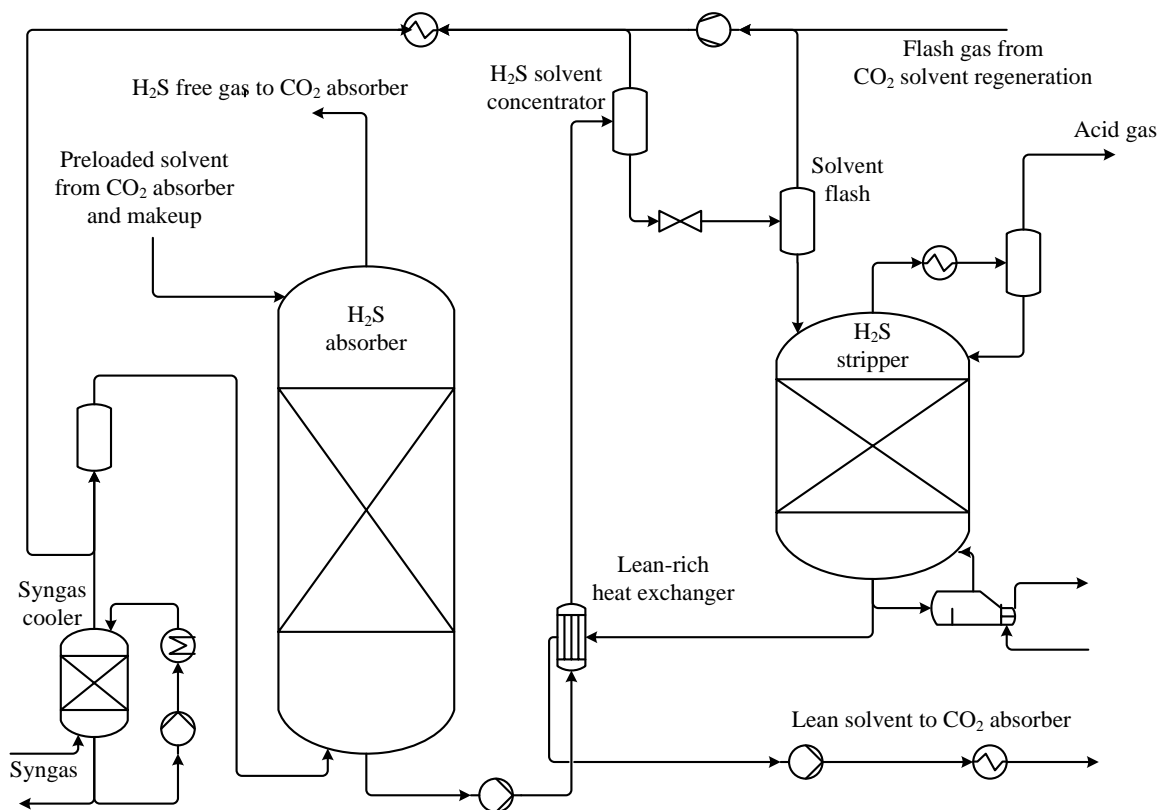


**Figure 21.** Pre-combustion $H_2S$ capture section with Selexol (after [52]).

The $H_2S$-free syngas leaving the $H_2S$ absorber is then directed to the $CO_2$ absorber as shown in Figure 22. The same applies to the regenerated lean solvent from the $H_2S$ capture section.

The layout shown here is based on the UOP Selexol process as reported by Breckendridge [52].

In the $CO_2$ capture section, regeneration of the solvent is achieved by depressurisation in flash drums (FD). The $CO_2$ released in flash drums 3 and 4 is then compressed for mixing with the $CO_2$ leaving FD2. After water condensation, the $CO_2$ stream is then compressed for transport and storage.
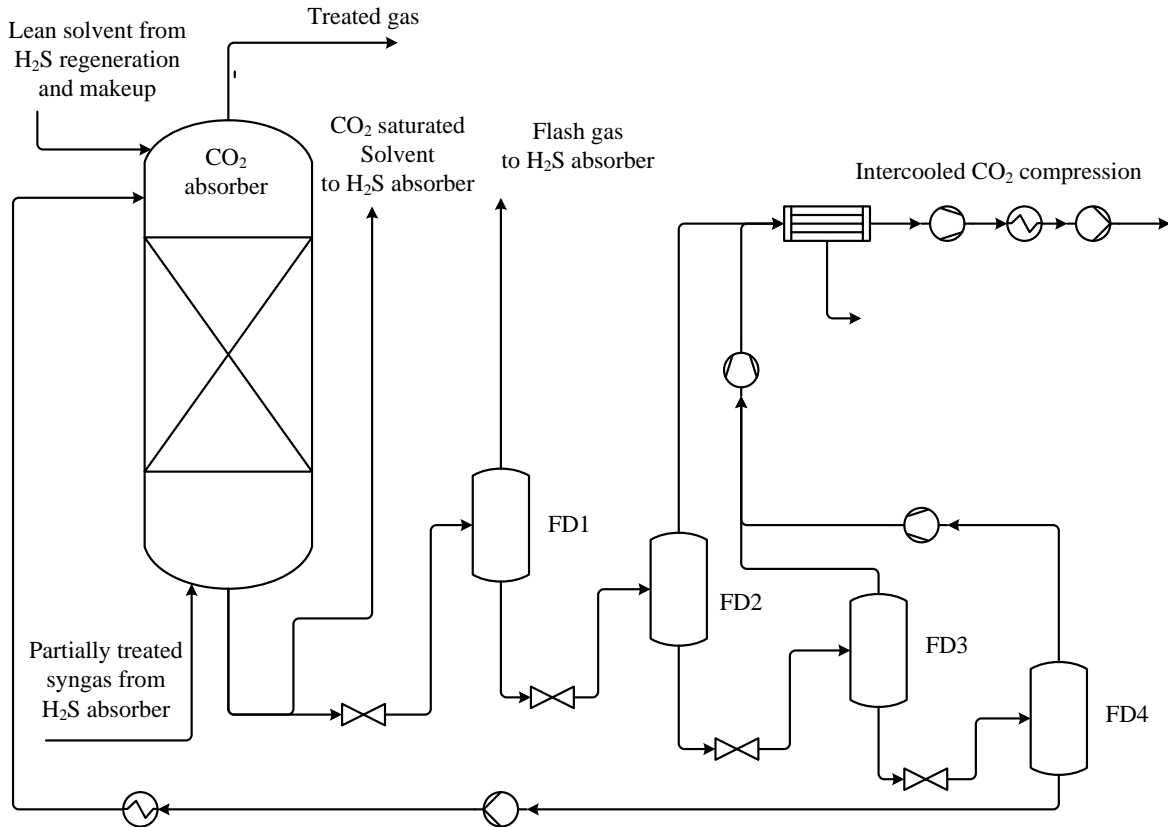


**Figure 22.** Pre-combustion $CO_2$ capture section with Selexol (after [52]).

All columns are modelled with RATESEP blocks, which are used in Aspen Plus for the simulation of rate-based processes. For modelling the absorption of acid gas components into the Selexol solvent, the PC-SAFT equation of state was applied [53]. This EOS is used to describe VLE in polymer solvents over a wide range of temperatures and pressures [54, 55, 56].

With this model , a sufficiently high concentration of $H_2S$ in the acid gas stream leaving the $H_2S$ stripper column could not be achieved here. Higher values would make its use in a Claus process for the production of sulphur attractive. Different researchers [29, 52] claim to achieve an $H_2S$ concentration of more than 45% in this process.

The maximum height of the columns with the Flexipac 1Y packing in this process was assumed to be 20m. The diameter was calculated for a maximum flooding of 80% for a stable operation. The key parameters obtained from the model are summarised for both capture sections in Table 20. The model was set to achieve an acid gas removal as reported in Table 24, where the performance of this model is compared to a second model, which was used for the co-capture of $H_2S$ and $CO_2$.

**Table 20.** Key parameters of rate-based $H_2S$ capture and $CO_2$ capture sections with Selexol.

| **$H_2S$ capture section** | |
|---|---|
| Preloaded solvent flow, $CO_2$ loading, $H_2S$ loading | 471 kg/s, 1.13 mol/mol, 0.0056 mol/mol |
| Gas inlet and solvent temperature | 24.1 °C, 25 °C |
| $H_2S$ rich loading | 0.03 mol/mol |
| $H_2S$ lean loading after stripper | 0.0098 mol/mol |
| Column packing and design parameter for diameter | Flexipac 1Y, 80% flooding |
| Pressure, height and diameter of packed absorber column | 41.5 bar, 20 m, 6 m |
| Pressure, height and diameter of packed stripper column | 4 bar, 3 m, 2.1 m |
| Reboiler duty (MW) and temperature | 20 $MW_{th}$, 113 °C |
| Solvent concentrator pressure, solvent flash pressure | 43 bar, 8 bar |
| Solvent makeup | 0.005 kg/s |
| **$CO_2$ capture section** | |
| Solvent flow from $H_2S$ regeneration, $CO_2$ loading | 403 kg/s, 0.0336 mol/mol |
| Solvent flow from $CO_2$ regeneration, $CO_2$ loading | 1513 kg/s, 0.0525 mol/mol |
| Gas inlet and solvent temperature | 25.3 °C, -1.1 °C |
| Column packing and design parameter for diameter | Flexipac 1Y, 80% flooding |
| Pressure, height and diameter of packed absorber column | 41 bar, 20 m, 8.4 m |
| Flash drum pressures (FD1 - 4) | 8 bar, 4 bar, 2 bar, 1 bar |

### 2.3.3. Rate-based pre-combustion co-capture of $CO_2$ and $H_2S$ with Selexol

In the other capture configuration $H_2S$ and $CO_2$ are captured simultaneously. This configuration, as shown in Figure 23, resembles the $CO_2$ capture configuration described in the previous section. Here, the gas from the first flash drum after the absorber is recycled to raise the amount of hydrogen rich syngas. Solvent regeneration is achieved solely by depressurisation so that no energy penalty due to steam extraction from the IGCC is introduced. The captured gas mixture may have to be stored in a site close to the power plant or it may have to be separated in an additional energy consuming process to prevent corrosion in the transport equipment.
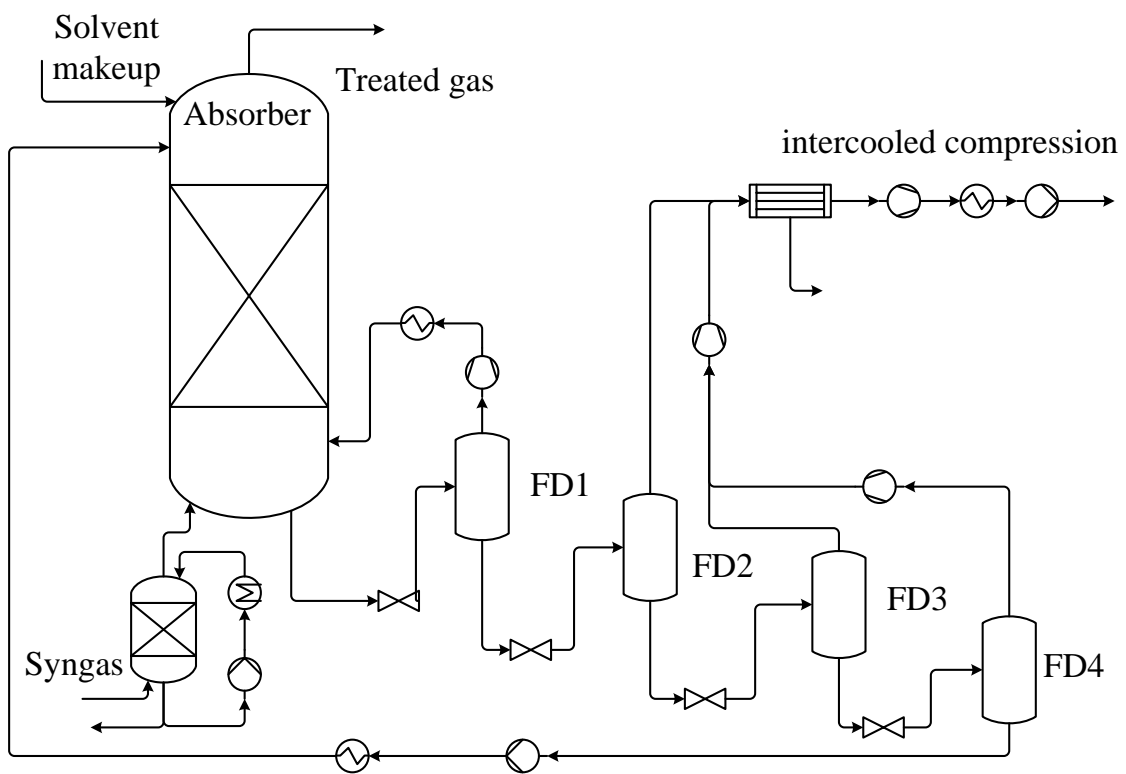


**Figure 23.** Flowsheet for pre-combustion co-capture installation with Selexol.

Compared to the model for separate acid gas removal, solvent flow and column height could be reduced for a $CO_2$ capture efficiency of 90%. The key parameters for this capture option can be found in Table 21. The pressure of flash drum 1 has a major influence on the performance of the capture process. Since the gas stream leaving this component needs to be recompressed before recycling to the absorber column, higher pressures lead to lower energy consumption in the recycle compressor. Lower pressures lead to a higher hydrogen flow in the purified gas stream and thus to a higher energy content of this fuel gas stream that is the burned in the gas turbine. The pressures of the other flash drums were selected to allow for the more economical use of identical compressors due to equal pressure ratios.

**Table 21.** Key parameters of rate-based co-capture section with Selexol.

| | |
|---|---|
| Solvent flow | 825 kg/s |
| Lean loading, rich loading for $CO_2$ | 0.0496 mol/mol, 0.7141 mol/mol |
| Lean loading, rich loading for $H_2S$ | 0.0051 mol/mol, 0.0082 mol/mol |
| Gas inlet and solvent temperature | 32.5 °C, -1.1 °C |
| Column packing and design parameter for diameter | Flexipac 1Y, 80% flooding |
| Pressure, height and diameter of packed absorber column | 41 bar, 11 m, 5.3 m |
| Flash drum pressures (FD1 - 4) | 18 bar, 5 bar, 2.25 bar, 1 bar |

The compositions and flows of the syngas streams and of the streams leaving the capture sections are listed in Table 22. As was to be expected, the purity of the purified gas stream and that of the $CO_2$ stream are higher in the case of separate acid gas removal. However, only an $H_2S$ concentration of 4.5% was achieved there for the $H_2S$-rich stream.

**Table 22.** Composition and flow of gas streams.

| | | | separate capture | | | co-capture | |
|---|---|---|---|---|---|---|---|
| | syngas | shifted | purified | H$_2$S rich | CO$_2$ stream | purified | acid gas |
| Mass Flow in kg/sec | 88.54 | 118.40 | 14.95 | 3.93 | 92.23 | 24.14 | 114.68 |
| Mole Fractions | | | | | | | |
| CO | 0.436 | 0.002 | 0.004 | 0.000 | 0.000 | 0.004 | 0.000 |
| $CO_2$ | 0.125 | 0.397 | 0.040 | 0.953 | 0.996 | 0.070 | 0.990 |
| $H_2$ | 0.286 | 0.512 | 0.923 | 0.000 | 0.000 | 0.896 | 0.004 |
| $H_2O$ | 0.130 | 0.072 | 0.000 | 0.002 | 0.000 | 0.000 | 0.000 |
| $N_2$ | 0.009 | 0.007 | 0.032 | 0.000 | 0.001 | 0.030 | 0.001 |
| $H_2S$ | 0.003 | 0.002 | 518 ppm | 0.045 | 0.003 | 262 ppm | 0.005 |

As reported in Table 24, shifting the syngas leads to a slight drop in power plant efficiency and would not make sense without capture of the acid gas components. The flue gas parameters of the IGCC with and without pre-combustion capture is reported in Table 23.

**Table 23.** Composition and flow of burned gas streams.

|  | no shift, no capture | separate capture | co-capture |
|---|---|---|---|
| Mass Flow in kg/sec | 694.44 | 656.62 | 644.94 |
| Mole Fractions |  |  |  |
| $N_2$ | 0.688 | 0.721 | 0.717 |
| $O_2$ | 0.121 | 0.131 | 0.128 |
| Ar | 0.011 | 0.009 | 0.009 |
| $H_2O$ | 0.082 | 0.133 | 0.135 |
| $CO_2$ | 0.098 | 0.006 | 0.010 |
| $SO_2$ | 463 ppm | 69 ppm | 37 ppm |
| HCl | trace | -- | -- |

As can be seen from these data, the $CO_2$ and $SO_2$ contents in the flue gas stream is significantly reduced due to pre-combustion capture. The capture efficiencies of the two investigated options are reported in Table 24.

### 2.3.4.   Influence of pre-combustion capture (rate-based models) on IGCC performance

The use of the different capture configurations led to different impacts on the power plant, mainly due to the difference in the energy requirements for solvent regeneration. Calculated values for the main parameters are presented in Table 24.

The theoretical advantage of separate capture, i.e. a concentrated acid gas stream for production of elementary sulphur in a Claus plant could not be achieved in the simulations, as the $H_2S$ concentrations yielded were too low. Therefore, the recommended option here is co-capture of $H_2S$ and $CO_2$, possibly with later separation of these gases in another process.

**Table 24.** Parameters for IGCC with and without pre-combustion capture of $CO_2$ and $H_2S$.

|  | shift no capture | no shift, no capture | separate capture | co-capture |
|---|---|---|---|---|
| Power plant output in $MW_{el}$ | 573.75 | 576.25 | 561.25 | 567.5 |
| ASU in $MW_{el}$ | 120 | 120 | 120 | 120 |
| Capture efficiency for $CO_2$ and $H_2S$ | -- | -- | 94.4%, 84.7% | 90.0%, 91.9% |
| $CO_2$ compression in $MW_{el}$ | -- | -- | 16.25 | 23.75 |
| Solvent chilling in $MW_{el}$ (COP = 4.5) | -- | -- | 10.01 | 1.88 |
| Work in $H_2S$ capture section | -- | -- | 9.98 | -- |
| Work in $CO_2$ capture section | -- | -- | 12.53 | 8.75 |
| Power plant net output in $MW_{el}$ | 453.8 | 456.3 | 392.5 | 412.5 |
| Power plant efficiency (HHV-based) | 38.40% | 38.60% | 33.20% | 34.90% |
| Energy penalty for capture in $MW_{el}$ | -- | -- | 63.75 | 43.75 |
| Specific energy penalty in $GJ_{el}/t$ | -- | -- | 0.67 | 0.48 |
| Specific $CO_2$ production in kg/MWh | 647.7 | 644.1 | 78.1 | 74.4 |
| Effective $CO_2$ removal | -- | -- | 87.9% | 88.5% |

In the simulations studied here, separate capture of the acid gas components led to a lower capture efficiency for $H_2S$, even though the $CO_2$ capture rate was raised above 90%. This also led to a higher energy penalty for the capture process. The high necessary solvent flow required more energy for solvent cooling and pumping, as well as for the recompression of the gas streams. Raising $CO_2$ capture efficiency to the reported level was necessary to achieve a similar effective $CO_2$ capture efficiency as with the co-capture option [51].

# 3. Post-combustion capture

Most anthropogenic point sources of $CO_2$ are combustion systems such as power plants, cement kilns and furnaces as used for iron and steel production, where the fuel is burned with air. Post-combustion capture is the removal of greenhouse gases at the end of the conversion process. Therefore, this second capture method discussed in the following is a very important process for reducing $CO_2$ emissions. Since these combustion processes are of large scale, occur at low pressure and due to the large nitrogen content of air, they produce very large gas flows with a low content of $CO_2$. This content ranges from 3 %vol. for a NGCC to about 15% for a coal-fired power plant. Due to the low partial pressure of $CO_2$ in the gas stream, liquid separation is a possible candidate. However, the development of ceramic or metallic membranes would possibly yield more efficient solutions of $CO_2$ separation [57, 58]. Another approach is the use of liquid membranes that combine chemical solvents with membranes [59, 60, 61]. Other capture technologies are pressure swing adsorption on molecular sieves and cryogenic gas separation. Of these approaches, this chapter will focus on the use of chemical solvents for post-combustion $CO_2$ capture. Chemical solvent absorption is currently the most promising and cost-effective technology [30].

Impurities such as $SO_X$, $NO_X$, particulates, HCl, HF, metals (mercury etc.) and other contaminants may negatively affect capture performance by causing solvent degradation. Especially the most widely used solvent monoethanolamine (MEA) is prone to degradation [62], which is caused by oxygen and oxygen-containing components such as $NO_X$ and $SO_X$, by producing oxidised amine fragments, $NH_3$, formate, acetate and peroxides [63, 64]. Degradation can be catalysed by metal cations present in the absorption section [65]. Iron is often present due to corrosion, which is especially pronounced in carbon steel equipment. Corrosion is mainly influenced by $CO_2$ loading of the solvent and by the solvent type [66], but also by the presence of degradation products, and by temperature and solvent concentration [65]. Corrosion inhibitors such as carboxylic acids act as oxygen scavengers and can significantly reduce steel corrosion in the capture plant [67]. In the presence of oxygen, $SO_2$ dissolved in MEA reacts very quickly to form heat stable sulphates that have to be removed to maintain solvent performance [64]. $NO_X$ are easily dissolved in water forming corrosive acids, and like $SO_2$ they can react irreversibly with alkanolamines [68, 69], causing a continuous loss of solvent [30]. Therefore, these components have to be removed to very low levels in the flue gas prior to entering the absorption section [65]. In Figure 24, a schematic diagram of a PC power plant with emission controls is shown.
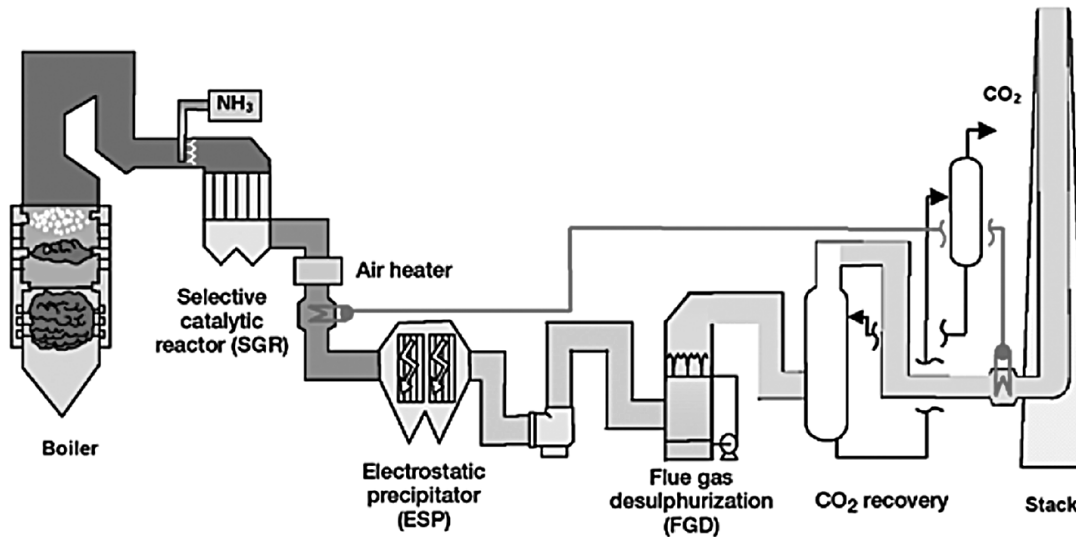
**Figure 24.** Pulverised coal power plant with amine $CO_2$ capture and other emission controls [12].

Chemical $CO_2$ absorption makes use of the reaction of a weak alkanolamines base with $CO_2$, which is a weak acid, to form a water-soluble salt [65]. This reversible and temperature dependent reaction can be written in simplified form as:

$$CO_2 + 2RNH_2 \underset{\text{hot}}{\overset{\text{cold}}{\rightleftarrows}} RNHCOO^- + RNH_3^+ \tag{32}$$
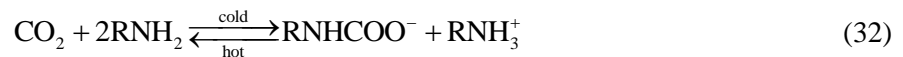
The carbamate ion RNHCOO⁻ can be formed by primary ions such as MEA and by secondary amines. From this reaction it can be seen that two moles of amine are necessary to remove one mole of $CO_2$. Tertiary amines such as MDEA do not form carbamate ions due to the lack of a hydrogen ion attached to the nitrogen. Then a different reaction forming bicarbonate ions takes place, which is catalysed by water:

$$CO_2 + R_3N \overset{H_2O}{\longleftrightarrow} HCO^{3-} + RNH^+ \tag{33}$$

Since only one mole of amine is needed for the removal of one mole of $CO_2$, the absorption capacity of tertiary and hindered amines is greater. However, their main disadvantage is the much slower $CO_2$ uptake rate (see 2.2.3). However, absorption kinetics for these solvents can be improved by adding small quantities of activators such as Piperazine [49]. Also primary amines such as MEA can be used as activator [70].

Although new amines such as KS-1 with very low degradation are being developed, MEA is still the most widely used solvent for $CO_2$ capture. It has very high reactivity, low solvent cost, reasonable thermal stability and thermal degradation rate [65].

A flow diagram that includes the most important steps of the post-combustion capture process is shown in Figure 25.
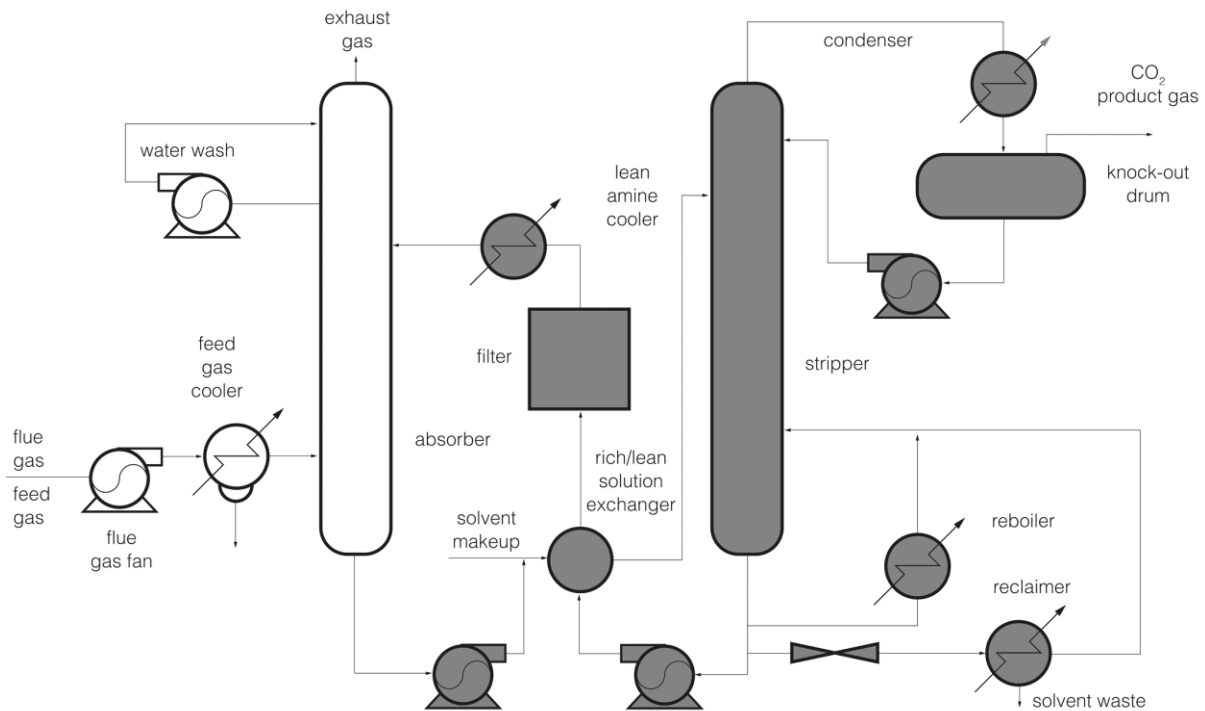


**Figure 25.** Process flow diagram for $CO_2$ capture by chemical absorption [12].

After passing a blower or fan to compensate for the pressure loss inside the absorber, the flue gas is cooled and enters the absorber. There, the flue gas comes into contact with the semi-lean solvent. Then a water wash is used to remove any solvent carried over with the scrubbed flue gas. Typical removal efficiencies are in the range of 80 to 95%. Higher efficiencies lead to taller absorber columns, higher energy penalties and thus to elevated costs. The $CO_2$-rich solvent is then pumped to the top of a stripper via a heat exchanger to minimise energy penalties. The regeneration of the solvent occurs at close to atmospheric pressure and at temperatures of 100 °C to 140 °C. The energy requirements of the reboiler for the stripper column is composed of the energy for i) bringing the solution to the boiling point, ii) for breaking the chemical bonds between $CO_2$ and solvent, and iii) for generating water vapour to establish an operating $CO_2$ partial pressure needed for $CO_2$ stripping [65].

Heat for solvent regeneration is generally supplied by low-pressure steam, leading to the main energy penalty for $CO_2$ capture. The necessary reboiler duty depends strongly on lean solvent loading [71, 72, 73]. Being the most influential factor on power plant output, the reboiler duty can be used as a variable for overall plant efficiency.

In this chapter, capture and power plant performances are compared mainly for chemical absorption with MEA and with ammonia, since several different studies showed that a significant reduction of up to 62% in regeneration energy is possible [74, 75]. Alstom is carrying out studies on a pilot

plant at the Pleasant Prairie coal-fired power plant by We Energies in Kinosha, WI, USA [76, 77, 78] and claim that this process uses only about 50% of the energy needed for a comparable MEA process, leading to an output reduction of only 10% in the power plant. Ammonia can also be used for the simultaneous removal of $CO_2$, $SO_2$, and $NO_X$ [79]. However, one of the major drawbacks of this process is the high loss of ammonia due to its high volatility and the formation of precipitates [80].

In the following, several post-combustion capture models will be developed and discussed.

## 3.1. Equilibrium-based $CO_2$ capture models and experiments

Due to the presence of ionic species in theses multi-component volatile weak electrolyte systems [17, 18], liquid and vapour properties were computed by the electrolyte NRTL method. Henry's law was used to calculate the solubility of $CO_2$ in water. All simulations were carried out with Aspen Plus, which has become a widely used standard application for computerised flowsheet simulations in the chemical industry.

### 3.1.1. PC power plant model

For all post-combustion capture processes the flue gas stream was assumed to exit from a 500 MW pulverised coal power plant with an SCR reactor (RSTOIC) for the removal of $NO_X$ with ammonia injection according to Reactions (34) - (36) and wet flue gas desulfurisation according to Reaction (37) in a RADFRAC column with a conversion factor of 0.26 for $CaCO_3$.

$$2\,NO_2 +\ 4\,NH_3 +\ O_2\ \leftrightarrow\ 3\,N_2 +\ 6\,H_2O \qquad\qquad (34)$$

$$NO +\ NO_2 +\ 2\,NH_3\ \leftrightarrow\ 2\,N_2 +\ 3\,H_2O \qquad\qquad (35)$$

$$4\,NO +\ 4\,NH_3 +\ O_2\ \leftrightarrow\ 4\,N_2 +\ 6\,H_2O \qquad\qquad (36)$$

$$CaCO_3\ +\ SO_2\ \leftrightarrow\ CaSO_3\ +\ CO_2 \qquad\qquad (37)$$

According to the IEA report on $CO_2$ capture [30], $NO_X$ and $SO_X$ levels have to be reduced to at least 20 ppm and 10 ppm respectively to prevent MEA degradation. With ammonia, these contaminants can be captured by the solvent. However, they would end up in the separated $CO_2$ stream, where they may have to be removed to prevent equipment damage due to acid formation. For thermal solvent regeneration in a stripper column steam is extracted after the medium pressure turbines. The parameters for the IEA coal used in the simulations are shown in Table 25.

**Table 25.** Coal analysis for PC power plant.

| Ultimate analysis | Dry basis %wt. | Proximate analysis | Dry basis %wt. | Sulphur analysis | Dry basis %wt. |
|---|---|---|---|---|---|
| Carbon | 71.38 | Moisture | 9.5 | Pyritic | 0 |
| Oxygen | 7.79 | Fixed Carbon (FC) | 50.51 | Sulfate | 100 |
| Nitrogen | 1.56 | Volatile Matter (VM) | 36.01 | Organic | 0 |
| Hydrogen | 4.85 | Ash | 13.48 | | |
| Sulfur | 0.952 | | | | |
| Chlorine | 0.026 | | | | |
| Ash | 13.48 | | | | |

The relevant parameters of this typical 3-stage Rankine cycle power plant can be found in Table 26. The Peng-Robinson EOS was used for this process, as recommended for the modelling of combustion processes.

**Table 26.** PC power plant parameters (after [72]).

| | |
|---|---|
| Coal Feed | 50.4 kg/s |
| Heating value coal | HHV = 27.06 MJ/kg, LHV = 25.87 MJ/kg |
| HP Turbine | $p_{in}$ = 152 bar    $T_{in}$ = 533 °C    P = 130.7 MW |
| IP Turbine | $p_{in}$ = 42.5 bar    P = 190.1 MW |
| LP Turbine | $p_{in}$ = 4.67 bar    P = 243.7 MW |
| Condenser | $p_{cond}$ = 0.04 bar    $Q_{Cooling}$ = 265 MW |
| Ammonia for SCR | 1.436 kg/s |
| Limestone slurry for FGD | 20.548 kg/s (6.74 %wt.), 1.871 kg/s gypsum produced |

To show the effect of SCR and FGD on the flue gas, the compositions of the treated and of the untreated flue gas stream are given in Table 27. It is plausible that the water content in the flue gas increases due to the use of wet FGD.

**Table 27.** Flue gas composition of PC power plant.

| flue gas components | composition of untreated flue gas in %mol | composition with SCR and FGD in %mol |
|---|---|---|
| $N_2$ | 74.0 | 70.3 |
| $H_2O$ | 7.0 | 12.3 |
| $CO_2$ | 13.8 | 13.1 |
| $O_2$ | 3.5 | 3.2 |
| CO | 0.2 | 0.2 |
| $NO_X$ | 0.4 | 19 ppm |
| $SO_2$ | 0.07 | 9 ppm |

The energy penalty involved with the thermal solvent regeneration in a stripper column will be discussed later.

### 3.1.2. Simulations of regenerative $CO_2$ capture with MEA, DGA, and $NH_3$

The most mature technology of $CO_2$ absorption in gas purification processes uses amines such as Monoethanolamine (MEA) as absorbent [47]. As already discussed in the introduction to this chapter, especially MEA is easily degraded in the presence of $SO_2$ and $O_2$ by the formation of irreversible by-products, reducing the absorption capacity of the amine and making its recovery difficult.

A standard absorber-desorber configuration as shown in Figure 26 (with a packed absorption column of 6 theoretical stages and a packed desorption column of 10 theoretical stages) was used for the simulation of the absorption process with MEA, diglycolamine (DGA), and ammonia as reactive solvents.

The columns were of the type RADFRAC, which is used in Aspen Plus for the calculation of chemical equilibrium processes.
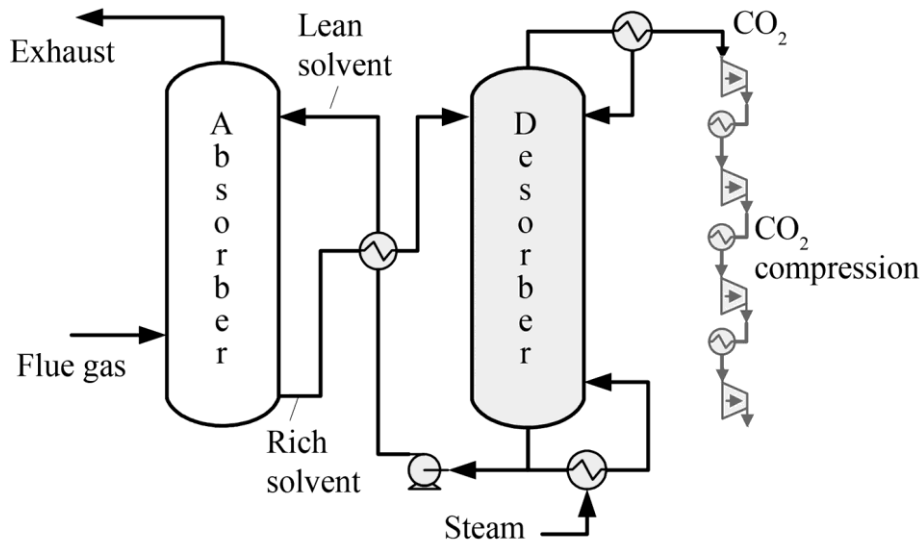


**Figure 26.** Absorption section for post-combustion $CO_2$ scrubbing [81].

The reactions used for $CO_2$ absorption with MEA, DGA and the ammonia solvent are listed in Table 28. This table also shows the parameters used for the calculation of the equilibrium constants. The kinetic parameters for the slower formation and dissociation of bicarbonate can be found in Table 12. The important reaction of carbamate formation (Reactions (39) and (41)) was described to proceed very fast by a so-called shuttle mechanism [82] via a zwitter-ionic intermediate.

**Table 28.** Equilibrium constants for absorption with MEA, DGA, and $NH_3$ [83, 84, 85].

| Reaction | | | A | B | C | D | |
|---|---|---|---|---|---|---|---|
| $2\,H_2O$ | $\leftrightarrow$ | $H_3O^+ + OH^-$ | 132.899 | -1345.9 | -22.4773 | | (11) |
| $CO_2 + 2\,H_2O$ | $\leftrightarrow$ | $H_3O^+ + HCO_3^-$ | 231.465 | -12092.1 | -36.7816 | | (14) |
| $HCO_3^- + H_2O$ | $\leftrightarrow$ | $H_3O^+ + CO_3^{-2}$ | 216.049 | -12431.7 | -35.4819 | | (15) |
| $MEAH^+ + H_2O$ | $\leftrightarrow$ | $MEA + H_3O^+$ | -3.03833 | -7008.36 | | -0.003135 | (38) |
| $MEACOO^- + H_2O$ | $\leftrightarrow$ | $MEA + HCO_3^-$ | 231.466 | 12092.1 | 36.7816 | | (39) |
| $DGAH^+ + H_2O$ | $\leftrightarrow$ | $DGA + H_3O^+$ | -13.3373 | -4218.71 | | | (40) |
| $DGACOO^- + H_2O$ | $\leftrightarrow$ | $DGA + HCO_3^-$ | 3.66110 | -3696.17 | | | (41) |
| $NH_3 + H_2O$ | $\leftrightarrow$ | $NH_4^+ + OH^-$ | -1.257 | -3335.7 | 1.4971 | -0.037057 | (18) |
| $NH_3 + HCO_3^-$ | $\leftrightarrow$ | $NH_2COO^- + H_2O$ | -4.583 | 2900 | | | (42) |
| $NH_4HCO_3$ | $\xrightarrow{SALT}$ | $NH_4^+ + HCO_3^-$ | 554.818 | -22442.5 | -89.0064 | 0.064732 | (43) |
| $(NH_4)_2CO_3$ | $\xrightarrow{SALT}$ | $2\,NH_3 + CO_2 + H_2O$ | by minimisation of Gibbs free energy | | | | (44) |
| $NH_2COONH_4$ | $\xrightarrow{SALT}$ | $NH_4^+ + NH_2COO^-$ | by minimisation of Gibbs free energy | | | | (45) |

$$\ln K(T) = A + B/T + C \cdot \ln(T) + D \cdot T, \quad T \text{ in Kelvin}$$

A comparison of the $CO_2$ removal efficiency per unit mass of solvent is shown in Figure 27. Ammonia has by far the best absorbent qualities among the substances investigated. For this comparison, the solvent flow was held constant for every individual solvent while the solvent concentration was raised (range of concentrations in % wt.: MEA: 0.17–0.33, DGA: 0.17–0.5, $NH_3$: 0.02–0.2).
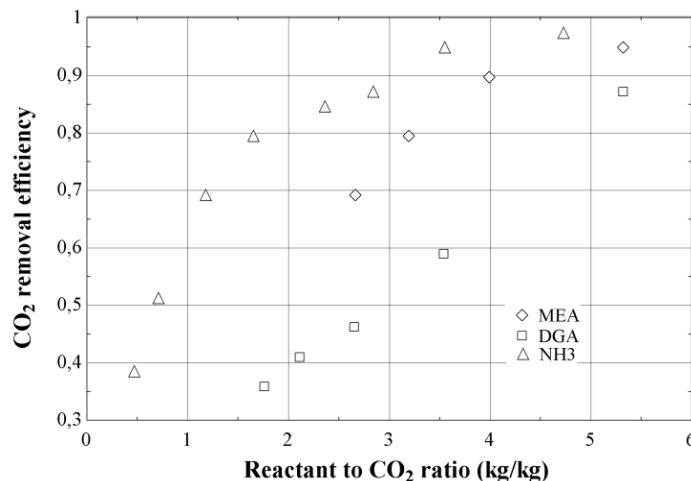


**Figure 27.** $CO_2$ removal eff. at 20 °C of MEA, DGA, and $NH_3$ at different solvent-to-$CO_2$ ratios.

$NH_3$ shows a very high removal efficiency at ambient pressure. For a $CO_2$ removal efficiency of 80% an ammonia-to-$CO_2$ ratio of ca. 1.5 (a solvent concentration of 7 %wt.) is sufficient, while for

the same removal efficiency using MEA an amine-to-$CO_2$ ratio greater than 3 (solvent concentration of 20 %wt.) is necessary. Solvent concentrations are limited by corrosion and by solvent losses.

Due to the assumption of chemical equilibrium, larger absorption columns of more than 6 stages did not give a significantly higher absorption efficiency in the simulations.

### 3.1.3. CO$_2$ capture simulations with ammonia in a non-regenerative process

The role of ammonia as a promising solvent in CO$_2$ capture is even more enhanced by a novel method to reduce CO$_2$ emissions from power plants by the use of an aqueous ammonia solution, which makes it possible to capture CO$_2$ as a valuable solid product [86, 87]. Thus, in this chapter a special focus is laid on the capture of ammonia salts, as this allows for a much more rational use of the CO$_2$ than the energy intensive compression and necessary storage of the gaseous carbon dioxide leaving the absorption process in the case of MEA and DGA. A possible configuration for this capture option, which was used in the simulations here, is presented in Figure 28. The model configuration included a packed absorber column of 10 theoretical stages and a filter for the extraction of salt products from the rich solvent leaving the absorber. The lean solvent is recycled to the absorber after inserting fresh solvent to make up for the losses attributed to the removal of ammonia salts.

The produced salts are a basic ingredient of fertilizers [88] and could hence be exploited commercially. NH$_3$ has frequently been used as reactant for the De-NO$_X$ process in power plants, and it is also interesting for the removal of SO$_2$ and HCl from flue gases [79].
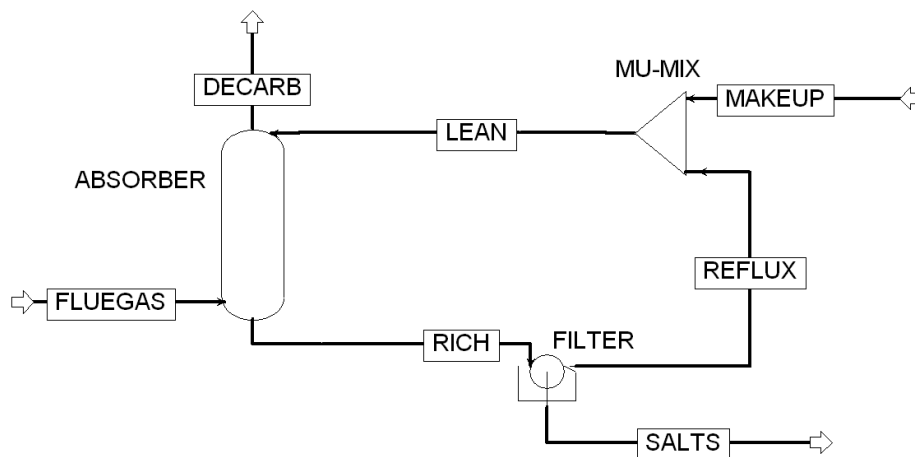


**Figure 28.** Schematic diagram of non-regenerative CO$_2$ capture with ammonia.

CO$_2$ scrubbing with ammonia is economically very attractive [81], if salts can be separated, since the conventional production of the ammonia salts requires an energy input of around 32 GJ/t salt [89], which is about twice the value for the production of NH$_3$.

As shown in Figure 29, salt formation increases with solvent loading (mol CO$_2$/mol solvent agent). The salts separated from the solvent stream by filtration or by sedimentation have commercial appeal for fertilizer production.
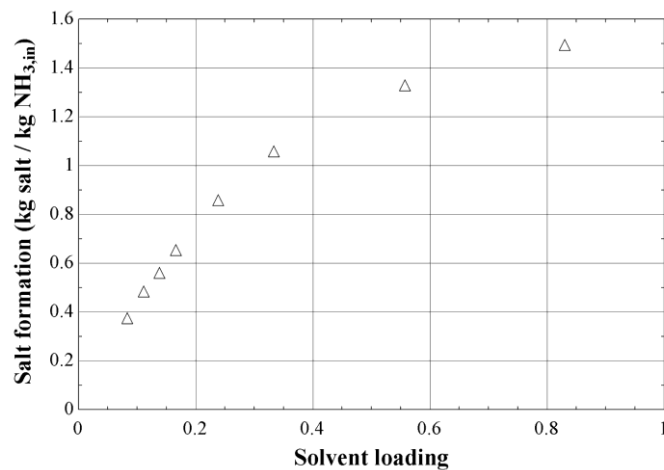
**Figure 29.** Ammonia salt formation for different loadings (mol/mol) of the ammonia solvent [90].

Values for the solubility of the ammonia salts are differing between manufacturers. Data sets for two major manufacturers are given in Table 29.

**Table 29.** Ammonia salt solubilities [91, 92].

| Salts | BASF (g/l) | Sigma - Aldrich (g/l) |
|---|---|---|
| $NH_4HCO_3$ | 178 | 220 |
| $NH_4COONH_2$ | 423 | 790 |
| $(NH_4)_2CO_3$ | 320 | 320 |

In the non-regenerative ammonia process, at 20 °C approximately 20% of the ammonia exits the absorber with the gas stream and has to be removed.

### 3.1.4. Experiments for $CO_2$ capture with ammonia and EAA solvent

A series of experiments for the investigation of $CO_2$ capture with ammonia solvents was carried out in a small-scale setup in the laboratory of the Inorganic Chemistry department at the University of Florence. The semi-continuous flow reactor shown in Figure 30 consisted of a glass column containing 240 ml of aqueous ammonia solution (5 %wt. ammonia concentration) [87].
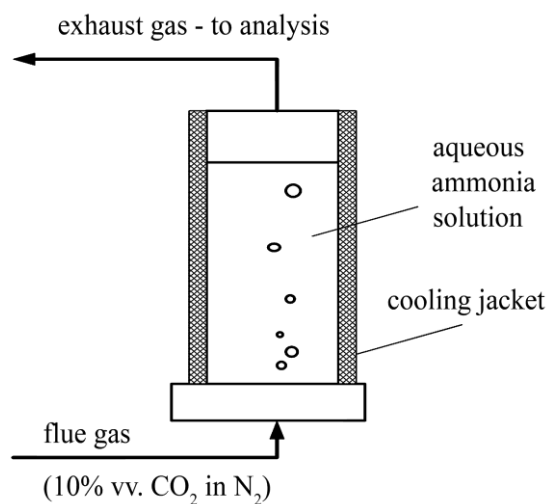


**Figure 30.** Schematic diagram of semi-continuous flow absorber for $CO_2$ [90].

A substitute flue gas stream (10 %vv. $CO_2$ in $N_2$) of ca. 4.2 ml/s was fed continuously to the bottom of the absorber through a sintered glass diffuser (Ø 16-40 μm pores). The exhaust gas left the absorber at the top. The inlet gas mixture was humidified by bubbling it through water before it entered the reactor. All experiments were carried out at atmospheric pressure. The $CO_2$ capture performance of the system is easily determined by weight measurements of all system components before the tests and after certain time intervals. The pH-value and the species in solution were analysed with a $^{13}$C-NMR apparatus. A gas chromatograph was used to measure the losses of $CO_2$ from the system.

Although the reaction between carbonate and bicarbonate reached equilibrium very fast, this was not the case for the reaction of carbamate with its carbonate and bicarbonate products. Thus, the solution was given at least 1 h to react, allowing for the measurement of the equilibrium concentrations of bicarbonate, carbonate and carbamate ions. The concentrations of the components in solution after different time intervals are shown for two different absorption temperatures in

Table 30. The loss of ammonia from the absorber in the experiments proved to be very low (ca. 0.01%).

**Table 30.** Development of component concentrations (% wt.) in 5 %wt. ammonia solution [90].

| Time (h) | T = -5 °C | | | T = 20 °C | | |
|---|---|---|---|---|---|---|
| | $HCO_3^-$ | $CO_3^{-2}$ | $NH_2COO^-$ | $HCO_3^-$ | $CO_3^{-2}$ | $NH_2COO^-$ |
| 2 | 28. 1 | 28.6 | 43.3 | 28.2 | 28.8 | 43.0 |
| 3 | 42.8 | 21.9 | 35.3 | 45.3 | 22.7 | 32.0 |
| 7 | 52.0 | 18.3 | 29.7 | 60.2 | 16.5 | 23.3 |
| 8 | 63.3 | 14.8 | 21.9 | 71.0 | 11.9 | 17.1 |

Temperatures of down to -5 °C were investigated, as reduced salt solubility was expected. However, the $CO_2$ removal efficiency was nearly independent of absorber temperature, as shown in Figure 31. pH-measurements of the solution verified this behaviour.
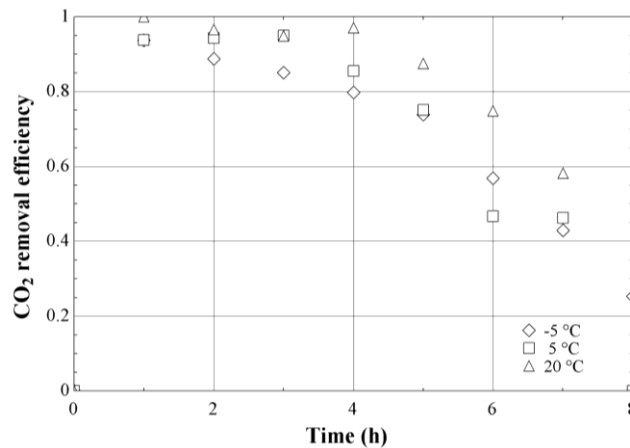


**Figure 31.** $CO_2$ removal efficiency by ammonia solution (5% wt.) at different temperatures [90].

Contrary to the simulation results, the experiments showed that at such low ammonia concentrations, it was not possible to separate the salts from the solution. The resulting lower removal efficiency of ammonia in the experiments (ca. 1.26 $kgCO_{2,removed}/kgNH_{3,in}$), however, is still higher than that found in the simulation results for MEA and DGA.

In order to separate the ammonia salts it is necessary to lower their solubility. This can be achieved by either raising the concentration of ammonia in the solvent stream [93, 94] or by using an alternative solvent. In this work, the latter option was chosen, as otherwise ammonia losses with the exhaust gas become very large.

Aiming at a reduction of these losses, the hydro-alcoholic solvent EtOH–$H_2O$–$NH_3$ was investigated [87], resulting in a so-called Ethanol-Aqueous-Ammonia (EAA) solution, consisting of 85 %wt. ethanol and a varying percentage of ammonia, the remaining amount being water. Ethanol was chosen due to its similar characteristics to water and its good availability. A new series of tests was

carried out for various ammonia concentrations and absorber temperatures without changing the described experimental setup.

After giving the solution 3 h to react, the $CO_2$ outlet concentration in the gas stream exceeded 20 %wt. for an ammonia concentration of 2 %wt., while it took more than 6 h until the same outlet concentration of $CO_2$ was observed at ammonia concentrations of 4 %wt. and 6 %wt. Also, the amount of produced salts confirmed that removal efficiency improved with increasing ammonia concentration. At the end of the experiment, when the $CO_2$ outlet concentration exceeded 25 %wt., the salts are removed from the absorption column. Then, they were dried and weighed to measure their relative amount, and a sample of the produced salts underwent an NMR analysis to determine the salt composition. In the end, the absorption column is weighed again and the test is restarted. At an absorber temperature of 5 °C, about 8.3 g were obtained for a solvent concentration of 2 %wt., while it were 12.8 g and 13.7 g respectively for solvent concentrations of 4 %wt. and 6 %wt. However, higher ammonia concentrations in the entering solvent stream also lead to elevated losses of ammonia with the exiting gas stream.

The results for different absorber temperatures clearly show a reduced formation of ammonia salts at higher temperature (above 0 °C). At a solvent concentration of 2 %wt. the amount of salts formed amounted to ca. 8.3 g at 5 °C, while at temperatures of 0 °C and 20 °C these values were reduced to 6.2 g and even 1.8 g respectively. A reduced salt formation consequently leads to lower $CO_2$ removal efficiencies and higher losses of the solvent components with the exhaust gas. The $CO_2$ outlet concentration exceeded 20 %wt. already after a reaction time of 90 min for an absorption temperature of 20 °C, while it took more than 150 min until the same outlet concentration of $CO_2$ was observed for the lower temperatures.

The experiments carried out with the EAA solvent confirmed the trends of the previous experiments without ethanol with respect to the response of component concentrations to the absorption conditions, i.e. absorption temperature.

While the trend for carbamate formation followed the decrease of free (or excess) $NH_3$ in the solution, the same trend could be observed for carbamate formation. The formation of bicarbonate increased with lower concentrations of free $NH_3$ (see Table 31).

**Table 31.** Development of component concentrations (%wt.) in EAA solution [90].

| Cycle | T = -5 °C | | T = 20 °C | |
| --- | --- | --- | --- | --- |
| | $HCO_3^- + CO_3^{-2}$ | $NH_2COO^-$ | $HCO_3^- + CO_3^{-2}$ | $NH_2COO^-$ |
| 1 | 13.8 | 86.2 | 35.4 | 64.6 |
| 2 | 20.8 | 79.2 | 69.6 | 30.4 |
| 3 | 73.5 | 26.5 | 100 | |
| 4 | 100 | | | |

With the hydro-alcoholic solution, the removal efficiency and thus the amount of produced salts improved with the increase of ammonia concentration. However, the ammonia losses increased as well. Therefore, an ammonia concentration of more than 10 %wt. is not recommended. Generally, lower temperatures lead to better capture performance and lower solvent losses. This is illustrated in Figure 32and in Figure 33. In Figure 32, the amount of salts produced by $CO_2$ capture with the EAA solvent at a solvent temperature of -5 °C is compared for different ammonia concentrations.
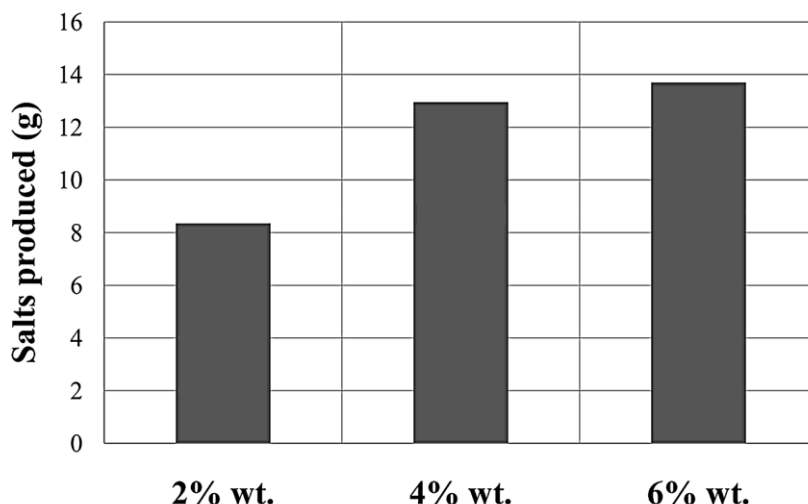


**Figure 32.** Salts produced in EAA solution at different $NH_3$ concentrations for T = -5 °C.

In Figure 33, the amount of salts produced by $CO_2$ capture with the EAA solvent at a constant ammonia concentration of 2 %wt. is compared for different absorption temperatures.
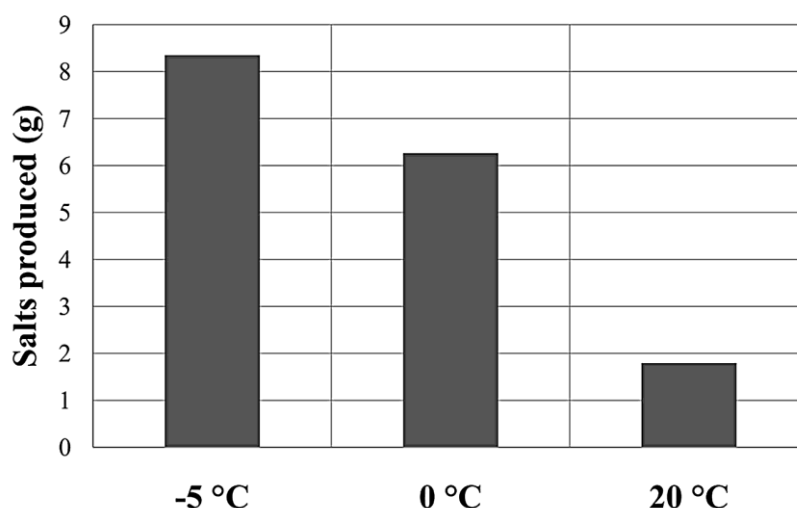


**Figure 33.** Salts produced in EAA solution at different $NH_3$ concentrations for T = -5 °C and at different temperatures for an $NH_3$ concentration of 2 %wt.

The development of $CO_2$ removal efficiency of the ammonia solution (AA) and the EAA solution are compared in Figure 34 for an absorption temperature of 20 °C and an ammonia concentration of 5 %wt. in the solvent stream. At any time, the removal efficiency of the salt-forming EAA is higher than the performance of AA.
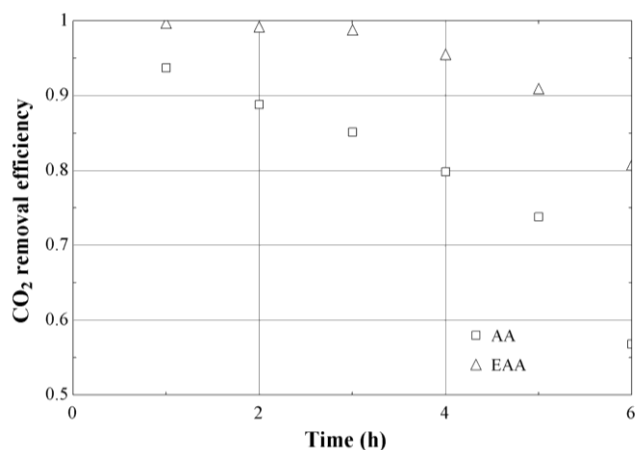


**Figure 34.** $CO_2$ capture efficiency of AA and EAA solutions at 20 °C with 5% wt. $NH_3$.

Finally, some remarks on the experimental error of the measurements. The precision of the balance, used to weigh all the components, is 0.01 g, corresponding to an error of ca. 1%. The accuracy of the gas chromatograph, used to measure the losses of $CO_2$ from the system, is ca. 5% around the value of calibration (a flow containing 10% vol. $CO_2$ and 90% vol. $N_2$ produced by Italian gas company Rivoira). This leads to an error of up to 4% in mass of $CO_2$ lost, depending on the total amount of $CO_2$ that has left the system. The NMR instrument measures frequency signals and compares them to a reference frequency, showing the composition of the produced salts.

### 3.1.5.  Comparison of post-combustion capture performance of investigated solvents

In a final comparison, the experimental findings show that for an aqueous ammonia solution (AA) of 5 %wt. and at an absorption temperature of 20 °C the non-regenerative absorption model with salt formation demonstrated the highest $CO_2$ removal efficiency, followed by the experimental results obtained with the EAS solution and the standard aqueous ammonia solvent. The last value in Figure 35 represents the result for 90% $CO_2$ removal in an absorber-desorber configuration. For the same parameters, the amount of $CO_2$ removed per unit mass of solvent agent was 0.18 kg/ kg of MEA and 0.17 kg/kg of DGA.
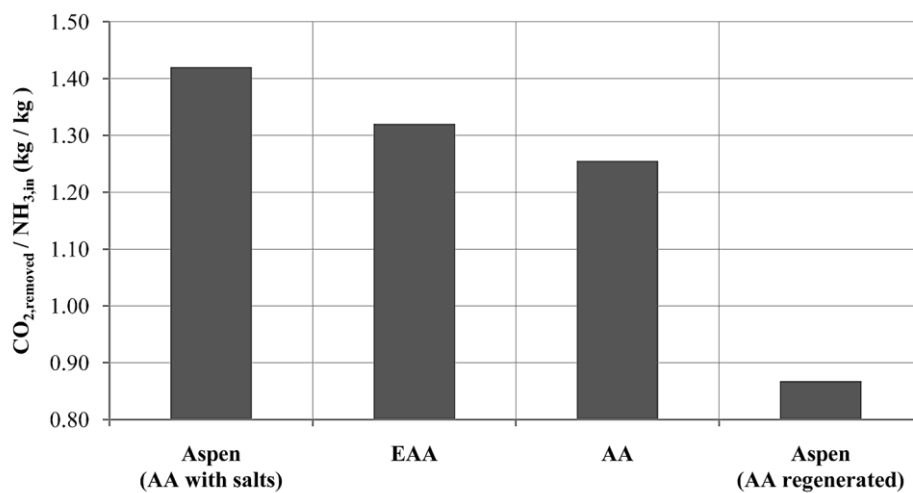


**Figure 35.** Comparison of simulations to experiments with AA and EAA solution at T = 20 °C.

The simulations show that ammonia is a very good absorbent for $CO_2$, which was verified by the experiments. However, crystalline salts (which may be used as a commercial product) could only be obtained by reduction of the very high solubility of the ammonia salts. This reduction was achieved by using a mixture of ethanol, water and ammonia. The solvent conditions are presented in Table 32.

**Table 32.** Solvents for equilibrium-based post-combustion capture simulations and experiments.

|  | MEA solvent | Ammonia solvent | EAA solvent | | |
|---|---|---|---|---|---|
|  | MEA | $NH_3$ | $NH_3$ | ethanol | water |
| Solvent concentration in %wt. | 33 | 10.5 | 4.4 | 85 | 10.6 |
| Solvent temperatures in °C | 40 | 20 | | -5 | |
| Reboiler temperatures in °C | 110 | 90 | | -- | |

Any capture process using ammonia, either by salt production or in an absorber-desorber configuration, benefits clearly from lower temperatures. This greatly reduces ammonia losses from the absorber and hence the necessary energy input for emission reduction. Chilling of the solvent introduces another penalty though. Using low concentrations of ammonia in the solution for $CO_2$ removal proved to be a good compromise between high removal efficiency and low ammonia losses with the exhaust gas stream.

Even if no salt formation occurs and the ammonia solvent is thermally regenerated in an absorber-desorber arrangement, the much lower absorption temperatures (due to the reactions between the $CO_2$ and the solvent) imply lower energy requirements for solvent regeneration compared to MEA and DGA.

The energy penalty for the thermal regeneration of the solvent in the traditional absorber-desorber process in post-combustion $CO_2$ capture with amines is currently in the range of 4-5 $GJ_{th}$/t $CO_{2,captured}$ [9, 95]. Applying the non-regenerative absorption process with ammonia greatly reduces energy requirements, since no heat for solvent regeneration and no compression of the separated $CO_2$ are necessary. However, a great amount of water is required for washing the exhaust gas stream in order to reduce emission of ammonia into the atmosphere, and the energy requirements for additional gas treatment in order to reduce ammonia emissions cannot be disregarded.

In case of ammonia regeneration, a great part of the $CO_2$ is released from the solvent requiring a far lower energy input than is necessary for the regeneration of MEA and DGA. The regeneration efficiency at different reboiler temperatures in the stripper column is shown in Figure 36 for the investigated solvents in the Aspen Plus desorber model.
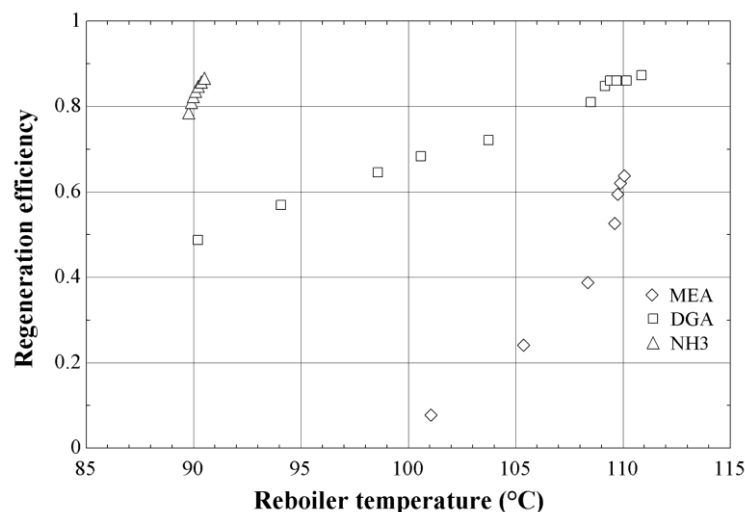


**Figure 36.** Regeneration efficiency for the investigated solvents at different reboiler temperatures.

So, even if no salt formation occurs and the ammonia solvent is thermally regenerated in an absorber–desorber arrangement, the much lower absorption temperatures (due to the reactions between the $CO_2$ and the solvent) imply much lower energy requirements for solvent regeneration as compared to MEA and DGA.

Using low concentrations of ammonia in the solution for $CO_2$ removal proved to be a good compromise between high removal efficiency and low ammonia losses with the exhaust gas stream. Any capture process using ammonia, either by salt production or in an absorber–desorber configuration, benefits clearly from lower temperatures. This greatly reduces ammonia losses from the absorber and hence the necessary energy input for emission reduction. However, the energy requirements for cooling the solvent and the absorber remain to be investigated. The production of fertilizers using the ammonia salts produced in the aforementioned process would of course lead to implications on the fertilizer market and on the producers of these fertilizers. This option will therefore only be implemented until the level of demand for fertilizers is met and probably in cooperation with the fertilizer producers, which this way could obtain an economical base ingredient from the power plant sector [90].

## 3.2. Rate-based post-combustion capture models

In order for the simulations of $CO_2$ capture to be more realistic, the kinetics of absorption has to be taken into account. With reaction kinetics, equipment sizing becomes a factor as well. Here, the performance of MEA and ammonia at two different solvent temperatures were compared with respect to their performance as solvent for $CO_2$ capture. Both solvents are thermally regenerated in a stripper column. Extra care has been taken to reduce solvent emissions to the environment [51, 96].

### 3.2.1.  PC power plant for rate-based post-combustion capture models

The same 500 MW PC power plant as described previously (see 3.1.1) served as basis for the investigation of the rate-based $CO_2$ capture models.

### 3.2.2.  Rate-based post-combustion $CO_2$ capture with ammonia

Although ammonia has a high loading capacity, the kinetics of $CO_2$ absorption is relatively slow. Thus, reaction kinetics should be taken into account in the absorption simulations.

Figure 37 shows the flow sheet for the modelled capture process. The cleaned flue gas passes through a cooler of circulating cold water, where contaminants such as HCl and HF get washed out. Another advantage is the removal of excess water and the reduction of the volume of the flue gases, which helps save energy for the flue gas blower (not presented in Figure 37). In order to save energy for the compression of the captured $CO_2$ and for the reduction of ammonia losses from the desorber, the stripper column operates at a higher pressure (2 bar). The $CO_2$ rich solvent gets preheated by the hot lean solvent leaving the desorber. This regenerated solvent needs to be cooled further to the operating temperature of the absorber column. Before re-entering the absorber, losses of water and ammonia have to be compensated for. Ammonia leaving at the top of both columns is washed out with water in additional packed columns. Since also $CO_2$ gets washed out this way, another desorption process is necessary to remove it. The remaining water containing the dissolved ammonia has to be sent to further treatment. In the simulations it was not possible to separate ammonia and water to satisfying levels in a stripper column. The energy necessary for this water treatment is not included in this study. Four of the capture installations as shown in Figure 37 are necessary for the removal of $CO_2$ from the flue gas stream. Their absorber heights and column diameters are 35 m and 11 m, respectively.
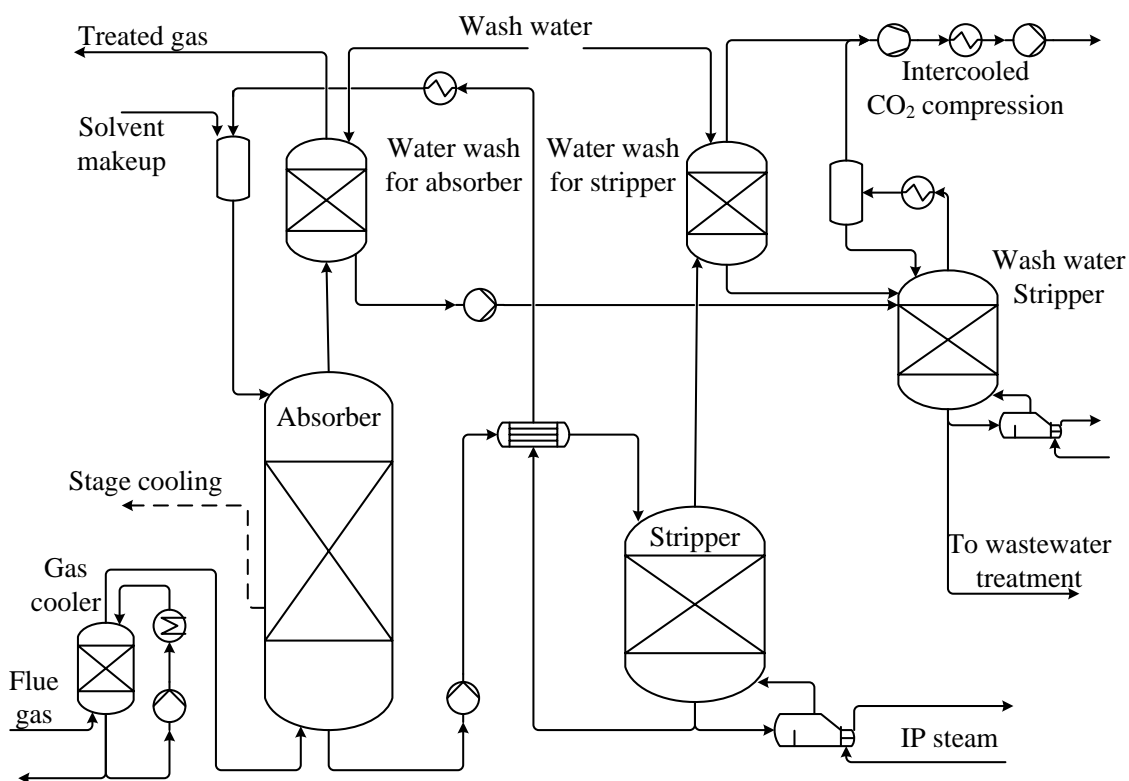
**Figure 37.** Flowsheet for rate-based model of $CO_2$ removal with ammonia solvent.

The same reactions as presented in the chapter on equilibrium models for $CO_2$ capture with ammonia have been used here. However, the components' property parameters and the absorber model were updated for the inclusion of kinetics. Due to the presence of ionic species, the electrolyte NRTL activity coefficient model is used for the liquid phase and the Redlich-Kwong equation of state for the vapour phase.

In order to achieve good absorption and to keep ammonia losses to a minimum, it is necessary to maintain a low temperature inside the absorber. Therefore intercooling at 80% from the top of the column is necessary. The solvent also needs to be cooled before entering the absorber from the top. Due to the slow kinetics of the absorption reactions with ammonia, the absorber column still has to be very tall. Without intercooling, using a taller absorber column does not improve absorption sufficiently in this case, and the absorption efficiency of the process drops from 90% to 80% with all other parameters unchanged. A comparison of the resulting temperature and absorption rate profiles (along the absorber axis Z) inside the absorber columns is shown in Figure 38 for a normal absorber column and in Figure 39 for the intercooled absorber.
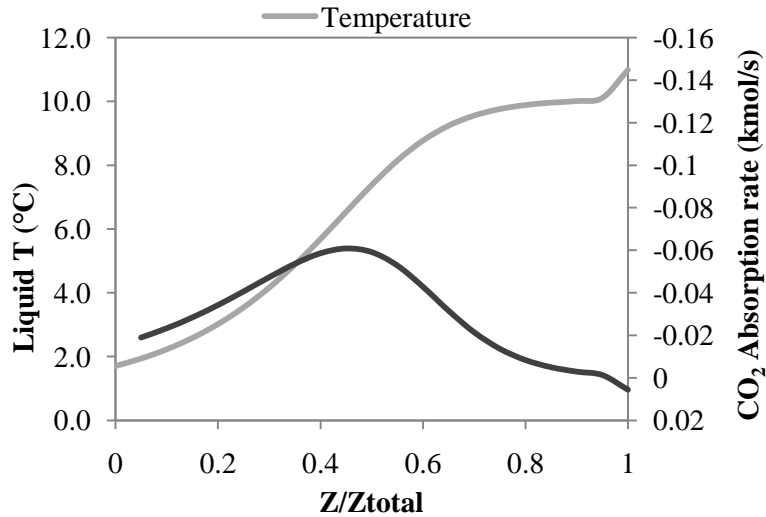
**Figure 38.** Temperature and absorption rate in absorber column with $NH_3$ solvent (T = 1.7 °C).

It can be seen for the not intercooled absorber that even desorption of $CO_2$ takes place at the lower end of the column, if there is no intercooling.
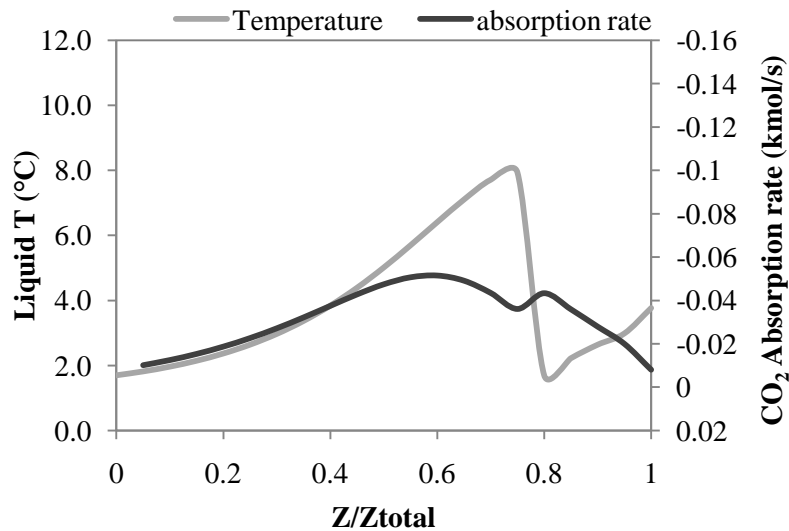


**Figure 39.** Temperature and absorption rate in intercooled absorber with $NH_3$ solvent (T = 1.7 °C).

For the intercooled absorber column, the absorption rate is maintained high along a much larger part of the column. Therefore, the absorber is used much more efficiently.

For ammonia, solvent performance improves at lower temperatures. Chilled ammonia as an option for post-combustion $CO_2$ capture was patented [97] in 2006 by Alstom. Alstom proposes a solvent temperature of 1.7 °C [98].

However, at these low temperatures cooling the solvent and intercooling the absorber column leads to a very significant energy penalty. We therefore investigated an alternative process with a sol-

vent temperature of 20 °C. The necessary solvent flow has to be higher, of course, since the loading capacity of the solvent is lower at this temperature. There is also an increase in the requirements for solvent makeup, wastewater treatment and above all for heat input to the stripper columns. The overall energy penalty of this capture process is discussed in a later section.

For this chilled ammonia process (CAP), the $CO_2$ loading of the lean stream should preferably be in the range of 0.33 to 0.67 mol of $CO_2$/mol of ammonia, and for the rich stream between 0.67 and 1 mol/mol [99]. In the rate-based simulations here, values at the lower end were found. A lean loading of 0.32 proved to lead to the lowest energy penalties. This lean loading resulted in rich loadings of 0.5 for the solvent temperature of 1.7 °C and 0.5 for 20 °C, both for a $CO_2$ capture rate of 90%.

A higher desorber pressure reduces ammonia losses and energy requirements for the compression of the captured $CO_2$, since the pressure is raised by pumping the rich solvent and not by gas compression. A pressure at the lower end of the recommended range was chosen here due to the size of the equipment.

In order to find the ideal solvent concentration for the capture process, the author investigated the necessary solvent flow rate to achieve a given $CO_2$ removal efficiency. With constant lean loading, solvent flow was varied for different solvent concentrations. Figure 40 shows the influence of ammonia solvent flow and concentration on $CO_2$ removal efficiency in one of the four absorbers necessary for the decarbonisation of the flue gas from the pulverised coal power plant. It can be observed that due to elevated losses, absorption efficiency is not improved for higher solvent concentrations. The ideal ammonia concentration was found to be 7.1 %wt.
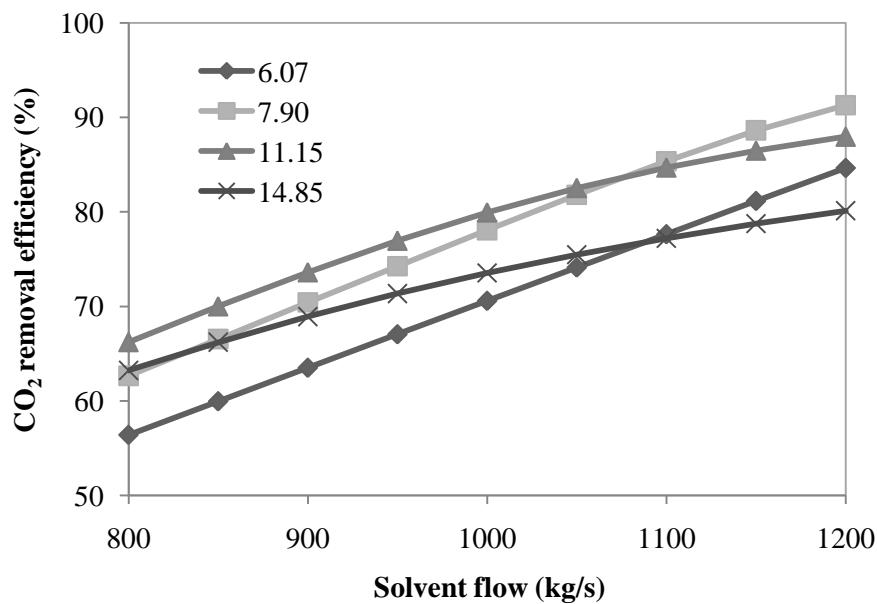


**Figure 40.** Removal efficiency for different solvent flows (T = 1.7 °C) and concentrations (% wt.).

In Figure 41 the influence of reboiler duty on the behaviour of one desorber (of four) is presented for the base solvent concentration of 7.1 %wt.. Based on the final simulation for 90% $CO_2$ capture, the reboiler duty was varied for unchanged properties of the incoming $CO_2$ rich stream. In the base case, a reboiler duty of 103.5 MW was needed to reach a bottom temperature of 100.5 °C in one of the four stripper columns.
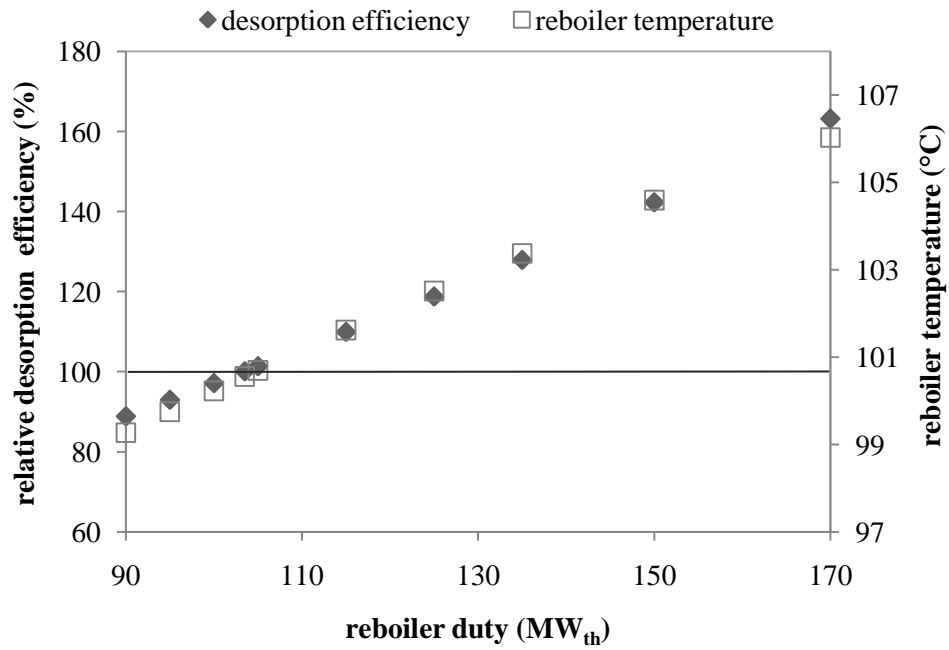


**Figure 41.** Relative $NH_3$ desorption eff. for varying desorber conditions compared to base case.

The key parameters and results of the capture installations with the ammonia solvent are presented in Table 33 for the two temperature cases.

**Table 33.** Key parameters of $CO_2$ capture installation (one of four) with ammonia solvent.

| | | |
|---|---|---|
| Lean solvent flow and solvent concentration | 1336 kg/s, 7.1 %wt. | 1596 kg/s, 7.1 %wt. |
| Gas inlet and solvent temperature | 25 °C, 1.7 °C | 25 °C, 20 °C |
| Lean loading | 0.318 mol/mol | 0.313 mol/mol |
| Rich loading | 0.493 mol/mol | 0.450 mol/mol |
| Column packing | Flexipac 1Y, 80% flooding | Flexipac 1Y, 80% flooding |
| Pressure, height and diameter of absorber column | 1.1 bar, 35 m, 10.7 m | 1.1 bar, 35 m, 11.2 m |
| Pressure, height and diameter of stripper column | 2 bar, 3 m, 6.8 m | 2 bar, 3 m, 7.7 m |
| Solvent makeup – ammonia, water | 1.253 kg/s, 4.450 kg/s | 1.880 kg/s, 6.260 kg/s |
| Wash water flow and temperature | 70 kg/s, 15 °C | 87 kg/s, 15 °C |
| Chilling for solvent and absorber intercooling | -86.7 $MW_{th}$ | -30.1 $MW_{th}$ |

### 3.2.3. Rate-based post-combustion $CO_2$ capture with MEA

Due to its higher molecular mass MEA has a lower mass loading capacity than ammonia, and it has to be regenerated at higher temperatures.

Based on equilibrium models, an ammonia concentration of 28 %wt. was found to lead to the least energy penalties at a rich loading of 0.67 mol/mol [100]. However, the low molecular mass of ammonia also facilitates its release with the treated gas from the absorber column, which makes it necessary to use ammonia in relatively low concentrations of around 8 %wt.

As a compromise between high capture efficiency and solvent losses, which both increase with solvent concentration, Liu *et al.* [101] recommend a solvent with 5 to 10 %wt. of ammonia. Therefore, as presented in Figure 42, the capture efficiency of MEA and ammonia is very similar on a molar basis. The data presented here were obtained from the $CO_2$ capture models discussed in this thesis. Starting with a capture efficiency of 90%, the composition (and thus the lean loading) of the lean solvent to the absorber was held constant. Then the solvent flow was reduced down to a $CO_2$ removal efficiency of 50%.
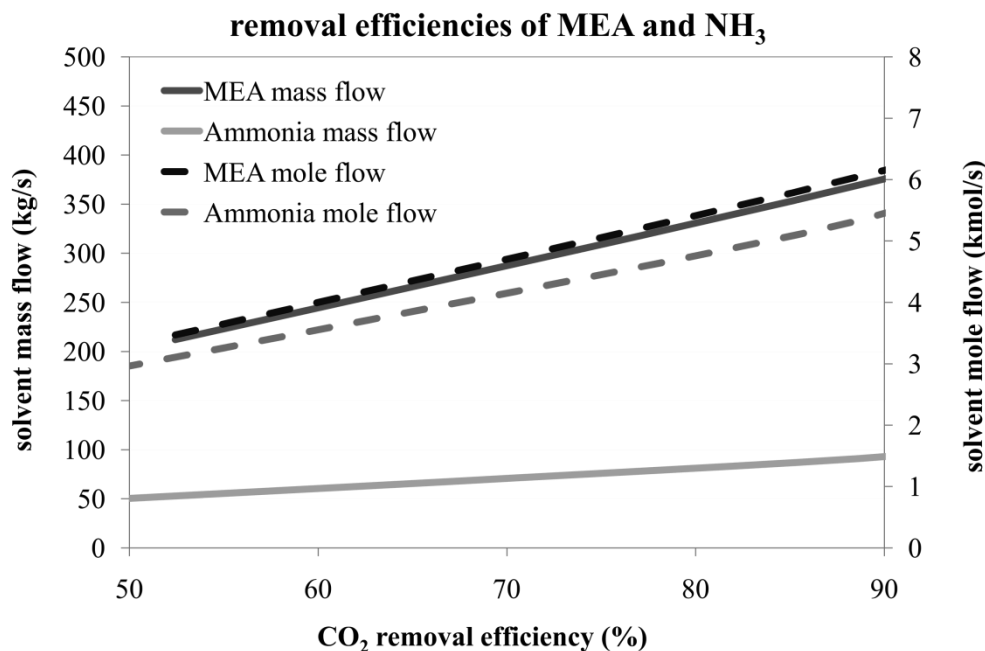


**Figure 42.** $CO_2$ removal efficiency for different molar and mass flows of ammonia and MEA.

Plaza *et al.* carried out experiments with different concentrations of MEA, DEA and ammonia in aqueous solution in a stirred reaction tank to determine the absorption rates of $CO_2$ at different temperatures. The ammonia solution (3 %wt. $NH_3$) showed an absorption rate, which was around half the rate obtained with the MEA solvent (30 %wt. MEA). This means that the absorption columns can be much smaller for capture operations with MEA. Esber [102] quotes G.T. Rochelle who gives a fac-

tor of 3 for the difference in necessary absorber heights when comparing ammonia and MEA as solvent. In my study, the absorbers had half the height of the absorbers used for the ammonia process, for which we assumed 35 m to be the maximum absorber height. However, the necessary absorber height for the capture process with MEA was found to be 2-3 times the height determined by Plaza *et al.* [103]. There, a three-stage flash configuration was compared to a conventional stripper. The three-stage flash stripper showed significantly better performance. This may be due to the usually slim stripper columns. In my simulations, however, it proved advantageous to use a desorber of low height and big diameter in agreement with a similar stripper design described in the work of Ziaii *et al.* [104]. Energy savings similar to the one reported in the work of Plaza *et al.* for the flash configuration could then be observed. A lower stripper allows for higher temperatures throughout the column and prevents re-absorption of the released $CO_2$ into the solvent. For the same reason condensed liquid on top of the stripper is not led back to the stripper but flows directly back to the washing section on top of the absorber. There, the liquid almost completely absorbs the MEA leaving with the gas stream and also supports the operation of the absorber. In contrast, Alie *et al.* found the necessary reboiler duty to decrease with increasing stripper height [72].

The capture process with MEA using the flowsheet simulation program Aspen Plus including reaction kinetics was previously modelled by Freguia [105], using kinetic data by Dang [106] modifying VLE data by Austgen [107], and including data by Jou *et al.* [108]. This work was further modified by Ziaii [109] by the inclusion of kinetic data that were obtained by Aboudheir [110] in experiments with a laminar jet. At the University of Texas at Austin, a model was developed that is based on a rigorous thermodynamic model by Hilliard [111] and Aboudheir kinetics. This electrolyte-NRTL model and vapour-liquid equilibrium (VLE) data that were adjusted to pilot plant data [103] are used here to model this system. It differs from previous models by including additional data on amine vapour pressure, enthalpies of absorption, heat capacity, and speciation. To guarantee thermodynamic consistency, Gibbs free energy and enthalpy values within Aspen plus were used for the calculation of chemical equilibrium. The reactions in Table 34 were used for this rate-based model of $CO_2$ absorption with MEA.

**Table 34.** Rate constants for kinetic reactions (Plaza *et al.*).

| Reaction | k | E | |
|---|---|---|---|
| $2\,MEA + CO_2 \rightarrow MEAH^+ + MEACOO^-$ | $4.734 \cdot 10^9$ | 19,342 kJ/kmol | (46a) |
| $MEAH^+ + MEACOO^- \rightarrow 2\,MEA + CO_2$ | $4.228 \cdot 10^5$ | 107,470 kJ/kmol | (49) |
| $MEA + CO_2 + H_2O \rightarrow HCO_3^- + MEAH^+$ | 9025 | 49,000 | (47a) |
| $HCO_3^- + MEAH^+ \rightarrow MEA + CO_2 + H_2O$ | 3113 | 112,736 | (48) |

$$r = k \cdot T^n \cdot \exp\left(-\frac{E}{RT}\right) \cdot \prod_{i=1}^{N} \left(\text{mole-frac}_i \cdot \alpha_i\right)^{a_i}, \quad \text{T in Kelvin}$$

In Figure 43 the schematic diagram of the Aspen Plus capture model with MEA is shown.
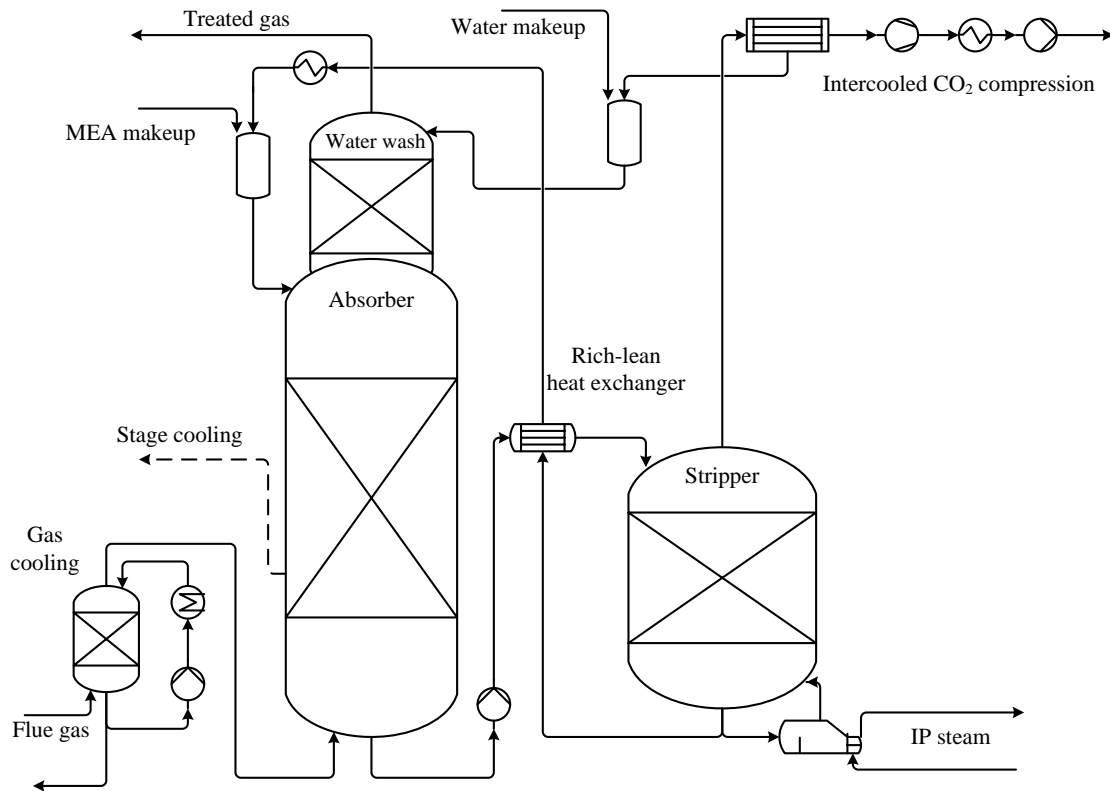


**Figure 43.** Flowsheet for rate-based model of $CO_2$ removal with MEA.

The key parameters and results of one of four necessary capture sections are presented in Table 35. They include the column sizes and solvent parameters such as loadings, losses and required makeup.

**Table 35.** Key parameters of $CO_2$ capture installation (one of four) with MEA solvent.

| | |
|---|---|
| Lean solvent flow and solvent concentration | 1204 kg/s, 31 %wt. |
| Gas inlet and solvent temperature | 40 °C, 40 °C |
| Lean loading | 0.400 kmol/kmol |
| Rich loading | 0.513 kmol/kmol |
| Column packing | Flexipac 1Y, 80% flooding |
| Pressure, height and diameter of absorber | 1.1 bar, 18 m, 10.2 m |
| Height and diameter of wash section of absorber | 4 m, 6.4 m |
| Pressure, height and diameter of stripper | 1.6 bar, 4 m, 6.6 m |
| Solvent makeup – MEA | 0.224 kg/h for losses, 161 kg/h due to degradation [71] |
| Solvent makeup – water | 0.32 kg/s |

In [103], a lean loading of 0.4 mol/mol was shown to present the least energy penalty in $CO_2$ capture with MEA. Other studies found a lean loading of 0.25 mol/mol [72] or of 0.32 mol/mol [71] to give the least energy requirements for solvent regeneration. In agreement with literature, a lean loading of 0.3 mol/mol was found this study to give the minimum necessary reboiler duty for solvent regeneration. However, a hydraulic and a thermal analysis of the absorber revealed that i) more solvent flow is necessary to prevent liquid being carried out at the top of the absorber and ii) that otherwise stage temperatures above 76 °C can be found. Therefore, a lean loading of 0.4 was chosen here. For good absorption, it is necessary to maintain a low temperature inside the absorber. A solvent and gas inlet temperature of 40 °C was found to give the best results.

In order to achieve this solvent temperature inside the absorber, intercooling at 80% from the top of the column is necessary here as well. A comparison of the temperature and absorption rate profiles inside the absorber columns is shown in Figure 44 for a normal absorber column and in Figure 45 for the intercooled absorber.
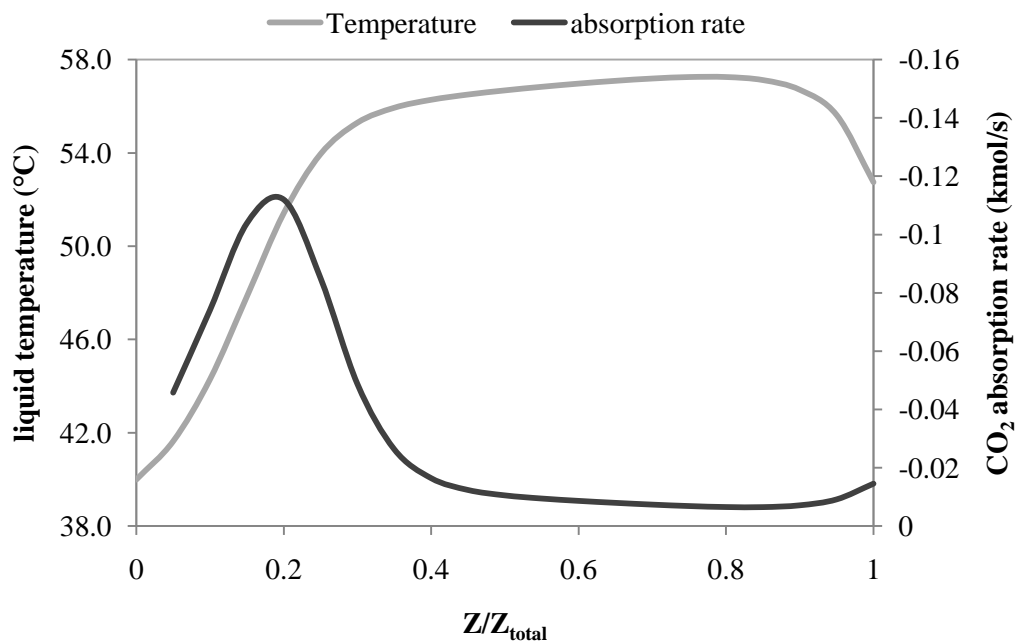


**Figure 44.** Temperature and absorption rate profiles in absorber column with MEA solvent.
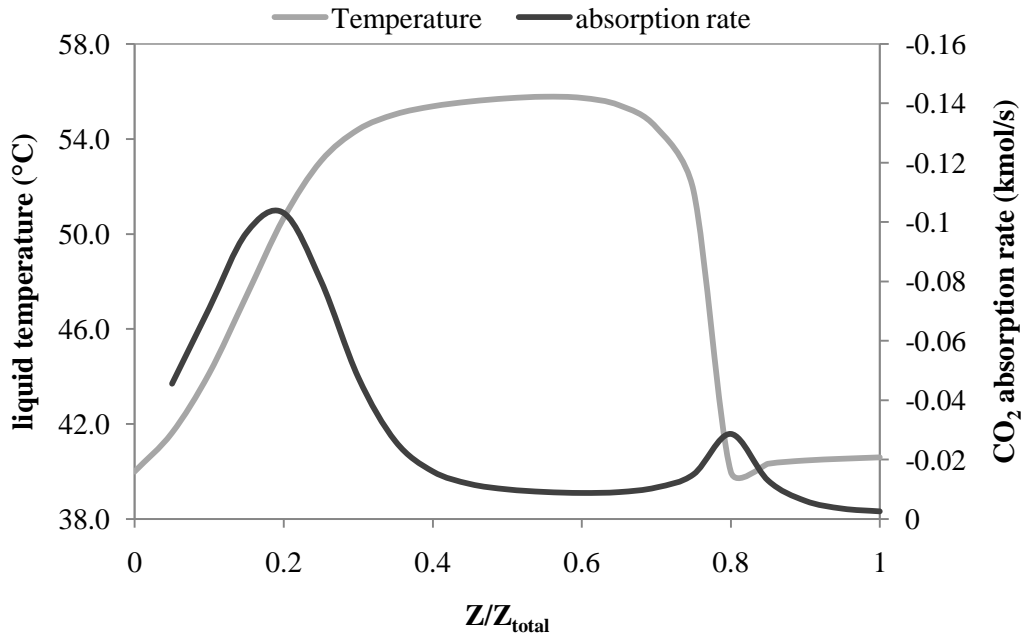
**Figure 45.** Temperature and absorption rate in intercooled absorber column with MEA solvent.

As shown in Figure 40 for ammonia, the ideal solvent concentration was investigated for the capture process with MEA. Figure 46 shows the influence of MEA solvent flow and concentration on $CO_2$ removal efficiency in one of the four absorbers necessary for the decarbonisation of the flue gas from the pulverised coal power plant. It can be observed that in this variation of the base case, compared to the ammonia process, less solvent flow is necessary to achieve a $CO_2$ capture efficiency of 90%.
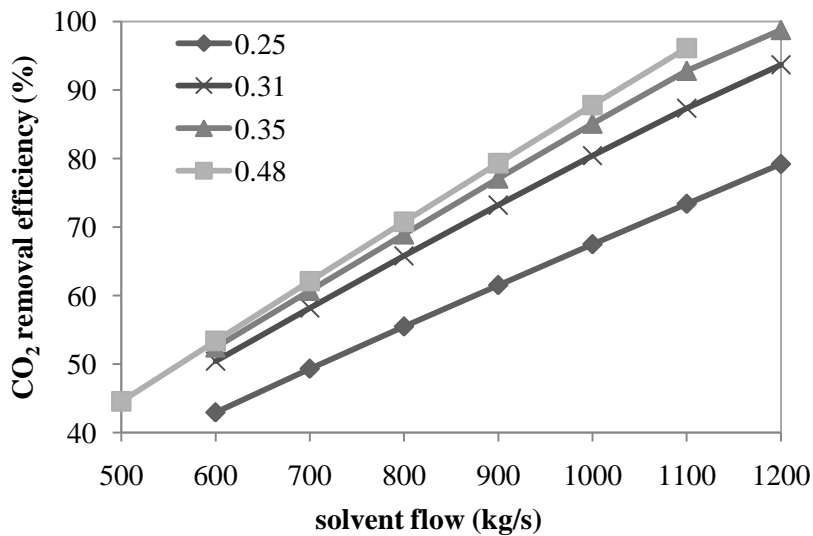


**Figure 46.** $CO_2$ removal efficiency for different solvent flows and MEA concentrations (% wt.).

Higher concentrations than ca. 40% wt. do not significantly reduce the necessary solvent flow rate for a desired removal efficiency. A higher solvent concentration, however, leads to elevated losses of solvent with the gas stream from the absorber. This makes it necessary to raise the flow rate of the wash water stream, which in turn dilutes the solvent. A compromise solvent concentration was found to be in the range of 30-40 %wt. In Figure 47 the influence of reboiler duty on the behaviour of one of the four desorbers is presented for the base case solvent concentration of 31 %wt. The MEA concentration of 31 %wt. required a 10 percent higher solvent flow than achieved with a solvent concentration of 35 %wt. However, due to possible degradation issues, this lower solvent concentration was chosen for this study.

Based on the final simulation for 90% $CO_2$ capture, the reboiler duty was varied for unchanged properties of the incoming $CO_2$ rich stream. In the base case, a reboiler duty of 113.5 MW was needed to reach a bottom temperature of 106.8 °C in one of the four stripper columns. This means that even though the necessary solvent flow rate for 90% $CO_2$ capture was lower than in the case of the ammonia solvent with a temperature of 1.7 °C, the necessary reboiler duty was higher for sufficient solvent regeneration.
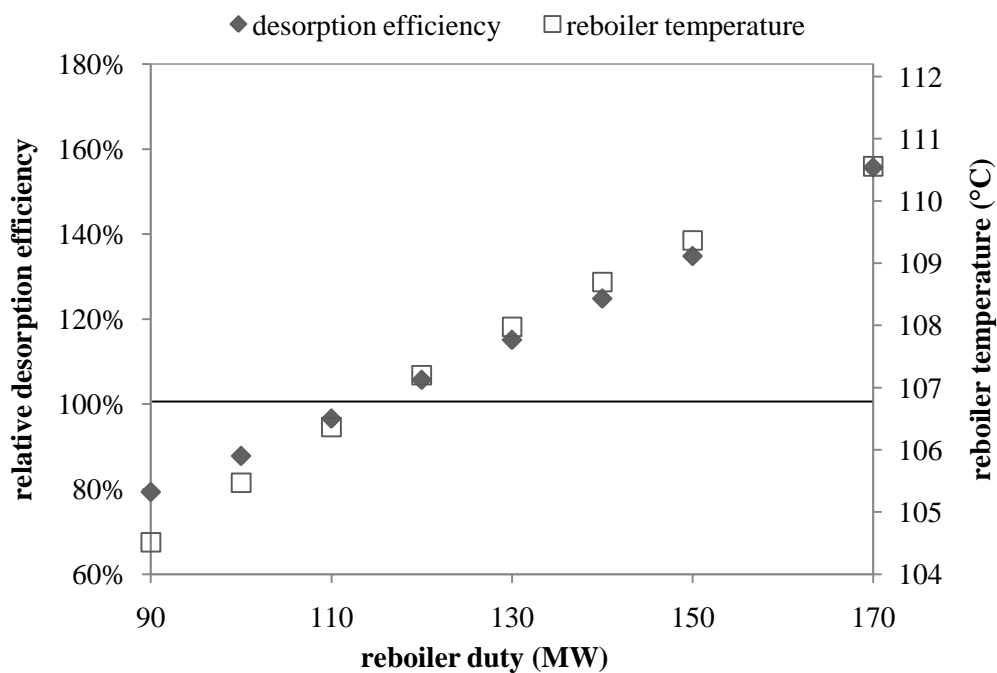


**Figure 47.** Relative MEA desorption eff. for varying desorber conditions compared to base case.

Data for the streams entering and leaving the capture sections with the solvents MEA and ammonia at the two investigated solvent temperatures (see 3.2.2) are presented in Table 36.

**Table 36.** Stream data for post-combustion $CO_2$ capture with MEA and ammonia.

| | MEA | | | Ammonia at 1.7 °C | | | | Ammonia at 20 °C | | |
|---|---|---|---|---|---|---|---|---|---|---|
| | flue gas | treated | $CO_2$ | flue gas | treated | $CO_2$ | waste | treated | $CO_2$ | waste |
| Temperature in °C | 39.9 | 40.6 | 28.5 | 25 | 1.8 | 27.9 | 100.9 | 20.4 | 27.98 | 104.9 |
| Pressure in bar | 1.19 | 1.1 | 110 | 1.19 | 1.1 | 110 | 1.9 | 1.1 | 110 | 1.9 |
| Mass Flow in kg/sec | 590.16 | 471.72 | 108.36 | 567.64 | 448.00 | 107.20 | 230.84 | 446.05 | 108.04 | 285.68 |
| Mole Fractions | | | | | | | | | | |
| $H_2O$ | 0.0875 | 0.0699 | 0.0023 | 0.027 | 0.006 | 0.002 | 0.968 | 0.007 | 0.0022 | 0.964 |
| $CO_2$ | 0.1357 | 0.0153 | 0.9976 | 0.145 | 0.011 | 0.996 | 35 ppm | 0.008 | 0.9965 | 97 ppm |
| $N_2$ | 0.7439 | 0.8761 | 132.7 ppm | 0.793 | 0.941 | 0.001 | trace | 0.944 | 0.0011 | trace |
| $O_2$ | 0.0329 | 0.0387 | 11.1 ppm | 0.035 | 0.042 | 114 ppm | trace | 0.042 | 100 ppm | trace |
| $NH_3$ | -- | -- | -- | -- | 595 ppb | trace | 0.032 | 1.1 ppm | trace | 0.036 |

$CO_2$ capture with MEA leads to a greater purity of the $CO_2$ stream. Higher temperatures in the capture process lead to a reduced absorption of the lighter gas components and thus to a lower concentration of these components in the captured stream.

### 3.2.4.  Influence of post-combustion capture (rate-based) on PC power plant performance

In power plants with post-combustion capture it is important to also consider process changes necessary for the solvents to function properly. For example, $NO_X$ and $SO_X$ levels have to be reduced to very low levels [30] upstream of the $CO_2$ capture section, in order to prevent MEA degradation. This, however, introduces an additional energy penalty to the power plant. With ammonia, these contaminants can be captured by the solvent [75]. They would eventually end up in the separated $CO_2$ stream, however, where they may have to be removed to prevent equipment damage due to acid formation. The amount of the ammonia salts $(NH_4)_2SO_4$ and $NH_4HCO_3$ that precipitate under realistic conditions in the chilled ammonia process remains to be investigated. These salts could be used for fertilizer production [90].

However, all options studied here assume the same amount of flue gas desulphurisation and denitrification prior to $CO_2$ capture and in the power plant without $CO_2$ capture.

The choice of the different capture configurations leads to different impacts on the power plant, mainly due to the difference in the energy requirements for solvent regeneration in a stripper column, for which steam is extracted after the medium pressure turbines. The main parameters for power plant performance without $CO_2$ capture and for a $CO_2$ removal efficiency of 90% are presented in Table 37.

Ciferno *et al.* [81] investigated the use of aqueous ammonia for $CO_2$ capture and for multi-pollutant capture based on the Powerspan ECO® process [112], in which the fertilizers $(NH_4)_2SO_4$ and $NH_4NO_3$ are produced by reaction with the $SO_2$ and the $NO_2$ in the flue gas. The energy penalty found there for both cases was about half the penalty found in this study and therefore lower than for the capture option with MEA. However, ammonia losses were not considered in [81] and energy requirements were calculated with the heat of reaction of only three basic equilibrium reactions. No steam extraction for solvent stripping was assumed to be necessary.

If $SO_X$ and/or $NO_X$ removal with the ammonia solvent are included, this would lower the energy penalties for the ammonia process due to a reduction of the energy consumption in the flue gas desulphurisation (FGD) section compared to the $CO_2$ capture with MEA. However, the minimum achievable penalty would then still be somewhat higher than the penalty introduced by the MEA process. Fisher et al. [113] proposed the heat integration of the $CO_2$ compressor with the reboiler of the stripper column and obtained energy savings of 5% or 13 $MW_{el}$. Even more significant savings were possible by integrating the flue gas cooling with the stripper column. Therefore both heat sources were used in the simulations to minimize the energy penalty due to $CO_2$ capture [51].

Although ammonia is a more economical solvent, its slow kinetics makes very large absorber towers necessary, as resulted from the simulations (see 3.2.2). Additional absorbers are necessary to limit ammonia emission to the atmosphere. Solvent chilling and emission reduction lead to further

energy penalties, so that despite the good qualities of ammonia as an absorbent for $CO_2$, the absorption with MEA is the more economical option here.

**Table 37.** Parameters for 500 MW PC power plant with and without $CO_2$ capture.

| Gross power plant output: 517 MW$_{el}$ | No Capture | Capture with MEA | Capture with NH$_3$ (1.7 °C) | Capture with NH$_3$ (20 °C) |
|---|---|---|---|---|
| Blower and pump work for FGD in MW$_{el}$ | 21.6+2.2 | 21.6 + 2.2 | 21.6 + 2.2 | 21.6 + 2.2 |
| Reboiler duty (including ammonia wash) in MW$_{th}$ | -- | 454 | 414 + 56 | 540 + 72 |
| Heat integration of gas cooling to reboiler in MW$_{th}$ | -- | 123 | 127 | 125 |
| Heat integration of $CO_2$ compr. to reboiler in MW$_{th}$ | -- | 47 | 47 | 47 |
| Penalty for remaining steam extraction in MW$_{el}$ | -- | 67 | 70 | 104 |
| Flue gas blower and pump work in MW$_{el}$ | -- | 9 | 9 | 9 |
| $CO_2$ compression in MW$_{el}$ | -- | 31 | 26 | 26 |
| Solvent chilling in MW$_{el}$ (COP of chiller = 4.5) | -- | -- | 92 | 31 |
| Energy savings due to heat integration in MW$_{el}$ | -- | 41 | 41 | 40 |
| Power plant net output in MW$_{el}$ | 493 | 386 | 296 | 323 |
| Power plant efficiency (HHV-based) | 36.3% | 28.4% | 21.8% | 23.8% |
| Energy penalty for $CO_2$ capture in MW$_{el}$ | -- | 107 | 197 | 169 |
| Specific energy penalty in GJ$_{el}$/t | -- | 1.00 | 1.84 | 1.58 |
| Specific $CO_2$ production in kg/MWh | 868.2 | 110.9 | 144.6 | 132.5 |
| Effective $CO_2$ removal | -- | 87.2% | 83.3% | 84.7% |

As the simulation results show, the necessary additional gas treatment for the limitation of ammonia emission introduces a significant energy penalty. For $CO_2$ capture with ammonia at 1.7 °C, this leads to a combined reboiler duty that is more elevated than in case of capture with MEA. At the higher solvent temperature, the increase in solvent flow and release of ammonia from the absorber lead to a further increase in reboiler requirements. This penalty can be reduced by eliminating the stripper column for the separation of $CO_2$ from the solvent wash. However, the same capture efficiency could only be achieved with higher solvent flows and increased energy for solvent cooling and reboiler duty in the main stripper. $CO_2$ compression is less energy intensive in case of the ammonia processes due to the lower temperature of the released $CO_2$.

Solvent chilling presents the biggest energy penalty in case of the model with the lower solvent temperature for $CO_2$ capture with ammonia. The combined cooling effect of cooling water and chiller reduces this penalty to about a third for the 20 °C ammonia solvent. Overall energy penalty due to $CO_2$ capture is significantly larger for use of the ammonia solvent compared to MEA. Therefore, the effective $CO_2$ removal is also reduced, although all options have a nominal capture efficiency of 90%.

Introduction of absorption kinetics lead to higher solvent flows that need to be cooled for the absorber and heated for stripping. The slower absorption rate with ammonia makes it necessary to use very tall absorber columns. Together with the extra equipment for the ammonia wash, this leads to elevated investment costs compared to $CO_2$ capture with MEA [51, 96].

It should, however, be mentioned that a VLE model for the chilled ammonia process described by Valenti *et al.* [99] reports a specific energy penalty, which is about 2.4 times lower than the values given here, although cooling was considered to be achieved with compression chillers.

# 4. Oxy-fuel combustion

A completely different approach to $CO_2$ capture eliminates the need for solvent processes. The application of oxy-fuel technology as retrofit option for existing power plants was reported to be technically feasible and at costs comparable to other $CO_2$ capture technologies [114]. In that respect it is similar to the previously described post-combustion capture. Only minor burner modifications, a new oxygen injection system and a new flue gas recycle line are needed [12]. The high temperature of the recycled gas stream leads to an increase in the thermal efficiency of the boiler. However, boiler modifications are more complex due to the need to reduce air leakage to a minimum.

The Oxy-fuel process uses the energy of the fuel by combusting it with pure oxygen, effectively reducing the nitrogen content and thus the mass flow of the flue gas that has to be treated. Since combustion with pure oxygen leads to combustion temperatures of 3500 °C, the $CO_2$ rich flue gas has to be recycled to keep the temperature within the limits, which are about 1300-1400 °C for gas turbines and about 1900 °C for coal-fired boilers [12]. Conditions similar to fuel burning with air lead to a nearly complete combustion [115] with very low excess oxygen levels of only 1-3% [12]. The flue gas stream is therefore mainly composed of $CO_2$ and water. Air leakage, not completely pure oxygen and fuel inerts lead to impurities in the flue gas stream such as $NO_X$, $SO_X$, HCl and Hg as well as the inerts nitrogen and argon. Due to the lack of nitrogen in the feed gas, the formation of $NO_X$ is greatly reduced [116], leading to reductions of up to 75% when compared to burning with air [117]. The inclusion of an SCR section can thus be often avoided as was done in the investigated model.

A key process step in the oxy-fuel technology is the necessary production of nearly pure oxygen, which has a major influence on power plant efficiency. Technologies for $O_2$ production from air separation are cryogenic distillation, pressure swing adsorption, and polymeric membranes. While for lower requirements multi-bed pressure swing adsorption may be economical, for larger applications such as power plants with an oxygen consumption of more than 200 t/d cryogenic air separation is the economic solution [114]. This technology is also used in pre-combustion capture for the gasification process. Oxygen production by distillation at cryogenic temperatures [118] has been used for more than 100 years [12].

Typically, in an air separation plant as shown in Figure 48, air is compressed to 50 to 60 bar and purified to remove water, $CO_2$, $N_2O$ and trace hydrocarbons that could otherwise accumulate to dangerous levels in oxygen-rich parts of the plant such as the reboiler condenser. This is usually achieved by switching fixed bed adsorbers with low pressure waste nitrogen as purge stream, where the absorbers are regenerated either by temperature or by pressure swing. To cool down the air stream the product nitrogen and oxygen streams are used in a multi-stream aluminium heat exchanger. The air stream is separated in a double distillation column with aluminium packing. Handling gas streams with oxygen levels above 40 %vol. must comply with strict rules for metals selection and vapour ve-

locity to avoid hazards. The introduced lighter inerts due to unavoidable air leakage need to be re-moved in the $CO_2$ purification section to produce sufficiently pure $CO_2$ for geological storage or EOR, so that designing the air separation unit for 95% pure oxygen instead of producing oxygen with 99.5% purity is more economical [119].
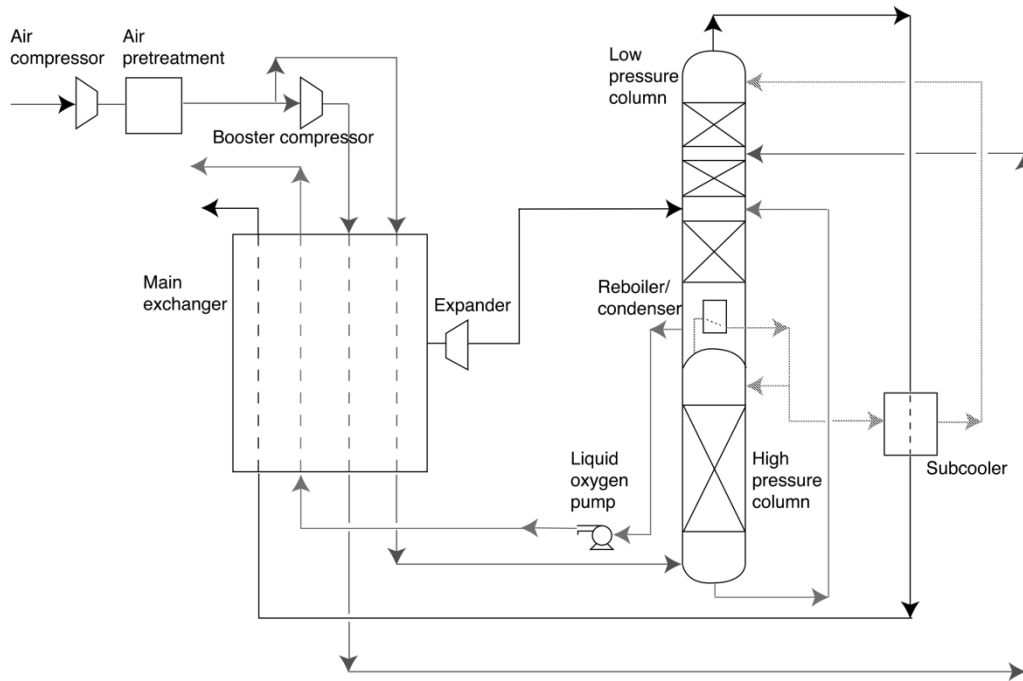


**Figure 48.** Cryogenic air separation unit [12].

After cooling, compression and drying of the flue gas stream, the impurities are separated from the $CO_2$ at low temperatures of about -55 °C. The product gas is usually composed of 96% $CO_2$, as well as nitrogen, argon, oxygen and $SO_2$. For storage, oxygen levels as well as $SO_X$ and $NO_X$ levels have to be very low. The required component concentrations in the $CO_2$ product stream are listed in Table 38. Especially the limit for oxygen levels is crucial, if the $CO_2$ stream is to be used in EOR. Higher oxygen levels may otherwise cause equipment damage.

**Table 38.** $CO_2$ purity issues for storage and for use in EOR [120].

| Components in product CO₂ stream | For storage | For EOR |
|---|---|---|
| $H_2O$ | < 500 ppm | < 50 ppm |
| $CO_2$ | > 90% | > 90% |
| $SO_2$ | from H&MB | < 50 ppm |
| NO | from H&MB | from H&MB |
| $O_2$ | < 4 % mol | < 100 ppm |
| $Ar + N_2 + O_2$ | < 4 % mol | < 4 % mol |

Regulations for on-shore and off-shore disposal of $CO_2$ are being drafted worldwide. A sensitive issue is the disposal of other wastes such as $SO_X$, $NO_X$ and Hg [120].

# 4.1. Oxy-fuel power plant

The third capture option investigated in this study is a 500 MW$_{el}$ Oxy-fuel power plant as presented in Figure 49 that uses the same coal type as the pulverised coal power plant with post-combustion $CO_2$ capture. The basic model was developed by Mitsui Babcock, Alstom Power, Air Products and the IEA GHG R&D programme [119]. This model served as basis for the investigation of $CO_2$ purification as described in the following subchapters [51].

In order to keep the temperature in the desired range, part of the flue gas is recycled to the boiler as the secondary recycle flue gas stream. In order to avoid ash accumulation in the boiler and damage to the recycle fan solids have to be removed in an ESP. The recycle stream must have a temperature of about 300 °C and may need to be premixed with oxygen to promote ignition. The excess level of oxygen needs to be in the range of 10-20% to ensure sufficient fuel burnout. The theoretical percentage of oxygen that needs to be added to the recycled gas stream would be in the range of 50 %vol. Due to material constraints, however, oxygen levels in the secondary recycle stream should not exceed 23 %vol. Therefore, additional oxygen is introduced separately to the boiler.
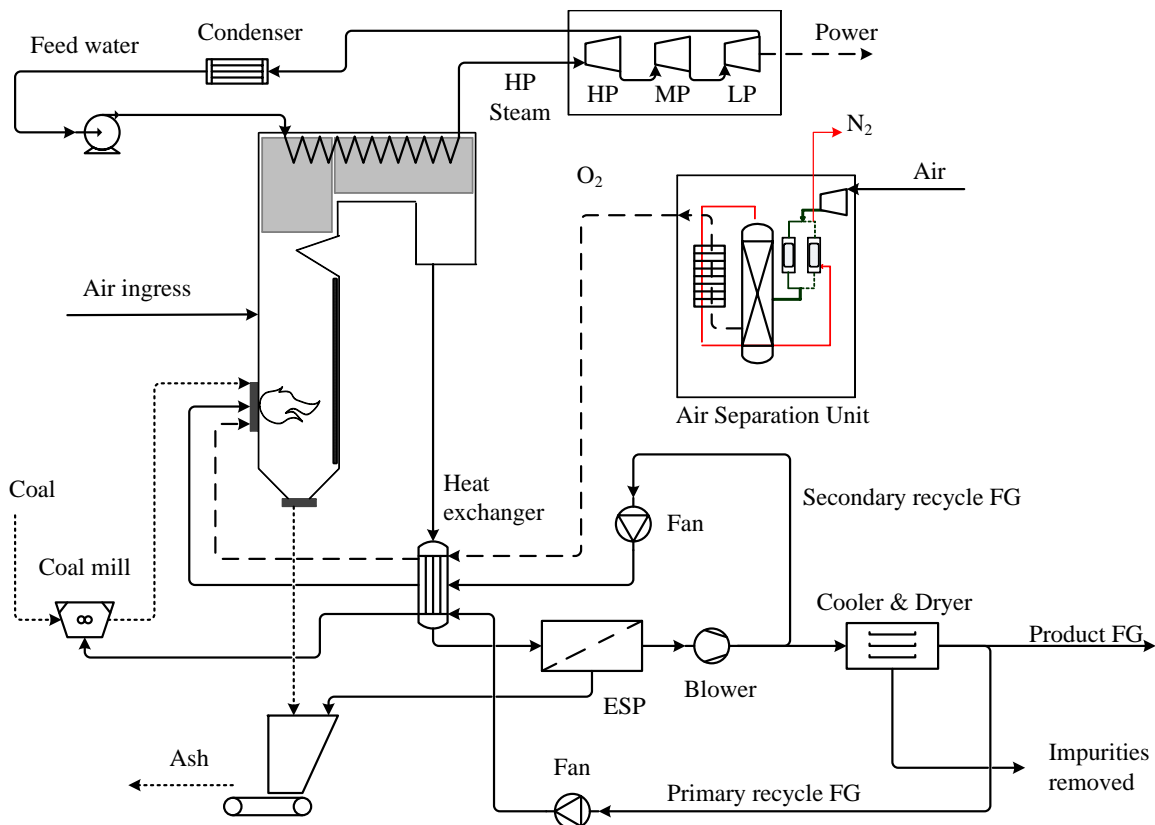


**Figure 49.** Schematic diagram of 500 MW ASC PC oxy-fuel power plant (after [119]).

After a first cooling and drying stage another part of the flue gas is recycled and used for the preheating and the transport of the coal to the boiler. This primary recycle needs to be cooled, and its moisture and acid gas components, e.g. $SO_3$ and HCl, need to be removed. Then the recycle is reheated before being fed to the coal mills. This stream has to be dry in order to be able to carry the coal moisture as vapour at low temperatures, since mill exit temperatures are limited to about 60-80 °C due to risk of ignition and possible coal melting. The temperature of this recycle is limited to 250-300 °C by the milling equipment. The flow of the secondary recycle stream is also very important to keep oxygen levels low in the primary recycle due to the risk of explosion in the coal mills [119].

Oxygen of about 95% is supplied by two trains of a three-column ASU with aluminium packing as presented in Figure 50 with two levels of air compression. Due to unavoidable air ingress, inerts always have to be removed in the $CO_2$ purification section. The increase in power to produce 99.5% pure oxygen is greater than the increase in power consumption for $CO_2$ compression there. The inclusion of a medium pressure column leads to a reduction in power consumption of ca. 10-12% down to 201 kWh/t, since it minimises the amount of air that needs to be compressed to high pressure [121].
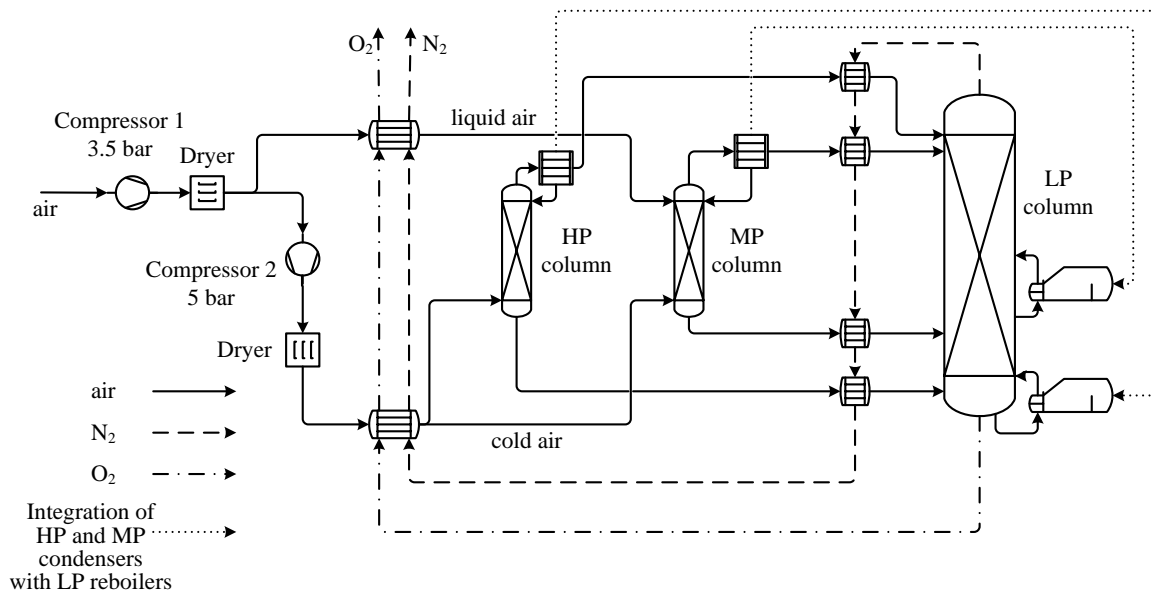


**Figure 50.** Three-column ASU with two levels of air compression (after [121]).

In order to prevent damage to the cryogenic equipment due to blockage or safety problems, water vapour, carbon dioxide and other trace hydrocarbons are removed in two dual bed adsorbers.

The main parameters of the IEA GHG 500 $MW_{el}$ oxy-fuel power plant including the ASU are shown in Table 39. These parameters were obtained by feedback from the authors simulation results for the flue gas stream to the already existing Excel model at the IEA GHG. Since $NO_X$ and $SO_X$ will be removed in the $CO_2$ purification section, there is no need for FGD and De-$NO_X$ processes in the

power plant. The actual power plant output and efficiency are discussed in a later section, where different $CO_2$ purification systems and their influence on plant performance will be compared.

**Table 39.** Oxy-fuel power plant parameters [122].

| | |
|---|---|
| Coal consumption | 55.54 kg/s |
| Heating value coal | HHV = 27.06 MJ/kg, LHV = 25.87 MJ/kg |
| Oxygen excess level | 12% |
| %wt. $O_2$ in the ASU | 94.45 |
| %wt. $N_2$ in the ASU | 1.72 |
| %wt. Ar in the ASU | 3.83 |
| $O_2$ stream supplied from ASU | 116.95 kg/s |
| Amount of air ingress | 23.29 kg/s (0.03 kg / kg of flue gas) |
| Total Flue Gas after the furnace / boiler | 772.66 kg/s |
| Primary recycled FG | 150.01 kg/s |
| Secondary recycled FG | 433.98 kg/s |
| Product Flue Gas | 165.94 kg/s |
| Impurities removed in cooler and dryer | $H_2O$ 21.64 kg/s, $SO_3$ 0.056 kg/s |

In order to optimise system performance feed water preheating is achieved by heat integration with heat rejection from air compressors in the ASU and with the $CO_2$ compressors. This reduces steam extraction from the low-pressure steam turbine and allows for a higher power output [119].

## 4.2. CO₂ flue gas pre-compression and purification

The product flue gas of the Oxyfuel power plant shown in Figure 49 contains about 72 %vol. $CO_2$ at atmospheric pressure. Before further drying and purification, the flue gas stream needs to be compressed to about 30 bar. Then all water is removed to prevent blockage in the successive cryogenic purification step. There the inerts are removed from the $CO_2$ by liquefying the $CO_2$ at around -55 °C.

Different patent applications by Air Products, Air Liquide, and by Praxair served the author of this thesis as basis for the development of Aspen Plus models of the described processes for $CO_2$ precompression and purification [51].

### 4.2.1. CO₂ flue gas pre-compression

Air Products have developed a method of $CO_2$ compression [123] that removes the heavier gas contaminants such as $SO_2$, $NO_X$, and Hg by reactive distillation in the presence of water and oxygen prior to the cryogenic $CO_2$ purification. In a first compressor, the flue gas is compressed adiabatically to 15 bar with no water removal as shown in Figure 51. Intercooling significantly reduces the work necessary for the compression of the gas stream. However, reduced intercooling to a gas outlet temperature of 307 °C allows for the use of this stream to heat up the inerts leaving the cryogenic purification section. These reheated inerts can then expand in a gas turbine in order to recover some of the compression energy.

After additional cooling down to 30 °C, the gas stream is fed to a distillation column where it is washed with a recycled condensate stream. In the distillation columns, which were modelled with RADFRAC blocks, the lead chamber reactions as listed in Table 40 take place. NO is oxidised to $NO_2$, which then oxidises $SO_2$ to $SO_3$ with NO acting as a catalyst. Then $SO_3$ is converted to sulphuric acid and $NO_2$ to nitric acid, while the formation of nitric acid only occurs after all $SO_2$ is converted. The pressure needs to be high for this process because reaction rate increases with pressure to the third power. Since the gas phase reactions already take place in the heat exchangers due to the high pressure, they have been modelled with RSTOIC blocks in Aspen Plus. For this section, the VLE model NRTL was applied, as this EOS resulted in gas compositions closest to the ones reported in the patent applications.
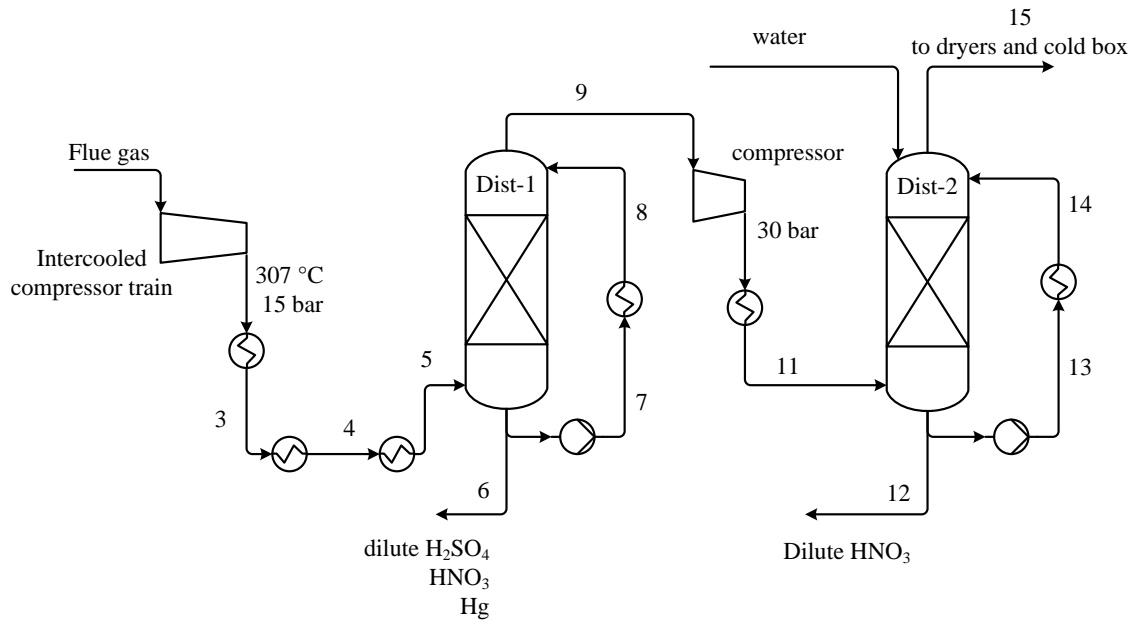
**Figure 51.** Reactive pre-compression of $CO_2$ (after [123]).


Before entering the second distillation column, the gas stream is compressed to 30 bar and cooled down again. Water needs to be added to make up for losses due to the removal of the diluted acids in the second column.


**Table 40.** Reactions in reactive compression with distillation [123].

| lead chamber reactions | phase | |
|---|---|---|
| $NO + 0.5\,O_2 \leftrightarrow NO_2$ | gas, slow | (48) |
| $NO_2 + SO_2 \leftrightarrow NO + SO_3$ | gas, fast | (49) |
| $SO_3 + H_2O \leftrightarrow H_2SO_4$ | liquid, fast | (50) |
| $2\,NO_2 + H_2O \leftrightarrow HNO_2 + HNO_3$ | liquid, fast | (51) |
| $2\,NO_2 \leftrightarrow N_2O_4$ | liquid, fast | (52) |
| $3\,HNO_2 \leftrightarrow HNO_3 + 2\,NO + H_2O$ | liquid, slow | (53) |


After this process, 95% of the NO are converted and removed as acid, while the conversion rate for $SO_2$ is about 99.5%. The water content is also effectively reduced by this treatment, leading to a concentration of about 75 %mol of $CO_2$ in the gas stream.

In Table 41, the key parameters for the flows in this section are compared to an alternative compression process used for modelling $CO_2$ purification according to patent applications by Air Liquide and Praxair. In the alternative configurations the compression section is held simpler by the elimination of distillation columns that normally help remove the heavier contaminants from the flue

gas stream. Ultra-pure $CO_2$ can then only be obtained by removing these substances with an additional distillation column in the cryogenic purification section.

As explained in a later section of this thesis, in the case of Air Liquide, the inerts are only heated up to relatively low temperatures, since the twice expanded inerts stream is used as a coolant. Therefore, intercooling in the flue gas compressor train can be used to lower the necessary compression work.

**Table 41.** Flue gas parameters in $CO_2$ pre-compression.

| | Air Products | | | | | | Air Liquide | Praxair |
|---|---|---|---|---|---|---|---|---|
| | flue gas | 2 | 5 | 6 (contaminants) | 12 (contaminants) | 15 (compressed) | compressed gas (intercooling) | compressed gas ($T_{out}$=307 °C) |
| Temperature in °C | 35 | 307 | 30 | 33 | 29 | 30 | 105 | 307 |
| Pressure in bar | 1.013 | 15 | 15 | 15 | 30 | 30 | 30 | 30 |
| Mass Flow in kg/s | 148.47 | 148.47 | 148.47 | 4.50 | 1.00 | 143.22 | 144.32 | 145.32 |
| Mole Fractions | | | | | | | | |
| $CO_2$ | 0.717 | 0.717 | 0.717 | 0.071 | 0.138 | 0.753 | 0.753 | 0.744 |
| $N_2$ | 0.175 | 0.175 | 0.175 | 0.001 | 0.016 | 0.185 | 0.184 | 0.181 |
| AR | 0.029 | 0.029 | 0.029 | 521 ppm | 0.006 | 0.031 | 0.030 | 0.030 |
| $O_2$ | 0.029 | 0.029 | 0.029 | 541 ppm | 0.007 | 0.029 | 0.029 | 0.028 |
| $H_2O$ | 0.045 | 0.045 | 0.045 | 0.851 | 0.833 | 0.001 | 0.003 | 0.015 |
| $SO_2$ | 0.003 | 0.003 | 0.003 | trace | trace | 3 ppm | 15 ppm | 15 ppm |
| NO | 710 ppm | 710 ppm | 721 ppm | trace | trace | 38 ppm | 37 ppm | 37 ppm |
| $NO_2$ | 11 ppm | 11 ppm | trace | 319 ppb | 229 ppb | 10 ppb | 906 ppb | 22 ppm |
| CO | 0.001 | 0.001 | 0.001 | 14.6 ppm | 174 | 0.002 | 0.002 | 0.001 |
| $SO_3$ | 2 ppm | 2 ppm | 96 ppm | trace | trace | trace | trace | trace |
| $N_2O_4$ | | | | trace | trace | trace | trace | 6 ppb |
| $HNO_2$ | | | | trace | trace | trace | trace | 9 ppb |
| $HNO_3$ | | | | 0.015 | 257 ppm | 208 ppb | 11 ppm | 173 ppm |
| $H_2SO_4$ | | | | 0.062 | trace | trace | trace | 5 ppb |
| Conversion of NO | | | | 95.0% | | | 95.0% | 95.0% |
| Conversion of $SO_2$ | | | | 99.9% | | | 99.5% | 99.5% |

As can be seen, the compression system employing distillation columns leads to far lower concentrations of $NO_2$, $SO_2$, $HNO_3$ and even to a lower water content in the compressed gas stream. The stream numbers for the Air Products pre-compression section refer to Figure 51.

### 4.2.2. CO$_2$ flue gas purification according to Air Products patent application

As described previously, the CO$_2$ needs to be purified after the pre-compression step. Also for this process Air Products filed a patent application [124], which the author then modelled in Aspen Plus. Three alternative configurations described in the aforementioned document were investigated in detail here.

The compressed flue gas stream passes through a dual bed adsorptive dryer that removes all water from the gas stream to prevent ice formation in the cold box. The cold box is a multi-stream heat exchanger, in which the gas mixture is cooled down to -54 °C by depressurised streams in the system.

In the base case, a first separation of the inert gases is achieved in a flash drum at 30 bar and -33 °C. Thereafter, additional cooling brings the temperature of the gas stream down to -54 °C at which point the CO$_2$ becomes a liquid and the lighter inert gases can be separated further. The CO$_2$ streams coming from the flash drums are depressurised to provide cooling to the other streams in the cold box, while the inerts can be reheated and their expansion work is used in a turbine.
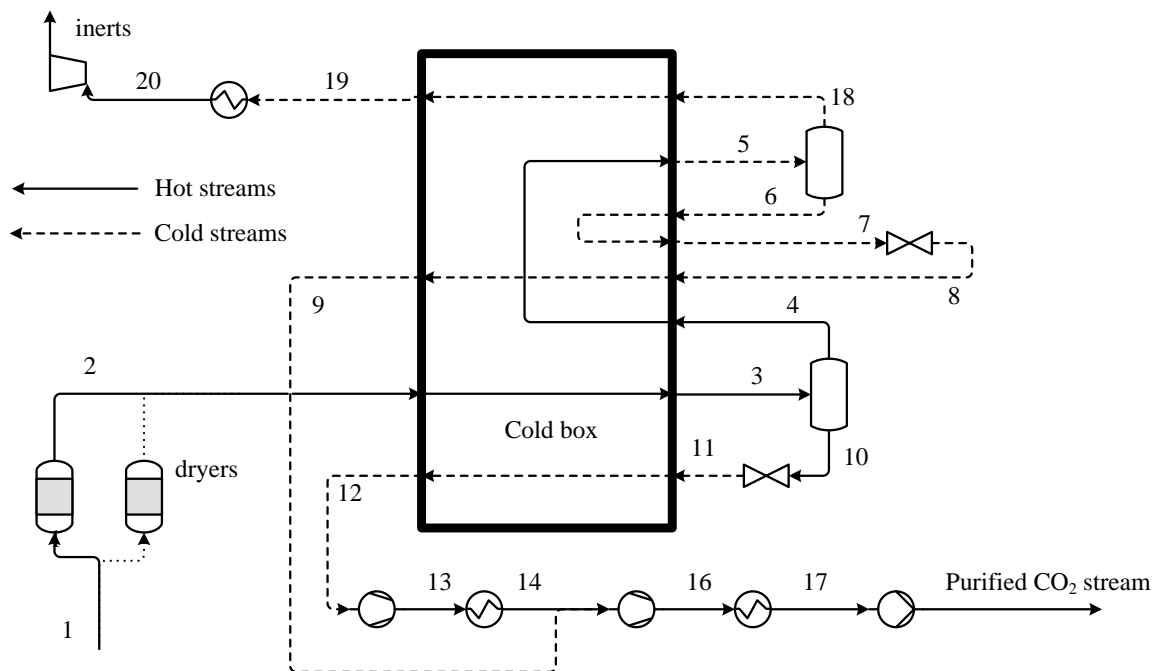


**Figure 52.** Base case for CO$_2$ purification (after [124]).

As shown in Table 42, this configuration leads to a CO$_2$ purity of 96% with an oxygen content of 0.7 %mol. If greater purity is required, e.g. for the use of the gas stream in EOR, then a stripper column for separation of the lighter inert gases needs to be included in the purification section. This is done in the next CO$_2$ purification option shown in Figure 53.
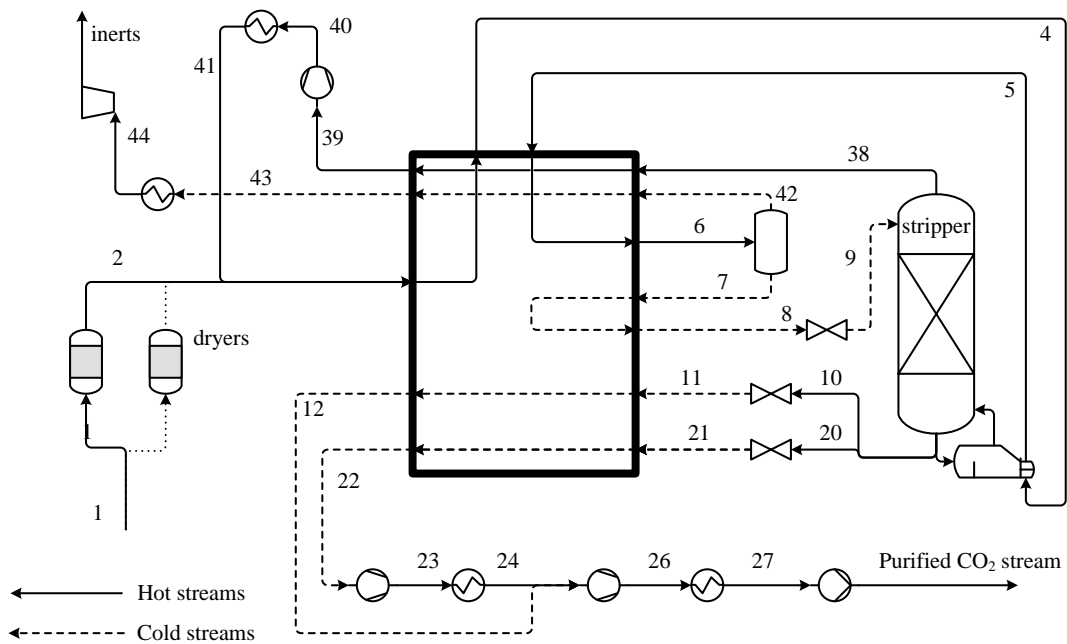
**Figure 53.** $CO_2$ purification (Air Products) with stripper column at 17 bar (after [124]).

After a first pass through the cold box, the stream is used to provide heat to the stripper column in which the liquefied $CO_2$ gets purified. Then the gas is cooled further down to -54 °C, causing the $CO_2$ to reach liquid state. The major part of the inert gases is then separated in a flash drum, while the liquid $CO_2$ stream is depressurised to 17 bar and fed to the stripper column. The remaining inerts leaving at the top are recompressed and recycled to the entering gas stream. This facilitates their separation from the gas mixture in the flash drum. Cooling of the flue gas stream is provided by decompression of the gas streams of different purity, pressure, and temperature.

An alternative version of the previously described Air Products design is presented in Figure 54. It uses two flash stages and a stripper column that is kept at a pressure of 30 bar. Here, two flash stages are used for separation of the inerts. The first separation occurs at -23 °C and the second at -54 °C. Inerts leaving the stripper column are recycled to increase their concentration in the system and to improve separation.
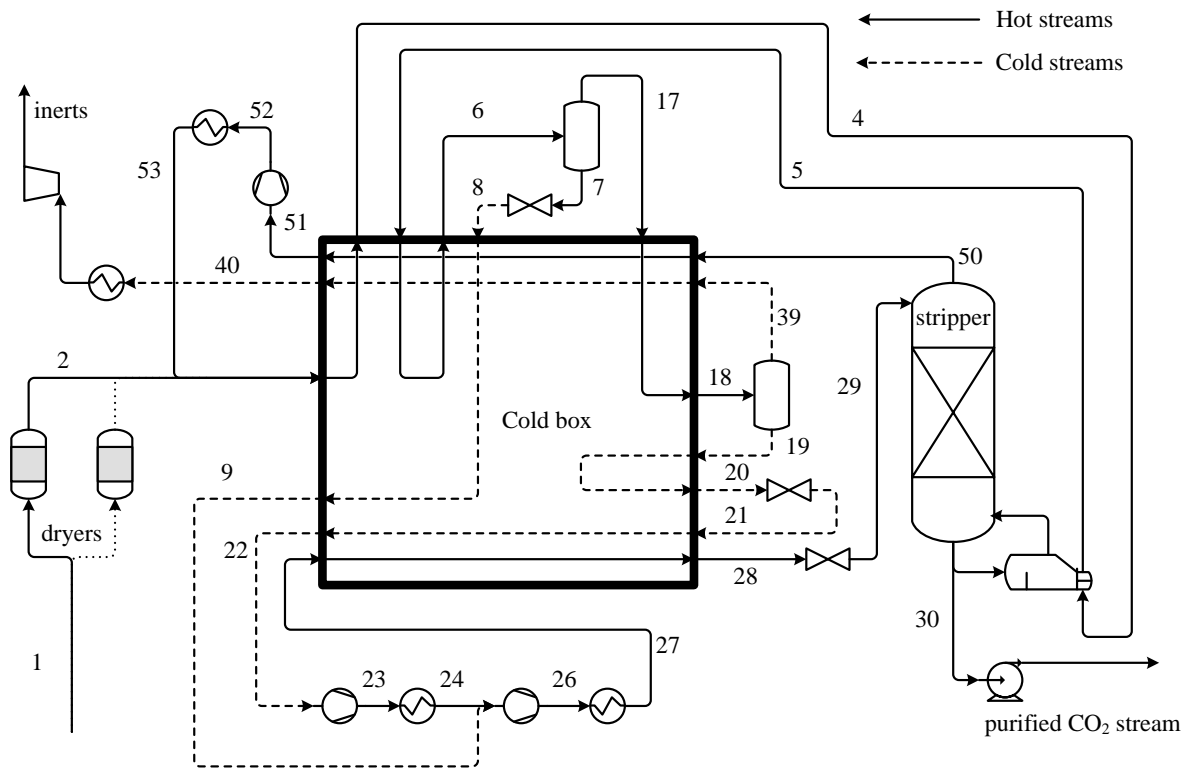


**Figure 54.** $CO_2$ purification (Air Products) with stripper column at 30 bar (after [124]).

A higher pressure in the stripper column should allow for a greater purity of the product $CO_2$ stream. The price to be paid is an increased compression work of the intermediate gas streams. In order to cool the stream entering the stripper column to -8 °C, it needs to expand from a pressure of 78.6 bar. Part of this expansion work is regained by not expanding and recompressing the product stream, since this stream is extracted from the process as a liquid and then pumped to the required pressure of 110 bar.

Cooling of the flue gas stream down to -54 °C inside the cold box has to be optimised for efficient use of the depressurised streams. Figure 55, a heat vs. temperature diagram for the cold box of the above installation, shows the hot and the cold curve for the streams inside the multi-stream heat exchanger in the Aspen Plus cold box model. The profile of the curves is shaped by passing the streams at different temperatures, pressures, and flows.

As an example, in the configuration presented in Figure 54, the flows of streams 7 and 17 are dependent on the temperature of the first separation stage, while the flow stream 50 is controlled by the temperature inside the stripper. The closer both curves are, the better the energy transfer between cold and hot streams is used. A minimum temperature difference of 1 °C was assumed for all cold boxes [125].
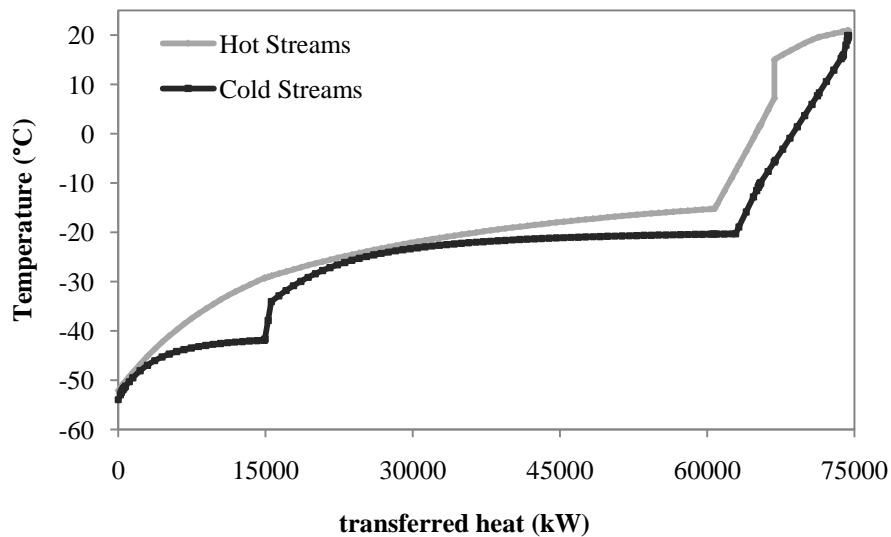


**Figure 55.** T-Q Diagram for Air Products cold box ($dT_{min} = 1$ °C) with stripper column at 30 bar.

### 4.2.3. CO$_2$ purification of Oxy-fuel flue gas according to Air Liquide patent application

An alternative patent application for the CO$_2$ purification process was filed by Air Liquide [126]. As with the Air Products patent application, the process description found in the patent application served the author of this thesis as basis for modelling the process with Aspen Plus [51].

If no distillation is used in the compression of the flue gas stream, the heavier contaminants have to be separated in a distillation column in the cryogenic purification process, such as in the cold box configuration by Air Liquide [126], which is presented in Figure 57. After separation of these components in the distillation column at -17.4 °C, part of the stream leaving at the top of the column is used to provide heating for the stripper. The main separation of the lighter inerts occurs in the second flash vessel at -54 °C. The liquid CO$_2$ stream from the bottom of the stripper is split into streams of different pressure to provide cooling inside the cold box. Then the streams are mixed and compressed to 110 bar for transport and storage.
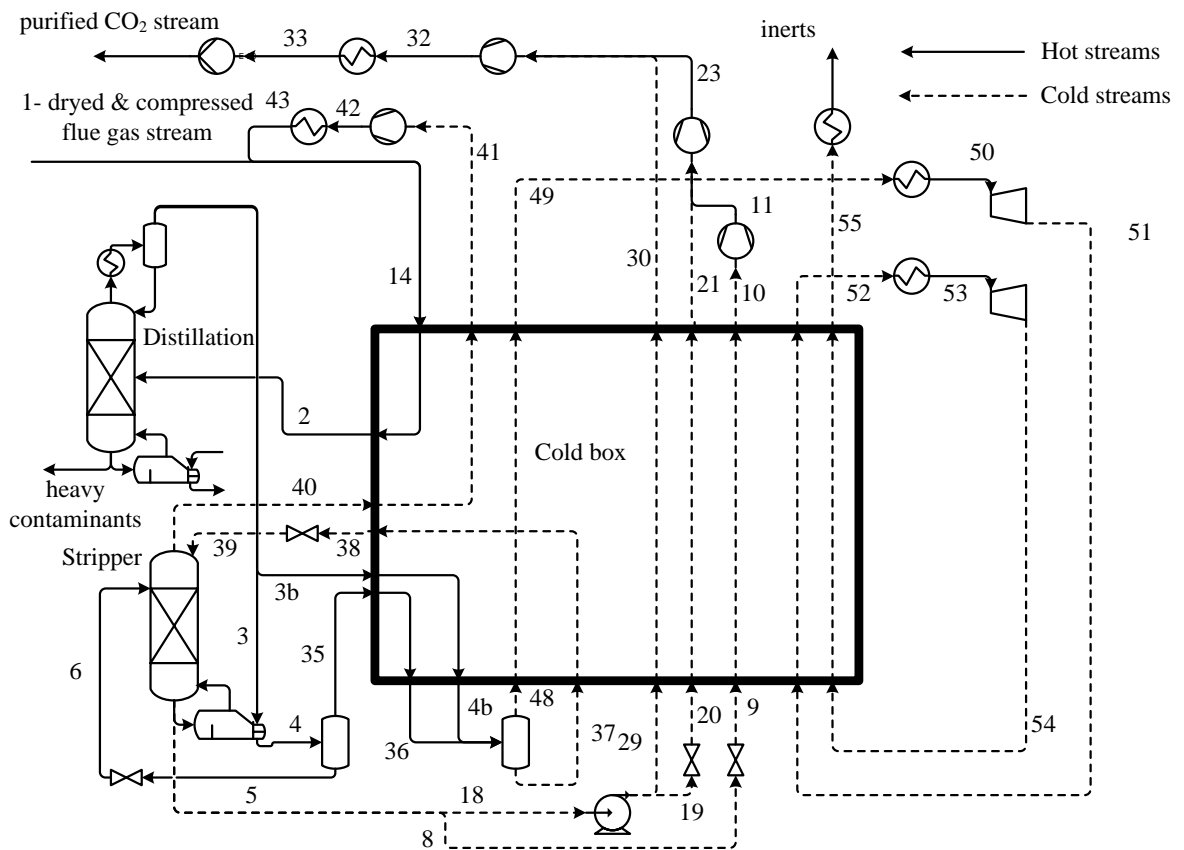


**Figure 56.** CO$_2$ purification (Air Liquide) with distillation column (after [126]).

In the Air Liquide cold box the inerts go through a staged expansion driving turbines that provide energy to the compressors for the purified CO$_2$ stream and for the recycled inerts from the stripper column (compander configuration). The expanded inert streams are also used for cooling.

### 4.2.4. CO$_2$ purification of Oxy-fuel flue gas according to Praxair patent application

The third patent application for the CO$_2$ purification process was filed by Praxair [127]. The CO$_2$ purification according to this document does not include a column for the removal of the heavier gas components, neither in the pre-compression section nor in the cold box section. Therefore, the product CO$_2$ purity reached with this configuration is lower than the one achieved with the previous configurations. This was verified by the author's simulations [51].
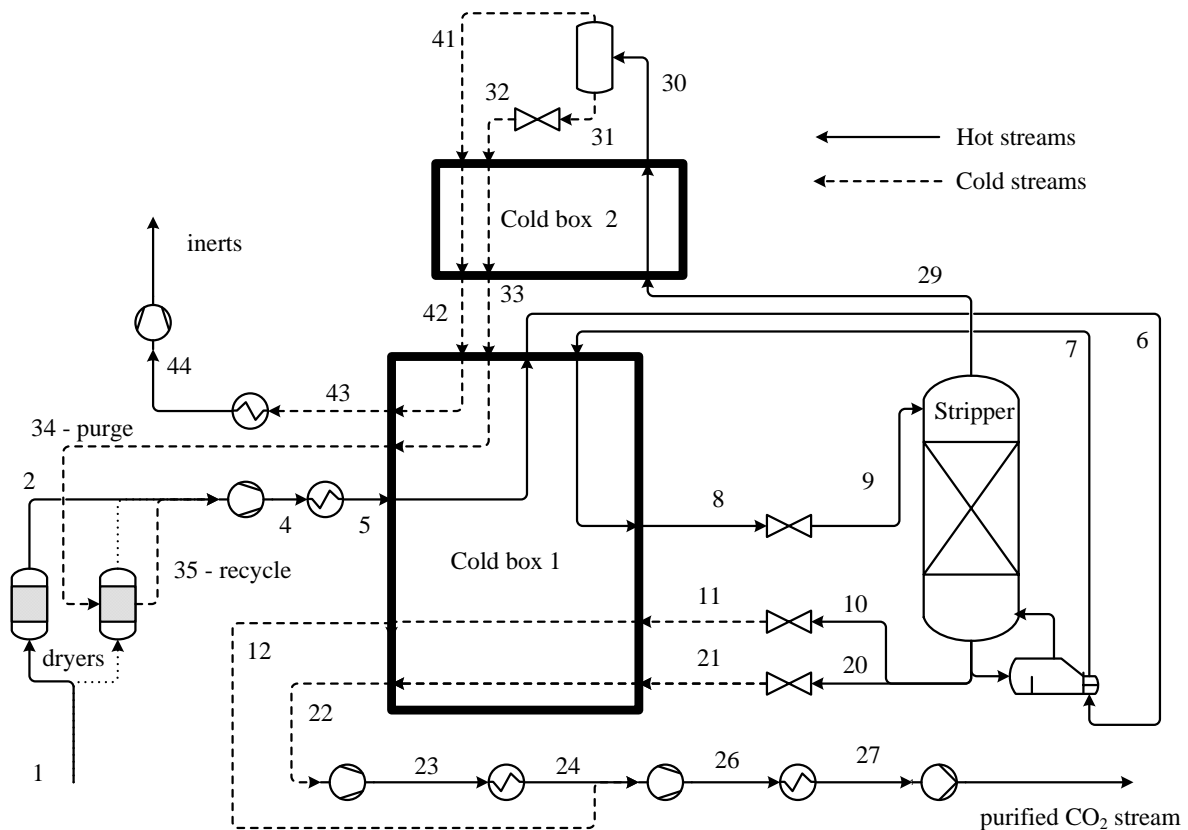


**Figure 57.** CO$_2$ purification (Praxair) without distillation column (after [127]).

Here, the inerts leaving at the top of the stripper column are separated further in a flash stage after additional cooling. The inerts can be reheated to 300 °C by the hot flue gas stream in the compression section and used in a turbine similar to the Air Products configurations. The separated liquid stream from the flash stage still contains 95.4% of CO$_2$ and is used as purge stream for the inactive adsorber bed in the dryer. Then it is mixed to the dry flue gas stream entering the cold box. This recycle raises the inerts content, facilitating their removal in the stripper column.

In conclusion, the stream data of all three configurations for CO$_2$ compression and purification can be found in Table 42.

**Table 42.** Stream compositions for the investigated $CO_2$ purification systems.

| | Air Products no distillation | | Air Products 17 bar | | Air Products 30bar | | Air Liquide | | | Praxair | |
|---|---|---|---|---|---|---|---|---|---|---|---|
| | inerts | purified | inerts | purified | inerts | purified | inerts | purified | acids | inerts | purified |
| Temperature in °C | 8.5 | 28.6 | 8.5 | 32.9 | 8.5 | 2.3 | 8.5 | 32.9 | -5.2 | 8.5 | 32.9 |
| Pressure in bar | 1.1 | 110 | 1.1 | 110 | 1.1 | 110 | 1.1 | 110 | 30 | 1.1 | 110 |
| Mass Flow in kg/s | 36.15 | 107 | 39.25 | 103.90 | 39.46 | 103.69 | 39.32 | 103.88 | 0.94 | 44.96 | 99.40 |
| Mole Fractions | | | | | | | | | | | |
| $CO_2$ | 0.2780 | 0.9609 | 0.2573 | 0.9997 | 0.2599 | 0.9999 | 0.2573 | 0.9999 | 0.9965 | 0.3314 | 0.9990 |
| $N_2$ | 0.5554 | 0.0242 | 0.5595 | 18.5 ppm | 0.5572 | 8.48 ppm | 0.5589 | 20.5 ppm | 118 ppm | 0.5039 | 17.2 ppm |
| AR | 0.0840 | 0.0074 | 0.0922 | 14 ppm | 0.0920 | 40 ppm | 0.0924 | 32 ppm | 77.2 ppm | 0.0828 | 290 ppm |
| $O_2$ | 0.0780 | 0.0073 | 0.0863 | 176 ppm | 0.0862 | 46.5 ppm | 0.0867 | 35.6 ppm | 79.3 ppm | 0.0776 | 363 ppm |
| $SO_2$ | 6.5 ppb | 4.4 ppm | 39.2 ppb | 4.6 ppm | 2.8 ppb | 4.6 ppm | 61 ppb | 11.5 ppm | 0.0013 | 41 ppb | 24 ppm |
| NO | 102 ppm | 9.56 ppm | 114 ppm | 0.16 ppm | 113 ppm | 18.7 ppb | 114 ppm | 33.2 ppb | 61.9 ppb | 102 ppm | 0.14 ppm |
| $NO_2$ | trace | 14.3 ppm | trace | 14.9 ppb | trace | 14.9 ppb | trace | 0.22 ppm | 127 ppm | 5 ppb | 34.70 ppm |
| CO | 0.0046 | 0.0020 | 0.0046 | 0.14 ppm | 0.0046 | 58.5 ppb | 0.0046 | 0.16 ppm | 0.91 ppm | 0.0041 | 0.11 ppm |
| $N_2O_4$ | trace | trace | trace | trace | trace | trace | trace | trace | 7.2 ppb | trace | 9 ppb |
| $HNO_2$ | trace | 0 | trace | 0 | trace | 0 | trace | trace | 41.2 ppb | trace | 14.3 ppb |
| $HNO_3$ | trace | 0.299 ppm | trace | 0.311 ppm | trace | 0.312 ppm | trace | 54.2 ppb | 0.0018 | trace | 271 ppm |

As can be seen from these data, the compression system employing distillation columns leads to far lower concentrations of $NO_2$, $SO_2$, $HNO_3$ and even to a lower water content. This confirms the findings presented in 4.2.1. The only purification options able to sufficiently reduce oxygen levels to EOR requirements are the Air Products patent application with a stripper column at 30 bar and the Air Liquide configuration (see Table 38).

## 4.3. Influence of CO$_2$ purification on power plant performance

While the previous subchapters were concerned with details of the different configurations for the CO$_2$ purification process, it is interesting to find out how these configurations affect power plant performance. As described, leaving the outlet temperature of the first compressor in the reactive compression at 307 °C for heating up the inerts leads to an elevated power consumption in this process. To see, if the introduction of intercooling would reduce power needs, the author carried out a comparative simulation with intercooling of all compressor stages to 30 °C. It was found that the energy savings (10.75 MW$_{el}$) due to intercooling are in the same range as the energy regained by the expansion of the inerts, but without the need for an extra turbine [51].

Intercooling, however, increases the complexity of the compressor and requires cooling water. In any case, if the expansion of the inerts is to be used, the necessary energy for reheating the inerts should be taken from a part of the power plant where it causes the least penalties. Since the temperature prior to the expansion of the inerts needs to be about 300 °C, using heat released between compressor stages is adequate. Then the data in Table 43 for capture efficiencies and the important energy flows that influence power plant performance are obtained for the aforementioned different patent approaches.

**Table 43:** Parameters for Oxy-fuel power plant with cryogenic CO$_2$ purification.

| Gross power plant output: 584.6 MW$_{el}$ <br> Gross efficiency (%LHV): 40.7% | no capture | Air Products no distillation | Air Products 17 bar | Air Products 30bar | Air Liquide | Praxair |
|---|---|---|---|---|---|---|
| Power consumption of ASU in MW$_{el}$ | 84.6 | 84.6 | 84.6 | 84.6 | 84.6 | 84.6 |
| Nominal capture efficiency | -- | 87.9% | 87.8% | 87.6% | 87.8% | 84.0% |
| CO$_2$ pre-compression in MW$_{el}$ | -- | 50.9 | 50.9 | 50.9 | 39.6 | 48.0 |
| Compression in CO$_2$ purification in MW$_{el}$ | -- | 10.5 | 13.1 | 25.2 | 10.7 | 13.4 |
| Expansion in CO$_2$ purification in MW$_{el}$ | -- | -10.2 | -11.1 | -11.1 | -7.5 | -12.5 |
| Power plant net output in MW$_{el}$ | 500 | 449 | 447 | 435 | 457 | 451 |
| Power plant eff. (%LHV) | 34.8% | 31.2% | 31.1% | 30.3% | 31.8% | 31.4% |
| Spec. penalty in GJ$_{el}$/t | -- | 0.492 | 0.509 | 0.627 | 0.412 | 0.492 |
| Specific CO$_2$ production in kg/MWh | 852.1 | 114.73 | 116.1 | 121.5 | 114.0 | 151.3 |
| Effective CO$_2$ removal | -- | 86.5% | 86.4% | 85.7% | 86.6% | 82.2% |

The CO$_2$ purification according to the Air Liquide patent application shows the highest effective CO$_2$ removal efficiency due to the lowest energy penalty. In combination with the high CO$_2$ pu-

rity achieved here (see Table 42), this option should be given preference over the other purification configurations. This option also leads to the lowest oxygen levels in the purified $CO_2$ stream. Apart from the purification according to Air Products with a stripper column at a pressure of 30 bar, it is the only purification option that produces EOR grade $CO_2$, but at a far lower energy penalty.

The patent application of Praxair needs to be revised because without distillation columns neither in the pre-compression step nor in $CO_2$ purification, effective $CO_2$ removal and product purity are low. This is caused by elevated losses of $CO_2$ with the lighter inerts in order to achieve a purity of 99.9%. A higher purity cannot be achieved, as there is no distillation step for the removal of the heavier substances as $SO_X$ and $NO_X$.

# 5. Life Cycle Assessment

Due to increasing environmental awareness, the environmental performance of processes has become an important issue. One tool to assess the environmental performance of products and industrial processes is Life Cycle Assessment (LCA). After an introduction to the methodology of LCA, the environmental impact of the studied capture solutions is investigated in this chapter.

## 5.1. Principles of LCA

LCA uses a holistic cradle-to-grave approach, meaning that all energy, material, and waste flows released to the environment, including extraction of raw materials, fabrication processes, transport, distribution, utilisation/production, re-use, internal recycle and final release or disposal are evaluated and accounted for [128]. The evaluation covers the whole life span or "life cycle" of the investigated product; and all stages in the product's life span are treated as interdependent. This system approach allows for a more accurate estimation of the cumulative environmental impact of a product. Typical measurable inputs and outputs and the possible life cycle stages considered in an LCA are shown in Figure 58.
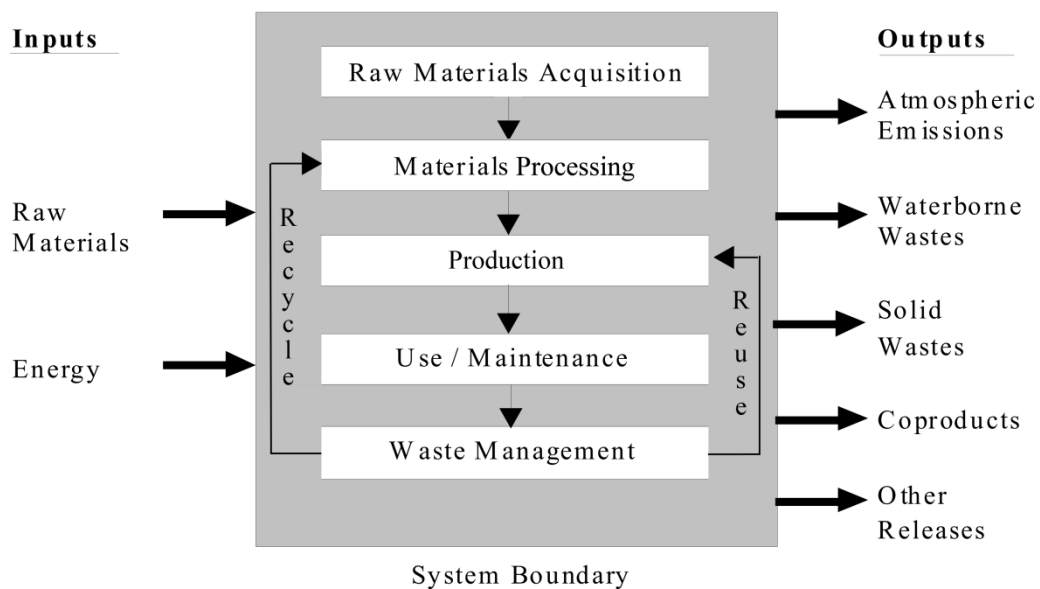


**Figure 58.** Life cycle stages (after [128, 129]).

LCA had its beginnings in the 1960s with the energy analyses of industrial processes by Boustead [89], when large companies started to be concerned about the limitation of raw materials and energy resources and about environmental issues. In the early 1990s, pressure from environmental organizations and concerns over inappropriate use of LCA by product manufacturers led to the development of international LCA standards [130]. These standards are grouped in the ISO 14000 series. The development of the international standards (ISO 14040:1997, ISO 14041:1999, ISO 14042:2000, ISO 14043:2000) was an important step to consolidate procedures and methods of LCA [131]. Their contribution to the general acceptance of LCA by stakeholders and by the international community was crucial. These standards were updated in 2006, the new standards now being ISO 14040 and 14044, the latter incorporating the previous standards ISO 14041-14043. In 2002, the international Life Cycle Initiative was launched by the United Nations Environment Programme (UNEP) and the Society of Environmental Toxicology (SETAC). The initiative incorporates three programmes that aim at putting life-cycle thinking into practice and to improve the supporting tools by better data and indicators [129]. The Life Cycle Management programme produces information materials, establishes forums for best practice, and carries out training courses all over the world in order to create awareness and to improve the skills of decision makers. The Life Cycle Inventory programme enables global access to transparent and reliable data by gathering the results of expert groups in web-based information systems. The Life Cycle Impact Assessment programme is a platform for the exchange of expert groups in order to establish high quality global life-cycle indicators.

The LCA is a systematic approach, consisting of the following four phases as shown in Figure 59. When deciding between two or more alternatives, LCA can help decision makers compare the quantity and quality of all major environmental impacts of all phases during the product's life cycle [128].

| - Goal and Scope definition: | Definition of the case study and the reasons behind it, definition of the audience the study is aimed at (Goal). |
| | Definition and description of the investigated product, process or activity, its purpose and functional units, as well as the identification of the boundaries and environmental effects to be considered in the assessment (Scope). |
| - Inventory Analysis: | Identification and quantification of all energy and material flows, such as raw materials and emissions, as shown in Figure 58. |
| - Impact Assessment: | Assessment of the environmental impacts on human health and ecological effects of all material usage and releases identified in the inventory analysis. |

- Interpretation:                    Evaluation of the results of inventory analysis and impact assessment to enable the selection of the adequate product, process or service with the identification of uncertainties and assumptions used to generate the results.
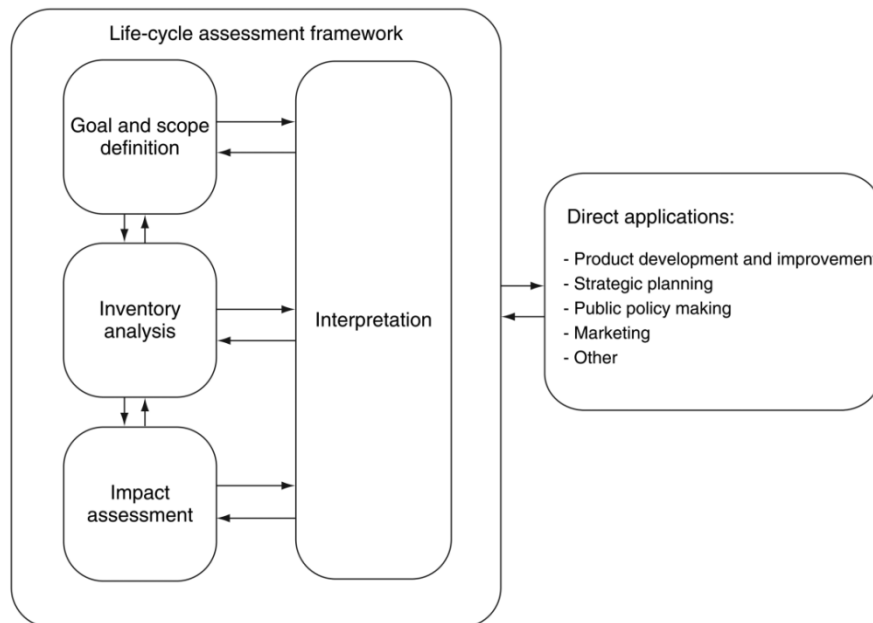


**Figure 59.** Life Cycle Assessment phases [129].

In the first phase, it is important to define a suitable functional unit as a prerequisite to adequately compare alternative products. The functional unit is the reference unit to which all inlet and outlet flows will be compared. The definition of the functional unit should be carried out under the principle of equivalent use. For e.g. alternative beverage containers, the equivalent use basis may be a fixed quantity of beverage transported to the consumer. The system boundaries are usually defined at the inlet of raw materials and the emission of waste and/or product flows. It may be necessary to adjust these boundaries, if important environmental issues would otherwise be excluded [130].

In the life-cycle inventory, all energy and raw material requirements, atmospheric and water-borne emissions, solid wastes, and other releases are quantified for the entire life-cycle period considered in the LCA. The level of detail required depends on the size of the system and the purpose of the study. In large systems incorporating several industries, some details may not have a major environmental effect. However, great care has to be taken as to the availability and accuracy of the data. The origin of the data used (measurements, literature, modelling, etc.) should therefore be clearly indicated. Another important point is the allocation of data. The considered mass flows have to be allocated to each production line. Care has to be taken not to duplicate emissions and emissions for the

different subprocesses. Recycling, which is often carried out on a global scale may complicate this allocation process and lead to a readjustment of the system boundaries [130].

In the third LCA phase, the impact assessment, the potential impacts on human health and on the environment are evaluated, which are caused by the resources and releases identified in the inventory step. For this phase, it has to be decided which impact categories, category indicators and characterisation models will be selected.

The key steps of a Life Cycle Impact Assessment (LCIA) are the following [129, 130]:

- Selection and Definition
  of Impact Categories: Identification of relevant environmental impact categories such as global warming, acidification, ozone depletion.

- Classification: Assigning inventory results to the impact categories (e.g. $CO_2$ emissions to global warming).

- Characterisation: Within the impact categories conversion factors are used to quantify the impact of the substances from the inventory such as the different potential impact of $CO_2$ and methane on global warming.

- Normalisation: The potential impacts are referenced to a standard in order to be able to compare them for different alternatives.

- Grouping: The indicators may be sorted and ranked, e.g. by location (local, regional, global).

- Weighting: Weighting is used to emphasise the importance of potential impacts.

- Evaluation and Reporting: Describing the methodology used, the analysed systems and their boundaries, and all assumptions made, which helps with understanding the reliability of the LCIA results.

For simplification purposes, LCIA is usually carried out at midpoint level instead of including all potential effects at specific endpoints, as shown on the example of ozone depletion in Figure 60.
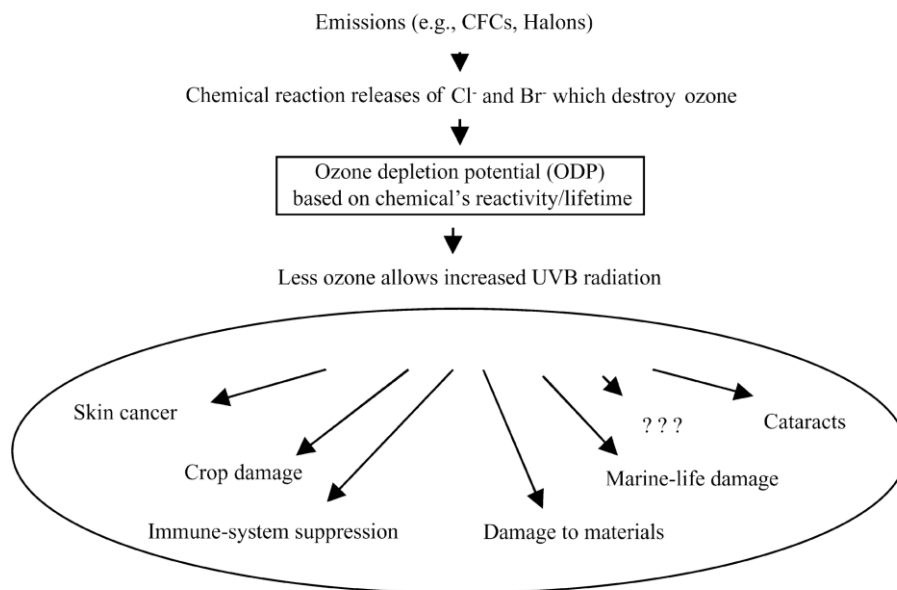
**Figure 60.** Midpoint versus endpoint modelling [132].

Analysis at midpoint level reduces the complexity of modelling and minimizes forecasting and necessary assumptions, and can therefore provide more comprehensive information that is more widely accepted.

With the Eco-indicator 95/99 method [133], all substances used or emitted are sorted into classes according to their effect on the environment as in Figure 61. Substances can be included in more than one effect class, like $NO_X$, which is toxic, acidifying by forming $HNO_3$, causes eutrophication, and contributes to ozone depletion. Another example is the emission of $SO_2$, which can cause damage in the categories acidification and human health. However, the effect depends completely on the phase in which the $SO_2$ is found. One should thus hypothesize a "phate" scenario (e.g., how much $SO_2$ is going to the ground, and how much is remaining as a gas) and divide the overall $SO_2$ flow rate accordingly [133].

A typical example for the characterisation step is the greenhouse effect. The main responsible is $CO_2$, which has a global warming potential (GWP) of 1. Emissions of $CH_4$ have a GWP of 42, because methane produces a forty-two times stronger greenhouse effect according to the models used in SimaPro [131].
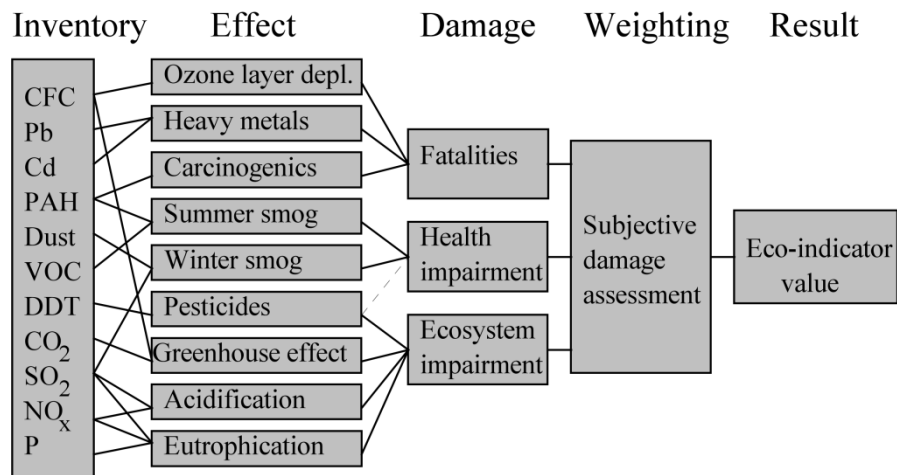
**Figure 61.** Principles of the Eco-indicator method [133].

In the normalisation step, another type of scaling is applied in order to gain a better understanding of the relative size of an impact. It is a benchmarking against the known total effect of a class. The Eco-Indicator method, for example, normalises with effects caused by the average European during a year.

Not all effects are considered to be equally important. Therefore, the normalised scores are finally multiplied by a weighting factor, representing the relative importance of the respective effect as listed in Table 44. The Eco-Indicator 95 and Eco-Indicator 99 weighting is based on a distance-to-target criterion: the method considers the distance between present value of the category indicator and the objective value which should be reached at European level. The larger the distance from the target, the higher is the weight for the category indicator.

In practice, the weighting factor $F_i$ is calculated as [130]:

$$F_i = N_i/T_i \tag{54}$$

with

$N_i$ = Current value for effect "i" per person, or "Normalisation Factor",

$T_i$ = Target value for effect "i".

**Table 44.** Weighting factors in Eco-indicator 99 method [130].

| Effect | Weighting factor |
|---|---|
| Greenhouse effect | 2,5 |
| Ozone layer depletion | 100 |
| Acidification | 10 |
| Eutrophication | 5 |
| Summer smog | 2,5 |
| Winter smog | 5 |
| Pesticides | 25 |
| Heavy metals in air | 5 |
| Carcinogenic substances | 10 |

As can be seen from this table, in the Eco-Indicator 99 method, the effects are weighted and referred to three damage macro-categories as shown in Table 45.

**Table 45.** Damage categories and weighting factors in Eco-indicator 99 method [133].

| Damage category | Category Indicator | Weighting Factor | Unit |
|---|---|---|---|
| Ecosystem Quality | Potentially Disappeared Fraction (PDF) | 400 | PDF*m$^2$*yr |
| Human Health | DALY (Disability Adjusted Life Years) Average Life Expectancy | 400 | Yr*person |
| Resource | Direct damage to resource | 200 | MJ/kg |

As can be seen from this table, with the Eco-indicator 99 method, the depletion of resources is given a lower weighting factor than the impact on ecosystem quality and human health.

The Eco-Indicator value I results from the weighted sum of all EcoPoints calculated for the different impact categories [130].

$$I = \sum_i \frac{E_i}{N_i} \cdot F_i$$

(55)

with

$N_i$ = Normalisation Value, i.e. current value for Europe of the i-th effect,

$E_i$ = Life Cycle contribution of a product/process to the i-th effect (EcoPoints),

$F_i$ = Weighting Factor = $N_i/T_i$,

$T_i$ = Target value for the i-th effect.

The interpretation of the LCA results is not just carried out in the final step of the LCA, but for all steps. The purpose of the interpretation is to check and evaluate the results and to compare them with the goal and scope definitions. This way, inconsistencies can be identified and necessary adjustments made.

The purpose of an LCA is to inform decision makers by providing a life-cycle perspective of environmental and human health impacts associated with alternative products or processes. Since LCA does not take into account technical performance, cost, or political and social acceptance, it is recommended to use the LCA results in connection with these other social and economic parameters. All of these parameters should then be based on the same system boundaries and the same functional unit [129].

This method LCA is not used for absolute evaluation, but rather for comparing the environmental impact of similar products. In the life-cycle approach, the term "product" is also used for processes and activities.

## 5.2. LCA of rate-based power plant models

The different capture options studied in this thesis reduce the emission of greenhouse gases, but they also lead to a reduction of the power plant output, i.e. to a higher specific consumption of resources. Especially in post-combustion $CO_2$ capture, the emissions and the necessary production of the solvents are potentially harmful to the environment.

For a good evaluation of these hazards, a life cycle assessment of the investigated power plants and capture options is carried out in the following. The commercial software SimaPro 7 with the Eco-Indicator 99 model was used in this study.

Since the rate-based models include reaction and mass transfer kinetics, only these power plant and capture models have been considered here. The data, assumptions and results are presented in the following sub-chapters.

### 5.2.1. Goal and Scope

This LCA is to give indications to decision makers and the sector of R&D on which capture options to focus, if the aim is a coal-fired power plant with the lowest environmental impact possible.

The investigated power plants are i) an IGCC with separate and co-capture of $CO_2$ and $H_2S$ with the physical solvent Selexol as pre-combustion capture option, ii) a conventional steam cycle power plant with post-combustion $CO_2$ capture with the chemical solvents MEA and ammonia, and lastly iii) an oxy-fuel power plant with $CO_2$ purification to an EOR grade $CO_2$ stream.

As the functional unit for comparison of all power plants the amount of energy produced during an assumed plant lifetime of 30 years was chosen. All results are therefore referenced to 1 $TJ_{el}$ of produced electricity by the power plants with or without acid gas removal.

The LCA included the impact of raw material extraction, transport, material processing, operation of the power plant, the use of cooling water and the emissions of flue gases and other substances during all life-cycle stages. $CO_2$ transport by pipeline and the energy for injection of the captured $CO_2$ into a geological storage site was also included here.

The LCA system boundaries for the PC power plant with and without $CO_2$ capture are shown in Figure 62 and for the IGCC in Figure 63. The boundaries for the oxy-fuel plant are the same as for the PC power plant except for the FGD and SCR requirements, since $SO_X$ and $NO_X$ are removed in the $CO_2$ purification section.

**Figure 62.** LCA boundaries for PC power plant a) without $CO_2$ capture and b) with capture [134].

a

Steel →
Concrete →
Aluminum →
Iron →

Material / fuel production

Material Transport → Power Plant Construction

Fuel →
Air →
Water →
Claus Plant Catalyst for Sulphur removal →
Transport Fuel (i.e. light or heavy fuel oil) →

Material Transport →

Fuel Handling

→ electricity

Power Generation

→ By-products Ash, Sulphur

→ Air emissions: $CO_2$, $H_2O$, $SOx$, $NOx$, $NH_3$, $HCl$, Particulates

Pollutant Removal (Sulphur removal, tail gas treatment)

→ Waste water

→ Solid waste: Claus plant catalyst, sludge, gasifier slag

Power Plant Decommissioning

Waste Transport

Waste Disposal: Landfilling / recycling

b

Steel →
Concrete →
Aluminum →
Iron →

Material Transport

Capture Plant Construction | Power Plant Construction | $CO_2$ Pipeline Construction

Material / fuel production

Fuel →
Air →
Water →
Selexol →
Claus Plant catalyst →
Transport Fuel (i.e. light or heavy fuel oil) →

Material Transport →

Fuel Handling

→ electricity

Power Generation

→ By-products: $CO_2$, Ash, Sulphur

→ Air emissions: $CO_2$, $H_2O$, $SOx$, $NOx$, $NH_3$, $HCl$, Particulates

Pollutant Removal (i.e.SCR, ESP, FGD, Sulphur removal, etc.)

→ Waste water

$CO_2$ Capture (Selexol process)

→ Solid waste: catalyst, Gasifier slag

$CO_2$ Compression

Power/Capture Plant Decommissioning

Waste Transport

Waste Disposal: Landfilling / recycling

**Figure 63.** LCA boundaries for IGCC a) without acid gas removal and b) with removal [134].

### 5.2.2. Life Cycle Inventory

The life-cycle has been divided in three phases: the assembly phase, the operational phase, and the waste management at the end of the life-cycle.

The assembly phase is the building of the power plant including capture section and $CO_2$ pipeline. The amount of materials needed was taken from different sources [134, 135] and include the fuel necessary for the construction work as well as the transport of the materials over different distances by road transport as listed in Table 46.

**Table 46.** Life Cycle Inventory (LCI) of investigated power plant structures.

| Material | PC power plant | Oxy-fuel power plant | IGCC | Capture Section MEA | pipeline |
|---|---|---|---|---|---|
| Diesel | 462 TJ | 462 TJ | 693 TJ | 3 TJ | 166 TJ |
| Electricity | 15 GWh | 15 GWh | 22.5 GWh | -- | -- |
| Sand | -- | -- | -- | -- | 97,500 t |
| Concrete | 150,240 t | 150,240 t | 200,360 t | 70 t | -- |
| Rock wool | 571 t | 571 t | 856.5 t | -- | -- |
| Aluminium | 332 t | 664 t | 498 t | -- | -- |
| Steel (95% low-alloy) | 44,801 t | 53,761 t | 67,202 t | 317 t | 12,000 t |
| Copper | 710 t | 710 t | 1065 t | 7 t | 710 t |
| Polyethylene | 401 t | 401 t | 601 t | 20 t | 232 t |
| Transport (x $10^3$ km) | 14,040 t | 14,700 t | 21,060 t | 131 t | 380 t |

For all metals, material processing such as sheet rolling (steel) and wire drawing (copper) are included in the LCA. Depending on the size of the capture or purification plant, a factorial approach was chosen. The multiplication factor was determined by the number and height of absorber towers relative to the reference capture section with MEA as solvent.

In the operational phase, materials have to be fed constantly to the power plants and capture sections. Coal has to be extracted and shipped, causing environmental impacts at the mining site and due to transport by ship, rail and road. Here, the average coal mix used in Europe was used to determine these impacts. Furthermore, solvent losses have to be compensated for. Additional material is needed in form of limestone for the FGD section and ammonia for the denitrification of the flue gas.

As an example for the impacts of solvent production, the production process for 1 kg of MEA is presented in Figure 64. This diagram also includes ammonia production from natural gas by partial oxidation and steam reforming as well as the use of ethylene oxide. Both substances are necessary for

the production of MEA. Furthermore energy and plant infrastructure is needed for the production of the solvent.
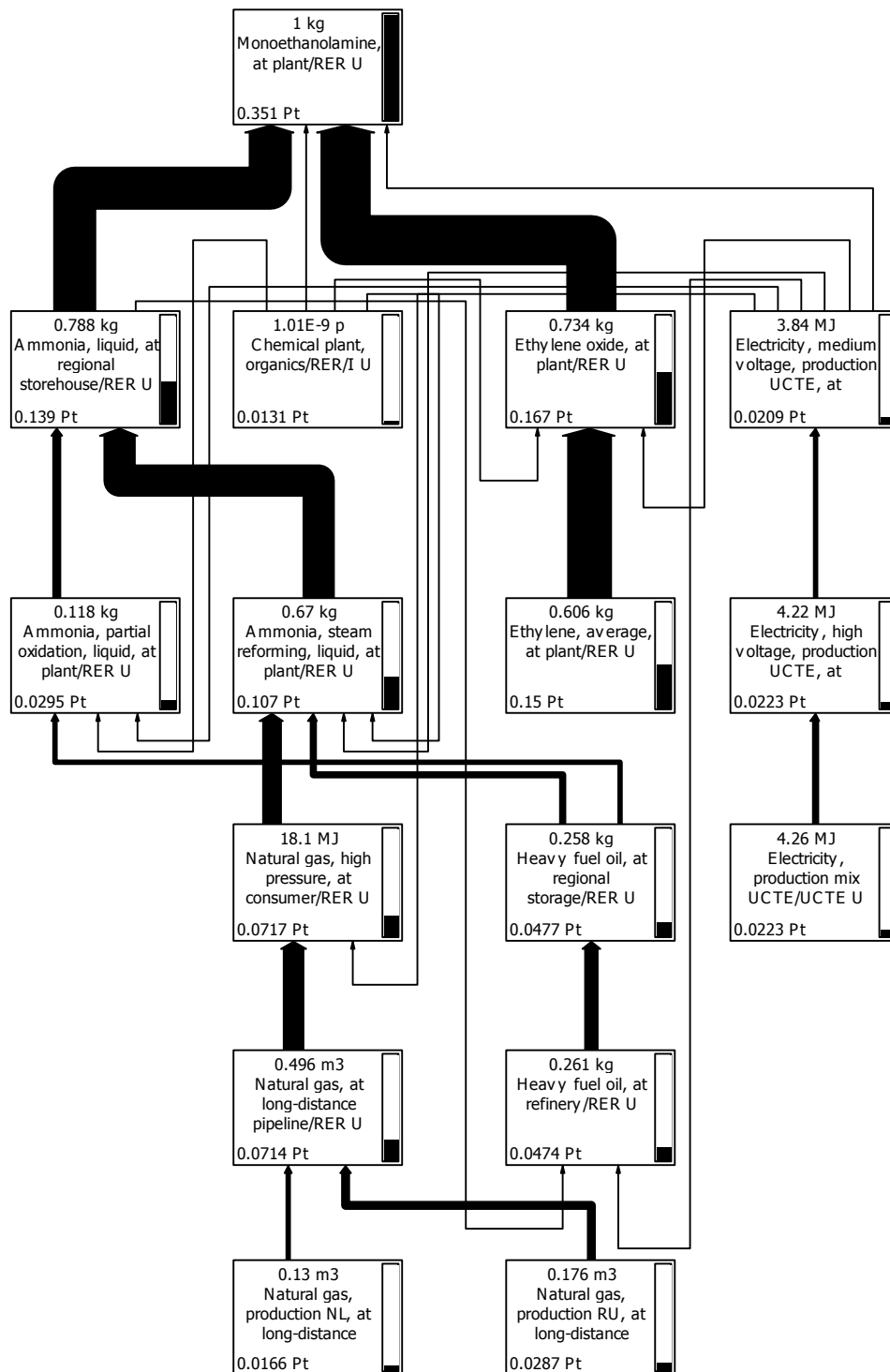


**Figure 64.** LCA process flow diagram for the production of 1 kg of MEA.

The above diagram also shows the interdepencies of the energy and material flows necessary for the solvent production. Apart from mass and energy units, this diagram includes Eco-point values, which will be discussed in the life-cycle impact assessment subchapter.

For all plant configurations in the respective chapters of this thesis the incoming material streams and emissions during operation can be found in the respective chapters of this thesis. These data were recalculated for a lifetime of 30 years with an average operation of 6,000 h/a at full capacity. Additional solvent to be produced and transported to the power plants was calculated to fill the used absorber and distillation columns completely. The excess amount compared to operational filling was assumed to fill the piping in the capture sections. For Selexol, no data could be found in the database of SimaPro. Since losses and makeup were negligible, no major influence of the exclusion of the process of Selexol production is expected on the results of this LCA. The limestone used for the wet FGD gets converted to the useful product gypsum. Therefore a beneficial impact of this gypsum production is expected. The waste water generated by the washing section to reduce ammonia emissions are sent to a water treatment plant. Due to uncertainties as to the treatment of the degradation products of scrubbing with MEA, these data were omitted here. The penalty for dealing with this waste stream was considered to be negligible in comparison with the penalty for the production and transport of the necessary solvent makeup. For the waste management at the end of the power plants' life cycle, the assumptions shown in Table 47 have been made.

**Table 47.** Waste management for materials used in power plants.

| Material | Waste scenario |
|---|---|
| Concrete | 100% reuse as filling material for construction work |
| Rock wool | 100% landfill |
| Aluminium | 100% recycling |
| Steel (95% low-alloy) | 80% recycling, 20% landfill |
| Copper | 100% recycling |
| Polyethylene | 100% incineration |

### 5.2.3. Life Cycle Impact Assessment

With the Eco-Indicator 99 method used here, every substance consumed or emitted in all sub-processes is given a specific impact value in the form of Eco-points. Before comparing the environmental impact of all investigated options, a Monte Carlo analysis was carried out with SimaPro to investigate the certainty of the data used. The PC power plant using the MEA solvent for $CO_2$ capture turned out to be the capture option with the highest data uncertainty. The results of its uncertainty analysis are presented in Table 48.

**Table 48.** Uncertainty of characterised LCA results for PC power plant with MEA scrubbing.

| Impact category | Unit | Mean | SD | CV (Coeff. of variation) | Standard error of Mean |
|---|---|---|---|---|---|
| Acidification / Eutrophication | PDF*m²yr | 4.11E08 | 1.42E06 | 0.35% | 0.000691 |
| Carcinogens | DALY | 1.10E04 | 15.2 | 0.14% | 0.000277 |
| Climate change | DALY | 3.93E03 | 14.9 | 0.38% | 0.00076 |
| Ecotoxicity | PAF*m²yr | 5.28E09 | 3.59E07 | 0.68% | 0.00136 |
| Fossil fuels | MJ surplus | 2.12E10 | 2.15E08 | 1.02% | 0.00203 |
| Land use | PDF*m²yr | 5.04E08 | 2.44E06 | 0.48% | 0.000967 |
| Minerals | MJ surplus | 8.72E07 | 5.42E06 | 6.22% | 0.0124 |
| Ozone layer | DALY | 7.24 | 0.0163 | 0.23% | 0.000449 |
| Radiation | DALY | 63.4 | 1.81 | 2.86% | 0.00572 |
| Respiratory inorganics | DALY | 1.11E04 | 32.4 | 0.29% | 0.000582 |
| Respiratory organics | DALY | 21.9 | 0.0681 | 0.31% | 0.000621 |
| **Damage category** | | | | | |
| Ecosystem quality | PDF*m²yr | 1.44E09 | 5.40E06 | 0.37% | 0.000748 |
| Human health | DALY | 2.61E04 | 47.2 | 0.18% | 0.000361 |
| Resources | MJ surplus | 2.13E10 | 2.17E08 | 1.02% | 0.00203 |

As can be seen from these data, the highest uncertainty was found for the depletion of minerals. This value falls in the damage category "resources", where the uncertainty due to the use of fossil fuels is influential and leads to a maximum coefficient of variation of slightly more than 1 percent. All other options investigated had coefficients of variation below this value. The uncertainty of the data used in this LCA should therefore be reliable.

For comparative reasons the unit Eco-points per $TJ_{el}$ of produced electricity during a plant lifetime of 30 years, which here are presented in weighted form according to the seriousness of the environmental impact.

The influence of the construction phase and end-of-life phase, including dismantling, reuse, recycling, and disposal, plays only a very minor role for the environmental impact of a power plant with a lifetime of 30 years is shown in Figure 65 for the case of the PC power plant without capture. For all configurations with capture the impact of the operation phase is even higher.

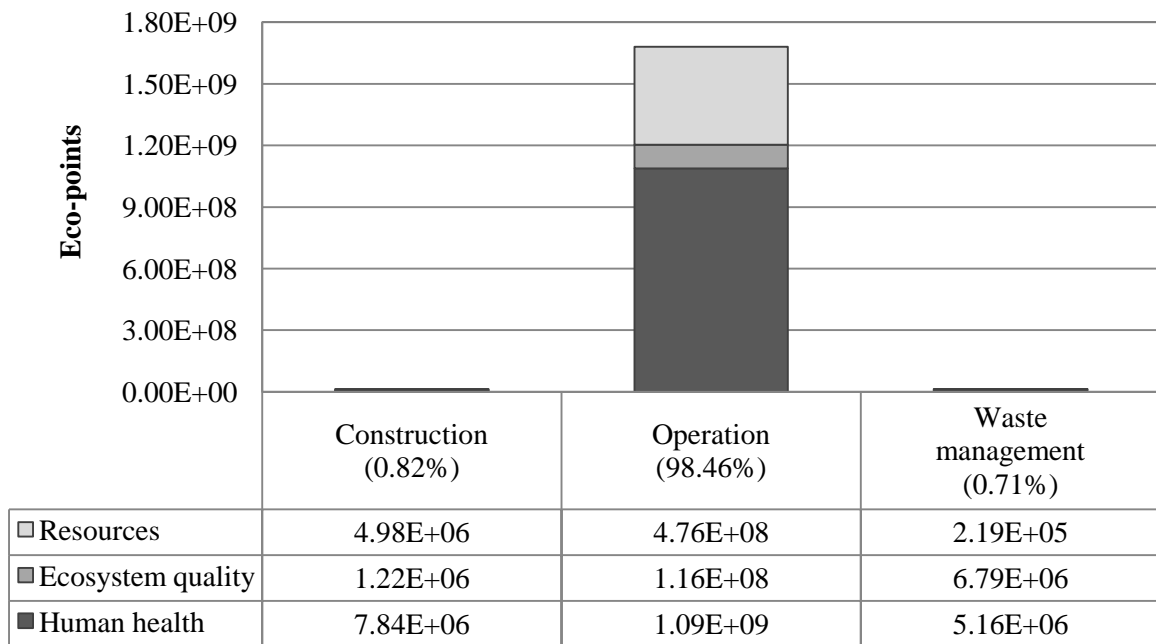| | Construction (0.82%) | Operation (98.46%) | Waste management (0.71%) |
|---|---|---|---|
| ☐ Resources | 4.98E+06 | 4.76E+08 | 2.19E+05 |
| ☐ Ecosystem quality | 1.22E+06 | 1.16E+08 | 6.79E+06 |
| ■ Human health | 7.84E+06 | 1.09E+09 | 5.16E+06 |

**Figure 65.** Influence of LCA phases on weighted results of PC power plant without $CO_2$ capture.

All environmental impacts of the different power plants with and without $CO_2$ capture are presented in weighted form with the weighting factors listed in Table 44 and Table 45.

All capture options have a nominal capture efficiency of ca. 90% for $CO_2$. The achieved net reduction in greenhouse gas emission, however, is significantly lower, as shown in the respective chapters for the effective $CO_2$ capture rate based on the emissions per TJ of produced energy (see 2.3.4, 3.2.4, 4.3). This net capture efficiency reported in the mentioned subchapters is calculated for an endogenous penalty compensation approach ("endo"), i.e. assuming compensation for the drop in the power plants' energy output by additional fuel consumption. However, this approach is not very realistic, because of the limitations of the investigated power plant. Compensation for energy penalties by higher fuel consumption is in fact equivalent to compensation by other identical power plants, i.e. plants with the same net efficiency, in which the same fuel is used and the same capture method applied. A second more realistic approach to determine the energy compensation of the penalties introduced by $CO_2$ capture considers the amount of compensational energy to be imported from the grid. In this exogenous compensation approach ("exo"), the environmental impact then depends on the energy mix used in the considered region [51]. In this study, the energy mix of Italy was assumed to be the supplier of electricity to the grid. The impact values according to this "exo" approach are higher, because in Italy electricity is mostly generated by conventional power plants using oil and gas. For both compensation approaches, the weighted environmental impact due to the emission of greenhouse gases of all analysed power plant configurations is shown in Figure 66 to Figure 68.

For the IGCC, separate capture of the acid gases led to a slightly higher capture efficiency for $CO_2$. However, this effect is almost completely compensated for, if exogenous compensation for the loss in power plant efficiency is taken into account.

For the PC power plant with post-combustion capture, the use of fossil fuels for solvent production, especially of oil and gas, in the case of post-combustion capture further reduces the net greenhouse effect of $CO_2$ capture to only 49% to 73%, as presented in Figure 67.

For the oxy-fuel power plant, only the plant including $CO_2$ purification is analysed here, since it would not make much sense to build an oxy-fuel power plant with the penalty introduced by the ASU without capturing the highly concentrated $CO_2$ in the flue gas stream. The results for the oxy-fuel plant should therefore be compared with the pulverised coal power plant without $CO_2$ capture. As for the base case of oxy-fuel flue gas purification, the Air Products patent application without a stripper column in the cold box section led to a $CO_2$ purity of only about 96%. As the main energy penalty is caused by the compression of the $CO_2$ and not by the purification process, this base case configuration had approximately the same detrimental effect on net power output as the other purification configurations, but without resulting in a highly pure $CO_2$ product. This option was therefore excluded from the LCA.

For pre-combustion capture and the oxy-fuel $CO_2$ purification processes, the contribution of methane emissions due to coal mining increases, since the net $CO_2$ capture efficiency is higher and equal to the net capture efficiency reported in the respective chapters with these options. Without $CO_2$ capture, the contribution to the greenhouse effect is directly dependent on power plant efficiency.
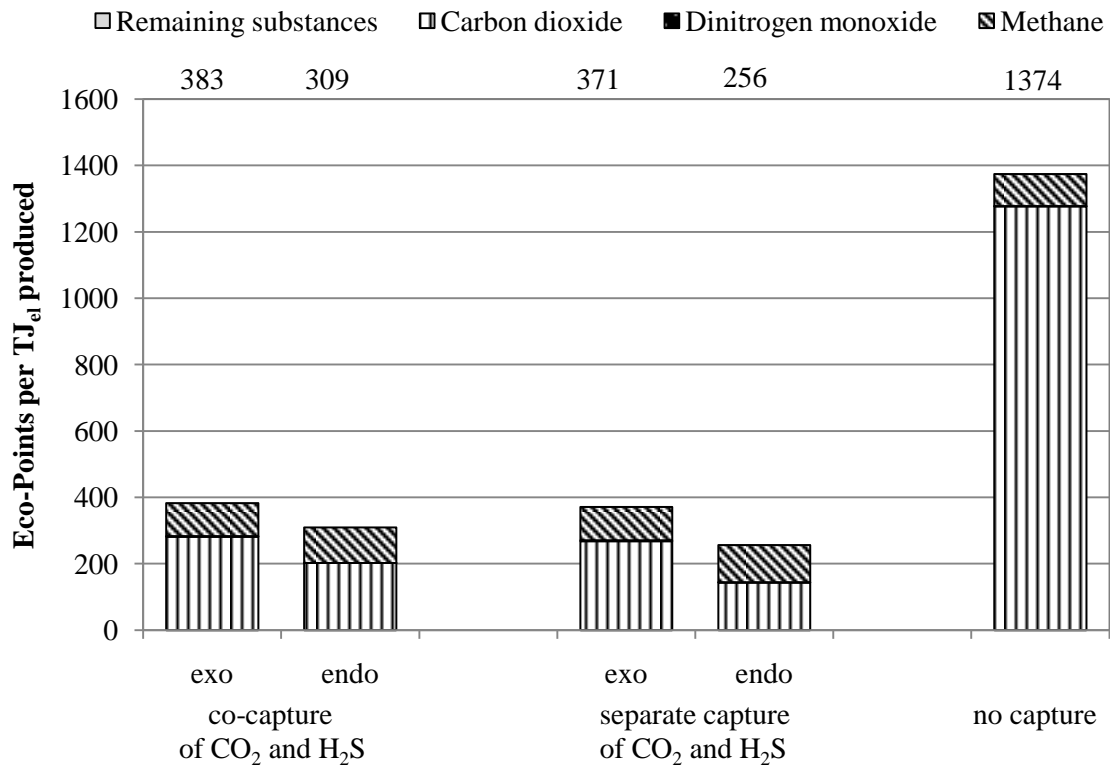
**Figure 66.** Impact of GHG emissions for IGCC with and without acid gas removal.
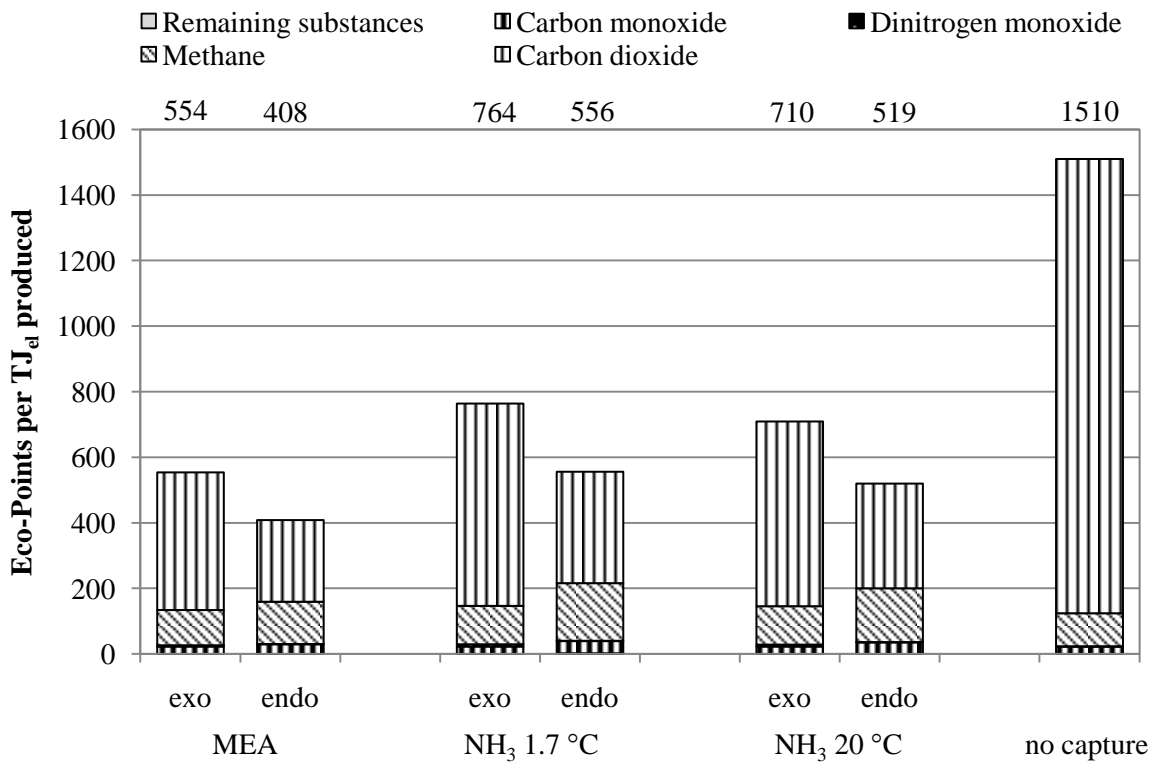


**Figure 67.** Impact of GHG emissions for PC power plant with and without CO$_2$ capture.
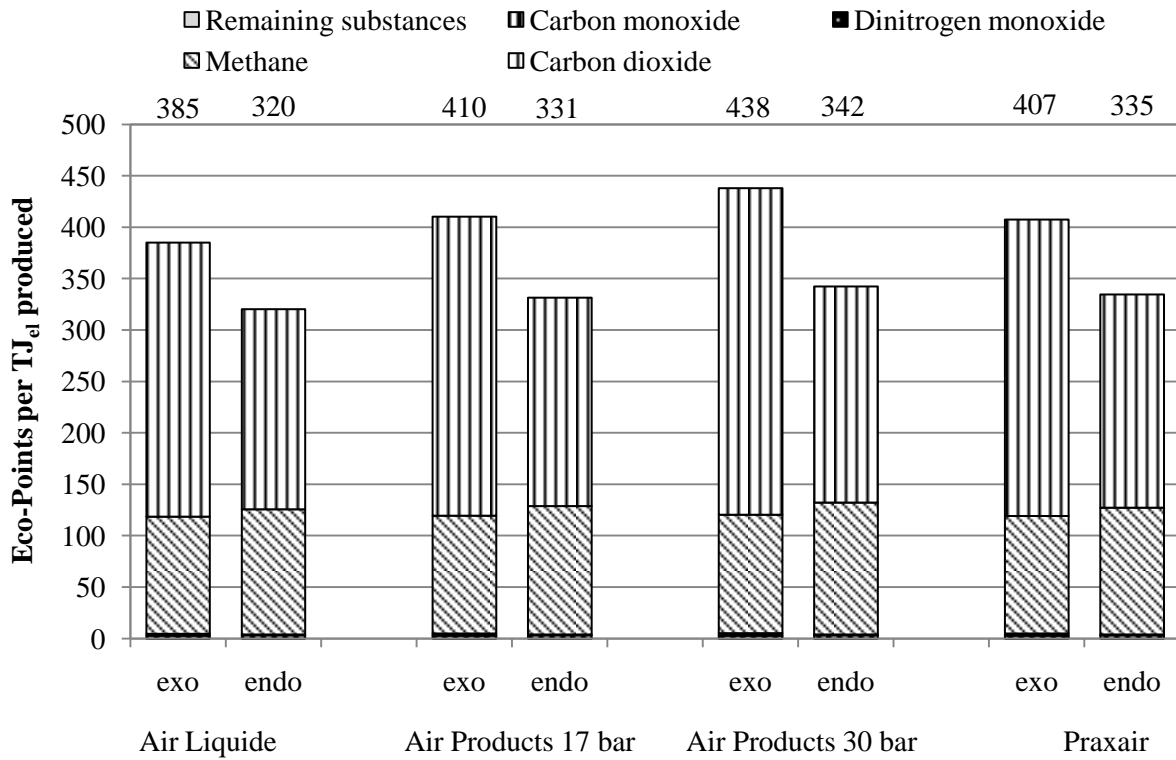
**Figure 68.** Impact of GHG emissions for oxy-fuel power plant with $CO_2$ purification.

As mentioned, the power plants in Italy currently use mainly oil and gas. Therefore the impact on fossil resource depletion determined by the exogenous compensation approach therefore differs considerably from the impact caused by higher coal consumption in the power plants with $CO_2$ capture. This effect is shown in Figure 69 to Figure 71 for the example of resource consumption for all capture configurations.
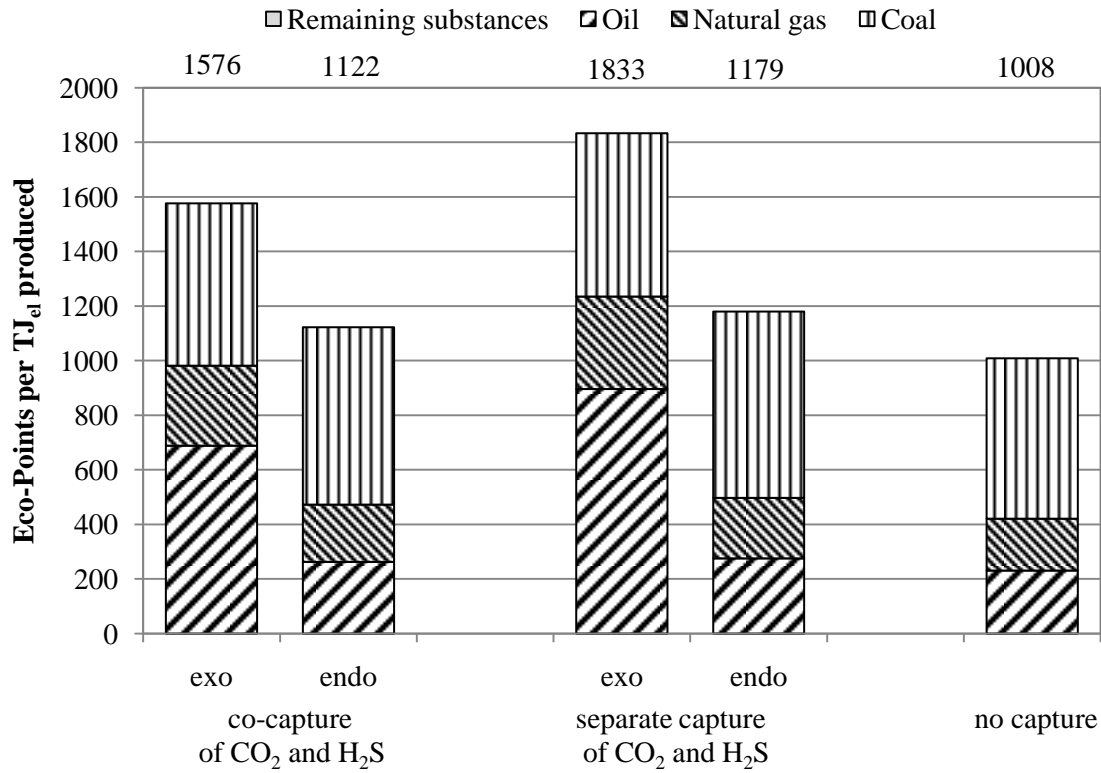
**Figure 69.** Impacts of resource consumption for IGCC with and without acid gas removal.
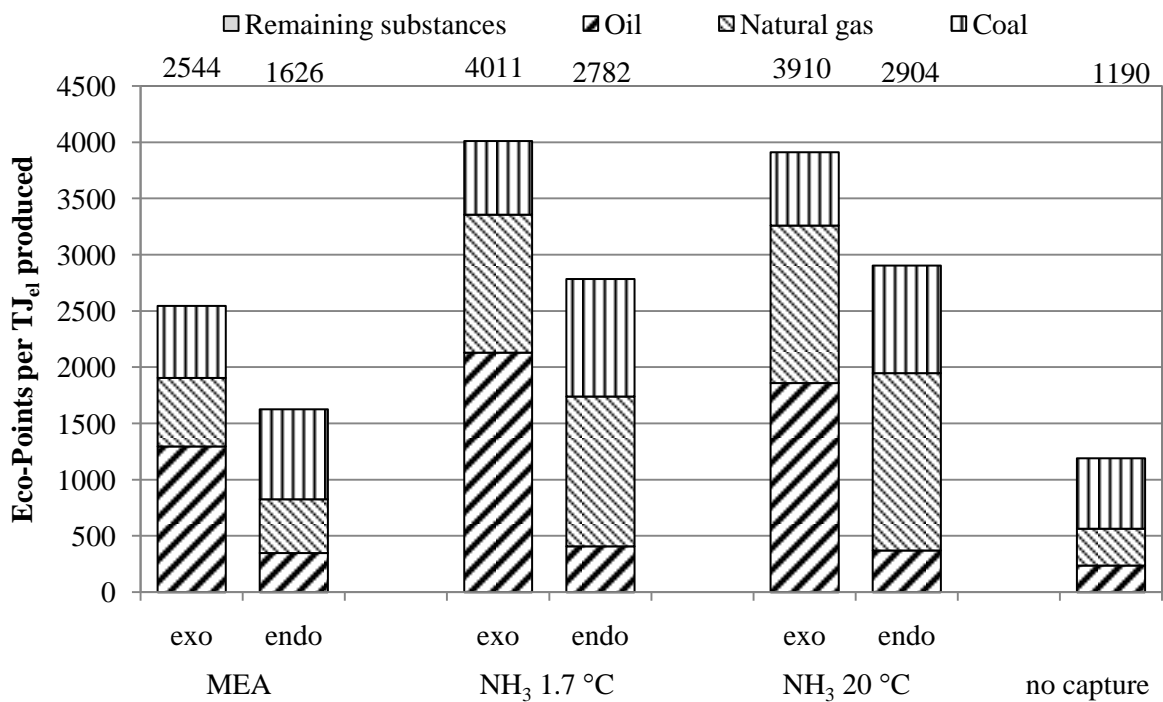


**Figure 70.** Impacts of resource consumption for PC power plant with and without $CO_2$ capture.
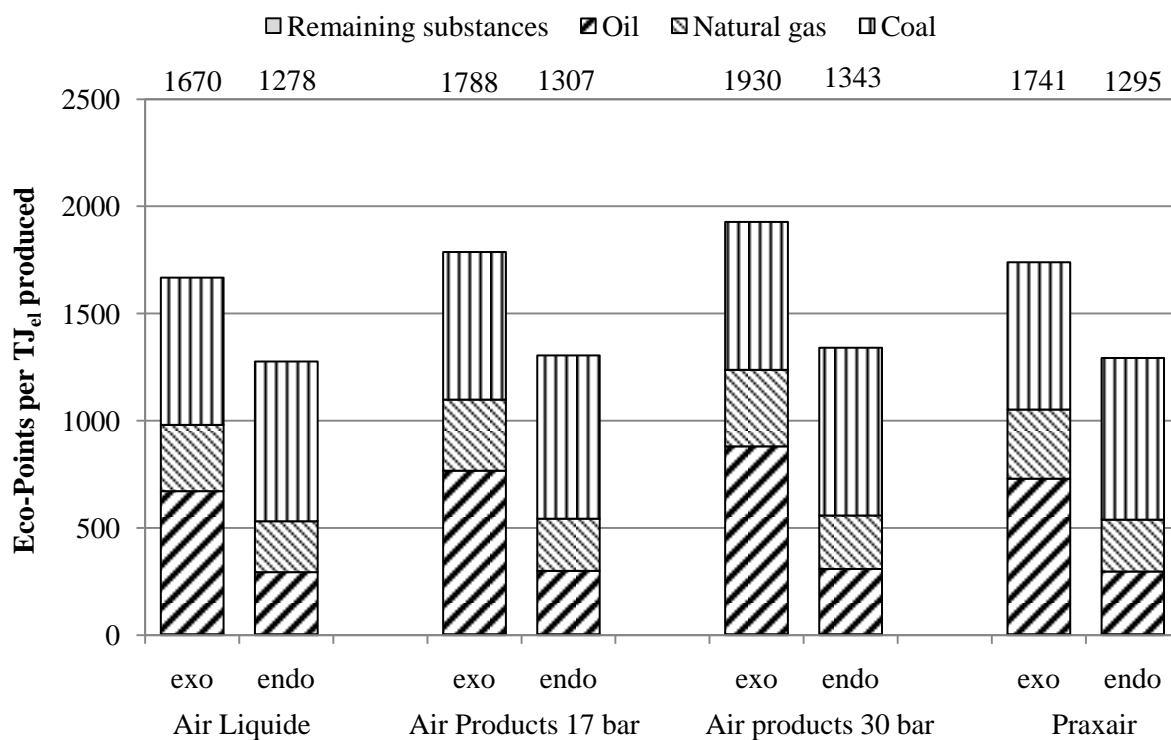
**Figure 71.** Impacts of resource consumption for oxy-fuel power plant with $CO_2$ purification.

It can be seen that even without $CO_2$ capture, oil and gas are consumed for coal processing and transport. Furthermore, in the post-combustion capture options, the production of solvents to make up for losses and degradation has a very prominent effect on overall fossil fuel consumption [51].

The complete weighted environmental impact, divided into different impact categories, is shown for all capture options in Figure 72 to Figure 74.
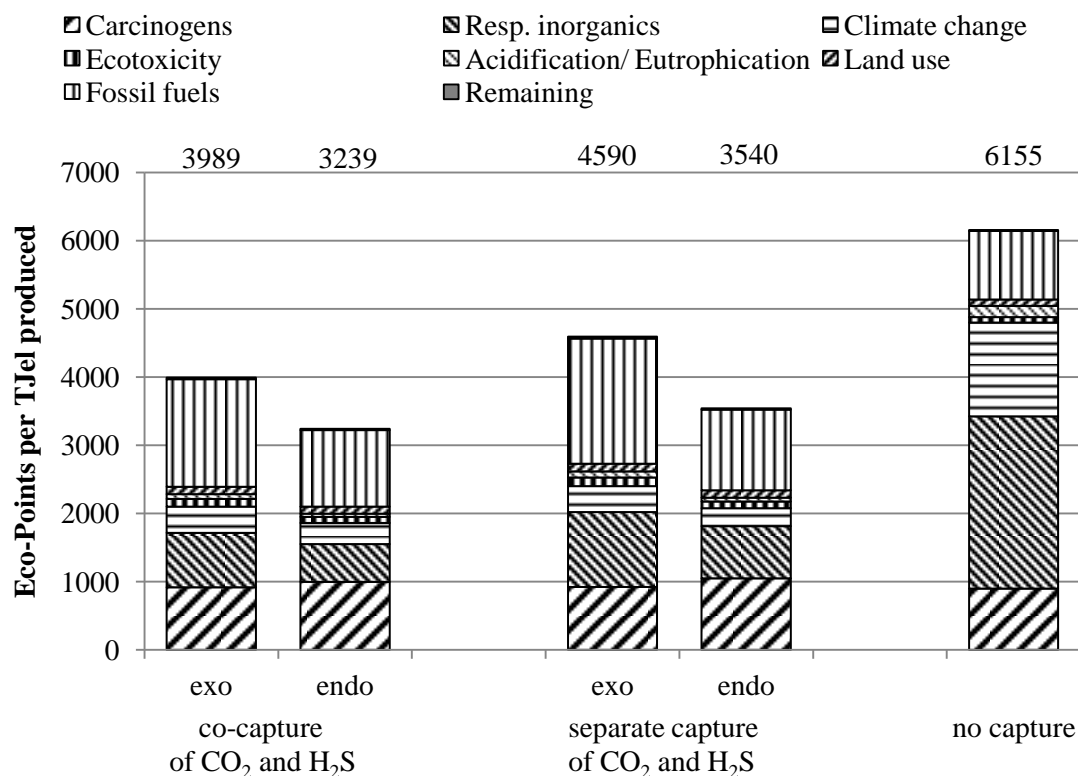


**Figure 72.** Environmental impacts IGCC with and without acid gas removal.
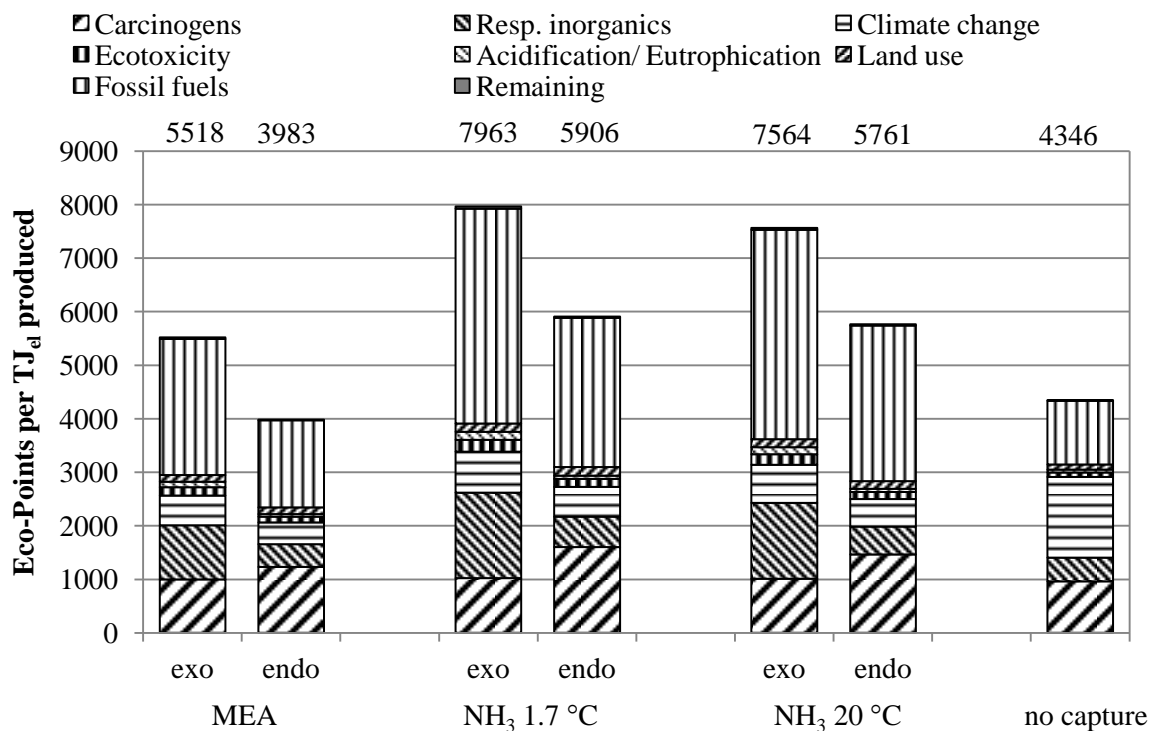


**Figure 73.** Environmental impacts of PC power plant with and without $CO_2$ capture.
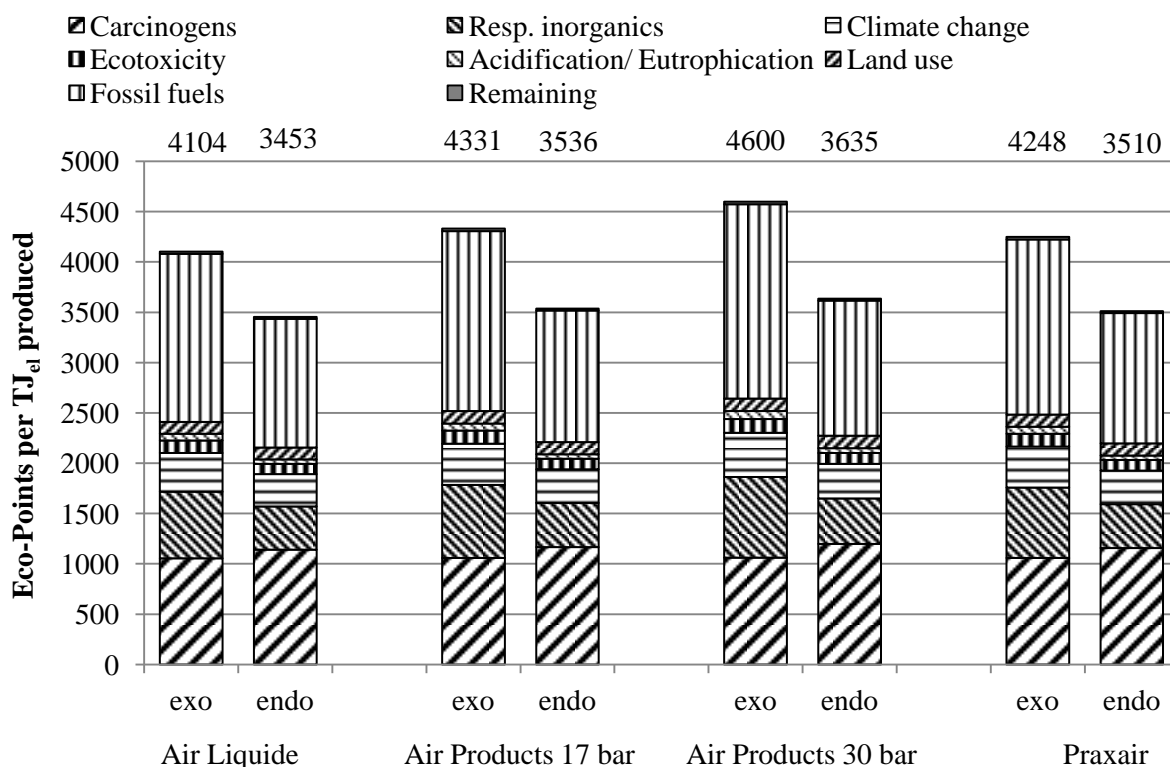
**Figure 74.** Environmental impacts of oxy-fuel power plant with and without $CO_2$ purification.

The only impact category for which the effect of endogenous compensation by higher coal consumption is significantly more pronounced than with exogenous compensation, is the release of carcinogens that are emitted during coal mining, processing, and transport.

The IGCC shows the highest environmental impact of all studied power plants due to the higher sulphur content of the burned coal. This leads to a major release of $SO_2$ and therefore to a high impact in the impact category "respiratory inorganics". It is also the only power plant here, in which this impact category is the major contributor to the overall environmental impact. However, all pre-combustion capture options are able to obtain lower impact values than the ones observed for post-combustion capture.

Although the emission of post-combustion capture solvents could be effectively reduced, the necessary makeup for solvent losses leads to a higher overall environmental impact for post-combustion capture than the impact caused by the PC power plant without $CO_2$ capture. Only for the $CO_2$ post-combustion capture option using MEA, this depends on which penalty compensation approach is chosen ("endo" or "exo").

For the same coal usage, the environmental impact is significantly reduced with all oxy-fuel options except for the Air Products purification option employing a stripper column at 30 bar pressure. For the latter option, this effect again depends on the approach for the compensation of plant efficiency reduction.

138

The complete weighted environmental impact, now divided into damage categories according to the Eco-indicator 99 method, is shown for all capture options in Figure 75 to Figure 77.
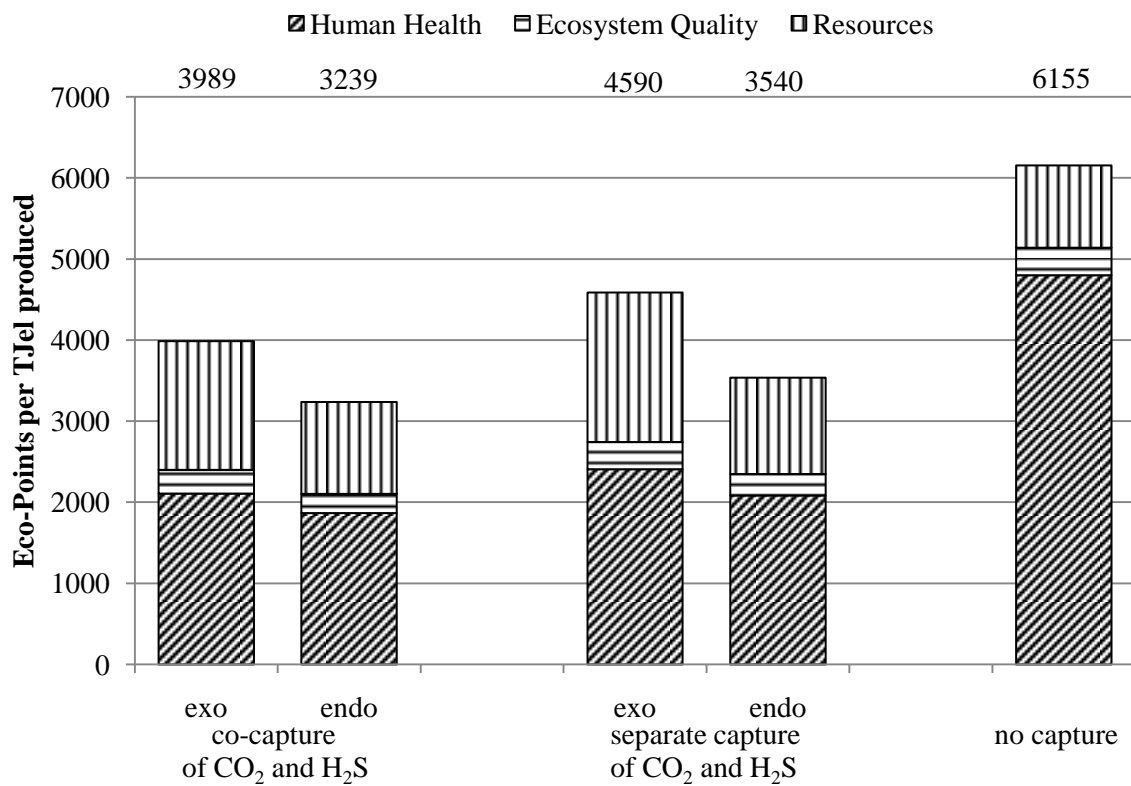


**Figure 75.** Potential environmental damages caused by IGCC with and without acid gas removal.
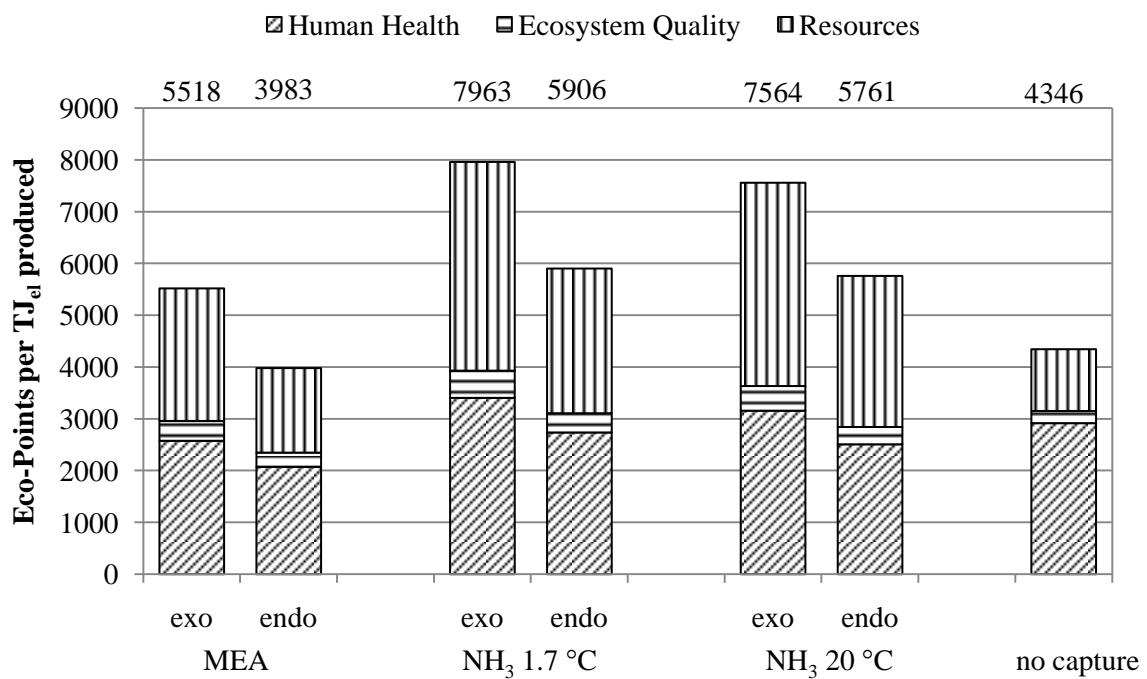


**Figure 76.** Potential environmental damages caused by PC plant with and without $CO_2$ capture.
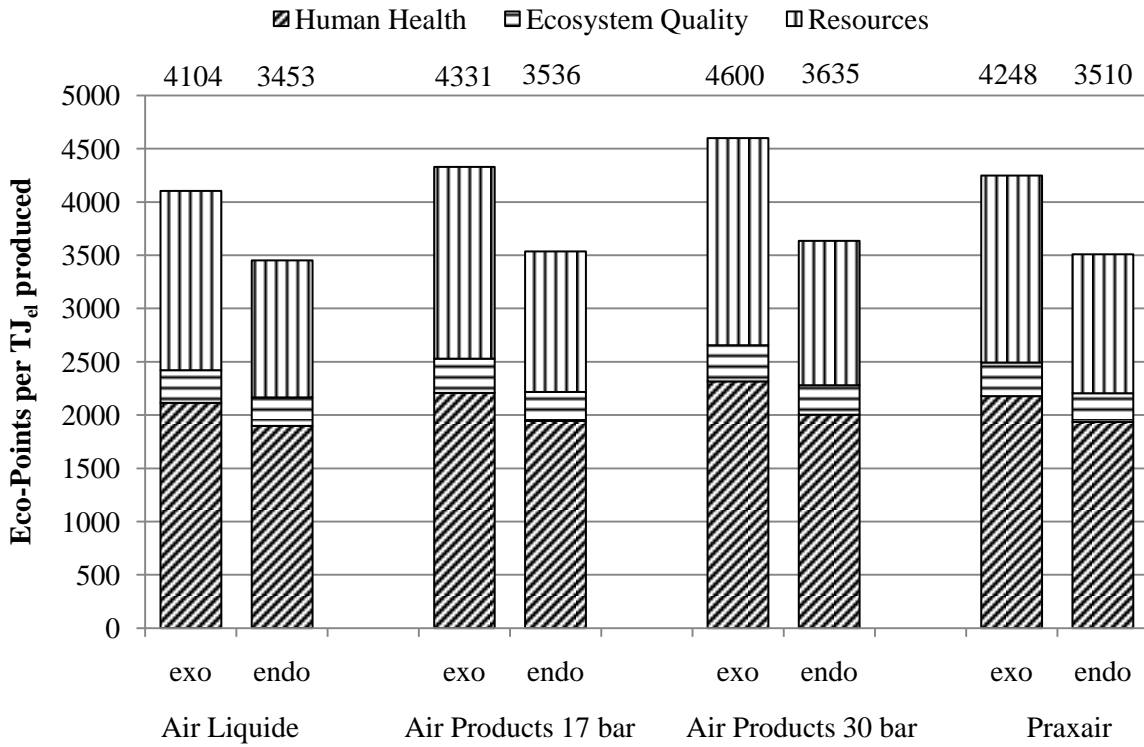
**Figure 77.** Potential environmental damages caused by oxy-fuel plant with $CO_2$ purification.

The environmental impact grouped into damage categories shows a very high value for potential damage to human health in case of the IGCC without acid gas removal. This value is greatly affected by the release of $SO_2$. However, all pre-combustion capture options lead to similar environmental impacts, as observed for the oxy-fuel power plant with $CO_2$ purification.

The highest impact values for the power plants with capture, especially in the damage category "resources", are obtained for the post-combustion capture options. Here, the necessary solvent makeup due to losses and degradation leads to a major consumption of fossil fuels for solvent production [51].

### 5.2.4. Interpretation of LCA results

The IGCC shows the highest energy efficiency of all options studied here, and the penalties introduced by $CO_2$ capture are the lowest as well. Therefore, the environmental impact due to fossil fuel consumption is the lowest for this power plant. Due to the low energy penalty introduced by the use of physical solvents, pre-combustion acid gas removal has also one of the lowest overall environmental effects here. Furthermore no additional harmful substances, e.g. solvents, are emitted, which also leads to a negligible impact caused by solvent production. The total impact of the IGCC may be further reduced by the use of coal with a lower sulphur content.

Of the post-combustion capture options only the use of MEA is capable of reducing the overall environmental impact according to the Eco-indicator 99 method. However, solvent production leads to a major environmental impact due to fossil resource consumption. Solvent emissions are considered harmful respiratory inorganic substances, i.e. they are potentially dangerous to the human health. However, if MEA is to be used, solvent degradation needs to be minimised thorough desulphurisation and denitrification, and possibly also by addition of corrosion inhibitors. For ammonia, alternative processes are necessary to minimise or recuperate ammonia losses due to the high volatility of the solvent.

In the oxy-fuel power plant, compression and purification of the $CO_2$ do not introduce a large penalty. However, due to the large energy requirements for the ASU and for the gas recycle blowers, this power plant has a relatively low energy efficiency. However, with the expected development of more efficient air separation, the energy efficiency is expected to increase [119], leading to a reduced environmental impact.

It can be seen for the majority of impact categories that the impact of energy penalties introduced by $CO_2$ capture is more harmful, if the penalties are compensated for by electricity production in other power plants (according to the energy mix of the considered region Italy) rather than by additional fuel consumption in the investigated power plants. The latter is equivalent to the compensation of the decrease in energy output by identical power plants, i.e. by coal power plants with $CO_2$ capture [51]. The unfavourable effect of exogenous compensation shown here can be explained by the fact that in Italy most energy is still produced by conventional fossil fuel power plants without $CO_2$ capture. The impact of this exogenous compensation may eventually become lower, when a transition to low-carbon power production is made. In other regions with a different energy mix than Italy, the environmental impacts will also be different then.

# 6. Exergetic Life Cycle Assessment

As shown in the previous chapter, the environmental sustainability of processes can be evaluated and compared within the framework of the well-established methodology of Life Cycle Assessment [136, 137]. However, until recently the concept of exergy as a measure for sustainability was omitted from this analysis. Exergy and the depletion of natural resources are directly related, as described by Cornelissen [138]. Therefore, the traditional LCA can be improved by applying this exergy concept, resulting in Exergetic Life Cycle Assessment (ELCA).

## 6.1. Principles of ELCA

Exergy can be regarded as a measure for available energy. Exergy analysis is used to determine the amount of potential work lost during a process and to identify the sources of the greatest losses. For the calculation of the exergy content of a stream, the main components are physical and chemical exergy. Kinetic, potential, nuclear and magnetic influences are usually neglected. The total exergy content of a stream is then calculated by

$$e = e_{ph} + e_{ch} \qquad (56)$$

Physical exergy $e_{ph}$ is defined to be equal to the maximum amount of work obtainable when the stream of a substance is brought from its initial state to the environmental state by physical processes involving only thermal interaction with the environment [139]. The environmental is defined by the pressure $p_0$ and the temperature $T_0$ .

The physical exergy of a stream is then given by

$$e_{ph} = h - h_0 - T_0 \cdot (s - s_0) \qquad (57)$$

Here h and s are the enthalpy and the entropy of the stream at its temperature T and its pressure p. The properties $h_0$ and $s_0$ are the same properties at the environmental conditions $T_0$ and $p_0$.

Chemical exergy $e_{ch}$ is defined to be equal to the maximum amount of work obtainable by bringing a substance from the environmental state to the dead state by processes involving heat transfer and exchange of substances only with the environment [139].

So, while for the calculation of physical exergy, the final state of the stream is the environmental state, for the calculation of chemical exergy the latter is the initial state. The final state in the

case of chemical exergy, the dead state, is reached, when the substance is in thermal, mechanical, and chemical equilibrium with the environment. The tabulated reference values for the substances are obtained at the environmental and partial pressure at which they exist in the environment.

For a mixture of ideal gases the chemical exergy is calculated by

$$e_{ch} = \sum_i (x_i \cdot e_i) + R \cdot T_0 \cdot \sum_i (x_i \cdot \ln(x_i)) \qquad (58)$$

The last part of the equation is identical to the Gibbs energy of mixing

$$dG_{mix} = n \cdot R \cdot T \cdot \sum_i (x_i \cdot \ln(x_i)) \qquad (59)$$

This means that the chemical exergy is the sum of the exergy of the components and the contribution of mixing the pure components [139].

In all real world processes exergy is consumed as entropy is produced [140, 141]. The so-called exergy destruction is proportional the total entropy production

$$dE = T_0 \cdot dS \qquad (60)$$

Here $T_0$ is the temperature of the environment.

The exergy balance can also be written as

$$\dot{E}_{in} + \dot{E}_q = \dot{E}_{out} + \dot{I} + \dot{W} \qquad (61)$$

$\dot{E}_{in}$ and $\dot{E}_{out}$ represent the exergy associated with the mass streams, while $\dot{E}_q$ represents the exergy of heat and $\dot{W}$ the work exchanged with the environment. From the second law of thermodynamic follows that the irreversibility $\dot{I}$ has to be positive.

An exergy analysis can be used to determine the thermodynamic perfection of a system and to show where the work potential of natural resources in relation to the surrounding environment is lost [142]. The maximum work is obtained in a completely reversible process.

In an ELCA, all irreversibilities of the investigated processes are considered for their entire lifetime, so that all life cycle stages have to be included. Furthermore, it is important to not include only the processes within the system, but also the processes related to all incoming and outgoing material and energy streams. A first step was the introduction of the Cumulative Exergy Consumption (CExC) of a product, i.e. the total exergy consumption from the extraction of raw materials to the final product [143]. However, this method does not take into account the exergy destruction associated with the disposal, recycling, or reuse of the product [138].

The irreversibilities due to emissions and the depletion of resources of a non-ideal process can be identified with an exergy analysis. On the basis of such an analysis, it is possible to compare the environmental burden of the investigated processes caused by exergetic resource consumption and emissions. A special case are the zero-exergy emission processes. There all emissions are harmless to the environment because their chemical composition and physical properties are identical to the environment itself [138]. In this case the ELCA will give the same ranking as a conventional LCA, while being able to provide information on the location of the major process irreversibilities. In the special case of a so-called Zero-ELCA, the exergy consumption for the reduction of all harmful emissions to zero in an additional process is included. With the inclusion of this abatement exergy, the life cycle irreversibility can be used as single criterion for the comparison of different processes with the same function, since all other environmental effects will be similar.

Both the LCA and the ELCA have a similar framework with identical goal and scope definitions. If the aim of the ELCA is to identify the process components with the highest irreversibilities or exergy destruction, the inventory has to be much more extensive than in the case of an LCA. A complete flowsheet of the mass and energy streams in the different process steps is then required, and all energy and mass balances need to be closed. A more simplified black box approach may be used if the aim is to compare complete systems. Then, as in an LCA, only the inputs and outputs of the investigated processes are considered.

## 6.2. Exergy analysis of rate-based power plant models

In order to determine the performance of the investigated capture options in terms of process irreversibilities and exergetic efficiencies, an exergy analysis was carried out for the same key processes as in the LCA in the previous chapter.

As a first step all important inputs and outputs of the power plants were identified. For the IGCC with and without pre-combustion capture these exergetic inputs and outputs are shown in Figure 78.
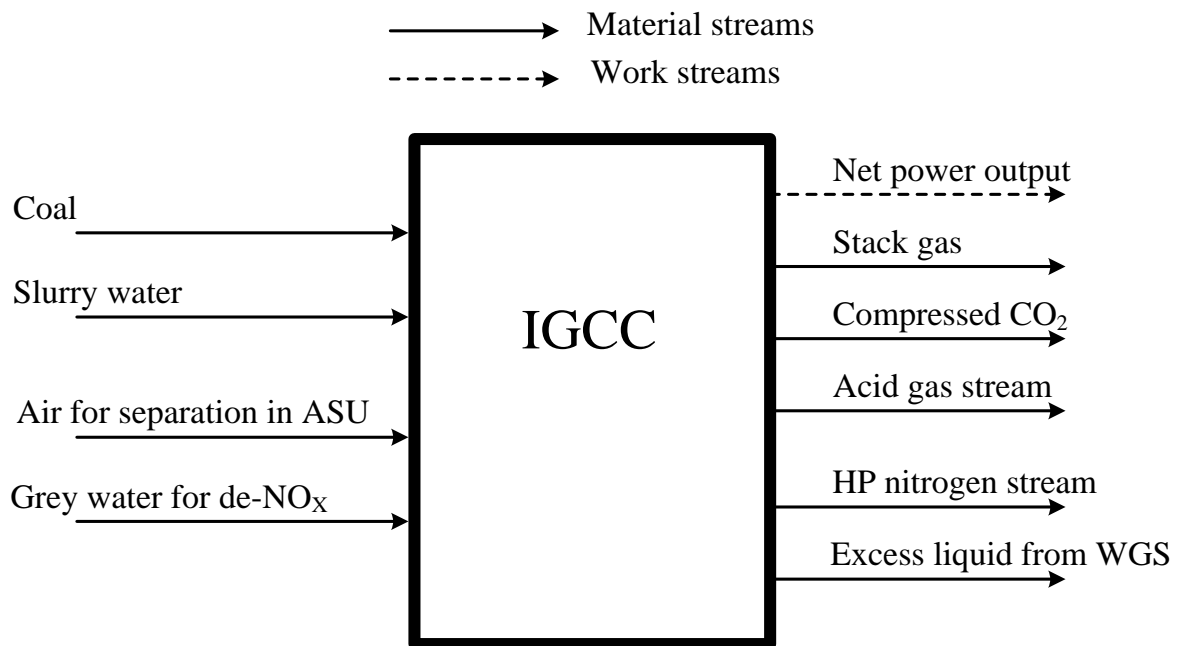


**Figure 78.** Main exergy stream for IGCC with and without acid gas removal.

The flows and exergy contents of the important inputs and outputs of the IGCC are summarised in Table 49.

For the pulverised coal power plant these streams are shown in the form of a diagram in Figure 79, and the data for these streams can be found in Table 50.

For all processes, only the streams directly connected to the power plants were considered here.

**Table 49.** Exergies of main energy and mass flows of IGCC.

| Stream | mass flow (kg/s) | exergy (kJ/kg) | $\dot{E}_{ch}$ (kW) | $\dot{E}_{ph}$ (kW) | Exergy (kW) |
|---|---|---|---|---|---|
| Coal | 43.8 | 29441.0 | 1288000.0 | 0.0 | 1288000.0 |
| Slurry water | 23.5 | 3637.0 | 16214.0 | 69360.0 | 85574.0 |
| Air for separation in ASU | 170.1 | 0.7 | 113.5 | 0.0 | 113.5 |
| HP nitrogen from ASU | 125.2 | 757.8 | 20169.0 | 74686.0 | 94856.0 |
| Grey water for de-NO$_X$ | 18.3 | 65.5 | 1196.0 | 0.0 | 1196.0 |
| Excess liquid from WGS | 29.0 | 310.9 | 7269.0 | 1755.0 | 9024.0 |
| Stack gas (no capture, no shift) | 694.4 | 77.6 | 34556.0 | 19345.0 | 53901.0 |
| Stack gas (separate capture) | 656.3 | 66.3 | 10165.0 | 33361.0 | 43526.0 |
| Stack gas (co-capture) | 652.8 | 56.1 | 10697.0 | 25904.0 | 36601.0 |
| Acid gas stream (separate capture) | 3.1 | 1350.0 | 3976.0 | 261.6 | 4238.0 |
| Compressed CO$_2$ (separate capture) | 73.4 | 706.8 | 33135.0 | 18737.0 | 51872.0 |
| Compressed CO$_2$ (co-capture) | 73.8 | 706.8 | 33311.0 | 18837.0 | 52147.0 |
| Net power output (no capture, no shift) | | | | | 456300.0 |
| Net power output (separate capture) | | | | | 392500.0 |
| Net power output (co-capture) | | | | | 412500.0 |
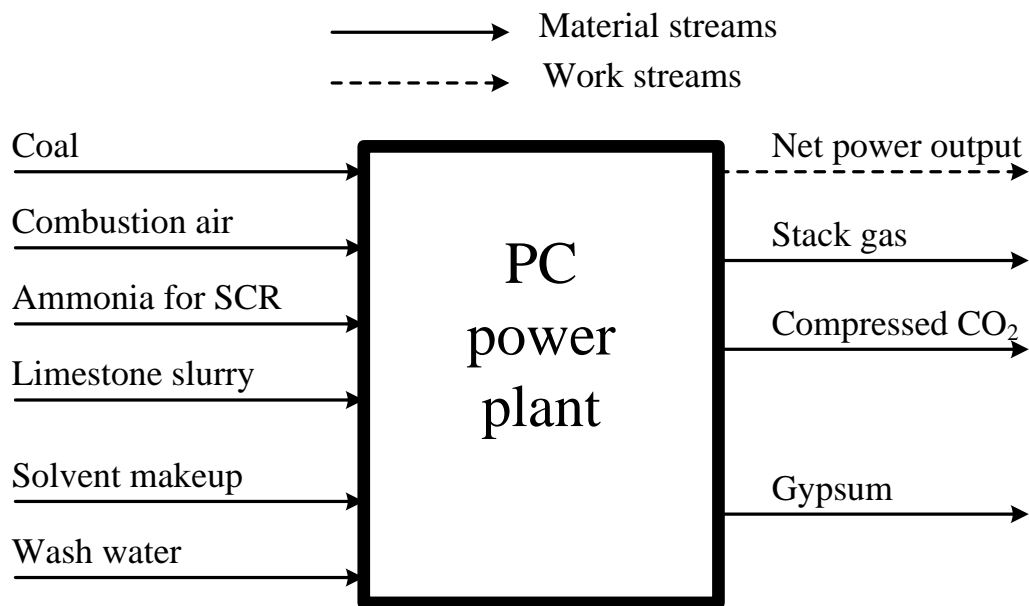


**Figure 79.** Main exergy stream for PC power plant with and without CO$_2$ capture.

**Table 50.** Exergies of main energy and mass flows of PC power plant.

| Stream | mass flow (kg/s) | exergy (kJ/kg) | $\dot{E}_{ch}$ (kW) | $\dot{E}_{ph}$ (kW) | Exergy (kW) |
|---|---|---|---|---|---|
| Coal | 50.4 | 27685.0 | 1395000.0 | 0.0 | 1395000.0 |
| Combustion air | 539.5 | 0.7 | 377.7 | 0.0 | 377.7 |
| Ammonia for SCR | 1.4 | 19307.0 | 27715.0 | 0.0 | 27715.0 |
| Limestone slurry | 20.6 | 47.3 | 971.2 | 0.0 | 971.2 |
| Gypsum | 1.9 | 69.8 | 110.8 | 19.1 | 129.9 |
| Solvent makeup (MEA) | 1.5 | 6935.0 | 10119.0 | 0.0 | 10119.0 |
| Solvent makeup ($NH_3$ 1.7 °C) | 22.8 | 4197.0 | 95748.0 | 0.0 | 95748.0 |
| Solvent makeup ($NH_3$ 20 °C) | 32.6 | 4411.0 | 143637.0 | 0.0 | 143637.0 |
| Waste water stream ($NH_3$ 1.7 °C) | 290.3 | 366.6 | 106396.0 | 0.0 | 106396.0 |
| Waste water stream ($NH_3$ 20 °C) | 359.5 | 349.9 | 125773.0 | 0.0 | 125773.0 |
| Condensate (MEA) | 9.7 | 637.8 | 6156.0 | 0.0 | 6156.0 |
| Stack gas (no capture) | 604.8 | 280.7 | 56895.0 | 112869.0 | 169764.0 |
| Stack gas (MEA) | 471.7 | 20.6 | 9717.0 | 0.0 | 9717.0 |
| Stack gas ($NH_3$ 1.7 °C) | 448.0 | 36.8 | 16493.0 | 0.0 | 16493.0 |
| Stack gas ($NH_3$ 20 °C) | 446.0 | 15.8 | 7051.0 | 0.0 | 7051.0 |
| Compressed $CO_2$ (MEA) | 108.4 | 796.8 | 49351.0 | 36986.0 | 86336.0 |
| Compressed $CO_2$ ($NH_3$ 1.7 °C) | 107.2 | 796.7 | 48822.0 | 36587.0 | 85410.0 |
| Compressed $CO_2$ ($NH_3$ 20 °C) | 108.0 | 817.3 | 49414.0 | 38870.0 | 88284.0 |
| Net power output (no capture) | | | | | 493000.0 |
| Net power output (MEA) | | | | | 386000.0 |
| Net power output ($NH_3$ 1.7 °C) | | | | | 296000.0 |
| Net power output ($NH_3$ 20 °C) | | | | | 323000.0 |

For the oxy-fuel power plant these streams are shown in Figure 80, while the data for these streams can be found in Table 51.
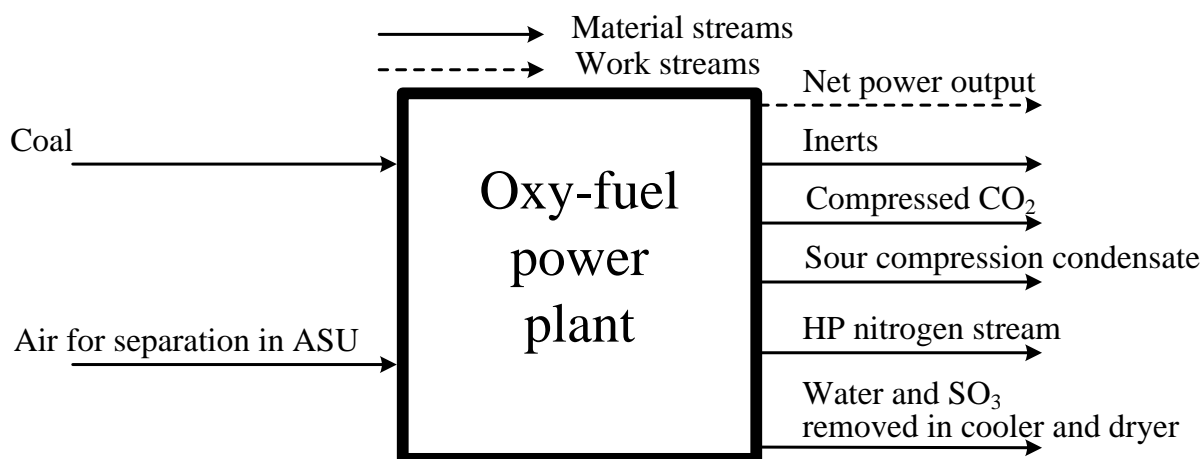
**Figure 80.** Main exergy stream for oxy-fuel power plant with $CO_2$ purification.

**Table 51.** Exergies of main energy and mass flows of oxy-fuel power plant.

| Stream | mass flow (kg/s) | exergy (kJ/kg) | $\dot{E}_{ch}$ (kW) | $\dot{E}_{ph}$ (kW) | Exergy (kW) |
|---|---|---|---|---|---|
| Coal | 55.5 | 27685.0 | 1538000.0 | 0.0 | 1538000.0 |
| Air for separation in ASU | 506.3 | 0.7 | 337.8 | 0.0 | 337.8 |
| HP nitrogen from ASU | 384.2 | 649.2 | 20169.0 | 229208.0 | 249377.0 |
| Water and $SO_3$ removed in cooler and dryer | 22.0 | 2991.0 | 1170.0 | 64624.0 | 65794.0 |
| Condensate Air Products | 5.5 | 357.2 | 1964.0 | 0.0 | 1964.0 |
| Condensate Air Liquide | 5.7 | 379.1 | 2179.0 | 0.0 | 2179.0 |
| Condensate Praxair | 4.8 | 365.0 | 1765.0 | 0.0 | 1765.0 |
| Inerts (Air Products 17 bar) | 39.3 | 131.8 | 5169.0 | 6.2 | 5175.0 |
| Inerts (Air Products 30 bar) | 39.5 | 132.9 | 5237.0 | 6.2 | 5244.0 |
| Inerts (Air Liquide) | 39.3 | 131.7 | 5172.0 | 6.2 | 5179.0 |
| Inerts (Praxair) | 39.3 | 131.8 | 5169.0 | 6.2 | 5175.0 |
| Compressed $CO_2$ (Air Products 17 bar) | 103.9 | 706.8 | 46901.0 | 26521.0 | 73422.0 |
| Compressed $CO_2$ (Air Products 30 bar) | 103.7 | 706.8 | 46815.0 | 26473.0 | 73288.0 |
| Compressed $CO_2$ (Air Liquide) | 103.9 | 706.8 | 46923.0 | 26534.0 | 73457.0 |
| Compressed $CO_2$ (Praxair) | 104.0 | 706.8 | 46955.0 | 26552.0 | 73507.0 |
| Net power output (no capture) | | | | | 500000.0 |
| Net power output (Air Products 17 bar) | | | | | 447000.0 |
| Net power output (Air Products 30 bar) | | | | | 435000.0 |
| Net power output (Air Liquide) | | | | | 457000.0 |
| Net power output (Praxair) | | | | | 451000.0 |

In Table 52, the calculated irreversibilities and exergetic efficiencies of the power plants are listed. Here, the irreversibility or exergy destruction is calculated according to

$$\dot{E}_D = \dot{E}_{in} - \dot{E}_{out} \tag{62}$$

And the simple exergetic efficiency is defined by

$$\varepsilon = \frac{\dot{E}_{out}}{\dot{E}_{in}} \tag{63}$$

For most processes, the output is not only the product but in part also waste.

$$\dot{E}_{out} = \dot{E}_{product} + \dot{E}_{waste} \tag{64}$$

For the exergetic efficiencies based on the useful product of the process, the following definition for the so-called rational exergetic efficiency [139] is used:

$$\psi = \frac{\dot{E}_{product}}{\dot{E}_{in}} \tag{65}$$

The exergy efficiency obtained by this definition depends strongly on which process outputs are considered as useful products.

Both definitions have been applied in the exergy analysis of the power plants. In Table 52, their exergy destruction and exergetic efficiencies are reported. Three different options were considered for the definition of the product of the power plants. The first option considers the produced power to be the only useful product here. The second option also considers the use of the compressed $CO_2$ stream, e.g. in EOR operations, while the last efficiency value includes the use of the compressed nitrogen stream leaving the ASU. In the case of $CO_2$ purification in oxy-fuel combustion, this nitrogen stream could be used for power generation in a turbine when being mixed to the separated inerts.

**Table 52.** Exergy destruction $\dot{E}_D$ and exergetic efficiencies of all power plant configurations.

| Capture option | $\dot{E}_D$ (MW) | $\varepsilon$ | $\psi$ (electricity) | $\psi$ (+ $CO_2$) | $\psi$ (+ $N_2$) |
|---|---|---|---|---|---|
| **Pre-combustion capture** | | | | | |
| No capture | 761 | 44.7% | 33.2% | -- | 40.1% |
| Separate capture | 779 | 43.4% | 28.5% | 32.6% | 39.5% |
| Co-capture | 770 | 44.0% | 30.0% | 33.8% | 40.7% |
| **Post-combustion capture** | | | | | |
| No capture | 764 | 46.5% | 34.6% | -- | -- |
| MEA | 949 | 34.0% | 26.9% | 32.9% | -- |
| $NH_3$ (1.7 °C) | 1018 | 33.2% | 19.4% | 25.0% | -- |
| $NH_3$ (20 °C) | 1026 | 34.7% | 20.6% | 26.2% | -- |
| **Oxy-fuel** | | | | | |
| Air Products (17 bar) | 827 | 48.4% | 27.9% | 32.4% | 48.0% |
| Air Products (30 bar) | 839 | 47.7% | 27.1% | 31.7% | 47.2% |
| Air Liquide | 817 | 49.1% | 28.5% | 33.1% | 48.6% |
| Praxair | 823 | 48.7% | 28.1% | 32.7% | 48.2% |

The difference between the simple exergetic efficiency $\varepsilon$ and the exergy definition distinguishing between exergy product and losses shows that a significant amount of the exergy leaving the process is lost. For more efficient energy generation these losses should be reintegrated to the power plants whenever and wherever possible. If for example the exergy content of the compressed nitrogen stream from the ASU could be used either in the gasification process or by expansion in a turbine, exergy losses could be reduced to a minimum. In the case of post-combustion capture, losses are caused by solvent degradation (MEA) and to a significant amount by solvent losses in the case of ammonia. These losses cannot be compensated for.

With electricity as the only useful product, the highest rational exergy efficiency $\psi$ was observed for pre-combustion acid gas removal. If the compressed nitrogen stream were to be integrated, the highest exergy efficiency would be obtained with the oxy-fuel processes.

## 6.3. ELCA of rate-based power plant models

For the investigated power plant configurations, the same lifetime as in the LCA was assumed, i.e. the power plants run an average of 6000 h/a at 100% capacity for 30 years. The goal and scope definition as well as the complete inventory for the different power plants with and without $CO_2$ capture can be found in chapter 5.2, where the Life Cycle Analysis of these power plant configurations was discussed. The possible use of the compressed $CO_2$ in EOR and the use of the compressed nitrogen were disregarded in this ELCA. However, as listed in Table 53, the Cumulative Exergy Consumption (CExC) of the used materials for the power plant construction was taken into account [144].

**Table 53.** Cumulative exergy consumption of resources and utilities for plant construction.

| Material or Utility | CExC |
|---|---|
| Concrete | 1.1 MJ/kg |
| Rock wool | 21.1 MJ/kg |
| Aluminium | 250 MJ/kg |
| Steel (95% low-alloy) | 54 MJ/kg |
| Copper | 67 MJ/kg |
| Polyethylene | 86 MJ/kg |
| Truck transport | 3.13 MJ/tkm |

**Table 54.** CExC and end-of-life irreversibilities related to power plant construction.

| Capture option | CExC | CExC + waste scenario |
|---|---|---|
| **Pre-combustion capture** | | |
| No capture | 5883.2 | 11001 |
| Separate capture | 5905.9 | 11044 |
| Co-capture | 5928.7 | 11086 |
| **Post-combustion capture** | | |
| No capture | 4249.9 | 7947 |
| MEA | 4272.7 | 7990 |
| $NH_3$ | 4295.5 | 8033 |
| **Oxy-fuel** | | |
| All configurations | 4771.1 | 8922 |

Since the CExC values do not include the exergy destruction at the end of the life cycle of the power plants [138], the same relationship as found in Figure 65 was used to include this influence here. The total CExC and the end-of-life exergy destruction of the used materials are shown in Table 54.

For the power plants already selected in the previous chapter on Life Cycle Assessment of the rate-based capture options, the cumulated irreversibilities or exergy destruction over the entire life cycle are presented in Figure 81 to Figure 83. The environmental cost for coal mining, processing, and transport was included here and found to be an additional 3 per cent of the exergy content of the used coal [145].
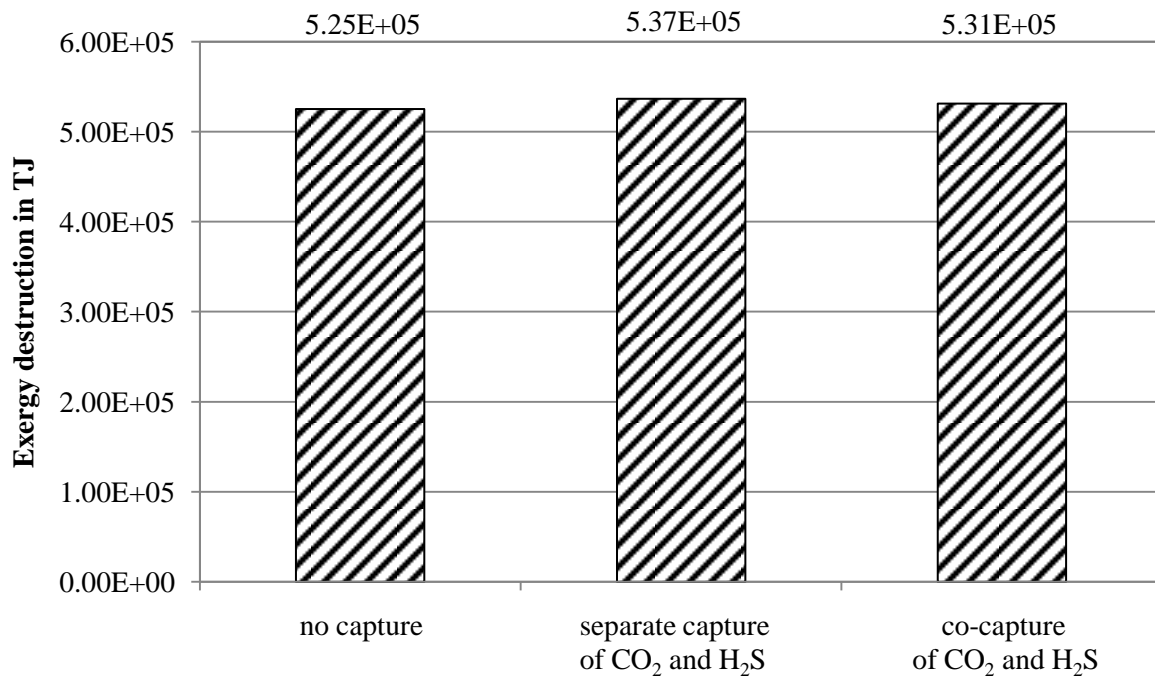


**Figure 81.** Life cycle irreversibilities of IGCC with and without acid gas removal.

The addition of acid gas removal to the power plant leads only to a minor increase in exergy destruction inside the power plant. Here, the co-capture of $H_2S$ and $CO_2$ had a lower exergetic impact than the separate capture of these acid gas components.
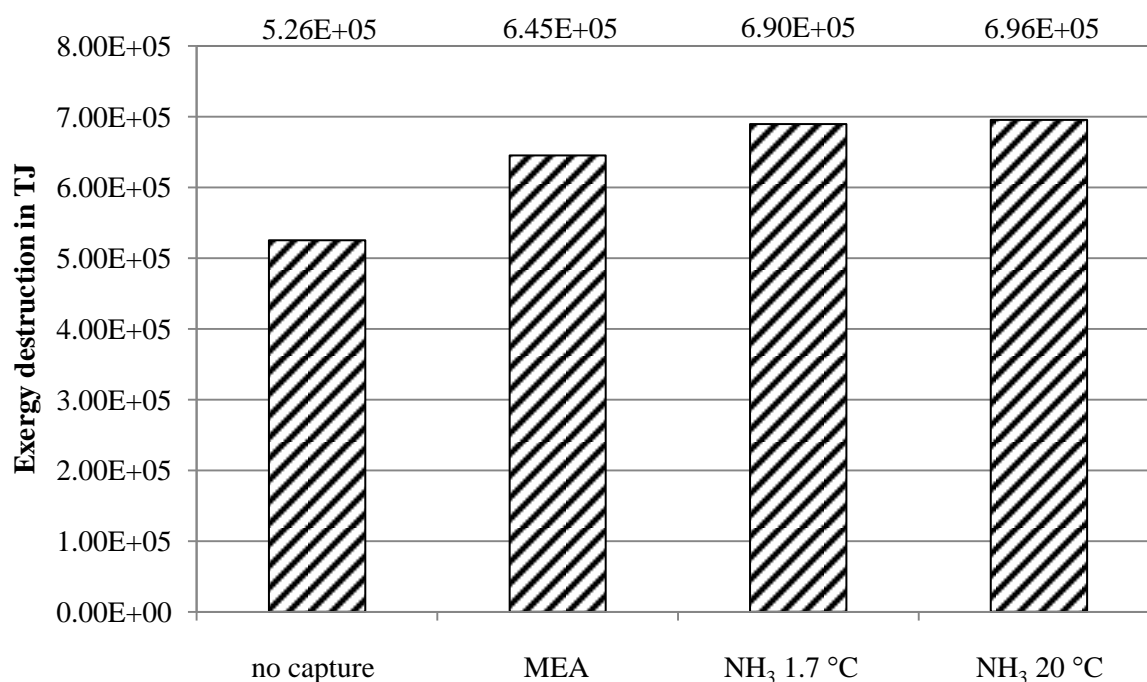
**Figure 82.** Life cycle irreversibilities of PC power plant with and without $CO_2$ capture.

As can be seen in Figure 82, the exergetic impact of $CO_2$ capture was more pronounced for post-combustion capture. The lowest impact could be observed for monoethanolamine. Contrary to the LCA, the lower ammonia solvent temperature (1.7 °C) led to slightly lower irreversibilities than the use of the ammonia solvent at 20 °C. This can be explained by the fact that the higher solvent temperature requires an increased exergetic input in the form of solvent makeup. Since much of this added solvent leaves the process with the wash water from the secondary gas treatment, the overall exergy destruction is higher, although the exergetic efficiency of the power plant with the low-temperature solvent is lower.
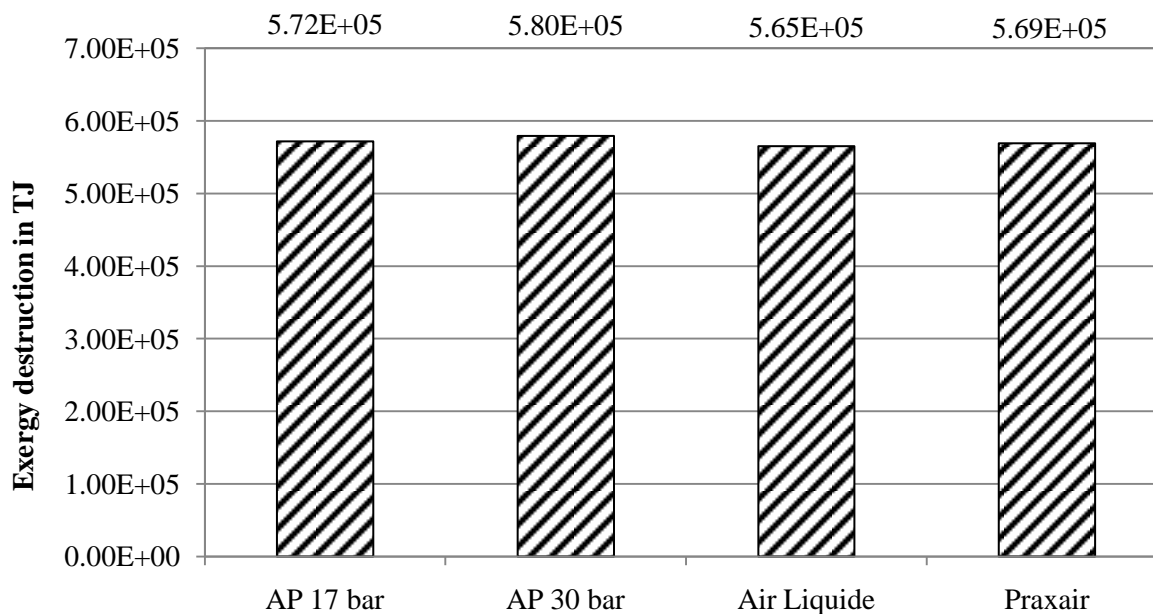
**Figure 83.** Life cycle irreversibilities of oxy-fuel power plant with $CO_2$ purification.

The results for the cumulated irreversibilities in the oxy-fuel processes as presented in Figure 83 show good agreement with the LCA results previously shown in Figure 74. The lowest impact was again observed for the gas treatment according to the Air Liquide patent application [126].

To summarise the results shown in Figure 81 to Figure 83, the lowest exergy destruction was observed for pre-combustion $CO_2$ capture, followed by oxy-fuel $CO_2$ purification. The exergy destruction in the latter power plant type could be significantly reduced, if the exergy content of the compressed nitrogen stream leaving the ASU could be integrated, e.g. by expansion in a gas turbine together with the inerts separated in the $CO_2$ purification section. Without $CO_2$ capture the irreversibilities in the pulverised coal power plant are similar to the IGCC plant.

Few values for the exergy destruction related to minimizing all harmful emissions to an absolute minimum can be found in the literature [138]. The reported values are mainly based on fixed standard values related to the treatment of these emissions. Furthermore, these values are based on realistic levels of emission reduction and not on 100% emission abatement. As can be observed from this study, the irreversibilities introduced by the gas treatment vary considerably, depending on the nature of the power plant and the adopted abatement technology. With all capture options, $SO_X$ and $NO_X$ emissions were significantly reduced. $CO_2$ emissions were reduced by approximately 90%. Further reduction using the investigated methods would lead to drastically increased penalties and cannot be considered to be practical. An additional Zero-ELCA was therefore not carried out here. For the respective capture method (pre-combustion, post-combustion, oxy-fuel process), the lowest calculated cumulative irreversibility or exergy destruction should be considered as synonymous to the result for a zero-emission process.

# 7. Conclusions

Power plant performance with and without capture was modelled with the flowsheet simulation program Aspen Plus. In a first step, models were developed that assume chemical and vapour-liquid equilibrium. In order for the models to be as realistic as possible, rate-based models that take into account the kinetics of the occurring chemical reactions and of mass transfer were investigated.

The rate-based models studied in this thesis are for

i)        a 500 MW pulverised coal power plant using monoethanolamine (MEA) and ammonia as chemical solvents for post-combustion $CO_2$ capture,

ii)       a 500 MW Internal Gasification Combined Cycle (IGCC) with the physical solvent for either separate or co-capture of $CO_2$ and $H_2S$, and

iii)      a 500 MW oxy-fuel power plant with cryogenic $CO_2$ purification.

The results obtained by flowsheet simulations and by Life Cycle Assessment show the advantages and disadvantages of all three groups of capture options studied here.

## 7.1.  Technical performance

The IGCC shows the highest energy efficiency of all options studied here, and the penalties introduced by $CO_2$ capture are the lowest as well. However, IGCC are very complex and require high capital costs [30]. These costs are even higher from the beginning, since retrofitting an IGCC with $CO_2$ capture is not feasible. The $CO_2$ captured with this option has also the lowest purity, so that the storage site should be near the power plant, especially for co-capture of $CO_2$ and $H_2S$. If the $CO_2$ is to be transported or used in EOR, further treatment may be necessary to prevent equipment damage.

The simplest option, which may also be used to retrofit existing power plants, is the post-combustion capture option, provided that $SO_X$ and $NO_X$ are reduced to the required levels to minimise solvent degradation. Due to the thermal regeneration of the solvent with medium-pressure steam, power plant output is reduced significantly. If solvent cooling by water is not sufficient, a further energy penalty is introduced by the chiller. Chilling was necessary to minimise solvent evaporation in post-combustion capture with ammonia. The $CO_2$ captured with this method is very pure, however. This makes it very attractive for transport to more distant storage sites, or for its use in EOR.

The oxy-fuel power plant is an attractive option, since compression and purification of the $CO_2$ do not introduce a large energy penalty. Relatively high purities of the $CO_2$ stream can be reached, so that it is suitable for EOR. However, due to the large energy requirements for the ASU and for the gas recycle blowers, this type of power plant has a relatively low energy efficiency.

155

## 7.2. Environmental performance

A major impact in the IGCC is caused by the emission of $SO_X$ due to the high sulphur content of the coal used in the investigated model. This impact may be reduced by burning coal with lower sulphur content, although this choice of fuel may usually not be possible. However, due to the pre-combustion capture of $H_2S$ alongside $CO_2$ significantly reduces this impact. Moreover, the use of a physical solvent with very low volatility in pre-combustion acid gas removal leads to one of the lowest overall environmental effects of all studied capture options here.

In post-combustion capture, solvent production leads to a major environmental impact caused by increased fossil resource consumption. Fresh solvent needs to be continuously fed to the capture installation due to degradation in the case of MEA and due to solvent emissions, which are especially pronounced for the use of ammonia due to its high volatility. Solvent emissions are also considered harmful respiratory inorganic substances, which are potentially harmful to the human health.

Oxy-fuel combustion with $CO_2$ purification according to the Air Liquide patent application shows also the lowest environmental impact of all investigated capture options, since emissions are relatively low and no environmentally harmful substances are added for capture.

## 7.3. Exergo-environmental performance

The lowest impact caused by process irreversibilities, i.e. exergy destruction was observed for pre-combustion $CO_2$ capture, followed by oxy-fuel $CO_2$ purification. The exergy destruction in the latter power plant type would be significantly reduced, if the exergy content of the compressed nitrogen stream leaving the ASU could be integrated, e.g. by expansion in a gas turbine together with the inerts separated in the $CO_2$ purification section. Without $CO_2$ capture the irreversibilities in the pulverised coal power plant are similar to the IGCC plant.

For the respective capture method, i.e. pre-combustion, post-combustion, or oxy-fuel, the lowest calculated cumulative irreversibility or exergy destruction should be considered as synonymous to the result for a zero-emission process.

# 7.4. Comparison

Finally, Table 55 summarises all findings from the flowsheet simulations and the LCA described above by showing in compact form quantitative results for the most relevant investigated capture options.

**Table 55.** Technical, environmental, and exergo-environmental performance of capture options.

| | Pre-combustion | | Post-combustion | | Oxy-fuel |
| --- | --- | --- | --- | --- | --- |
| | separate capture | co-capture | Capture with MEA | Capture with $NH_3$ (20 °C) | Air Liquide |
| Power plant net output in $MW_{el}$ | 393 | 413 | 386 | 323 | 457 |
| Power plant efficiency (HHV-based) | 33.2% | 34.9% | 28.4% | 23.8% | 31.8% |
| Reduction of power plant output | 13.5% | 9.1% | 21.7% | 34.5% | 8.6% |
| Specific energy penalty in $GJ_{el}$/t $CO_2$ | 0.67 | 0.48 | 1.00 | 1.58 | 0.41 |
| Effective $CO_2$ removal | 87.9% | 88.5% | 87.2% | 84.7% | 86.6% |
| Eco-points / $TJ_{el}$ ("exo" approach) | 4590 | 3989 | 5518 | 7564 | 4104 |
| Eco-points / $TJ_{el}$ ("endo" approach) | 3540 | 3239 | 3983 | 5761 | 3453 |
| Rational exergetic eff. (electricity) | 28.5% | 30.0% | 26.9% | 20.6% | 28.5% |
| Life cycle irreversibilities in $10^5$ TJ | 5.37 | 5.31 | 6.45 | 6.96 | 5.65 |

In Table 56, the advantages and disadvantages of all investigated capture methods are compared. Despite different favourable technical and environmental performances, no final recommendation for one capture method can be made.

**Table 56.** Overview of advantages and disadvantages of studied capture processes.

| | **Pre-combustion capture** | **Post-combustion capture** | **Oxy-fuel plant with CO$_2$ purification** |
|---|---|---|---|
| **Advantages** | Highest effective CO$_2$ removal efficiency.<br><br>Highest power plant efficiency.<br><br>Relatively low efficiency reduction in power plant.<br><br>If co-capture of H$_2$S and CO$_2$ is viable, lowest environmental impact. | Possible retrofit option.<br><br>Can be applied to fuel burning with air at atmospheric pressure, the most widespread fuel conversion process.<br><br>High CO$_2$ purity. | Possible retrofit option for existing power plants (although air leakage needs to be reduced to a minimum).<br><br>Lowest efficiency reduction in power plant.<br><br>Low environmental impact.<br><br>Ultra-pure CO$_2$ product. |
| **Disadvantages** | Not a retrofit option.<br><br>Complex and costly power plant design.<br><br>Low CO$_2$ purity may cause problems in transport and storage. | Lowest power plant efficiency.<br><br>Energy and exergy penalty and plant efficiency reduction much higher than for other capture options. | ASU introduces high energy and exergetic penalty. |

The choice of one capture technology depends on various factors. These factors are mainly costs (complexity of plant design, retrofit option), available coal type and the intended use of the CO$_2$ stream and its necessary purity. Despite showing the highest impact on plant performance and the environment, post-combustion capture could therefore be the method of choice, as its applicability is not limited to power plants, so that it can be used in a wide range of industrial processes. Decision parameters may change in the future, e.g. depending on developments for chemical solvents or liquid membranes for post-combustion capture, or more effective air separation for oxy-fuel processes and gasification.

# References

[1]     IEA-GHG. $CO_2$ Emissions from Fuel Combustion. OECD/IEA. 2009.

[2]     Pachauri, R K, Reisinger, A. Climate Change 2007: Synthesis Report. Contribution of Working Groups I, II and III to the Fourth Assessment Report of the Intergovernmental Panel on Climate Change. IPCC, Geneva, Switzerland. 2007.

[3]     UNFCCC. Uniting on climate: A guide to the Climate Change Convention and the Kyoto Protocol. 2007.

[4]     Hein, K R G. Carbon dioxide capture - Reasons, requirements and technology. In: IEA GHG International Interdisciplinary Summer School. 2007.

[5]     Forster, P, Ramaswamy, V, Artaxo, P, Berntsen, T, Betts, R, Fahey, D W, et al. Changes in atmospheric constituents and in radiative forcing. In: Climate Change 2007: The Physical Science Basis. Contribution of Working Group I to the Fourth Assessment Report of the Intergovernmental Panel on Climate Change. 2007.

[6]     Solomon, S, Qin, D, Manning, M, Chen, Z, Marquis, M, Averyt, K B, et al. Summary for policymakers. In: Climate Change 2007: The Physical Science Basis. Contribution of Working Group I to the Fourth Assessment Report of the Intergovernmental Panel on Climate Change. 2007.

[7]     UNFCCC. 2009. Available from: http://www.unfccc.int.

[8]     Kyoto2.org. 2009. Available from: http://www.kyoto2.org/page112.html.

[9]     IEA-GHG. Prospects for $CO_2$ capture and storage. IEA GHG. 2004.

[10]    IEA-GHG. World Energy Outlook 2009 - presentation to the press. OECD/IEA. 2009.

[11]    Kohl, A L, Nielsen, R B. Gas dehydration and purification by adsorption. In: Gas Purification (Fifth Edition). Gulf Professional Publishing. 1997. pp. 1022 – 1135.

[12]    Metz, B, Davidson, O, de Coninck, H C, Loos, Meyer , L A (eds ). Carbon dioxide capture and storage. In: IPCC Special Report on Carbon Dioxide Capture and Storage. Prepared by Working Group III of the Intergovernmental Panel on Climate Change. 2005.

[13]    Sims, R E H, Schock, R N, Adegbululgbe, A, Fenhann, J, Konstantinaviciute, I, Moomaw, W, et al. Energy supply. In: Climate Change 2007: Mitigation. Contribution of Working Group III to the Fourth Assessment Report of the Intergovernmental Panel on Climate Change. 2007.

[14]    Haefeli, S, Bosi, M, Philibert, C. Carbon dioxide capture and storage issues – Accounting and baselines under the United Nations Framework Convention on Climate Change (UNFCCC). IEA. 2004.

[15]    Wilson, M, Monea, M. IEA GHG Weyburn $CO_2$ monitoring and storage project summary report 2000-2004. In: Proceedings of the 7th International Conference on Greenhouse Gas Control Technologies. 2004.

[16]    IEA GHG. 2009. Available from: http://www.co2captureandstorage.info.

[17]    MIT. 2009. Available from: http://sequestration.mit.edu/tools/projects/index.html.

[18]    CO2net. 2009. Available from: http://www.co2net.eu/public/index.asp.

[19]    BP, Statoil, Sonatrach. 2009. Available from: http://www.insalahco2.com.

[20] Strömberg, L, Lindgren, G, Anheden, M, Simonsson, N, Köpcke, M; Vattenfall AB. Vattenfall's 30 MWth oxyfuel pilot plant project. 2006.

[21] Kubek, D. Large CO2 sources & capture systems. In: Workshop on Future Large $CO_2$ Compression Systems. Gas Processing Solutions LLC. 2006.

[22] Thomas, D C, Kerr, H R. Introduction. In: Carbon Dioxide Capture for Storage in Deep Geologic Formations. Elsevier Science. 2005.

[23] Feron, P H M, Jansen, A E. 2002. $CO_2$ separation with polyolefin membrane contactors and dedicated absorption liquids: Performances and prospects. Separation and Purification Technology. Vol 27, no. 3. pp. 231 – 242.

[24] Klaassen, R, Feron, P H M, Jansen, A E. 2005. Membrane contactors in industrial applications. Chemical engineering research and design. Vol 83, no. 3. pp. 234 – 246. Process Developments in Membrane Contactors and Reactors.

[25] Marano, J J, Ciferino, J P. 2009. Integration of gas separation membranes with IGCC identifying the right membrane for the right job. Energy Procedia. Vol 1, no. 1. pp. 361 – 368. Greenhouse Gas Control Technologies 9, Proceedings of the 9th International Conference on Greenhouse Gas Control Technologies (GHGT-9), 16-20 November 2008, Washington DC, USA.

[26] Dijkstra, J W, Jansen, D. Novel concepts for $CO_2$ capture with SOFC. In: Gale, J, Kaya, Y, editors. Greenhouse Gas Control Technologies - 6th International Conference. Pergamon. 2003. pp. 161 – 166.

[27] Lee, M C, Seo, S B, Chung, J H, Kim, S M, Joo, Y J, Ahn, D H. 2009. Gas turbine combustion performance test of hydrogen and carbon monoxide synthetic gas. Fuel. Vol In Press, Corrected Proof. pp–.

[28] Wright, I G, Gibbons, T B. 2007. Recent developments in gas turbine materials and technology and their implications for syngas firing. International Journal of Hydrogen Energy. Vol 32, no. 16. pp. 3610 – 3621. TMS06: Symposium on Materials in Clean Power Systems.

[29] Chen, C. A technical and economic assessment of $CO_2$ capture technology for IGCC power plants. Carnegie Mellon University, USA. 2005.

[30] IEA-GHG. $CO_2$ capture in low rank coal power plants. IEA GHG. 2006.

[31] Sciamanna, S, Lynn, S. 1988. Solubility of hydrogen sulfide, sulfur dioxide, carbon dioxide, propane, and n-butane in polyglycol ethers. Industrial & Engineering Chemistry Research. Vol 27. pp. 492 – 499.

[32] IEA-GHG. Potential for improvements in gasification combined cycle power generation with $CO_2$ capture. IEA GHG. 2003.

[33] ZEP. Strategic research agenda. The European Technology Platform for Zero Emission Fossil Fuel Power Plants. 2006.

[34] Lombardi, L. LCA comparison of technical solutions for $CO_2$ emissions reduction in power generation. University of Florence, Italy. 2000.

[35] Epps, R. Use of Selexol solvent for hydrocarbon dewpoint control and dehydration of natural gas. In: Laurance Reid Gas Conditioning Conference. 1994.

[36] Doctor, R D, Molburg, J C, Thimmapuram, P R, Berry, G F, Livengood, C D. Gasification combined cycle: Carbon dioxide recovery, Transport, and Disposal. Argonne National laboratory. 1994.

[37] Kubek, D I, Polla, E, Wilcher, F P. Purification and recovery options for gasification. UOP. 2000.

[38]   Lampert, K, Ziebik, A. 2007. Comparative analysis of energy requirements of $CO_2$ removal from metal-lurgical fuel gases. Energy. Vol 32, no. 9. pp. 521 − 527.

[39]   Lampert, K. Energy analysis of $CO_2$ removal in CHP plant fired with Corex export gas. University of Florence, Italy. 2003.

[40]   Bolhàr-Nordenkampf, M, Friedl, A, Koss, U, Tork, T. 2004. Modelling selective $H_2S$ absorption and desorption in an aqueous MDEA-solution using a rate-based non-equilibrium approach. Chemical Engineering and Processing. Vol 43, no. 6. pp. 701 − 715.

[41]   FosterWheeler,. Precombustion decarbonisation. IEA GHG. 1998.

[42]   Klinkenbijl, J M, Dillon, M L, Heyman, E C. Gas pre-treatment and their impact on liquefaction processes. In: GPA Nashville TE meeting. 1999.

[43]   Aspen Technology Inc. 2008. Rate-based model of the $CO_2$ capture process by MDEA using Aspen Plus.

[44]   Jou, F Y, Mather, A E, Otto, F D. 1982. Solubility of hydrogen sulfide and carbon dioxide in aqueous methyldiethanolamine solutions. Industrial and Engineering Chemistry Process Design and Development. Vol 21. p. 539.

[45]   Jou, F Y, Carroll, J J, Mather, A E, Otto, F D. 1993. Solubility of mixtures of hydrogen sulfide and carbon dioxide in aqueous n-methyldiethanolamine solutions. Journal of Chemical and Engineering Data. Vol 38. p. 75.

[46]   Jou, F Y, Carroll, J J, Mather, A E, Otto, F D. 1993. The solubility of carbon dioxide and hydrogen sulfide in a 35 wt aqueous solution of methyldiethanolamine. Canadian Journal of Chemical Engineering. Vol 71. p. 264.

[47]   Kohl, A L, Nielsen, R B. 1985. Gas Purification (Fourth Edition). Gulf Professional Publishing. Houston, TX, USA.

[48]   Patil, P, Malik, Z, Jobson, M. Prediction of $CO_2$ and $H_2S$ solubility in aqueous MDEA solutions using an extended Kent and Eisenberg model. In: IChemE Distillation and Absorption Conference. 2006.

[49]   Closmann, F, Nguyen, T, Rochelle, G T. 2009. MDEA/Piperazine as a solvent for $CO_2$ capture. Energy Procedia. Vol 1, no. 1. pp. 1351 − 1357. Greenhouse Gas Control Technologies 9, Proceedings of the 9th International Conference on Greenhouse Gas Control Technologies (GHGT-9), 16-20 November 2008, Washington DC, USA.

[50]   Aspen Technology Inc. 2008. Using Aspen Plus to model coal gasification.

[51]   Strube, R, Manfrida, G. Different Strategies of $CO_2$ Capture from Coal Fired Power Plants: Effect on Performance and Environmental Impact. In: Proceedings of the International Conference on Optimization Using Exergy–Based Methods and Computational Fluid Dynamics. 2009.

[52]   Breckendridge, W, Holiday, A, Ong, J O Y, Sharp, C. Use of Selexol Process in Coke Gasification to Ammonia Project. In: Laurance Reid Gas Conditioning Conference. 2000.

[53]   Aspen Technology Inc. 2008. Aspen Plus Model of the $CO_2$ Capture Process by DEPG.

[54]   Tumakaka, F, Gross, J, Sadowski, G. 2002. Modeling of Polymer Phase Equilibria using Perturbed-Chain SAFT. Fluid Phase Equilibria. Vol 194-197. pp. 541 − 551.

[55]   Grenner, A, Kontogeorgis, G M, von Solms, N, Michelsen, M L. 2007. Application of PC-SAFT to Glycol containing Systems - PC-SAFT towards a Predictive Approach. Fluid Phase Equilibria. Vol 261, no.

1-2. pp. 248 – 257. Properties and Phase Equilibria for Product and Process Design, 11th International Conference on Properties and Phase Equilibria for Product and Process Design.

[56] Perfetti, E, Thiery, R, Dubessy, J. 2008. Equation of state taking into account dipolar interactions and association by hydrogen bonding: II–Modelling liquid-vapour equilibria in the $H_2O$-$H_2S$, $H_2O$-$CH_4$ and $H_2O$-$CO_2$ systems. Chemical Geology. Vol 251, no. 1-4. pp. 50 – 57.

[57] Aaron, D, Tsouris, C. 2005. Separation of $CO_2$ from flue gas: A review. Separation Science and Technology. Vol 40, no. 1. pp. 321 – 348.

[58] Davison, J, Thambimuthu, K. Technologies for capture of carbon dioxide. In: Rubin, E S, Keith, D W, Gilboy, C F, Wilson, M, Morris, T, Gale, J, et al., editors. Greenhouse Gas Control Technologies 7. Elsevier Science Ltd. 2005. pp. 3 – 13.

[59] Wang, R, Zhang, H Y, Feron, P H M, Liang, D T. 2005. Influence of membrane wetting on $CO_2$ capture in microporous hollow fiber membrane contactors. Separation and Purification Technology. Vol 46, no. 1-2. pp. 33 – 40.

[60] Bao, L, Trachtenberg, M C. 2006. Facilitated transport of $CO_2$ across a liquid membrane: Comparing enzyme, amine, and alkaline. Journal of Membrane Science. Vol 280, no. 1-2. pp. 330 – 334.

[61] Figueroa, J D, Fout, T, Plasynski, S, McIlvried, H, Srivastava, R D. 2008. Advances in $CO_2$ capture technology–The U.S. Department of Energy's Carbon Sequestration Program. International Journal of Greenhouse Gas Control. Vol 2, no. 1. pp. 9 – 20.

[62] Yeh, A C, Bai, H. 1999. Comparison of ammonia and monoethanolamine solvents to reduce $CO_2$ greenhouse gas emissions. The Science of The Total Environment. Vol 228, no. 2-3. pp. 121 – 133.

[63] Goff, G S, Rochelle, G T. Oxidative degradation of aqueous monoethanolamine in CO2 Capture Systems Under Absorber Conditions. In: Gale, J, Kaya, Y, editors. Greenhouse Gas Control Technologies - 6th International Conference. Pergamon. 2003. pp. 115 – 120.

[64] Sexton, A J, Rochelle, G T. 2009. Catalysts and inhibitors for MEA oxidation. Energy Procedia. Vol 1, no. 1. pp. 1179 – 1185. Greenhouse Gas Control Technologies 9, Proceedings of the 9th International Conference on Greenhouse Gas Control Technologies (GHGT-9), 16-20 November 2008, Washington DC, USA.

[65] IEA-GHG. Post combustion carbon capture from coal fired power plants - solvent scrubbing. IEA GHG. 2007.

[66] Soosaiprakasam, I R, Veawab, A. 2009. Corrosion inhibition performance of copper carbonate in MEA-$CO_2$ capture unit. Energy Procedia. Vol 1, no. 1. pp. 225 – 229. Greenhouse Gas Control Technologies 9, Proceedings of the 9th International Conference on Greenhouse Gas Control Technologies (GHGT-9), 16-20 November 2008, Washington DC, USA.

[67] Veawab, A. Corrosion in $CO_2$ Capture Unit for Coal-Fired Power Plant Flue Gas. In: Gale, J, Kaya, Y, editors. Greenhouse Gas Control Technologies - 6th International Conference. Pergamon. 2003. pp. 1595 – 1598.

[68] Wilson, M, Tontiwachwuthikul, P, Chakma, A, Idem, R, Veawab, A, Aroonwilas, A, et al. 2004. Test results from a $CO_2$ extraction pilot plant at boundary dam coal-fired power station. Energy. Vol 29, no. 9-10. pp. 1259 – 1267. 6th International Conference on Greenhouse Gas Control Technologies.

[69]     Tanthapanichakoon, W, Veawab, A. Heat stable salts and sorrosivity in amine treating units. In: Gale, J, Kaya, Y, editors. Greenhouse Gas Control Technologies - 6th International Conference. Pergamon. 2003. pp. 1591 – 1594.

[70]     van Loo, S, van Elk, E P, Versteeg, G F. 2007. The removal of carbon dioxide with activated solutions of methyl-diethanol-amine. Journal of Petroleum Science and Engineering. Vol 55, no. 1-2. pp. 135 – 145. Petroleum Production Research in the Middle East.

[71]     Abu-Zahra, M R M, Schneiders, L H J, Niederer, J P M, Feron, P H M, Versteeg, G F. 2007. $CO_2$ capture from power plants: Part I. A parametric study of the technical performance based on monoethanolamine. International Journal of Greenhouse Gas Control. Vol 1, no. 1. pp. 37 – 46. 8th International Conference on Greenhouse Gas Control Technologies - GHGT-8.

[72]     Alie, C. $CO_2$ capture with MEA: Integrating the absorption process and steam cycle of an existing coal-fired power plant. University of Waterloo, Canada. 2004.

[73]     Alie, C, Backham, L, Croiset, E, Douglas, P L. 2005. Simulation of $CO_2$ capture using MEA scrubbing: a flowsheet decomposition method. Energy Conversion and Management. Vol 46, no. 3. pp. 475 – 487.

[74]     Yeh, J T, Pennline, H W. Absorption and Regeneration Studies for $CO_2$ Capture by Aqueous Ammonia. In: Third Annual Conference on Carbon Capture & Sequestration. 2004. .

[75]     Yeh, J T, Resnik, K P, Rygle, K, Pennline, H W. 2005. Semi-batch absorption and regeneration studies for $CO_2$ capture by aqueous ammonia. Fuel Processing Technology. Vol 86, no. 14-15. pp. 1533 – 1546. Carbon Dioxide Capture and Sequestration.

[76]     Modern-Power-Systems,. 2006. Chilling news for carbon capture. Modern Power Systems. Vol 26. pp. 17 – 18.

[77]     Kozak, F, Petig, A, Morris, E, Rhudy, R, Thimsen, D. 2009. Chilled ammonia process for $CO_2$ capture. Energy Procedia. Vol 1, no. 1. pp. 1419 – 1426. Greenhouse Gas Control Technologies 9, Proceedings of the 9th International Conference on Greenhouse Gas Control Technologies (GHGT-9), 16-20 November 2008, Washington DC, USA.

[78]     Rhudy, R. Chilled ammonia process update. In: International Test Network for $CO_2$ Capture: report on 10th workshop. 2007.

[79]     Resnik, K, Yeh, J. 2004. Aqua ammonia process for simultaneous removal of $CO_2$, $SO_2$, and $NO_X$. Int J of Environmental Technology and Management. Vol 4.

[80]     Dave, N, Do, T, Puxty, G, Rowland, R, Feron, P H M, Attalla, M I. 2009. $CO_2$ capture by aqueous amines and aqueous ammonia - A Comparison. Energy Procedia. Vol 1, no. 1. pp. 949 – 954. Greenhouse Gas Control Technologies 9, Proceedings of the 9th International Conference on Greenhouse Gas Control Technologies (GHGT-9), 16-20 November 2008, Washington DC, USA.

[81]     Ciferno, J, DiPietro, P, Tarka, T. An economic scoping study for $CO_2$ capture using aqueous ammonia, final report. NETL. 2005.

[82]     Astarita, G, Savage, D W, Longo, J M. 1981. Promotion of $CO_2$ mass transfer in carbonate solutions. Chemical Engineering Science. Vol 36, no. 3. pp. 581 – 588.

[83]     Aspen Technology Inc. 2008. Rate-based model of the $CO_2$ capture process by MEA using Aspen Plus.

[84]     Aspen Technology Inc. 2008. Rate-based model of the $CO_2$ capture process by DGA using Aspen Plus.

[85]     Aspen Technology Inc. 2008. Rate-based model of the CO2 capture process by NH3 using Aspen Plus.

[86]   Fiaschi, D, Manfrida, G, Pellegrini, G, Massin, M. Some innovative applicable proposals for chemical separation and sequestration of $CO_2$ emission plants. In: ASME ESDA Conference. 2004.

[87]   Pellegrini, G. An LCA analysis of different solutions of zero $CO_2$ emission plants. University of Florence, Italy. 2008.

[88]   Lee, J W, Li, R. 2003. Integration of fossil energy systems with $CO_2$ sequestration through $NH_4HCO_3$ production. Energy Conversion and Management. Vol 44, no. 9. pp. 1535 – 1546.

[89]   Boustead, I, Hancock, G F. 1979. Handbook of Industrial Energy Analysis. John Wiley & Sons. New York, USA.

[90]   Pellegrini, G, Strube, R, Manfrida, G. 2009. Comparative study of chemical absorbents in postcombustion $CO_2$ capture. Energy. Vol In Press, Corrected Proof.

[91]   BASF Group. 2007. Available from: http://www.inorganics.basf.com.

[92]   Sigma Aldrich. 2007. Available from: http://www.sigmaaldrich.com.

[93]   Bai, H. 1997. Removal of $CO_2$ greenhouse gas by ammonia scrubbing. Ind Eng Chem Res. Vol 36. pp. 2490–2493.

[94]   Diao, Y-F, Zheng, X-Y, He, B-S, Chen, C-H, Xu, X-C. 2004. Experimental study on capturing $CO_2$ greenhouse gas by ammonia scrubbing. Energy Conversion and Management. Vol 45, no. 13-14. pp. 2283 – 2296.

[95]   Abu-Zahra, M R M, Niederer, J P M, Feron, P H M, Versteeg, G F. 2007. $CO_2$ capture from power plants: Part II. A parametric study of the economical performance based on mono-ethanolamine. International Journal of Greenhouse Gas Control. Vol 1, no. 2. pp. 135 – 142. 8th International Conference on Greenhouse Gas Control Technologies - GHGT-8.

[96]   Strube, R, Pellegrini, G, Manfrida, G. The environmental impact of postcombustion $CO_2$ capture with MEA and with ammonia for a coal-fired power plant. In: Proceedings of the ECOS 2009 Conference. 2009.

[97]   Gal, E. Ultra cleaning combustion gas including the removal of $CO_2$. Alstom. 2006. WO 2006022885.

[98]   PowerMag. 2008. Alstoms chilled ammonia $CO_2$ capture process advances toward commercialization. Power Magazine. pp. 1–4.

[99]   Valenti, G, Bonalumi, D, Machi, E. 2009. Energy and exergy analyses for the carbon capture with the Chilled Ammonia Process (CAP). Proceedings of the 9th International Conference on Greenhouse Gas Control Technologies (GHGT-9). Vol 1, no. 1. pp. 1059–1066.

[100]  Darde, V, Thomsen, K, van Well, W J M, Stenby, E H. 2009. Chilled ammonia process for $CO_2$ capture. Energy Procedia. Vol 1, no. 1. pp. 1035 – 1042. Greenhouse Gas Control Technologies 9, Proceedings of the 9th International Conference on Greenhouse Gas Control Technologies (GHGT-9), 16-20 November 2008, Washington DC, USA.

[101]  Liu, J, Wang, S, Zhao, B, Tong, H, Chen, C. 2009. Absorption of carbon dioxide in aqueous ammonia. Energy Procedia. Vol 1, no. 1. pp. 933 – 940.

[102]  Esber, G S. Carbon dioxide capture technology for the coal-powered electricity industry: A systematic prioritization of research needs. Massachusetts Institute of Technology, USA. 2006.

[103]  Plaza, J M, van Wagener, D, Rochelle, G T. 1999. Modeling $CO_2$ capture with aqueous monoethanolamine. Energy Procedia. Vol 1, no. 1. pp. 1171–1178.

[104] Ziaii, S, Cohen, S, Rochelle, G T, Edgar, T F, Webber, M E. 2009. Dynamic operation of amine scrubbing in response to electricity demand and pricing. Energy Procedia. Vol 1, no. 1. pp4047 – 4053.

[105] Freguia, S, Rochelle, G T. 2003. Modeling of $CO_2$ capture by aqueous monoethanolamine. AIChE Journal. Vol 49, no. 7. pp. 1676 – 1686.

[106] Dang, H. CO2 Absorption Rate and Solubility in MEA/PZ/$H_2O$. The University of Texas at Austin, TX, USA. 2000.

[107] Austgen, D M, Rochelle, G T, Peng, X, Chen, C C. 1989. Model of vapor liquid equilibria for aqueous acid gas alkanolamine systems using the electrolyte NRTL equation. Ind Eng Chem Res. Vol 28, no. 7. pp. 1060 – 1073.

[108] Jou, F Y, Mather, A E, Otto, F D. 1994. Vapor-liquid equilibrium of carbon dioxide in aqueous mixtures of monoethanolamine and methyldiethanolamine. Ind Eng Chem Res. Vol 33, no. 8. pp. 2002 – 2005.

[109] Ziaii, S, Fisher, K S, Searcy, K, Schubert, C, Rochelle, G T. Advanced amine solvent formulations and process integration for near-term capture success, final report. DOE. 2007. DE-FG02-06ER84625.

[110] Aboudheir, A. Kinetics modeling and simulation of carbon dioxide absorption into highly concentrated and loaded monoethanolamine solutions. University of Regina, USA. 2002.

[111] Hilliard, M D. A predictive thermodynamic model for an aqueous blend of potassium carbonate, Piperazine, and monoethanolamine for carbon dioxide capture from flue gas. The University of Texas at Austin, TX, USA. 2008.

[112] Powerspan, Clean Energy Technology. 2009. Available from: http://www.powerspan.com.

[113] Fisher, K S, Rochelle, G T. Integrating MEA regeneration with $CO_2$ compression and peaking to reduce CO2 capture costs. U.S. Department of Energy. 2005.

[114] Buhre, B J P, Elliott, L K, Sheng, C D, Gupta, R P, Wall, T F. 2005. Oxy-fuel combustion technology for coal-fired power generation. Progress in Energy and Combustion Science. Vol 31, no. 4. pp. 283 – 307.

[115] Tan, Y, Croiset, E, Douglas, M A, Thambimuthu, K V. 2006. Combustion characteristics of coal in a mixture of oxygen and recycled flue gas. Fuel. Vol 85, no. 4. pp. 507 – 512.

[116] Chui, E H, Douglas, M A, Tan, Y. 2003. Modeling of oxy-fuel combustion for a western Canadian sub-bituminous coal[small star, filled]. Fuel. Vol 82, no. 10. pp. 1201 – 1210.

[117] Croiset, E, Thambimuthu, K V. 2001. $NO_X$ and $SO_2$ emissions from $O_2/CO_2$ recycle coal combustion. Fuel. Vol 80, no. 14. pp. 2117 – 2121.

[118] Castle, W F. 2002. Air separation and liquefaction: recent developments and prospects for the beginning of the new millennium. International Journal of Refrigeration. Vol 25, no. 1. pp. 158 – 172.

[119] IEA-GHG,. Oxy combustion processes for $CO_2$ capture from power plant. IEA GHG. 2005.

[120] White, V, Allam, R, Miller, E. Purification of oxyfuel-derived $CO_2$ for sequestration or EOR. In: Gale, J, Kaya, Y, editors. Proceedings of the 8th International Conference on Greenhouse Gas Control Technologies (GHGT-8). 2006. pp. 1595 – 1598.

[121] Santos, S. Oxyfuel combustion for coal fired power plant with $CO_2$ capture. In: IEA GHG R&D Programme Summer School. 2008.

[122] Personal communication with S. Santos, IEA GHG. 2009.

[123] Allam, R J. Purification of carbon dioxide. Air Products. 2008. US7416716B2.

[124] White, V. Purification of carbon dioxide. Air Products. 2008. US20080173585A1.

[125]  .Personal communication with V. White, Air Products. 2009.

[126]  Bao, H A. $CO_2$ separation apparatus and process for oxy-combustion coal power plant. Air Liquide. 2008. US20080196587A1.

[127]  Shah, M M. Carbon dioxide purification method. 2007. US20070231244A1.

[128]  Curran, M A. Purification and recovery options for gasification, EPA/600/R-06/060. Scientific Applications International Corporation (SAIC), National Risk Management Laboratory, U.S. Environmental Protection Agency, Cincinnati, Ohio, USA. 2006.

[129]  Curran, M A. Life-Cycle Assessment. In: Jorgensen, S E, Fath, B, editors. Encyclopedia of Ecology. Academic Press. 2008. pp. 2168 – 2174.

[130]  Manfrida, G. Introduction to Life Cycle Analysis. University of Florence. 2006.

[131]  Goedkoop, M, Schryver, A D, Oele, M. Introduction to LCA with SimaPro 7. 2008. 4.2.

[132]  Bare, J C, Norris, G A, Pennington, D W, McKone, T. 2002. TRACI − The tool for the reduction and assessment of chemical and other environmental impacts. Journal of Industrial Ecology. Vol 6, no. 3-4. pp. 49 – 78.

[133]  Goedkoop, M, Spriensma, R. The Eco-indicator 99: A damage oriented method for Life Cycle Impact Assessment, Methodology Report, Third edition. PRé Consultants. 2001.

[134]  Odeh, N A, Cockerill, T T. 2008. Life cycle GHG assessment of fossil fuel power plants with carbon capture and storage. Energy Policy. Vol 36, no. 1. pp. 367 – 380.

[135]  Koornneef, J. 2008. Life Cycle Assessment of a pulverised coal power plant with post-combustion capture, transport and storage of $CO_2$. International Journal of Greenhouse Gas Control. Vol 2. pp. 448–467.

[136]  Rebitzer G, Ekvall T, Frischknecht R, Hunkeler D, Norris G, Rydberg T, et al. Life cycle assessment: Part 1: Framework, goal and scope definition, inventory analysis, and applications. Environment International. 2004;30(5):701 – 720.

[137]  Meester BD, Dewulf J, Verbeke S, Janssens A, Langenhove HV. Exergetic life-cycle assessment (ELCA) for resource consumption evaluation in the built environment. Building and Environment. 2009;44(1):11 – 17.

[138]  Cornelissen RL. Thermodynamics and Sustainable Development - The use of Exergy Analysis and the Reduction of Irreversibility. University Twente, Netherlands; 1997.

[139]  Kotas TJ. Exergy concepts for thermal plant : First of two papers on exergy techniques in thermal plant analysis. International Journal of Heat and Fluid Flow. 1980;2(3):105 – 114.

[140]  Finnveden G, Östlund P. Exergies of natural resources in life-cycle assessment and other applications. Energy. 1997;22(9):923 – 931.

[141]  Szargut J. International progress in second law analysis. Energy. 1980;5(8-9):709 – 718. Second law analysis of energy devices and processes.

[142]  Szargut JT. Optimization of the design parameters aiming at the minimization of the depletion of non-renewable resources. Energy. 2004;29(12-15):2161 – 2169. Efficiency, Costs, Optimization, Simulation and Environmental Impact of Energy Systems.

[143]  Szargut J. Sequence method of determination of partial exergy losses in thermal systems. Exergy, An International Journal. 2001;1(2):85 – 90.

[144] Dewulf J, Langenhove HV, Dirckx J. Exergy analysis in the assessment of the sustainability of waste gas treatment systems. The Science of The Total Environment. 2001;273(1-3):41 – 52.

[145] Szargut J, Ziebik A, Stanek W. Depletion of the non-renewable natural exergy resources as a measure of the ecological cost. Energy Conversion and Management. 2002;43(9-12):1149 – 1163.